AD_____

Award Number: DAMD17-99-1-9402

TITLE: Training Program in the Molecular Basis of Breast Cancer Research

PRINCIPAL INVESTIGATOR: Z. Dave Sharp, Ph.D.

CONTRACTING ORGANIZATION: The University of Texas Health Sciences Center at San Antonio
San Antonio, TX 78229-3900

REPORT DATE: August 2002

TYPE OF REPORT: Annual Summary

PREPARED FOR: U.S. Army Medical Research and Materiel Command
Fort Detrick, Maryland 21702-5012

DISTRIBUTION STATEMENT: Approved for Public Release;
Distribution Unlimited

The views, opinions and/or findings contained in this report are those of the author(s) and should not be construed as an official Department of the Army position, policy or decision unless so designated by other documentation.

929 011

REPORT DOCUMENTATION PAGE

Form Approved
OMB No. 074-0188

Public reporting burden for this collection of information is estimated to average 1 hour per response, including the time for reviewing instructions, searching existing data sources, gathering and maintaining the data needed, and completing and reviewing this collection of information. Send comments regarding this burden estimate or any other aspect of this collection of information, including suggestions for reducing this burden to Washington Headquarters Services, Directorate for Information Operations and Reports, 1215 Jefferson Davis Highway, Suite 1204, Arlington, VA 22202-4302, and to the Office of Management and Budget, Paperwork Reduction Project (0704-0188), Washington, DC 20503

1. AGENCY USE ONLY (Leave blank)	2. REPORT DATE	3. REPORT TYPE AND DATES COVERED
	August 2002	Annual Summary (1 Aug 2001 - 31 Jul 2002)

4. TITLE AND SUBTITLE
Training Program in the Molecular Basis of Breast Cancer Research

5. FUNDING NUMBERS
DAMD17-99-1-9402

6. AUTHOR(S)
Z. Dave Sharp, Ph.D.

7. PERFORMING ORGANIZATION NAME(S) AND ADDRESS(ES)
The University of Texas Health Sciences Center at San Antonio
San Antonio, TX 78229-3900

E-Mail: ting@uthscsa.edu

8. PERFORMING ORGANIZATION REPORT NUMBER

9. SPONSORING / MONITORING AGENCY NAME(S) AND ADDRESS(ES)
U.S. Army Medical Research and Materiel Command
Fort Detrick, Maryland 21702-5012

10. SPONSORING / MONITORING AGENCY REPORT NUMBER

11. SUPPLEMENTARY NOTES

20030929 011

12a. DISTRIBUTION / AVAILABILITY STATEMENT
Approved for Public Release; Distribution Unlimited

12b. DISTRIBUTION CODE

13. ABSTRACT (Maximum 200 Words)

The objective of the program is to train highly qualified doctoral students in the genetic, cellular, and molecular basis of Breast Cancer. The training program, conducted within the Molecular Medicine Ph.D. Program, was administered by a select group of faculty whose research projects were intimately involved in breast cancer. An additional goal of the program was to promote synergistic interactions between the various laboratories engaged in breast cancer research. Breast cancer meetings, Molecular Medicine Distinguished Seminar Series were integral parts of the training program for students supported by the Breast Cancer Training Program. The major strengths of the program were the high quality of the Program faculty, and the interactive nature of the Breast Cancer research community in San Antonio. The program faculty encompassed scientists and physicians studying different aspects of breast cancer and cancer therapy, as well as fundamental mechanisms of DNA repair, cell growth and cell differentiation. Key research accomplishments during the 2002-2003 reporting period were: **1)** publication of 10 peer-reviewed articles by students in the program; **2)** DOD BCRP pre-doctoral grants awarded to three students in the program, **3)** seven faculty awarded DOD BCRP Idea and/or Career Development grants totaling $3.6 million; **4)** four Ph.D. students supported by the program graduated.

14. SUBJECT TERMS	15. NUMBER OF PAGES
Breast cancer, research training, cancer therapy, DNA repair and Tumor suppressor genes, cell growth regulation and cell differentiation	149
	16. PRICE CODE

17. SECURITY CLASSIFICATION OF REPORT	18. SECURITY CLASSIFICATION OF THIS PAGE	19. SECURITY CLASSIFICATION OF ABSTRACT	20. LIMITATION OF ABSTRACT
Unclassified	Unclassified	Unclassified	Unlimited

Table of Contents

INTRODUCTION

Brief Description of the Training Program and Its Objectives

The aim of the program is to establish at the University of Texas Health Science Center in San Antonio an in-depth training program in the Molecular Genetics of Breast Cancer. An important goal of the program is to train highly qualified Ph.D. students in the genetic, cellular, and molecular basis of Breast Cancer. Toward these ends, the program has been extremely successful. Based on the publication record of our trainees, our expectation for significant discoveries is being realized. During the reporting period, students supported by the training program achieved a total of 10 publications relevant to breast cancer.

The training program is administered within the Molecular Medicine Ph.D. Program by a select group of faculty whose research projects are relevant to breast cancer. An additional goal of the program is to promote synergistic interactions between the various laboratories engaged in breast cancer research. An important meeting was the Annual Breast Cancer Symposium held in San Antonio. All students supported by the program are required to attend. Finally, an outstanding Molecular Medicine Seminar Series sponsored by the Department of Molecular Medicine is also a requirement for all trainees. The following seminars in this series were pertinent to breast cancer:

- **Fall Semester: 2002**

Anindya Dutta	"p21 and geminin: Lessons from two inhibitors of the cell-cycle"
Tim G. Formosa	"Getting the FACTs on chromatin: How polymerases manage nucleosomes"
Michael A. Resnick	"DNA double-strand breaks: An endless pursuit"
Eric E. Alani	"Mismatch repair proteins: Are they just spellcheckers?"
Scott N. Keeney	"Initiating meiotic recombination in yeast and mouse"
Carl Wu	"ATP-dependent chromatin remodeling protein complexes for transcription"
Peter M. J. Burgers	"Rings around the DNA: A family of sliding clamps in DNAmetabolism"
Erica S. Johnson	"Factors that control protein modification by SUMO"
Chawnshang Chang	"Androgen receptor and androgen receptor coregulators in prostate cancer"
Rolf Sternglanz	"Studies on transcriptional silencing in yeast"
Vicki Lundblad	"Recruitment of multiple complexes to the chromosome terminus"

Spring Semester: 2003

Gerald R. Smith	"Meiotic recombination in *S. pombe*: Hotspots, DNA breaks and remote control"
Debu Chakravarti	"Hormones, HATs, and INHAT: Roles in circadian timing and transcriptional regulation"
Benoit deCrombrugghe	"Transcriptional controls in formation of the skeleton"
Vincent Chau	"Mechanism underlying proteasome inhibition in cancer therapy"
Helen Hansma	"The atomic force microscope and molecular force probes as tools for molecular medicine"
Patrick J. Concannon	"Identifying genes for human inherited radiation sensitivity disorders"
Kerry Bloom	"Dynamics of DNA repair in live cells"
Eileen Adamson	"High throughput methods to identify targets of Early Growth Responses gene 1 (EGR1)"
Michael Christman	"Molecular events in genome instability"
Antonio Iavarone	"Id2 in development and cancer"
Anthony Firulli	"Transcriptional control of specification and differentiation: a 'HANDFUL' of factors"
Mirit Aladjem	"Initiation of DNA replication in mammalian cell: Coordination of Sites and timing

Breast Cancer Research Programs and Faculty.

One of the major strengths of the program is the high quality of the Program faculty, and the interactive nature of the Breast Cancer research community in San Antonio, which encompass scientists and physicians studying different aspects of breast cancer and cancer therapy, as well as fundamental mechanisms of to maintain genomic stability, cell growth, differentiation and molecular genetics. These faculty groupings are listed below; detailed descriptions of individual research programs were included in the original application.

Breast Cancer Research Training Faculty

W.-H. Lee, Ph.D. (Director, **Note:** Dr. Lee recently moved his laboratory to UC Irvine – see comments in changes to faculty).
C. Kent Osborne, M.D. (Co-Director)

Powell H. Brown, M.D., Ph.D.
Peter O'Connell, Ph.D.
Gary M. Clark, Ph.D.
Suzanne Fuqua, Ph.D.
Alan Tomkinson, Ph.D.
E. Lee, Ph.D. Note: Dr. Lee recently moved her laboratory to UC Irvine – see comments in changes to faculty
Z. Dave Sharp, Ph.D. (**Note**: Appointed Director as of July, 2003)
Patrick Sung, Ph.D.
Greg R. Mundy
Bettie Sue Masters, Ph.D.
Bandana Chatterjee, Ph.D.
Arun K. Roy, Ph.D.
Judy M. Teale, Ph.D.
Peter M. Ravdin, M.D. Ph.D.
Phang-Lang Chen, Ph.D
Renee Yew, Ph.D.
Tom Boyer, Ph.D.
Maria Gazynska, Ph.D.
Paul Hasty, DVM
Jan Vijg, Ph.D.
Tadayoshi Bessho, Ph.D.
Sang Eun Lee, Ph.D.
Hai Rao, Ph.D.

Relationship between the Breast Cancer Training Program and the Molecular Medicine Graduate Ph.D. Program

The Breast Cancer Training Program was implemented within the context of the Molecular Medicine Graduate Ph.D. Program. The Molecular Medicine Ph.D. Program is an interdisciplinary Ph.D. training program in the Graduate School of Biomedical Sciences at the UTHSCSA. For the academic year 2002-03, there were a total of 49 Ph.D. students enrolled in the Molecular Medicine Program.

The Breast Cancer Training program takes advantage of the internationally recognized breast cancer research programs existing in the institution for many years, and offers a unique opportunity for students interested in starting careers in breast cancer research. The participating scientists in this breast cancer program represent diverse departments including the Divisions of Medical Oncology and Endocrinology in the Department of Medicine, and the Departments of Cellular and Structural Biology, and Biochemistry. In addition, the University of Texas Institute of Biotechnology and the San Antonio Cancer Institute (SACI), an NIH-designated Cancer Center, represent outstanding resources for training opportunities in clinical and basic science research. The national and international reputation of the participating faculty serve to attract a large number of excellent applicants to the breast cancer research track in the Molecular Medicine program.

The rationale for administering the breast cancer training program in the Molecular Medicine Ph.D. program remains based on several important criteria: (1) The Molecular Medicine curriculum is specifically designed to provide basic science training while integrating fundamental principles of molecular biology with modern medicine. A Molecular Medicine Core course provides students with the mechanisms underlying human disease and provides intensive review of specific diseases (including breast cancer) that may serve as models for how

human diseases can be studied at the molecular genetic level. (2) The Molecular Medicine program requires the participation of both clinical and basic scientists in the training process. The inclusion of MDs on all student advisory committees insures that every graduate of the program has a clear perspective on the clinical relevance of the basic research in their program that, in most instances, will serve as a guide for the project. (3) The Molecular Medicine program is an interdepartmental, interdisciplinary program that offers flexibility to students in terms of research laboratories, advisors and committee members. This arrangement offers a real potential for synergism in breast cancer research not possible in traditional department-bound programs. In summary, the Ph.D. program in Molecular Medicine offers a near perfect environment for Ph.D. training in breast cancer and has attracted many well-qualified applicants.

Research Support for Program Faculty

An essential component of maintaining a successful and aggressive training program in Breast Cancer Research is the continued research funding of the individual Program Faculty laboratories. The faculty has been extremely successful in obtaining research funding, including over $12 million in total direct costs for the 2002-2003 reporting period.

Key Research Accomplishments:

Research grants awarded to members of the faculty by the Defense Department's Breast Cancer Research Program (BCRP).

Tom Boyer, Ph.D., Career Development Award

Project Title: Regulation of BRCA1 function by DNA damage-induced site-specific phosphorylation.

Project Period: 05/15/02 - 06/15/06

Project Total: $176,516 Total for entire project

Considerable evidence implicates DNA-damage-induced site-specific phosphorylation of BRCA1 as a critical regulator of its caretaker properties. Dr. Boyer hypothesizes that DNA damage-induced site-specific phosphorylation of BRCA1 regulates its transcription and/or DNA double-strand break repair activities.

Tom Boyer, Ph.D., Idea Award

Project Title: Regulation of BRCA1 function by DNA damage-induced site-specific phosphorylation.

Project Period: 04/01/01 - 03/31/04

Project Total: $414,599 Total for entire project

Considerable evidence implicates DNA-damage-induced site-specific phosphorylation of BRCA1 as a critical regulator of its caretaker properties. Dr. Boyer hypothesizes that DNA damage-induced site-specific phosphorylation of BRCA1 regulates its transcription and/or DNA double-strand break repair activities.

Phang-Lang Chen, Ph.D., Idea Award

Project Title: BRCA2 and the DNA double strand break repair machinery

Project Period: 10/01/99 – 10/31/02 (obtained one-year no cost extension to 10/31/03)

Project Total: $304,500

To understand the cellular function of BRCA2, and to elucidate its role in the development and progression of breast cancer.

Phang-Lang Chen, Ph.D., Idea Award

Project Title: Small chemical molecules disrupt BRCA2 and Rad51 interaction for adjuvant BC

Project Period: 04/01/01 – 05/31/04

Project Total: $433,500

To isolate small molecules which disrupt the interactions between BRCA2 and Rad51 using reverse yeast two-hybrid screening. To evaluate the ability of the identified molecules to sensitize cultured breast cancer cells to the genotoxic and cytotoxic effects of ionizing radiation; and to assess the efficacy of the small molecules as adjuvant.

Maria Gaczynska, Ph.D., Idea Award

Project Title: Molecular characteristics of multicorn, a new large proteolytic assembly and potential anticancer drug target in human breast cancer cells

Project Period: 04/01/01 – 03/31/04

Project Total: $324,056

The goal of this project is to clone and express the gene of human multicorn monomer, study the mechanism controlling the multicorn activity through its oligomerization and phosphorylation, and test molecular characterization of the multicorn at different stages of the cell cycle.

Paul Hasty, DVM, Idea Award

Project Title: Development of anti-cancer therapeutics that modulate the RAD51-BRCA2 complex.

Project Period: 02/15/02 - 02/14/05

Project Total: $436,500

RAD51 is important for repairing double-strand breaks in DNA by recombination; interestingly, this function is likely to be essential since mammalian cells deleted for RAD51 exhibit chromosomal instability, are unable to sustain proliferation and senesce or die. Our specific aims are: characterize antp-26mer for biological activity on tissue culture cells, perform a

deletion and substitution analysis on the antp-26mer, and test peptides for potential as anti-cancer therapeutics in mice.

Patrick Sung, Ph.D., Career Development Award

Project Title: Interactions among BRCA1, BRCA2 & components of the recombination machinery

Project Period: 06/01/98 – 05/31/03

Project Total: $200,000

The main goal of this project is to purify BRCA1 and BRCA2 and study their biochemical properties.

(Note: Dr. Sung relocated to Yale University in 2003)

Patrick Sung, Ph.D., Idea Award

Project Title: BRCA2 & components of the recombination machinery

Project Period: 06/01/98 – 05/31/03

Project Total: $303,311

The main goal of this project is to purify BRCA1 and BRCA2 and study their biochemical properties.

(See Note above)

Renee Yew, Ph.D., Career Development Award

Project Title: The role of BRCA1-dependent ubiquitination in Breast Cancer

Project Period: 06/01/02 - 05/31/04

Project Total: $181,960

Mutational inactivation of the BRCA1 gene accounts for a large percentage of hereditary breast cancer. Although the BRCA1 gene product has been implicated to function in a number of different cellular processes including DNA repair and transcription, it is still unclear how BRCA1 biochemically mediates its cellular function as a tumor suppressor protein. It has been suggested that the BRCA1 gene product functions as an ubiquitin protein ligase or E3 enzyme in a manner similar to a growing number of proteins that comprise a family of ring finger proteins. If this putative E3 activity of BRCA1 can be shown to be a physiological function of full length BRCA1 in the cell, this could greatly aid in determining the molecular mechanisms by which BRCA1 mediates its cellular function.

Renee Yew, Ph.D., Idea Award

Project Title: The role of BRCA1-dependent ubiquitination in Breast Cancer

Project Period: 04/01/01 - 03/31/04

Project Total: $411,006

Mutational inactivation of the BRCA1 gene accounts for a large percentage of hereditary breast cancer. Although the BRCA1 gene product has been implicated to function in a number of different cellular processes including DNA repair and transcription, it is still unclear how BRCA1 biochemically mediates its cellular function as a tumor suppressor protein. It has been suggested that the BRCA1 gene product functions as an ubiquitin protein ligase or E3 enzyme in a manner similar to a growing number of proteins that comprise a family of ring finger proteins. If this putative E3 activity of BRCA1 can be shown to be a physiological function of full length BRCA1 in the cell, this could greatly aid in determining the molecular mechanisms by which BRCA1 mediates its cellular function.

Tadayoshi Bessho, Ph.D., Idea Award

Project Title: Biochemical Characterization of BRCA2

Project Period: 04/01/03 – 03/31/06

Project Total: $414,115

Nearly one third of the familial breast cancer patients have mutations in BRCA2 gene. Accumulating evidence implicate that BRCA2 functions in the maintenance of genomic stability. However, the molecular mechanism of tumor suppressor function of BRCA2 has not been understood yet, largely due to the lack of biochemical studies. Biochemical purification of BRCA2 will provide valuable insights into the functional role of BRCA2.

A deficiency of BRCA2 results in the hypersensitivity to a DNA crosslinking agent, mitomycin C (MMC), implicating a critical role of BRCA2 in crosslink repair. Our hypothesis is that BRCA2 functions as a multi-protein complex in crosslink repair, which is distinct from the previously isolated BRCA2 complex. We will purify a BRCA2 DNA repair complex using a cell free crosslink repair assay, which monitors removal of a psoralen crosslink in a defined substrate. By complementing a defect of crosslink removal activity in the extract from BRCA2 deficient cells with fractionated proteins from HeLa cells, we will isolate a functional and stoichiometric BRCA2 DNA repair complex. We will identify the components of the complex. The information obtained in this proposal will provide fundamentals to understand the regulation of the BRCA2 DNA repair complex during the cell cycle and after DNA damage and will reveal a link between DNA repair and the other cellular functions of BRCA2.

Predoctoral Breast Cancer Research Awards to Supported Trainees

Predoctoral training grants awarded to current trainees by the Defense Department's Breast Cancer Research Program (BCRP):

Sean Post, training in Dr. E. Lee's laboratory.

Project Title: Phosphorylation of hRad17 by ATR is required for cell cycle checkpoint activation

Project Period: 04/01/02 - 03/31/04

Total Award: $61,342

The goal of this study is to determine the relationship between ATR, hRad17, Chk2, and BRCA1 and demonstrate how these potential protein networks regulate checkpoint activation. Based on the reuqirement of SpRad3 and SpRad17 for checkpoint activation through SpCds1 in fission yeast and the ability of Chk2 to phosphorylate BRCA2 Ser988 in humans, it is my hypothesis that ATR mediated phosphorylation of hRad17 is required to activate cell cycle checkpoints, through Chk2 and BRCA1.

Stefan Sigurdsson, training in Dr. Patrick Sung's laboratory.

Project Title: Functions of Human Rad51 and Other Recombination Factors In DNA Double-Strand Break Repair.

Project Period: 06/01/01 - 05/31/04

Total Award: $66,000

Homologous recombination and recombinational repair of DNA double-strand breaks are mediated by proteins of the *RAD52* epistasis group. Rad51 is a key factor in these processes and the protein can assemble on ssDNA substrates to form a nucleoprotein filament. With the help from other factors, the Rad51-ssDNA nucleoprotein filament searches for a DNA homlog and catalyzes formation of a heteroduplex DNA joint with the homolog. The biochemical reaction that forms heteroduplex DNA joints is called □homologous DNA pairing and strand exchange. A number of Rad51-like proteins are known in human cells, but their function in recombination and DNA repair is currently unknown. I have shown that two of these Rad51-like proteins, Rad51B and Rad51C, are associated in a stable heterodimer. I will further define the homologous DNA pairing and strand exchange activity of human Rad51. In addition, a variety of experiments will be conducted to test the hypothesis that the Rad51B-Rad51C complex promotes the assembly of the Rad51-ssDNA nucleoprotein filament and enhances the efficiency of Rad51-mediate d homologous DNA pairing and strand exchange. The information garnered from this study should contribute significantly to our understanding of how DNA double-strand breaks are repaired in human cells.

Xining Zhu, training in Dr. Renee Yew's laboratory.

Project Title: Identification and Characterization of the BRCA1 Ubiquitin

Project Period: 05/01/03 – 04/30/06

Project Total: $90,000

Identification and Characterization of the BRCA1 Ubiquitin Ligase and its Substrates
The Breast Cancer susceptibility gene 1, BRCA1, is an 1863 amino acid, 220 kilodalton (Kd) nuclear phosphoprotein that is frequently mutated in inherited breast and ovarian cancer. The functional domains of BRCA1 interact with a variety of proteins, directly or indirectly implicating BRCA1 to function in a number of different cellular processes including cellular proliferation during embryogenesis, homologous recombination, transcription-coupled repair, double-strand break repair, transcriptional regulation, and functions as a tumor suppressor protein. However, it is unclear how BRCA1 mediates its normal function in the cell or how its multiple functions are coordinated. Germline mutations in BRCA1, including the ring finger domain, predispose women to breast and ovarian cancers. Within the last year, the highly conserved ring finger domain of BRCA1 has been shown to exhibit E3 ubiquitin ligase activity in vitro and in vivo with non-specific model substrates in a manner similar to a growing number of proteins that comprise the family of ring finger proteins. It has also been shown that the cancer predisposing ring finger mutations disrupt this ubiquitin ligase activity of BRCA1 both in vitro and in vivo. This ubiquitinating activity of BRCA1 has only recently been discovered. How this biochemical activity of BRCA1 may mediate the functions of BRCA1 in breast cancer prevention has yet to be addressed. If this putative E3 activity of BRCA1 can be shown to be a physiological function of full length BRCA1 in the cell, this could greatly aid in determining the molecular mechanism by which BRCA1 mediates its cellular function. Based on results showing that the ring finger domain of BRCA1 possesses ubiquitin protein ligase activity, our hypothesis is that BRCA1 mediates its biological function by targeting proteins for ubiquitination.

Dr. Yew's laboratory proposes that BRCA1 affects the ubiquitination of proteins involved in DNA repair or regulators of growth proliferation, leading either to their degradation or to an alteration of activity. The specific aims proposed here will address the physiological significance of a BRCA1 E3 activity, potential BRCA1 target substrates, and the significance of a BRCA1 E3 activity to breast cancer biology. The specific aims of this study are: (1) To develop an *in vitro* ubiquitination assay using full length BRCA1 and BRCA1-associated RING domain 1 protein (BARD1) proteins; (2) To identify potential BRCA1 substrates and to study the biological significance of the BRCA1-dependent ubiquitination of substrates. These studies will examine the ubiquitination of proteins in an extract by utilizing either baculovirus expressed and purified full length wild type and ring finger mutant of BRCA1, full length BARD1 or immunoprecipitated full length wild type and ring finger mutant of BRCA1 and BARD1 from stable cell lines in association with E1 and E2 proteins. Next, Ms. Zhu will study the predicted targets of BRCA1 for BRCA1-dependent ubiquitination. Predicted targets of BRCA1 ubiquitination include BRCA1-associated proteins and putative functional targets of BRCA1 such as the estrogen receptor alpha (ERalpha) and RNA Polymerase II. Ms. Zhu will use in vitro ubiquitination assays with 35S-Methionine labeled putative substrate and/or an immunoprecipitated putative substrate from the stable cells expressing wild type and ring finger mutant of BRCA1 and BARD1 to determine which substrate proteins are ubiquitinated by full length BRCA1. Ms. Zhu will also determine in vivo using the stable cells expressing wild type and ring finger mutant of BRCA1 or BARD1 which substrates are ubiquitinated in a BRCA1-dependent manner. By virtue of more stable interactions with the substrates, the ring finger mutant of full length BRCA1, devoid of E3 activity, will also be used to identify putative BRCA1 substrates. Once it is determined that a substrate is ubiquitinated in a BRCA1-dependent manner, the turnover of these BRCA1 substrates will be studied *in vivo* using the BRCA1 -/- and BRCA1 +/+ mouse embryonic fibroblast (MEF) cells. A bonafide BRCA1 substrate is expected to have an extended half-life in vivo in the absence of BRCA1. Ms. Zhu will also examine the turnover of BRCA1 substrates in non-cancerous versus BRCA1 mutated breast cancer cells to understand how the E3 activity of BRCA1 contributes to the prevention of cancer and especially breast cancer.

This study addresses a highly novel putative activity of BRCA1 that could have a large impact on our understanding of familial breast cancer development. It is Dr. Yew's laboratory's hope that these studies will identify a previously uncharacterized biochemical activity of BRCA1 in the cell and several important targets of this BRCA1 activity. This discovery could not only alter the manner in which all future studies are directed on the function of BRCA1 in the cell, but could also open many new avenues for the development and implementation of drugs for the treatment of breast cancer.

This project has obvious direct relevance to breast cancer and Dr. Yew is one of the world's experts in this important area of research. This is an important new function of the BRCA1 tumor suppressor, with a clear potential for translation into therapeutic applications.

Graduates During the Reporting Period (A description of supported student's research and future plans is below)

Stephen Van Komen, Ph.D.	October 2002
Stefan Sigurdsson, Ph.D.	May 2003
Ahmad Utomo, Ph.D.	March 2003
Song Zhao, Ph.D.	May 2003

Reportable Outcomes

Supported Trainees, Research Description and Publications

The following outstanding group of trainees was supported on the Breast Cancer Training Program during:

Reporting Period 8/1/02 – 7/31/03

1. Bingnan Gu (July 1-31, 2003 = 1 month) NEW APPOINTEE
2. Xianzhi Jiang (08/01/02 - 07/31/03)
3. Horng-Ru Lin (08/01/02 - 06/30/03 = 11 months)
4. Yi-Tzu Lin (08/01/02 - 07/31/03)
5. Aimin Peng (July 1-31, 2003 = 1 month) NEW APPOINTEE
6. Wei Tan (08/01/02 - 05/31/03 = 10 months)
7. Ahmad Utomo (08/01/02 - 03/11/03)
8. Sangeetha Vijayakumar (08/01/02 - 05/31/03 = 10 months)
9. Guikai Wu (08/01/02 - 02/28/03 = 7 months) he was on LOA from 3/1/03 through 7/31/03 due to visa/passport complications in China
10. Haiying Zhou (09/01/02 - 04/30/03 = 8 months)

The accomplishments of these students and their mentors are outstanding examples of how small investments in student training can be amplified in programs grounded in excellence.

The 2002-2003 academic year marks the tenth full year of operation for the Molecular Medicine Ph.D. Program, and is the eighth year for the Training Program in the Molecular Basis of Breast Cancer Research. The availability of highly qualified applicants to the Molecular Medicine Program was excellent. Overall, 86 applications were received for admission to the Fall 2002

entering class. Fourteen new students began classes in August of 2002. The total number of students at the start of the Fall semester 2002 in the Molecular Medicine Ph.D. Program at all levels was 49, which includes 23 women, and 3 underrepresented minority.

Project Summaries and Publications of Ph.D. Trainees (past and present supported by the currently active grant)

Note that the Program Director's comments regarding each student's research are in italics below each description.

David Levin ***Mentor -- Dr. Alan Tomkinson***

DNA joining events are required to maintain the integrity of the genome. Three human genes encoding DNA ligases have been identified. David is identifying the cellular functions involving the product of the LIG1 gene. Previous studies have implicated DNA ligase I in DNA replication and some pathways of DNA repair. During DNA replication, DNA ligase I presumably functions to join Okazaki fragments. However, under physiological salt conditions, DNA ligase I does not interact with DNA. It is Mr. Levin's working hypothesis that DNA ligase I involvement in different DNA metabolic pathways is mediated by specific protein-protein interactions which serve to recruit DNA ligase I to the DNA substrate. To detect proteins that bind to DNA ligase I, David has fractionated a HeLa nuclear extract by DNA ligase I affinity chromatography. PCNA was specifically retained by the DNA ligase I matrix. To confirm that DNA ligase I and PCNA interact directly, Mr. Levin found that in vitro translated and purified recombinant PCNA bind to the DNA ligase I matrix. In similar experiments, he has shown that DNA ligase I interacts with a GST (glutathione S transferase)-PCNA fusion protein but not with GST. Using in vitro translated deleted versions of DNA ligase I, Mr. Levin determined that the amino terminal 120 residues of this polypeptide are required for the interaction with PCNA. During DNA replication PCNA acts as a homotrimer that encircles DNA and tethers the DNA polymerase to its template. He showed that DNA ligase I forms a stable complex with PCNA that is topologically linked to a DNA duplex. Thus, it appears that PCNA can also tether DNA ligase I to its DNA substrate. A manuscript describing these studies was published in the Proc. Natl. Acad. Sci. U.S.A.

In addition to interacting with PCNA, the amino terminal domain of DNA ligase I also mediates the localization of this enzyme to replication foci. To determine whether these are separable functions David fine mapped the region that interacts with PCNA and, in collaboration with Dr. Montecucco's group, the region required for recruitment to replication foci. Since the same 19 amino acids are necessary and sufficient for both functions and the same changes in amino acid sequence inactivate both functions, we conclude that DNA ligase I is recruited to replication foci by its interaction with PCNA. A manuscript describing these studies was published in the EMBO Journal.

In recent studies, Mr. Levin has a constructed a mutant version of DNA ligase I that does not interact with PCNA. Importantly the amino acid substitutions do not affect the catalytic activity of DNA ligase I. By transfecting cDNAs encoding the mutant and wild type DNA ligase I into a DNA ligase I-mutant cell line, he has demonstrated the biological significance of the DNA ligase I/PCNA interaction in DNA replication and long patch base excision repair.

This project was relevant to breast cancer since problems with DNA replication and repair undoubtedly underlie the genomic instability associated with tumor formation.

Dr. Levin earned his Ph.D. in Molecular Medicine in the summer of 2000, and is currently a staff scientist at GeneTex, Inc., in San Antonio, Texas.

- ***John Leppard*** ***Mentor -- Alan Tomkinson***

Three genes, *LIG1*, *LIG3* and *LIG4*, encoding DNA ligases have been identified in the mammalian genome. Unlike the *LIG1* and *LIG4* genes, there are no homologues of the *LIG3* gene in lower eukaryotes such as yeast. Biochemical and genetic studies suggest that DNA ligase III participates in base excision repair and the repair of DNA single-strand break. A feature of DNA ligase III that distinguishes it from other eukaryotic DNA ligases is a zinc finger. In published studies we have shown that this zinc finger binds preferentially to nicks in duplex DNA and allows DNA ligase III to efficiently ligate nicks at physiological salt concentrations. These studies will be extended by determining how the zinc finger of DNA ligase III binds to DNA single-strand breaks but does not hinder access of the catalytic domain of DNA ligase III to ligatable nicks. Furthermore, we will reconstitute the base excision and single-strand break repair pathways mediated by DNA ligase III and elucidate the functional consequences of interactions between DNA ligase III and other DNA repair proteins such as Xrcc1, DNA polymerase beta and poly (ADP-ribose) polymerase that participate in these repair pathways.

Mr. Leppard's research is relevant to breast cancer since genomic instability is likely to be involved at several stages during the progression to malignant breast cancer. Methods to intervene and stabilize the genome could prevent progression and spread of the disease. In addition, information about DNA repair processes in normal and cancer cells may lead to the development of treatment regimes that more effectively kill cancer cells and minimize damage to normal tissues and cells.

Publications:

Tomkinson, A., and **Leppard, JB**., DNA ligases: Mechanism and function. Encyclopedia of Biological Chemistry.

- ***Teresa Motycka*** ***Mentor -- Alan Tomkinson***

DNA double-strand break repair is important for maintaining genomic stability. If left unrepaired, these lesions may cause cell death. The cell has evolved two major pathways for dealing with these lesions, nonhomologous end-jo ining and homologous recombination. Nonhomologous end-joining fuses the ends of broken DNA irrespective of the sequence at the site of the break, whereas homologous recombination preserves the sequence at the damaged site by using a sister chromatid as a template to copy the genetic information. Genetic studies in the budding yeast Saccharomyces cerevisiae have identified a number of genes important in this pathway, collectively named the RAD52 epistasis group. Of all of these genes, a del etion in rad52 produces the most severe phenotype. Mammalian homologs of RAD52 have been identified and the biochemical activity of the protein products is conserved from yeast to human. In order to gain further understanding of Rad52 function in higher eukaryotes, Ms. Motycka looked for interacting proteins by affinity chromatography and identified those polypeptides that were specifically bound by the resin. She has shown a direct interaction between XPF, a component of a multifunctional DNA structu re-specific endonuclease, with the N-terminus of hRad52. Complex formation between hRad52 and XPF/ERCC1 concomitantly stimulates the DNA structure-specific endonuclease activity of XPF/ERCC1 and attenuates the DNA strand annealing activity of hRad52. These results are consistent with previous genetic studies and provide a novel role for hRad52 in the modulation of XPF/ERCC1 activity. Ms. Motycka is currently examining the biological significance of a second protein-protein interaction identified in our screen. Hypersensitivity to DNA damage results from the deletion of the respective gene, suggesting we may have identified a novel player in Rad52-dependent DNA repair.

An understanding of the mechanisms of DSB in mammalian cells is relevant to breast cancer because the accumulating evidence linking the products of the breast cancer susceptibility genes, BRCA1 and BRCA2, with DSB repair.

- ***Suh-Chin(Jackie) Lin*** ***Mentor -- Dr. Eva Lee***

The tumor suppressor gene, p53, is frequently mutated in human tumors, including breast carcinoma. P53 null mice develop multiple spontaneous tumors, predominantly lymphoma and sarcoma, within the first 6 months of age. To establish a mouse model of p53-mediated mammary tumor development, Ms. Lin initiated a bigenetic approach employing the cre-loxp system. Through gene targeting in embryonic stem (ES) cells, mice carrying floxed p53 genes in which exons 5 and 6 are flanked by the loxp sequence were generated. A second mouse line carrying a cre transgene under the control of mouse mammary tumor virus LTR (MMTV-cre) has also been generated. Floxed p53 mice were mated with MMTV-cre transgenic mice to produce mice with p53 inactivation in mammary tissue. Indeed, we observed p53 excision in the tissues of double transgenic mice. In addition, adenoviral vectors carrying cre recombinase are being used to inactivate p53. These approaches should provide a mouse mammary tumor model for studies of mammary tumor progression resulting from p53 mutation and for testing therapeutic interventions of mammary tumorigenesis. The resulting mice have demonstrated interesting patterns of tumor development including those of the mammary gland. These animals will be valuable models for testing new approaches to breast cancer treatment and understanding its etiology.

Upon DNA damage, p53 protein becomes phosphorylated and stabilized, leading to subsequent activation of cell cycle checkpoints. It has been shown that ATM is required for IR induced phosphorylation on Ser15 residue of p53. Based on the involvement of p53 in mammary tumorigenesis and on the higher risk of ATM carriers for breast cancer, we have carried out studies to address the cancer susceptibility of ATM heterozygous and ATM null mammary epithelial cells by transplanting mammary gland to wild-type sibling mice. Initial studies have indicated differential checkpoint and apoptotic responses in cells harboring ATM mutation. These studies will establish whether ATM plays important roles in mammary tumorigenesis.

Both of these projects are highly relevant to breast cancer, especially the Dr. Lin's animal models which hold promise in terms of new therapies for breast cancer and its metastases.

Ms. Lin successfully defended her dissertation on December 18, 2000, and continues as a post-doctoral fellow in Dr. Lee's laboratory extending her work on the development of important animal models for human cancer.

- ***Sean Post*** ***Mentor -- Dr. Eva Lee***

Recent studies indicate that breast cancer susceptibility genes, BRCA1 and BRCA2, are involved in DNA repair. Cells harboring mutations in either gene are hypersensitive to ionizing radiation (IR). Extensive genetic evidence in yeast indicates that DNA double-stranded breaks are processed by Rad50/Mre11 nuclease complex. It has also been shown that in response to IR, Rad50 assembles into nuclear foci. In mammalian cells, such IR-induced Rad50 foci are not observed in cells established from Nijmegen breakage syndrome (NBS). We and others have shown that the protein product of gene mutated in NBS, Nibrin, forms a stable complex with

Rad50/Mre11 and the complex possesses nuclear activity. The E. Lee laboratory demonstrated that IR-induced Rad50 redistribution requires ATM kinase activity. Rad50 is phosphorylated upon IR. Their preliminary studies indicate that such IR-induced Rad50 foci formation and phosphorylation are defective in A-T cells. In addition, IR-induced Rad50 foci formation is aberrant in some sporadiac cancers that express normal ATM, Rad50, Mre11, nibrin, BRCA1 and BRCA2 suggesting involvement of additional protein in this DNA damage response.

Mr. Post characterized IR-induced Rad50 phosphorylation. How phosphorylation affects Rad50 function will be studied. In addition, cross-linking experiments will be carried out to investigate whether there is defective Rad50 protein complex formation in breast cancer cells. These studies will provide insights into the role of ATM kinase cascade in the assembly of double-stranded breakage repair protein. Furthermore, characterization of components in the repair protein complex may lead to the identification of additional players involved in breast carcinoma.

These projects are highly relevant to breast cancer since genomic instability is a hallmark of cancer and is thought to be a major contributor to the tumorigenic process. Mr. Post's research will contribute toward a greater understanding of the mechanisms responsible for maintaining genomic integrity that is undoubtedly involved in breast cancer development and progression.

Mr. Post successfully defended his dissertation research in July of 2003, and is in the process of revising his last paper for publication.

- ***Song Zhao*** ***Mentor – Dr. Eva Lee***

Mr. Zhao worked on the functional interactions between ATM and DNA repair proteins with a focus on NBS1. Ataxia-telangiectasia (A-T) and Nijmegen breakage syndrome (NBS) are recessive genetic disorders with susceptibility to cancer and similar cellular phenotypes. The protein product of the gene responsible for A-T, designated ATM, is a member of a family of kinases characterized by a carboxy-terminal phosphatidylinositol 3-kinase-like domain. The NBS1 protein is specifically mutated in patients with Nijmegen breakage syndrome and forms a complex with the DNA repair proteins Rad50 and Mrel1. Mr. Zhao showed that phosphorylation of NBS1, induced by ionizing radiation, requires catalytically active ATM. Complexes containing ATM and NBS1 exist in vivo in both untreated cells and cells treated with ionizing radiation. He, along with others in the lab, have identified two residues of NBS1, Ser 278 and Ser 343 that are phosphorylated in vitro by ATM and whose modification in vivo is essential for the cellular response to DNA damage. This response includes S-phase checkpoint activation, formation of the NBS1/Mrel1/Rad50 nuclear foci and rescue of hypersensitivity to ionizing radiation. Together, these results demonstrate a biochemical link between cell-cycle checkpoints activated by DNA damage and DNA repair in two genetic diseases with overlapping phenotypes

These projects have clear and compelling relevance to breast cancer since all of the proteins described are vital to the "caretaker" function of the DNA repair and response systems of all cells, to which mammary cells are especially dependent. Dr. Zhao made significant contributions as a graduate student and will undoubtedly continue this level of contribution as a postdoctoral fellow.

Dr. Zhao recently obtained his Ph.D., and is continuing his training as a postdoctoral fellow in Dr. Thomas Kelly's laboratory at the Memorial Sloan Kettering Institute. Dr. Zhao will be working to understand the regulation of DNA replication.

Publications:

Yuan SS, Su JH, Hou MF, Yang FW, **Zhao S**, Lee EY. Arsenic-induced Mre11 phosphorylation is cell cycle-dependent and defective in NBS cells. DNA Repair 2002, 1:137-42.

- ***Shang Li*** ***Mentor -- Dr. Wen-Hwa Lee***

Mutations of the *BRCA1* gene predispose women to the development of breast cancer. The *BRCA1* gene product [BRCA1] is a nuclear phosphoprotein whose cellular function is poorly understood. The C-terminal region of the BRCA1 protein contains an activation domain and two repeats termed BRCT (for BRCA1 C-terminal). In his recent work, Mr. Li identified a BRCT-interacting protein previously identified as CtIP, a protein that interacts with the C-terminal-binding protein (CtBP) of E1A. Together, CtIP and CtBP are postulated to form a transcription corepressor complex. The ability of BRCA1 to transactivate the p21 promoter can be inactivated by mutation of the C-terminal conserved BRCT domains. To explore the mechanisms of this BRCA1 function, the BRCT domains were used as bait in a yeast two-hybrid screen. A known protein, CtIP, a co-repressor with CtBP, was found. CtIP interacts specifically with the BRCT domains of BRCA1, both *in vitro* and *in vivo*, and tumor-derived mutations abolished these interactions. The association of BRCA1 with CtIP was also abrogated in cells treated with DNA-damaging agents including UV, γ-irradiation and adriamycin, a response correlated with BRCA1 phosphorylation. The transactivation of the p21 promoter by BRCA1 was diminished by expression of exogenous CtIP and CtBP. These results suggest that the binding of the BRCT domains of BRCA1 to CtIP/CtBP is critical in mediating transcriptional regulation of p21 in response to DNA damage.

This project was directly relevant to breast cancer since it involves the study of a protein whose function appears to central to the mobilizing the response of cells to DNA damage. Perturbations in the systems that maintain genomic integrity underlie initiation and progression of most cancers, including those of the breast.

Dr. Li defended his dissertation in Fall of 2000. He continues his training as a post doctoral fellow in the laboratory of Dr. Elizabeth Blackburn in the department of biochemistry and biophysics at the UCSF. He is working on a novel cancer therapy involving a mutated telomere RNA template.

- ***Qing Zhong*** ***Mentor -- Dr. Wen-Hwa Lee***

One of Mr. Zhong's projects in Dr. Lee's laboratory is a study of the tumor suppressor protein, TSG101. *tsg101* was identified as a tumor susceptibility gene by homozygous function inactivation of allelic loci in mouse 3T3 fibroblasts. To confirm its relevance to breast cancer that was originally reported, antibodies specific for the putative gene product were prepared and used to identify cellular 46 kDa TSG101 protein. A full size 46 kDa TSG101 protein was detected in a panel of 10 breast cancer cell lines and 2 normal breast epithelial cell lines with the same antibodies. A full-length *TSG101* mRNA was also detected using rtPCR. These results indicate that homozygous intragenic deletion of *TSG101* is rare in breast cancer cells. In more recent work, Mr. Zhong demonstrated that TSG101 is a cytoplasmic protein that translocates to the nucleus during S phase of the cell cycle. Interestingly, TSG101 is distributed mainly around the chromosomes during M phase. Microinjection of antibodies selective for TSG101 during G1 or S results in cell cycle arrest and overexpression leads to cell death. These data indicate that neoplastic transformation due to lack of TSG101 could be due to a bypass of cell cycle checkpoints.

Another more recent interest of Mr. Zhong is the role of the breast tumor suppressor BRCA1 in cancer formation. *BRCA1*, encodes a tumor suppressor that is mutated in familial breast and ovarian cancers. Mr. Zhong's work showed that BRCA1 interacts *in vitro* and *in vivo* with human Rad50, which forms a complex with hMre11 and p95/nibrin. BRCA1 was detected in discrete foci in the nucleus that colocalize with hRad50 after irradiation. Formation of irradiation-induced foci positive for BRCA1, hRad50, hMre11 or p95 were dramatically reduced in HCC1937 breast cancer cells carrying a homozygous mutation in *BRCA1*, but was restored by transfection of wild-type *BRCA1*. Ectopic expression of wild-type, but not mutated *BRCA1* in these cells rendered them less sensitive to the DNA damage agent, methyl methanesulfonate. These data suggest that BRCA1 is important for the cellular responses to DNA damage that are mediated by the hRad50-hMre11-p95 complex.

Dr. Zhong's work on BRCA1 was highly relevant for breast cancer research. By understanding the interaction and functional role of BRCA1 in the DNA repair process could lead to a greater understanding of its role in tumorigenesis and to new forms of cancer therapy aimed at interactions with the repair proteins.

Publications:

Nijhawan D, Fang M, Traer E, **Zhong Q**, Gao W, Du F, Wang X. Elimination of Mcl-1 is required for the initiation of apoptosis following ultraviolet irradiation. Genes Dev. 2003 17(12):1475-86.

Dr. Zhong successfully defended his dissertation in November, 2000, and obtained his Ph.D. He recently published additional work related to his doctoral research as a postdoctoral fellow in Dr. Wen-Hwa Lee's laboratory. Dr. Zhong is currently continuing his training in Xiaodong Wang's laboratory at the University of Texas Southwestern Medical Center at Dallas, where he is working on the biochemistry and cell biology of apoptosis.

As a contributing author on the above paper from Dr. Wang's laboratory, Dr. Zhong continues to add to the knowledge base concerning cellular responses to DNA damage, an important component of tumorigenesis.

- ***Lei Zheng*** ***Mentor -- Dr.Wen-Hwa Lee***

Lei accomplished a significant amount of work during this training period. His main goal was to elucidate the molecular basis of genomic instability that occurs in most of human cancers including breast cancer. He started working on a novel mitotic phase specific protein, Hec1, by demonstrating that Hec1 interacts with retinoblastoma protein for maintaining the genomic stability that was published in Mol. Cell. Biol. (1999). He then developed a method to examine the level of chromosome instability by using retrovirus carrying both positive and negative selectable marker that integrated randomly into individual chromosomes, and the frequency of loss of this selectable chromosomal marker (LOM) was measured. The results showed that normal mouse embryonic stem cells had a very low frequency of LOM, which was less than 10-8/cell/generation. In Rb-/- mouse ES cells, the frequency was increased to approximately 10-5/cell/generation, while in Rb+/- ES cells, the frequency was approximately 10-7/cell/generation. LOM was mainly mediated through chromosomal mechanisms and not due to point mutations.

These results revealed that RB haploinsufficiency plays a critical role in the maintenance of chromosome stability. The mystery of why RB heterozygous carriers have early onset tumor formation with high penetrance can be, at least, partially explained by this novel activity. Dr. Lei Zheng made very significant contributions toward this novel aspect with RB function.

Publications:

Zheng L, Roeder RG, Luo Y. S phase activation of the histone H2B promoter by OCA-S, a coactivator complex that contains GAPDH as a key component. Cell. 2003 114:255-66.

Dr. Zheng successfully defended his Ph.D. dissertation in Novermber, 2000. Lei is currently working on a project involving regulators of gene transcription in Dr. Robert Roeder's at the I Laboratory of Biochemistry and Molecular Biology, The Rockefeller University, New York. After completing his postdoctoral training in Dr. Roeder's laboratory, Dr. Zheng will begin an internal medicine residency program of Albert Einstein Medical College in New York, beginning in July, 2003. After that he is planning to do an Oncology subspecialty fellowship, all the while using his protected research time in Dr. Roeder's laboratory. Dr. Zheng will undoubtedly continue to make major contributions in both basic and clinical science of breast cancer.

The above cited paper is the product of Dr. Zheng's efforts in Dr. Roeder's laboratory. This paper is a very important contribution to our understanding of transcription factor function. The paper's importance is underscored by a perspective paper in the same issue of cell by Dr. Steve McKnight (Gene switching by metabolic enzymes--how did you get on the invitation list? Cell. 2003 114:150-2). Dr. Zheng is clearly going to be a very significant biomedical scientist, a further testament to the value of supporting graduate student-based research programs.

- ***Horng-Ru Lin***

BRCA1 or BRCA2 germline mutations predispose women to early onset, familial breast cancer. Current studies on BRCA1 and BRCA2 suggest their roles in the maintenance of genome integrity. However, in contrast to the clear studies of BRCA1, there has been very little characterization of the BRCA2 protein and evidence that speaks to a dynamic function of BRCA2 in this regard. That is, the intrinsic biological nature of the BRCA2 protein remains enigmatic. Therefore, this project is to try to reveal the physiological function of the BRCA2 protein by characterizing its posttranslational processing, such as phosphorylation.

The novelty of the work lies in the following. First, it demonstrates BRCA2 is a phosphoprotein in vivo. Second, BRCA2 is hyperphosphorylated specifically in mitosis. Third, dephosphorylation of BRCA2 corresponds to the timing of cells' exit from mitosis. These findings imply that BRCA2 may play an important role in mitosis. To further characterize the phosphorylated amino acids of BRCA2 will provide fresh insights into functional study of BRCA2, which has obvious relevance to breast cancer.

Publications:

Lin HR, Ting NS, Qin J, Lee WH. M-phase specific phosphorylation of BRCA2 by Polo-like Kinase 1 correlates with dissociation of p300/CBP-associated factor, P/CAF. J Biol Chem. 2003 Jun 17. [Epub ahead of print].

Mr. Lin's first paper is a very significant contribution to our understanding of BRCA2 functional regulation by an important kinase, which regulates the cell cycle.

Note: Because of personal issues, Mr. Lin did not accompany Dr. Wen-Hwa Lee when he recently moved his laboratory to UC Irvine. Mr. Lin is currently working in Dr. Renee Yew's laboratory on a project to better understand regulation of the cell cycle, a critically

important area in cancer biology. A description of this research will appear in the next progress report.

- ***Stephen Van Komen*** ***Mentor – Dr. Patrick Sung***

In yeast homologous recombination, Rad54, a member of Swi2/Snf2 family of proteins, functionally cooperates with the Rad51 recombinase in making D-loop, the first DNA joint formed between recombining chromosomes. Mr. Van Komen's biochemical studies have indicated that yeast Rad54 modulates DNA topology at the expense of ATP hydrolysis, producing extensive unconstrained supercoils in DNA. This supercoiling ability is likely to be indispensable for D-loop formation. Given the high degree of structural and functional conservation among yeast and human recombination factors, Mr. Van Komen hypothesize that human Rad51 and Rad54 also function together to make D-loop. This hypothesis is being tested with human Rad51 and Rad54 proteins purified from insect cells infected with recombinant baculoviruses. In addition, whether human Rad54 has ATP hydrolysis-driven DNA supercoiling ability is also being examined.

Mr. Van Komen's research is directly relevant to breast cancer since double strand breaks in DNA and their repair is an issue pertinent to breast cancer. Since the tumor suppressor, BRCA2, interacts with Rad51, it is critically important to understand the biochemistry of this important enzyme in DNA repair.

Wolner B, **van Komen S**, Sung P, Peterson CL. Recruitment of the recombinational repair machinery to a DNA double-strand break in yeast. Mol Cell. 2003 Jul;12(1):221-32.

Krejci L, **Van Komen S**, Li Y, Villemain J, Reddy MS, Klein H, Ellenberger T, Sung P. DNA helicase Srs2 disrupts the Rad51 presynaptic filament. Nature. 2003 May 15;423:305-9.

Jaskelioff M, **Van Komen S**, Krebs JE, Sung P, Peterson CL. Rad54p is a chromatin remodeling enzyme required for heteroduplex DNA joint formation with chromatin. J Biol Chem. 2003;278(11):9212-8.

Dr. Van Komen continues as a post doctoral fellow in Dr. Sung's laboratory, which has recently moved to Yale University. The above papers indicate his continued contributions to our understanding of DNA repair in response to damage, which is a vibrant area of cancer biology.

- **Deanna Jansen**

Ms. Jansen's husband was transferred to a new military base and, for family reasons, she decided to withdraw from the program. At some point, she plans to complete her Ph.D. training.

- **Stefan Sigurdsson** **Mentor – Dr. Patrick Sung**

The RAD51 encoded product exhibits structural and functional similarities to the Escherichia coli recombination protein RecA. RecA promotes the pairing and strand exchange between homologous DNA molecules to form heteroduplex DNA. We have shown that hRad51 also makes DNA joints avidly and promotes highly efficient DNA strand exchange. Two Rad51-like proteins, Rad51B and Rad51C, are found associated in a heterodimeric complex. We have co-expressed the Rad51B and Rad51C proteins in insect cells and purified the Rad51B-Rad51C complex to near homogeneity. Biochemical experiments have revealed that Rad51B-Rad51C binds DNA and enhances the recombinase activity of the Rad51 protein. This recombination mediator function of Rad51B-Rad51C is likely indispensable for efficient recombination in vivo.

Recently, hRad51 was shown to interact with the breast tumor suppressor BRCA2. The biochemical studies by Mr. Sigurdsson should be useful for understanding the molecular basis of breast tumor suppression by the recombination machinery.

Genomic caretaking by the recombination systems is vital to the "health" of the information residing in DNA. Corruption of the information by insults arising from internal and external sources is known to be involved in genesis of cancer. Thus, the system elucidated by Mr. Sigurdsson is very important for all cancers including those of the mammary glands.

Publications:

Dr. Sigurdsson recently successfully defended his dissertation. He is continuing to pursue research in DNA repair as a post doctoral fellow in Dr. Sung's laboratory. Upon his wife's graduation from Medical School, he will be pursuing other post doctoral training opportunities in breast cancer research.

Guikai Wu **Mentor – Dr. Phang-Lang Chen**

Immortalized cells maintain telomere length through either a telomerase-dependent process or a telomerase-independent pathway termed alternative lengthening of telomeres (ALT). Homologous recombination is implicated in the ALT pathway in both yeast and human ALT cells. In ALT cells, two types of DNA double-strand break repair and homologous recombination factors, the Rad50/Mre11/NBS1 complex and Rad51/Rad52 along with replication factors (RPA) and telomere binding proteins (TRF1 and TRF2), are associated with the ALT-associated PML body (APB). DNA synthesis in late S-G(2) is associated with APBs, which contain telomeric DNA and, are therefore, potential sites for telomere length maintenance. Mr. Gu showed that the breast cancer susceptibility gene product, breast cancer susceptibility gene 1, and the human homologue of yeast Rap1, hRap1, are also associated with APBs specifically during late S-G(2) phase of the cell cycle. He additionally show that the localization of the double-strand break repair factors with APBs is distinct from their association with ionizing radiation-induced nuclear foci. To systematically explore the mechanism involved in the assembly of APBs, we examine the role of Nijmegen breakage syndrome 1 (NBS1) and TRF1 in this process, respectively. He demonstrated that NBS1 plays a key role in the assembly and/or recruitment of Rad50, Mre11, and breast cancer susceptibility gene 1, but not Rad51 or TRF1, to APBs. The NH(2) terminus of NBS1, specifically the BRCA1 COOH-terminal domain, is required for this activity. Although TRF1 interacts with NBS1 directly, it is dispensable for the association of either Rad50/Mre11/NBS1 or Rad51 with APBs. Perturbation of the interactions between NBS1/Mre11 and APBs correlates with reduced BrdUrd incorporation associated with APBs, consistent with decreased DNA synthesis at these sites. Taken together, these results support a model in which NBS1 has a vital role in the assembly of APBs, which function to maintain telomeres in human ALT cells.

All of the proteins in Mr. Wu's project are vital to the DNA repair and response systems of normal and cancer cells. Telomeres are essential for the maintenance of chromosome length and are a target of both cancer and aging research. Accordingly, Mr. Wu's project could have important relevance to the age-related onset of cancer including those of the mammary gland.

Wu G, Jiang X, Lee WH, Chen PL. Assembly of functional ALT-associated promyelocytic leukemia bodies requires Nijmegen Breakage Syndrome 1. Cancer Res. 2003 63:2589-95.

Xianzhi Jiang **Mentor – Dr. Phang-Lang Chen**

Since joining Dr. Chen's lab, Mr. Jiang has been participating in the following two research projects: (I) A systematic study of the mechanism involved in the assembly of the ALT-associated promyelocytic leukemia body (APB), and (II) the characterization of a novel non-selenocysteine containing phospholipid hydroperoxide glutathione peroxidase (NPGPx). Regarding the first project, it has been known that NBS1 and TRF1 are associated with ALT-associated PML body (APB). NBS1 physically interacts with TRF1, a telomere-specific binding protein. In order to understand the potential roles of NBS1 and TRF1 in the assembly of APBs, Mr. Jiang made adenovirus constructs that expressed GFP-TRF1Dmyb fusion protein, which lacks the NBS1 interaction region. Overexpressed TRF1Dmyb protein can form a TRF1Dmyb/TRF1 dimer and thus acts as a dominant negative by depleting endogenous TRF1 from telomere DNA. In collaboration with Guikai Wu, Mr. Jiang demonstrated that NBS1 plays a key role in the assembly and/or recruitment of RAD50, MRE11, and BRCA1, but not RAD51 or TRF1, to APBs. Although TRF1 interacts with NBS1 directly, it is dispensable for the association of either RAD50/MRE11/NBS1 or RAD51 with APBs.

In the second project, Mr. Jiang identified a novel non-selenocysteine containing phospholipid hydroperoxide glutathione peroxidase named as NPGPx. In collaboration with Ahmad Utomo, Mr. Jiang demonstrated that ectopic expression of NPGPx in Brca1-null cells that were sensitive to oxidative stress induce by hydrogen peroxide conferred a similar resistance level to that of the wild-type cells, suggesting the importance of this enzyme in reducing oxidative stress. Unlike mammary gland and other normal tissues, the majority of breast cancer cell lines studied (11 out of 12) expressed very low or undetectable levels of NPGPx irrespective of BRCA1 status. Re-expression of NPGPx in breast cancer lines, MCF-7 and HCC1937, induced resistance to eicosapentaenoic acid (an omega-3 type of polyunsaturated fatty acid) mediated cell death and abrogated proliferative stimulation by linoleic acid (an omega-6 type). Thus NPGPx plays an essential role in breast cancer cells in alleviating oxidative stress generated from polyunsaturated fatty acid metabolism.

Mr. Jiang's projects are clearly important to breast cancer research. The proteins in project one are of obvious importance to DNA repair and genomic stability. Project two is novel and offers fresh insights into the role of oxidative damage and the proteins that participate in assuaging it. Thus the research plan of Mr. Jiang will be important in combating breast cancer on two critically important fronts.

Wu G, **Jiang X**, Lee WH, Chen PL. Assembly of functional ALT-associated promyelocytic leukemia bodies requires Nijmegen Breakage Syndrome 1. Cancer Res. 2003 63:2589-95.

Yi-Tzu Lin **Mentor – Dr. Wen-Hwa Lee**

Accurate chromosome segregation, a process essential for maintenance of genomic integrity, requires coordination between centrosomes, kinetochores, and chromosomes during M phase progression. Previously, we discovered a novel coil-coiled kinetochore protein, Hec1, which is essential for faithful chromosome segregation. Hec1 interacts directly with Hint1/HZWint1, which in turn binds to Zw10 at the kinetochore to facilitate spindle attachment. Ms. Lin showed that when Hec1 expression is down regulated by a small inhibitory RNA, localization of both Hec1 and Hint1 at kinetochores is abolished. When Hint1 expression is similarly down regulated by siRNA, Hec1 remains at kinetochores. Thus Hec1 is required for the recruitment of Hint1 to kinetochores. Down regulation of Hec1 expression resulted in chromosome missegregation characterized by lagging chromosomes during metaphase, and incomplete segregation during anaphase. These aberrations in turn lead to formation of micronuclei and multiple nuclei. Similar albeit less severe phenotypes were observed in cells treated with Hint1 siRNA. M phase is

prolonged in cells treated with Hec1 siRNA, but not completely arrested since cytokinesis occurs. The cells in which Hec1 expression is down regulated fail to activate the spindle checkpoint: they do not accumulate in metaphase after treatment with nocodazole, nor is BubR1 phosphorylated. Taken together, Ms. Lin's results suggest that Hec1 recruits Hint1/Zw10 to the kinetochore for spindle attachment and may serve as a platform for control of the spindle checkpoint. The findings thus provide a molecular mechanism by which Hec1 plays a crucial role in chromosome segregation.

Cells from solid tumors typically display chromosomal aberrations attributed to problems with their segregation during cell division. Ms. Lin's research is especially relevant to breast cancer since these tumors often demonstrate these types of chromosomal defects, which may contributed to their progression.

Ahmad Utomo **Mentor – Dr. Wen-Hwa Lee**

A drastic reduction in the expression of a novel phospholipid hydroperoxide glutathione peroxidase (PHGPx), which incorporates cysteine instead of selenocysteine in the conserved catalytic motif was observed in a microarray analysis using cDNAs amplified from mRNA of Brca1-null mouse embryonic fibroblasts (MEFs). This non-selenocysteine PHGPx named as NPGPx is a cytoplasmic protein with a molecular weight of approximately 22 kDa. Ectopic expression of NPGPx in Brca1-null cells, which are sensitive to oxidative stress induced by hydrogen peroxide, conferred a similar resistance level equal to that of the wild-type cells, suggesting the importance of this enzyme in reducing oxidative stress. Expression of NPGPx was found in many tissues, including developing mammary gland. However, the majority of breast cancer cell lines studied (11 out of 12) expressed very low or undetectable levels of NPGPx irrespective of BRCA1 status. Re-expression of NPGPx in breast cancer lines, MCF-7 and HCC1937, induced resistance to eicosapentaenoic acid (an omega-3 type of polyunsaturated fatty acid) mediated cell death, and abrogated proliferative stimulation by linoleic acid (an omega-6 type). Thus, NPGPx plays an essential role in breast cancer cells in alleviating oxidative stress generated from polyunsaturated fatty acid metabolism.

The data and novel insights derived from Mr. Utomo's research might help explain breast cancer development due to defects in responding to oxidative damage. If true, affected family members of families carrying alterations in BRCA1 might benefit from avoidance of situations where oxidative damage is increased.

Dr. Utomo successfully defended his dissertation and was recently awarded his Ph.D. He is continuing his training as a postdoctoral fellow at the Harvard Medical School in the laboratory of Dr. Tanya Mayadas.

Chang-Ching Liu **Mentor – Dr. Wen-Hwa Lee**

The Rad50/MRE11/NBS 1 complex is involved in a variety of cellular processes, including both non-homologous end-joining and homologous recombination pathways involved in DNA double-strand breaks repair, cell cycle checkpoint activation, telomere maintenance, and meiosis. In order to understand the mechanism underlying the function of this repair complex, a novel Rad50-interacting protein (RINT-1) was identified by a yeast two-hybrid screen in our laboratory. RINT-1, an evolutionarily conserved protein from Drosophila to human beings, has been shown to interact with Rad50 preferentially at late S and G2/M phases through its central and c-terminal conserved region. To further explore the function of interaction between RINT-1 and Rad50, several stable MCF7 clonal cell lines that express GFP fusions containing only the Rad50 binding region of RINT-1 were established. Overexpression of the fusion protein leads to

a defective radiation-induced G2/M checkpoint. This observation is related to the repair function of Rad50 and another Rad50-interacting protein, BRCA1, which is also thought to play a role in radiation-induced G2/M checkpoint control. Like Rad50 and BRCA1, inactivation of RINT-1 causes early embryonic lethality. Blastocysts were isolated at day 3.5 of pregnancy from Rint-1+/- intercross and were cultured in vitro for 7 days. Unlike wild type and Rint-1+/- embryos, whose inner cell mass continued to expand and differentiate, Rint-1-/- cells stop their expansion subsequent to day 4 and died.

To study the cellular function of RINT-1 besides its roles in response to DNA damage, Ms. Liu established an U2OS cell line expressing full-length RINT-1 protein coupled with GFP and discovered that RINT-1 localizes to the centrosome in a microtubule-independent manner. GFP-RINT-1 proteins localize at the centrosomes throughout the cell cycle and move to the midbody along with the mother centrosome before cytokinesis. Endogenous RINT-1 proteins reside in the centrosomal fractions isolated from LEM cells, and are found in purified centrosomes. Interestingly, GFP fusions with either the N-terminal coiled-coil domain or the conserved Rad50 binding region of RINT-1 are recruited to the centrosome. Using the N-terminal coiled-coil domain of RINT-1 as bait in a yeast two-hybrid screen, Ms. Liu found two centrosomal proteins potentially interacting with RINT-1; PA28b and p150glued. Similar to the p150glued component of the dynactin complex, adenovirally overexpressed N-terminal RINT-1 polypeptides decorated the entire length of interphase microtubules. Overexpressed N-terminal RINT-1 polypeptides also resulted in the formation of cytoplasmic dots outside the centrosome, a phenomenon also observed when peptides of a coiled-coil centrosomal protein, Cep135, were overexpressed. The centrosome is a major microtubule-organizing center in animal cells. It duplicates only once during the cell cycle and ensures the formation of bipolar spindles, which distribute replicated chromosomes equally to daughter cells. Defective centrosomes, exemplified by an excess number of centrioles and pericentriolar material, are characteristic of solid tumors in general and breast tumors in particular, and may contribute to their genomic instability by the formation of multipolar mitotic spindles. Recent molecular evidence suggests that centrosomes are also involve in stress response mechanisms, cell cycle checkpoint control, and cell cycle progression. It has been shown that inactivation of the other Rad50-interacting proteins, MRE11 and Brca1, lead to centrosome amplification and embryonic lethality. Future studies of the roles played by RINT-1 in regulation of centrosomal activities may provide insight about how DNA repair pathways coordinate with the cell cycle progression and the regulation of centrosome function.

This on the basic biology of centrosomes and their roles in cells division is applicable to all cells including those that form tumors. It is especially relevant to breast tumors since they often display chromosomal aberrations attributed to defects involving centrosomal proteins.

Note: Miss. Liu withdrew from the graduate program to return to home to assist with a critically ill member of her immediate family.

Wei Tan **Mentor – Dr. Thomas Boyer**

The breast and ovarian-specific tumor suppressor BRCA1 has been implicated in both activation and repression of gene transcription by virtue of its direct interaction with sequence-specific DNA-binding transcription factors. However, the mechanistic basis by which BRCA1 mediates the transcriptional activity of these regulatory proteins remains largely unknown. Mr. Tan has been studying the functional interaction between BRCA1 and ZBRK1, a BRCA1-dependent KRAB-zinc finger transcriptional repressor as a model system to understand the mechanistic basis by which BRCA1 mediates sequence-specific transcription control. During the reporting period, Mr. Tan succeeded in identifying and initiating the molecular characterization of a portable BRCA1-dependent transcriptional repression domain within the ZBRK1 C-terminus. Mr. Tan found that this C-terminal repression domain functions in a BRCA1-, HDAC-,

and promoter-specific manner, and is thus functionally distinguishable from the N-terminal KRAB repression domain in ZBRK1, which exhibits no BRCA1 dependency and broad promoter specificity. Significantly, Mr. Tan also found that the BRCA1-dependent transcriptional repression domain modulates sequence-specific DNA-binding by the minimal ZBRK1 DNA-binding domain. These findings thus reveal a dual function for the BRCA1-binding domain on ZBRK1 in sequence-specific DNA-binding and transcriptional repression by DNA-bound ZBRK1. Mr. Tan is currently engaged in experiments to complete the functional characterization of this BRCA1-dependent repression domain, and he is in the process of writing up his results in manuscript form.

This project is applicable to breast cancer since all of these proteins are involved in the transcriptional response to DNA damage medicated by BRCA1. Understanding this response system, which includes the ZBRK1 protein, is critical to preventing and treating breast cancer.

Sangeetha Vijayakumar **Mentor – Dr. Wen-Hwa Lee**

The Suv3 helicase of yeast *Saccharomyces cerevisiae* has been classified as a mitochondrial RNA helicase. Yeast genetic studies revealed that suv3-null yeast fails to grow in glycerol media and forms petite colonies, implicating a role in energy metabolism. Because the helicase domains in both yeast and human Suv3 vary considerably from typical RNA helicase motifs, homogenously purified Suv3 was required by Ms. Vijayakumar in order to verify its putative enzymatic activities. Ms. Vijayakumar expressed a form of human Suv3 carrying an N-terminal deletion of 46 amino acids (ΔNhSuv3) in yeast suv3 null mutants and demonstrated that ΔNhSuv3 fully complements the null phenotype. Through a five-step chromatographic procedure, ΔNhSuv3 (83 kDa) and its partially degraded 70 kDa protein (hSuv3-70), which constitutes amino acids 68 to 685, were purified to homogeneity. Both proteins have ATPase activities, but mutants with an invariant lysine in the ATP binding site, K213, changed to alanine (A) or arginine (R) lose activity. At pH 7.5, ΔNhSuv3 unwinds only RNA/DNA hetero duplex, while hSuv3-70, which retains all the core catalytic domains, can unwind multiple substrates including homoduplexes of RNA and DNA and heteroduplexes of RNA-DNA. However, under low pH (≤ 5.0) reaction conditions, ΔNhSuv3 also exhibits ATP-dependent multi-substrate specificity similar to that of hSuv3-70. Consistently, ΔNhSuv3 binds to homo duplexes of both RNA and DNA at pH 5.0, but not at pH 7.5, Moreover, data from circular dichroism analysis suggests that at pH 5.0, ΔNhSuv3 adopts a similar conformation to that of hSuv3-70, which in turn may govern its differential substrate specificity.

Human Suv3 is likely to be involved in critical functions in both normal and breast cancer cells. Knowledge regarding its function will, therefore, be a significant contribution toward understanding the development and/or maintenance of the tumorigenic state.

Bingnan Gu **Mentor – Dr. Phang-Lang Chen**

CtIP (CtBP-interacting protein) is a co-repressor of transcription that works with CtBP, which was originally identified as a transcriptional repressor that binds to the C-terminal region of oncoprotein E1A1. Published studies suggest a role for CtIP in transcription regulation through interactions with tumor suppressors Rb2, and BRCA1 and/or through interactions with transcription repressors CtBP, LMO4 and Ikaros. To systematically study the function of CtIP, Mr. Gu showed that CtIP protein localizes immunocytochemically to sites of BrdU-Incorporation representing replication foci (RF) in S-phase of the cell cycle. Deletion mutagenesis indicates that 84 amino acids in the middle of region 463-546 are sufficient to target CtIP to RF. Moreover, neither DNA damage by IR irradiation nor replication stress induced by hydroxy urea

impair the association of GFP-tagged wide type CtIP with foci, nor does mutations in CtIP (S664/745A) that prevents phosphorylation by the ATM kinase. Finally, small interference RNA-mediated CtIP protein level reductions are correlated with defects in cellular proliferation. These studies have revealed a pivotal role of CtIP in mammalian DNA replication, which is consistent with animal studies showing that homozygous knockout of mouse the CtIP gene is associated with early embryonic lethality.

This study is highly relevant to breast cancer research since CtIP is a BRCA1-associated protein. This association is DNA-damage dependent, and thus potentially links BRCA1 to S phase DNA replication, through its association with CtIP. Mr. Gu's research is in the very early stages, but is clearly on the way to a very significant contribution to breast cancer research.

Aimin Peng **Mentor – Dr. Phang-Lang Chen**

Cellular response to DNA double strand breaks (DSBs) comprises a cascade of molecules to transmit the DNA damage signals through sensor, and a transducer to effector proteins that activate DNA repair, cell cycle checkpoint and programmed cell death (apoptosis). Previously, Dr. Chen's laboratory showed that NFBD1 (aka, KIAA0170), which contains an N-terminal FHA, C-terminal tandem BRCT domains and internal Repeats, is an early participant in nuclear foci upon IR treatment. To systemically explore the role of NFBD1 in the DNA damage signaling pathway, Mr. Peng used the RNAi-mediated gene silencing technique to eliminate the expression of NFBD1, and showed that its elimination leads to IR sensitivity and G2/M checkpoint defects. NFBD1 was placed downstream of λ-H2AX in the DNA damage response pathway. Furthermore, Mr. Peng showed that the association of NFBD1 and 53BP1 with DSBs both rely on λ-H2AX.

Both NFBD1 and 53BP1 share a structural mtoif, C-terminal tandem BRCT domains, with Rad9 in budding yeast. Rad9 is an adaptor protein that mediates the phosphorylation and activation of transducer kinase Rad53. Using an ATM/ATR substrate specific antibody, Mr. Peng found that both NFBD1 and 53BP1 RNAi treated cells exhibited reduced IR-induced, ATM/ATR-dependent phosphorylation at DSB sites. Specifically, either NFBD1 or 53BP1 binds to CHK2, and RNAi treatment partially affected CHK2 phosphorylation at DSB sites, while silencing both NFBD1 and 53BP1 reduced phosphorylated CHK2 foci to a very low level, which is comparable to the H2AX RNAi-treated cells. In addition, both NFBD1 and 53BP1 are required for ATR-dependent RAD17 phosphorylation at Ser 645. These studies suggested that NFBD1 and 53BP1 play redundant role in mediating activation of CHK2 in response to DNA damage. NFBD1 and 53BP1 also have distinct roles in the DNA damage signaling pathway. For example, Mr. Peng showed that NFBD1 is not required for BRCA1 IRIF formation, but is responsible for the recruitment of the NBS1/MRE11/RAD50 complex and TopBP1 into IRIF. This activity is not shared by 53BP1.

To further understand the structural and functional relationship of NFBD1 with NBS1 and TopBP1, RNAi-resistant NFBD1 and deletion mutants were introduced into RNAi targeted cells. N-terminal FHA domain and internal repeats of NFBD1 were required for NBS1 and TopBP1 IRIF respectively. Unlike wild-type NFBD1, internal repeats deleted NFBD1 could not rescue G2/M checkpoint defect derived from NFBD1 RNAi treatment. Together with his previous functional studies of NBS1 and TopBP1, these observations support a model in which NFBD1 mediates the intra-S checkpoint through its N-terminal FHA domain and NBS1, while its internal repeats mediate G2/M checkpoint with TopBP1. This work was recently reported in the Journal of Biological Chemistry.

This work by Mr. Peng is clearly and compelling important in the breast cancer research field. The signaling control pathways operative in response to DNA-damage are a crucial aspect of

the overall cellular response to exogenous stress. This newly identified player, NFBD1, is an important addition to the knowledge base concerning the function of this important stress response pathway. It is clear that Mr. Peng will continue to make significant contributions to breast cancer research as student in Dr. Chen's laboratory.

Publications:

Peng A, Chen PL. NFBD1, like 53BP1, is an early and redundant transducer mediating Chk2 phosphorylation in response to DNA damage. J Biol Chem. 2003 278(11):8873-76.

Changes to the Program Faculty:

As noted above, Dr. Patrick Sung moved his laboratory to Yale University during the reporting period. However, he remains as a member of the training faculty in the Graduate Program and this training grant since one of his students, Wendy Bussen, who is an applicant for a DOD award, is a student is good standing within the program. Also, as noted above, the same status applies to Dr. Wen-Hwa Lee, and also to Dr. Eva Lee, who both have students in good standing within the Graduate Program in Molecular Medicine.

Additions: None during the reporting period.

Changes in the Program Courses: None during the reporting period.

SUMMARY: The Breast Cancer Training Program made excellent progress toward attracting and retaining excellently qualified students in breast cancer research. The students received a high level of training in the modern research methods and theory. A total of 10 publications on breast cancer were achieved by students supported by the program. Seven of the faculty had eleven grants totaling $3,600,063 in the reporting period. Three students in the program were funded by Defense Department's Breast Cancer Research Program in the period covered by this report. One key investigator relocated his laboratory, but remains on the training faculty. In summary, the overall progress of the students was excellent. Combined with the basic instruction they receive in the Molecular Medicine Ph.D. Program, students will graduate as highly skilled researchers who will be competitive for post doctoral positions in the premiere breast cancer laboratories in the world.

Appendix: NIH Biosketches and Reprints of Trainee Publications.

1) Tomkinson, A., and **Leppard, JB**., DNA ligases: Mechanism and function. Encyclopedia of Biological Chemistry.

2) Yuan SS, Su JH, Hou MF, Yang FW, **Zhao S**, Lee EY. Arsenic-induced Mre11 phosphorylation is cell cycle-dependent and defective in NBS cells. DNA Repair 2002;1:137-42.

3) Nijhawan D, Fang M, Traer E, **Zhong Q**, Gao W, Du F, Wang X. Elimination of Mcl-1 is required for the initiation of apoptosis following ultraviolet irradiation. Genes Dev. 2003 17(12):1475-86.

4) **Zheng L**, Roeder RG, Luo Y. S phase activation of the histone H2B promoter by OCA-S, a coactivator complex that contains GAPDH as a key component. Cell. 2003 114:255-66.

5) **Lin HR**, Ting NS, Qin J, Lee WH. M-phase specific phosphorylation of BRCA2 by Polo-like Kinase 1 correlates with dissociation of p300/CBP-associated factor, P/CAF. J Biol Chem. 2003 Jun 17. [Epub ahead of print].

6) Wolner B, **van Komen S**, Sung P, Peterson CL. Recruitment of the recombinational repair machinery to a DNA double-strand break in yeast. Mol Cell. 2003 July;Vol.12:221-32.

7) Krejci L, **Van Komen S**, Li Y, Villemain J, Reddy MS, Klein H, Ellenberger T, Sung P. DNA helicase Srs2 disrupts the Rad51 presynaptic filament. Nature. 2003 May 15;423:305-9.

8) Jaskelioff M, **Van Komen S**, Krebs JE, Sung P, Peterson CL. Rad54p is a chromatin remodeling enzyme required for heteroduplex DNA joint formation with chromatin. J Biol Chem. 2003;278(11):9212-8.

9) **Wu G, Jiang X,** Lee WH, Chen PL. Assembly of functional ALT-associated promyelocytic leukemia bodies requires Nijmegen Breakage Syndrome 1. Cancer Res. 2003 63:2589-95.

10) **Peng A,** Chen PL. NFBD1, like 53BP1, is an early and redundant transducer mediating Chk2 phosphorylation in response to DNA damage. J Biol Chem. 2003 278(11):8873-6.

DNA LIGASES: MECHANISM AND FUNCTIONS

ALAN E. TOMKINSON
JOHN B. LEPPARD
THE UNIVERSITY OF TEXAS HEALTH SCIENCE CENTER
AT SAN ANTONIO, INSTITUTE OF BIOTECHNOLOGY

DNA ligases are involved in DNA replication, genetic recombination, and DNA repair. These enzymes belong to a larger superfamily of nucleotidyl transferases that also includes RNA ligases and mRNA capping enzymes. Specifically, DNA ligases catalyze phosphodiester bond formation at breaks in the phosphate backbone of duplex DNA. The DNA ligase family can be subdivided into two groups based on cofactor specificity. Prokaryotic enzymes utilize either nicotinamide adenine dinucleotide (NAD) or adenosine triphosphate (ATP) as a cofactor, whereas viral, archael, and eukaryotic DNA ligases use ATP almost exclusively. DNA ligases share a common core catalytic domain but the regions flanking the core domain are widely divergent. These unique regions mediate the specific participation of DNA ligases in different DNA transactions.

I. Reaction Mechanism

DNA ligase activity was first identified in 1967 in five different laboratories. In the years that followed, the Lehman laboratory was primarily responsible for elucidating the three step reaction catalyzed by the NAD-dependent *E. coli* DNA ligase and the ATP-dependent DNA ligase encoded by bacteriophage T4 that is described below.

A. Adenylation

In the first step, DNA ligase reacts with either NAD or ATP to form a covalent enzyme-adenosine monophosphate (AMP) intermediate (Fig. 1). The AMP group is linked via a phosphoramidate bond to a conserved lysine residue that defines the active site of the core catalytic domain (Fig. 2). Formation of the enzyme-AMP intermediate

induces a conformational change that is required for recognition of a nicked DNA substrate in the next step.

B. AMP-DNA intermediate

The second step in the reaction involves the transfer of the AMP group to the 5' phosphate terminus at the nick in duplex DNA (Fig. 1). The previous step leaves the enzyme in an open conformation that exposes the DNA binding site. Specific amino acid residues in the enzyme coordinate the AMP group such that an oxygen atom of the 5' phosphate in the DNA substrate can attack the phosphoryl group of AMP generating a DNA-AMP intermediate.

C. Phosphodiester bond formation

The third and final step of ligation is catalyzed by the non-adenylated form of DNA ligase. In this reaction, esterification of the 5' phosphoryl group to the 3' hydroxyl group completes phosphodiester bond formation with the concomitant release of AMP (Fig. 1).

II. Structure

Gene cloning and, more recently, genome sequencing has led to a rapid growth in the number of DNA ligase genes identified. Alignment of DNA ligase amino acid sequences indicates that these enzymes share a conserved catalytic domain (Fig. 2). Furthermore, a comparison with the catalytic domains of mRNA capping enzymes revealed the presence of 6 conserved motifs (I, III, IIIa, IV, V, VI) that are characteristic of nucleotidyl transferases. In recent years, our understanding of how the DNA ligase catalytic domain catalyzes DNA joining has been advanced by a combination of

approaches that include the use of site-directed mutagenesis to elucidate the role of individual amino acids within the catalytic domain and the determination of the three-dimensional structure of several DNA ligases by X-ray crystallography.

A. Crystal structures

X-ray crystallographic studies of both NAD- and ATP-dependent DNA ligases have provided important insights into the three-dimensional structure of theses enzymes. In 1996, the Wigley laboratory solved the first crystal structure of an ATP-dependent DNA ligase, the bacteriophage T7 DNA ligase, in a complex with ATP. More recently, the structure of the enzyme-AMP intermediate formed by the *Chlorella* virus DNA ligase was determined by the Shuman laboratory. A comparison of these structures revealed a conformational change in the DNA ligase catalytic domain that allows binding to nicked DNA. The structures of the ATP-dependent DNA ligases together with those of NAD-dependent enzymes such as *Thermus filiformis* DNA ligase (Fig. 2) and other members of the nucleotidyl transferase superfamily represent snapshots of this family of enzymes at different stages of the catalytic cycle. Thus, they provide a framework for understanding the dynamic conformational changes that occur when nucleotidyl transferases interact with their nucleotide co-factor and polynucleotide substrate.

B. Domains constituting the core catalytic domain

There are two sub-domains known as the adenylation domain and the oligomer-binding (OB) fold (Fig. 2) within the DNA ligase catalytic domain. The larger adenylation domain is the minimum region required for formation of an enzyme-AMP intermediate whereas the OB fold allows the enzyme to bind to DNA and coordinates the ligation event. Residues from motifs I through V line a cleft formed between the two

subdomains to generate a positively charged nucleotide-binding pocket. The active-site lysine residue, which is contained within motif I, sits at the bottom of the cleft close to where the adenylation domain and the OB fold are linked. In the non-adenylated form, the enzyme is in an open conformation with the DNA-binding surface of the OB fold rotated away from the active site thus preventing non-productive DNA binding. Upon adenylation, the enzyme undergoes a conformational change such that the DNA binding surface of the OB fold faces in toward the cleft, making the active site accessible.

C. Other common domains of NAD-dependent DNA ligases

NAD-dependent DNA ligases are relatively uniform in size (~70 kDa). In addition to the adenylation domain and OB fold, they contain several other common motifs (Fig. 2) that are thought to mediate protein-DNA and protein-protein interactions. The zinc finger and helix-hairpin-helix (HhH) motifs confer DNA binding activity. The BRCT domain, which was first identified in the breast cancer susceptibility gene 1, is probably involved in protein-protein interactions that recruit the enzyme to its site of action.

D. Sequences flanking the core catalytic domain of ATP-dependent DNA ligases

Unlike NAD-dependent ligases, ATP-dependent DNA ligases are heterogeneous in size (40 kDa – 125 kDa) (Fig. 2). The amino acid residues that flank the catalytic domain of ATP-dependent DNA ligases contain a wide variety of sequences that mediate specific protein-protein interactions and protein-DNA interactions (Fig. 2). Intriguingly, recent sequencing studies have identified open reading frames in bacterial genomes whose sequences suggest that ATP-dependent DNA ligase activity may reside in the same polypeptide as nuclease and primase activities.

III. Biological functions

The notion that cells may contain more than one species of DNA ligase was based upon initial studies in the Lindahl laboratory describing the properties of different species of DNA ligase in mammalian cell extracts. These biochemical studies led to the cloning of three mammalian genes, *LIG1*, *LIG3* and *LIG4* that encode DNA ligases (Table I). More recent genome sequencing has led to the identification of additional DNA ligase genes in organisms such as *S. cerevisiae* and *E. coli* that were thought to have only a single DNA ligase gene. Since DNA joining is required to complete DNA replication, DNA repair, and genetic recombination, it appears likely that the multiple species of DNA ligase have evolved to participate in specific DNA transactions. Insights into the biological functions of the different DNA ligases has been obtained by examining the phenotype of DNA ligase-deficient cells and by identifying protein partners of the DNA ligases (Table I).

A. DNA replication

The ability to make a copy of their genetic information is essential for all organisms. During DNA replication, DNA joining events are required to link together DNA intermediates known as Okazaki fragments that are generated by discontinuous DNA synthesis on the lagging strand at the replication fork. As expected, inactivation of genes encoding replication proteins, including the replicative DNA ligase, results in cell lethality. Since DNA replication involves the co-ordinated actions of many different proteins, it seems reasonable to assume that the DNA ligase involved in DNA replication would interact with one or more of the other replication proteins. In mammalian cells,

proliferating cell nuclear antigen (PCNA), a homotrimeric ring-shaped clamp protein that was identified as an accessory factor of the replicative DNA polymerase, specifically interacts with the N-terminal region of DNA ligase I. This interaction is critical for the recruitment of DNA ligase I to the sites of DNA replication and for the efficient joining of Okazaki fragments. A similar protein-protein interaction occurs in *E. coli* between the NAD-dependent DNA ligase and β clamp, the functional homolog of PCNA, indicating that the interaction between the replicative DNA ligase and the clamp protein is conserved in prokaryotic and eukaryotic DNA replication.

B. DNA excision repair

Exposure to endogenous DNA damaging agents such as reactive oxygen species, and exogenous DNA damaging agents such as ultra-violet light results in damage to the nitrogenous bases of DNA. In addition, the DNA replication machinery makes errors that result in mispaired or unpaired nucleotides. Damaged and mispaired nucleotides are removed from the genome by excision repair pathways that share three common steps; (i) excision of the damaged or mispaired DNA; (ii) gap-filling DNA synthesis using the undamaged strand as template; (iii) DNA ligation to complete the repair.

The pathways for the repair of damaged bases can be divided into two types based on whether the damage is removed as a nitrogenous base, base excision repair (BER), or as a nucleotide, nucleotide excision repair (NER). In mammalian cells, there are two subpathways of BER, long patch and short patch, that appear to involve two different DNA ligases. Short-patch BER events are mostly completed by DNA ligase IIIα in a complex with its partner protein XRCC1, whereas long-patch BER is completed by DNA ligase I. Nucleotide excision repair events are probably completed by DNA ligase I.

In DNA mismatch repair, specific protein factors recognize the mispaired or unpaired nucleotides and direct the excision proteins to the newly synthesized strand. After removal of a section of newly synthesized DNA containing the mispaired or unpaired nucleotides, the resultant single-strand gap is filled-in by a DNA polymerase and repair completed by a DNA ligase, presumably DNA ligase I.

C. Genetic recombination and recombinational repair.

Genetic recombination is the major process by which diversity is generated in living organisms. In mammals, exchanges between homologous chromosomes that occur during meiosis contribute to the generation of genetically diverse gametes. It is assumed that DNA ligase I, the replicative DNA ligase, also completes the meiotic recombination events. However, in vertebrates, there is a germ-cell specific isoform of DNA ligase III, DNA ligase IIIβ, that may also participate in the completion of meiotic recombination. Alternatively, DNA ligase IIIβ may function in DNA transactions in haploid gametes.

Recombination pathways are also critical for the maintenance of genome stability in somatic cells, in particular for the repair of DNA double-strand breaks. This lesion presents a difficult challenge because both strands of the DNA duplex are broken. Recombinational repair pathways can be divided into two types based on whether they are dependent upon DNA sequence homology or not. It is generally assumed that homology-dependent recombinational repair pathways, in particular those involving sister chromatids, are completed by DNA ligase I. In the non-homology directed repair pathways, the ends of broken DNA molecules are simply brought together by DNA end-bridging factors, processed and then ligated. Surprisingly, this inaccurate repair pathway, which can result in a wide spectrum of genetic alterations ranging from small deletions to

chromosomal translocations, makes a major contribution to the repair of DNA double-strand breaks in mammalian cells. Genetic and biochemical studies have shown that this so-called non-homologous end-joining (NHEJ) is dependent upon DNA ligase IV and its partner protein XRCC4. The same DNA ligase IV/XRCC4 complex is also required for the completion of V(D)J recombination, a site-specific recombination mechanism that is required for the rearrangement of immunoglobulin genes to develop a diverse repertoire of antibodies and T-cell receptors.

D. Mitochondrial DNA metabolism.

The DNA transactions described above occur in the nucleus. However, the eukaryotic organelles, mitochondria and chloroplasts, contain their own genetic information which must be replicated and repaired. Studies in the Campbell laboratory have shown that nuclear and mitochondrial forms of DNA ligase III are generated by translation initiation at different sites within the same open reading frame encoded by DNA ligase IIIα mRNA. Although the yeast *S. cerevisiae* lacks a homolog of the *LIG3* gene, it uses the same mechanism to generate mitochondrial and nuclear forms of Cdc9 DNA ligase.

IV. Concluding Remarks

Although the basic reaction mechanism catalyzed by DNA ligases was elucidated over thirty years ago, the recent determination of the three dimensional structure of both NAD- and ATP-dependent DNA ligases has provided exciting new molecular insights into this reaction mechanism. However, structures of DNA ligases interacting with their DNA

substrate are needed for a better understanding of the final two steps of the ligation reaction. Because DNA strand breaks are a common intermediate in many different DNA transactions, the study of DNA ligases by genetic and biochemical approaches has provided and will continue to provide information about the molecular mechanisms of DNA replication, DNA repair and genetic recombination. Finally, mutations in DNA ligase genes have been associated with human diseases, highlighting the importance of these enzymes.

Glossary

Adenylation- the reaction in which DNA ligase interacts with ATP or NAD to form a covalent enzyme-adenylate complex.

Motif- amino acid sequence found to be conserved in different proteins.

Phosphoramidate bond- covalent bond formed between a phosphoryl group and an amino group. For DNA ligases, the phosphoryl group of AMP is linked to the amino group of the active site lysine.

Phosphodiester bond- these bonds link together deoxynucleotides in DNA, forming the sugar phosphate backbone of the DNA polymer.

Further Reading

Doherty, A.J. and Suh, S.W. (2000) Structural and mechanistic conservation in DNA ligase. *Mutation Res.* **28,** 4051-4058.

Lehman, I.R. (1974) DNA ligase: structure, mechanism and function. *Science* **186,** 790-797.

Lindahl, T. and Barnes, D.E. (1992) Mammalian DNA ligases. *Annu. Rev. Biochem.* **61,** 251-281.

Shuman, S. (1996) Closing the gap on DNA ligase. *Structure* **4,** 653-658.

Timmons, D.J., Singleton, M.R. and Wigley, D.B. *Mutat. Res.* **460,** 301-318.

Tomkinson, A.E. and Mackey, Z.B. (1998) Structure and function of mammalian DNA ligases. *Mutat. Res.* **407,** 1-9.

Biographical Statement

Dr. Alan Tomkinson is a professor in the Department of Molecular Medicine at The University of Texas Health Science Center at San Antonio. He holds a Ph.D degree from the University of Newcastle upon Tyne, U.K. and received postdoctoral training at the University of California, Berkeley and the Imperial Cancer research Fund, U.K. His laboratory focuses on the function of eukaryotic DNA ligases in DNA replication, DNA repair and genetic recombination.

Figure legends

Figure 1. Mechanism of phosphodiester bond formation by DNA ligase. Step 1, DNA ligase interacts with ATP or NAD forming a covalent enzyme-AMP intermediate. **Step 2,** after nick recognition, the AMP group is transferred to the 5' phosphate terminus forming a high energy phosphate bond. **Step 3,** DNA ligase catalyzes phosphodiester bond formation, releasing AMP.

Figure 2. Features of the core catalytic domain and alignment of NAD- and ATP-dependent DNA ligases. Top, Schematic representation of the core catalytic domain shared by all DNA ligases. **Bottom,** Comparison of a prokaryotic NAD-dependent DNA ligase (*Thermus filiformis*), and ATP-dependent DNA ligases from virus (bacteriophage T7), and humans (DNA ligases I, IIIα, and IV). Znf, zinc finger motif; HhH, helix-hairpin-helix domain; BRCT, BRCA1 C-terminus domain.

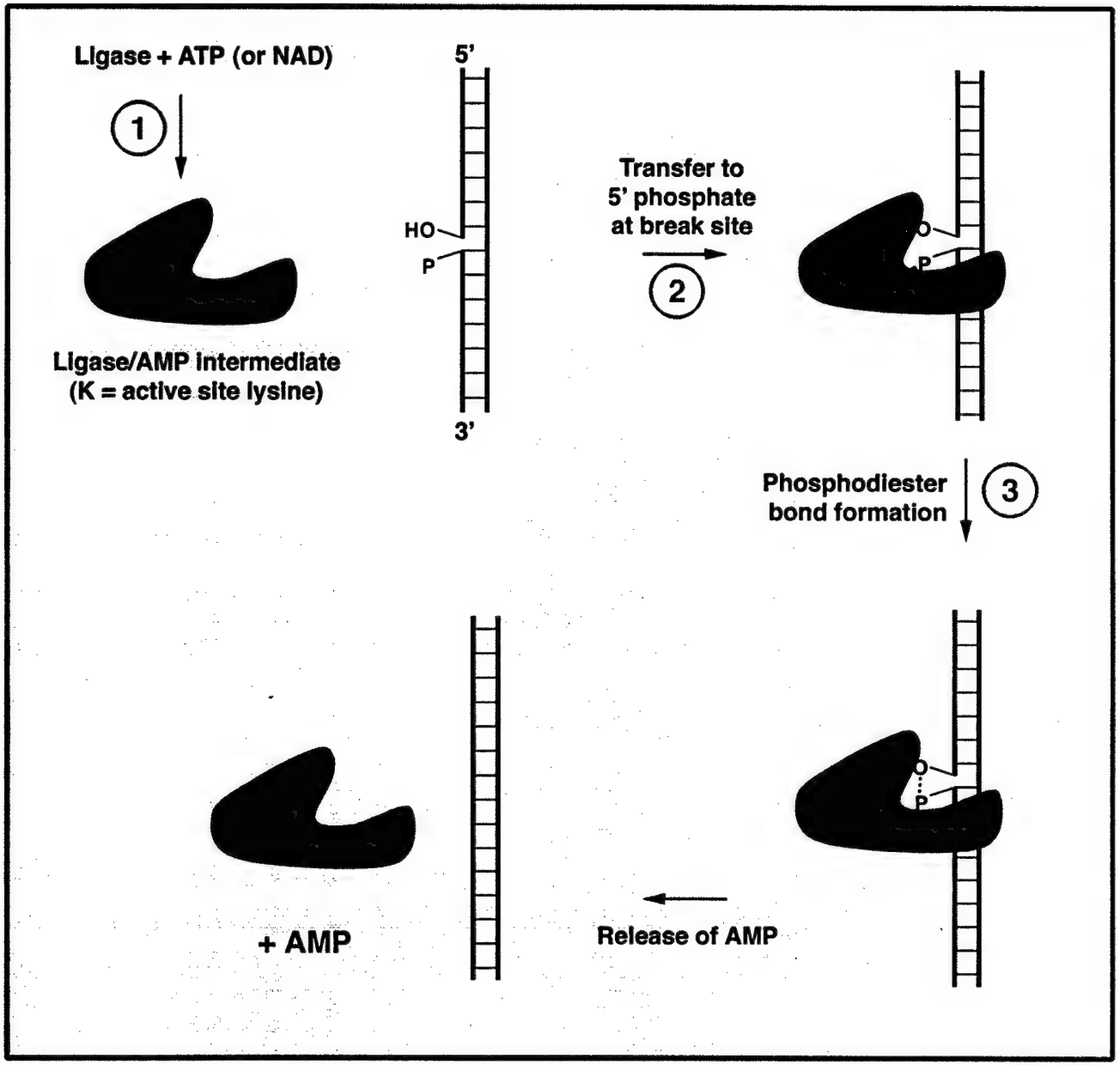
Ligase + ATP (or NAD)
1
Ligase/AMP intermediate
(K = active site lysine)
5'
HO
P
3'
Transfer to
5' phosphate
at break site
2
O
P
Phosphodiester
bond formation
3
O
P
Release of AMP
+ AMP

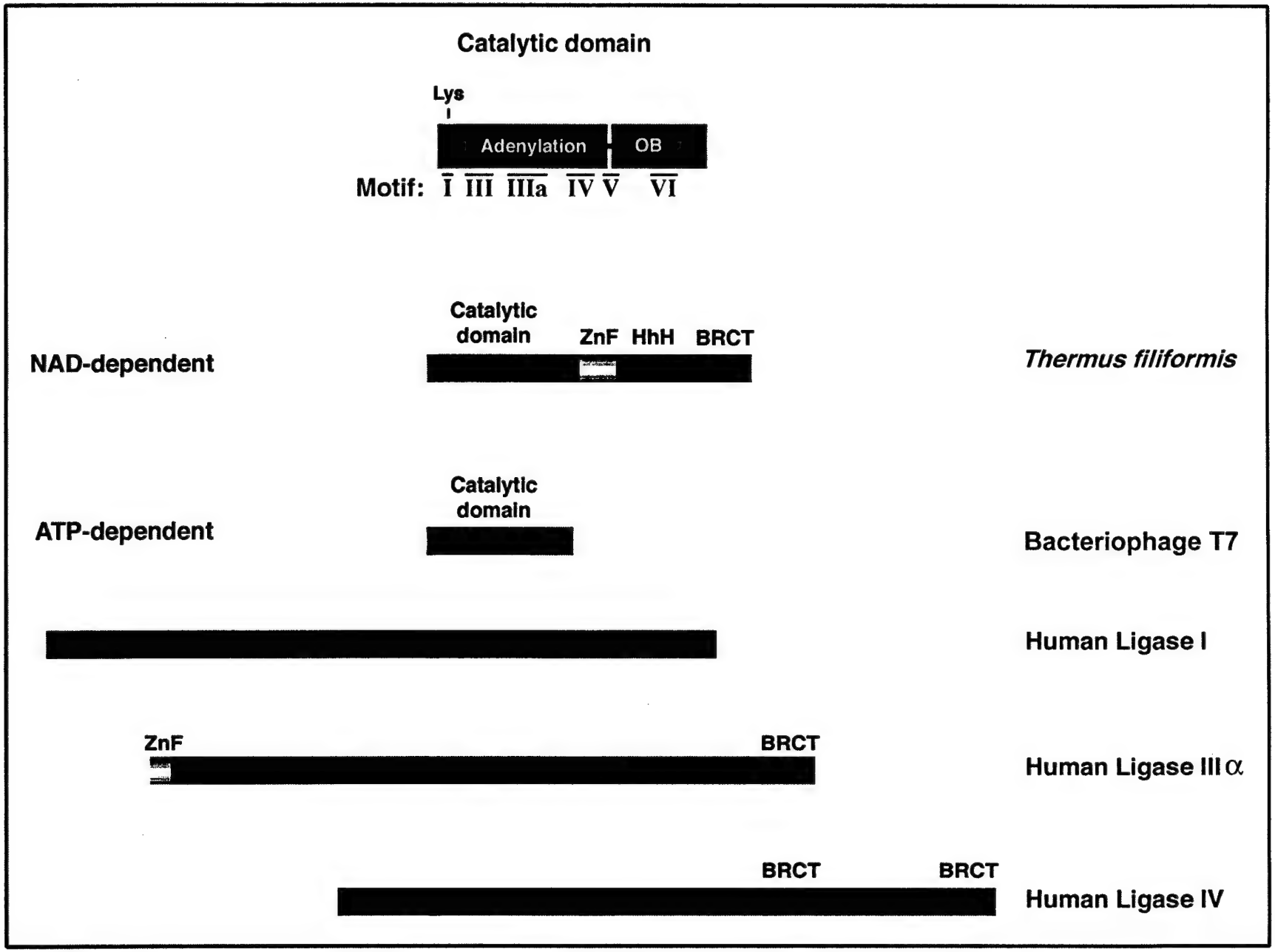
Catalytic domain
Lys
Adenylation
OB
Motif: I III IIIa IV V VI
NAD-dependent
Catalytic domain
ZnF
HhH
BRCT
Thermus filiformis
ATP-dependent
Catalytic domain
Bacteriophage T7
Human Ligase I
ZnF
BRCT
Human Ligase IIIα
BRCT
BRCT
Human Ligase IV

Table I. Mammalian DNA ligases

Gene	Gene product	Interacting protein	Function
LIG1	DNA ligase I	PCNA, Polβ	DNA replication, BER, NER, Recombination
LIG3	DNA ligase IIIα (nuclear)	XRCC1	Single-strand break repair, BER
	DNA ligase IIIα (mitochondrial)	?	Single-strand break repair, BER?
	DNA ligase IIIβ	?	Post-meiotic repair?, meiotic recombination?
LIG4	DNA ligase IV	XRCC4	NHEJ, V(D)J recombination

ELSEVIER

DNA Repair 1 (2002) 137–142

DNA REPAIR

www.elsevier.com/locate/dnarepair

Arsenic-induced Mre11 phosphorylation is cell cycle-dependent and defective in NBS cells

Shyng-Shiou F. Yuan[a,*], Jinu-Huang Su[a], Ming-Feng Hou[b], Fei-Wen Yang[a], Song Zhao[c], Eva Y.-H.P Lee[c]

[a] *Department of Obstetrics and Gynecology, Kaohsiung Medical University Hospital, Kaohsiung 807, Taiwan, ROC*
[b] *Department of Surgery, Kaohsiung Medical University Hospital, Kaohsiung 807, Taiwan, ROC*
[c] *Department of Molecular Medicine/Institute of Biotechnology, University of Texas Health Science Center, San Antonio, TX 78245-3207, USA*

Received 19 July 2001; received in revised form 20 October 2001; accepted 29 October 2001

Abstract

Cancer-prone diseases ataxia-telangiectasia (AT), Nijmegen breakage syndrome (NBS) and ataxia-telangiectasia-like disorder (ATLD) are defective in the repair of DNA double-stranded break (DSB). On the other hand, arsenic (As) has been reported to cause DSB and to be involved in the occurrence of skin, lung and bladder cancers. To dissect the repair mechanism of As-induced DSB, wild type, AT and NBS cells were treated with sodium arsenite to study the complex formation and post-translational modification of Rad50/NBS1/Mre11 repair proteins. Our results showed that Mre11 went through cell cycle-dependent phosphorylation upon sodium arsenite treatment and this post-translational modification required NBS1 but not ATM. Defective As-induced Mre11 phosphorylation was rescued by reconstitution with full length NBS1 in NBS cells. Although As-induced Mre11 phosphorylation was not required for Rad50/NBS1/Mre11 complex formation, it might be required for the formation of Rad50/NBS1/Mre11 nuclear foci upon DNA damage. © 2002 Elsevier Science B.V. All rights reserved.

Keywords: Ataxia-telangiectasia; Nijmegen breakage syndrome; Ataxia-telangiectasia-like disorder; DNA double-stranded breaks; Arsenic; Phosphorylation

1. Introduction

The maintenance of genomic integrity is essential for the cell surviving and functioning [1]. Ataxia-telangiectasia (AT), Nijmegen breakage syndrome (NBS) and ataxia-telangiectasia-like disorder (ATLD), caused by mutations in *ATM*, *NBS1* and *Mre11*, respectively, share the similar phenotypes of defective DNA double-stranded break (DSB) repair and aberrant checkpoint activation when treated with ionizing radiation (IR) or radio-mimetic drugs [2–4]. A function link between repair proteins ATM and NBS1 was demonstrated recently [5–8]. Furthermore, IR-induced Mre11 phosphorylation is abrogated in NBS cell lines [9]. All these results suggest that ATM, NBS1 and Mre11 may play important roles in DNA repair through protein–protein interaction and post-translational modification.

Arsenic (As) is a naturally occurring metalloid and broadly present in water, soil, air and food. Chronic As exposure has a strong correlation to the occurrence of bladder, lung and skin cancers [10]. However, the molecular basis for the carcinogenesis of As is mostly unclear. As treatment leads to DNA mutations, DSBs,

* Corresponding author. Tel.: +886-7-3805228; fax: +886-7-3110947.
E-mail address: yuanssf@ms33.hinet.net (S.-S.F. Yuan).

1568-7864/02/$ – see front matter © 2002 Elsevier Science B.V. All rights reserved.
PII: S1568-7864(01)00009-X

chromosome breaks and deletions, micronuclei induction and aneuploidy in the cells, events frequently observed in cancer cells [11–14]. As also induces cell proliferation and aberrant expression of genes involved in cell growth or cell cycle control [15–18].

To study the genetic requirement for the repair of As-induced DNA damage, cultured wild type, AT and NBS cells were treated with sodium arsenite to analyze post-translational modification of Rad50/NBS1/Mre11 protein complex and formation of Rad50/NBS1/Mre11 nuclear foci. Here, we showed that As-induced Mre11 phosphorylation required NBS1, not ATM. Although As-induced Mre11 phosphorylation was present in all phases of cell cycle, it was most dominant at M phase.

2. Materials and methods

2.1. Cell culture and treatment

Human AT fibroblast cell lines (GM05849C, and GM09607B) and NBS fibroblast cell lines (GM07166A and GM15989) were received from Coriell Institute and cultured in DMEM with 10% FBS. Human NBS fibroblast NBS-LBI, VA13 human fibroblast and T24 human bladder transitional cell carcinoma cell lines were all grown in DMEM with 10% FBS. NBS-LBI-V and NBS-LBI-WT stable cell lines were derived from NBS-LBI, a NBS cell line, after infection with pLXIN retroviral vector (Clontech) and retroviral vector expressing wild type NBS1, respectively. Both stable cell lines were selected under 500 μg/ml G418 (Sigma) and maintained in DMEM supplemented with 10% FBS and 200 μg/ml G418. Various cell cycle phases T24 cells were retrieved by density arrest accordingly [19] and cell cycle distribution of T24 cells was analyzed by EPICS flow cytometer (Beckman Coulter). M phase-enriched T24 cells were achieved by treating the cells, which were 32 h released from density arrest, with 0.4 μg/ml nocodazole (Sigma) for 10 h.

2.2. Immunoblotting and immunoprecipitation

The cultured cells were treated with sodium arsenite (Sigma) or γ-irradiation, harvested and lysed in EBC buffer (50 mM Tris, pH7.6, 120 mM NaCl, 0.5% Nonidet P-40, 1 mM EDTA, 1 mM β-mercaptoethanol, 50 mM NaF, and 1 mM Na_3VO_4) plus protease inhibitors. The detailed procedures for immunoblotting and immunoprecipitation were followed accordingly [20]. Phosphatase and phosphatase inhibitor (New England BioLab) were incubated with the Mre11 immunoprecipitate to study the As-induced Mre11 phosphorylation [7]. Rad50, NBS1 and Mre11 proteins were detected by enhanced chemiluminence (Amersham Pharmacia Biotech).

2.3. Immunofluorescent staining

The cultured cells were grown in 35 mm petri dish, treated with sodium arsenite and fixed for NBS1 nuclear foci study. Cell treatment and immunofluorescent staining were carried out as described [20]. In this assay, NBS1 monoclonal antibody and FITC-conjugated goat anti-mouse IgG (Jackson Immunochemicals) were used as the primary and secondary antibodies, respectively.

3. Results

3.1. The effect of cell cycle on arsenic-induced Mre11 phosphorylation

The cellular responses to As are complex and include DNA damage, aberrant cell growth and apoptosis ([10] for review). To study how As affects the DSB repair machinery, T24 cells were treated with sodium arsenite and Rad50/NBS1/Mre11 repair proteins were analyzed. Interestingly, exposure of T24 cells to sodium arsenite for 3 h at the concentration of 10 μM or more, before obvious cell death was noticed by morphology, resulted in the formation of a slower migrating form of Mre11 (Fig. 1A). This mobility shift was abolished after phosphatase treatment (Fig. 1B), suggesting it was caused by protein phosphorylation. As-induced Mre11 phosphorylation appeared 2 h after treatment and persisted for at least 8 h (Fig. 1C). For comparison, the dosage effect (Fig. 1A) and time course of IR-induced Mre11 phosphorylation (Fig. 1C) was also analyzed. In our study, IR-induced Mre11 phosphorylation was observed as early as 10 min after 20 Gy γ-irradiation treatment and decreased at 8 h after treatment (Fig. 1C).

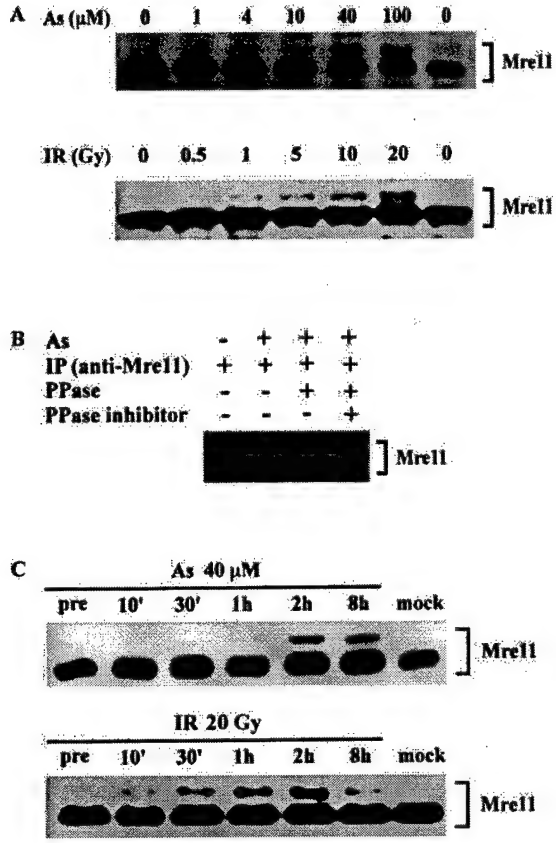

Fig. 1. Arsenic-induced Mre11 mobility shift was caused by phosphorylation. (A) Mobility shift of Mre11. Unsynchronized T24 cells were treated with various dosages of sodium arsenite (As) for 3 h or γ-irradiation (IR) and then subjected for immunoblotting analysis. (B) Phosphorylation of Mre11. Arsenic-treated T24 cell lysates were immunoprecipitated (IP) with anti-Mre11 antibody and the immunoprecipitate was incubated with phosphatase (PPase) in the absence or presence of phosphatase inhibitor. (C) The time course of arsenic-induced and IR-induced Mre11 phosphorylation. T24 cells were treated with 40 μM sodium arsenite or 20 Gy γ-irradiation and the kinetics of Mre11 phosphorylation was analyzed at different time points after treatment. (−) Without treatment; (+) with treatment; (pre) before sodium arsenite treatment; (mock) in arsenic-free medium or without γ-irradiation for 8 h.

To examine the effect of cell cycle progression on As-induced Mre11 phosphorylation, T24 cells of different cell cycle phases were obtained by density arrest [19] or nocodazole treatments. T24 cells of various phases were harvested for Mre11 immunoblotting analysis after As exposure for 3 h. Although the As-induced Mre11 phosphorylation was observed in T24 cells of all cell cycle phases, it was more significant at M phase (Fig. 2). This result was somewhat different from the IR-induced Mre11 phosphorylation, which is at similar levels in all cell cycle phases (Fig. 2).

3.2. The effect of arsenic on Rad50/NBS1/Mre11 protein complex maintenance and NBS1 nuclear focus formation

To study the functional significance of As-induced Mre11 phosphorylation on DSB repair, the effect of As on the maintenance of Rad50/NBS1/Mre11 protein complex and formation of NBS1 nuclear foci was analyzed. Although sodium arsenite treatment induced Mre11 phosphorylation in cultured cells, Rad50/NBS1/Mre11 complex remained unchanged before and after treatment (Fig. 3A), suggesting Mre11 phosphorylation was not required for Rad50/NBS1/Mre11 complex maintenance. However, the NBS1 nuclear foci formation is prompt in response to As (Fig. 3B). In our preliminary study, about 8% of the unsynchronized T24 cells showed NBS1 foci at 5 h after 40 μM sodium arsenite treatment, in comparison to 2% before treatment (data not shown).

3.3. The requirement of NBS1 for arsenic-induced Mre11 phosphorylation

It has been well documented that ATM and NBS1 are the key players in DSB repair ([21] for review). To study the requirement of ATM and NBS1 for the As-induced Mre11 phosphorylation, wild type, AT cells and NBS cells were treated with 40 μM sodium arsenite for 3 h and subjected for Mre11 analysis. The As-induced Mre11 phosphorylation was observed in wild type and AT cells but not NBS cell lines we analyzed (Fig. 4B). However, this post-translational modification reappeared in the NBS cells when they were reconstituted with full length NBS1 (Fig. 4B), suggesting NBS1 was required for As-induced Mre11 phosphorylation. Interestingly, an elevated basal level of Mre11 phosphorylation was observed frequently in GM09607B AT cells and less frequently in other AT and NBS cell lines we tested. The reason for this constitutive phosphorylation is unclear, but suggests certain ATM-independent kinase(s) may be involved [9].

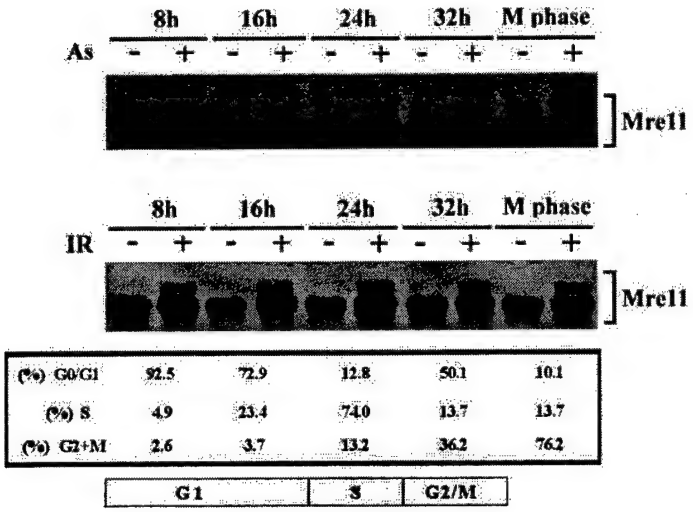

Fig. 2. Arsenic-induced Mre11 phosphorylation was cell cycle-dependent. T24 cells of various cell cycle phases were retrieved after releasing from density arrest for 8, 16, 24, and 32 h. M phase-enriched cells (M phase) were retrieved by treating the T24 cells, which were 32 h released from density arrest, with 0.4 μg/ml nocodazole for 10 h. Cell cycle distribution of T24 cells was analyzed by flow cytometer. T24 cells of different phases were treated with 40 μM sodium arsenite for 3 h or 20 Gy γ-irradiation and the cell lysates were subjected for immuoblotting analysis.

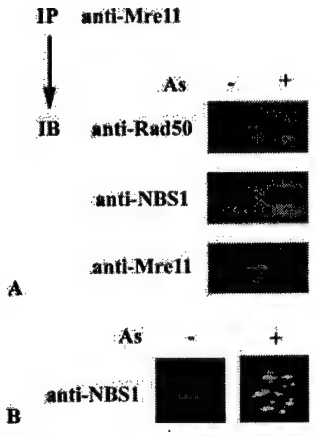

Fig. 3. The effect of arsenic-induced Mre11 phosphorylation on Rad50/NBS1/Mre11 complex maintenance and NBS1 nuclear focus formation. (A) For Rad50/NBS1/Mre11 complex study, unsynchronized T24 cells were treated with 40 μM sodium arsenite for 3 h and the cell lysates were immunoprecipitated (IP) with anti-Mre11 antibody, followed by immunoblotting (IB) using anti-Rad50, anti-NBS1 and anti-Mre11 antibodies, respectively. (B) For NBS1 nuclear foci analysis, unsynchronized T24 cells were treated with 40 μM sodium arsenite for 5 h and the cells were fixed and subjected for immunofluorecent staining.

ATM and NBS1 dependency of Mre11 phosphorylation following IR was also analyzed for comparison. Although As-induced Mre11 phosphorylation is NBS1-dependent but ATM-independent (Fig. 4B), both ATM and NBS1 are required for IR-induced Mre11 phosphorylation (Fig. 4C).

4. Discussion

As is a well documented environmental carcinogen [10]. Although it causes DSBs in the exposed cells, the role of DSB repair proteins in the repair process of As-induced DNA damage is not clear. To the best of our knowledge, this is the first report demonstrating the involvement of Rad50/NBS1/Mre11 DSB repair complex in As-induced DNA damage.

It has been reported that As-treated cells arrested at G1 and G2/M phases and then went through apoptosis eventually [22,23]. It was intriguing to notice that the As-induced Mre11 phosphorylation was dominant at M phase (Fig. 2). Since T24 cells were harvested 3 h after 40 μM sodium arsenite treatment, before cell apoptosis was observed, the functional significance of this M phase-dominant event remains to be explored.

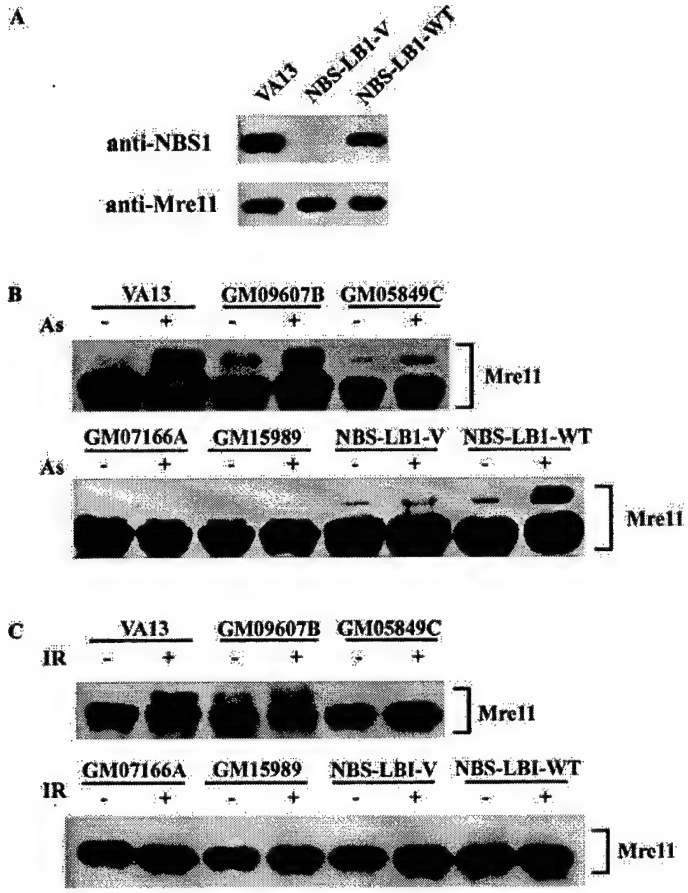

Fig. 4. The requirement of ATM and NBS1 for arsenic-induced Mre11 phosphorylation. (A) The expression of NBS1 and Mre11 in wild type fibroblasts (VA13), NBS fibroblasts (NBS-LBI-V) and NBS1-reconstituted NBS fibroblasts (NBS-LBI-WT). (B) VA13, AT fibroblasts (GM09607B and GM05849C), NBS fibroblasts (GM07166A, GM15989 and NBS-LBI-V) and NBS-LBI-WT were treated with 40 μM sodium arsenite for 3 h and the cell lysates were subjected for immunoblotting analysis. (C) The cells were treated with 20 Gy γ-irradiation, harvested at 3 h after treatment and subjected for immunoblotting analysis.

The involvement of Rad50/NBS1/Mre11 protein complex in DSB repair is well documented ([21] for review). In our study, As-induced Mre11 phosphorylation was observed at earlier time points than the formation of NBS1 foci. Although the Rad50/NBS1/Mre11 protein complex status was not affected by As treatment, the prompt NBS1 nuclear foci formation suggested a possible link between Mre11 phosphorylation and As-induced foci formation.

NBS1 is a downstream target for ATM and is phosphorylated upon IR in an ATM-dependent manner [5–8]. However, in our study, the As-induced Mre11 phosphorylation only required NBS1 but not ATM (Fig. 4B), suggesting that, in the repair of As-induced DNA damage, an ATM-independent but NBS1-dependent pathway, which linked Mre11 phosphorylation and downstream repair processes together, might exist. Further studies are required to rule out this possibility.

In agreement with the recent paper by Stewart et al. [24], we did not observe IR-induced Mre11 phosphorylation in any of the classical AT cell lines we tested. Nevertheless, As-, UV- or MMS-induced Mre11 phosphorylation is intact in the classical AT cell lines (Fig. 4B and [9]). More efforts are required to define the detailed mechanisms and biological

significance of Mre11 phosphorylation in response to DNA damages caused by different genotoxic agents.

Acknowledgements

This work is supported by grant from National Science Committee, Taiwan, ROC to S.S.Y. (NSC89-2320-B-037-070).

References

[1] D.C. van Gent, J.H. Hoeijmakers, R. Kanaar, Chromosomal stability and the DNA double-stranded break connection, Nat. Rev. Genet. 2 (2001) 196–206.
[2] Y. Shiloh, Ataxia-telangiectasia and the Nijmegen breakage syndrome: related disorders but genes apart, Ann. Rev. Genet. 31 (1997) 635–662.
[3] G. Rotman, Y. Shiloh, ATM: from gene to function, Hum. Mol. Genet. 7 (1998) 1555–1563.
[4] G.S. Stewart, R.S. Maser, T. Stankovic, D.A. Bressan, M.I. Kaplan, N.G. Jaspers, A. Raams, P.J. Byrd, J.H. Petrini, A.M. Taylor, The DNA double-strand break repair gene hMRE11 is mutated in individuals with an ataxia-telangiectasia-like disorder, Cell 99 (1999) 577–587.
[5] D.S. Lim, S.T. Kim, B. Xu, R.S. Maser, J. Lin, J.H. Petrini, M.B. Kastan, ATM phosphorylates p95/nbs1 in an S-phase checkpoint pathway, Nature 404 (2000) 613–617.
[6] M. Gatei, D. Young, K.M. Cerosaletti, A. Desai-Mehta, K. Spring, S. Kozlov, M.F. Lavin, R.A. Gatti, P. Concannon, K Khanna, ATM-dependent phosphorylation of nibrin in response to radiation exposure, Nat. Genet. 25 (2000) 115–119.
[7] S. Zhao, Y.C. Weng, S.S. Yuan, Y.T. Lin, H.C. Hsu, S.C. Lin, E. Gerbino, M.H. Song, M.Z. Zdzienicka, R.A. Gatti, J.W. Shay, Y. Ziv, Y. Shiloh, E.Y. Lee, Functional link between ataxia-telangiectasia and Nijmegen breakage syndrome gene products, Nature 405 (2000) 473–477.
[8] X. Wu, V. Ranganathan, D.S. Weisman, W.F. Heine, D.N. Ciccone, T.B. O'Neill, K.E. Crick, K.A. Pierce, W.S. Lane, G. Rathbun, D.M. Livingston, D.T. Weaver, ATM phosphorylation of Nijmegen breakage syndrome protein is required in a DNA damage response, Nature 405 (2000) 477–482.
[9] Z. Dong, Q. Zhong, P.L. Chen, The Nijmegen breakage syndrome protein is essential for Mre11 phosphorylation upon DNA damage, J. Biol. Chem. 274 (1999) 19513–19516.
[10] NRC (National Research Council), Arsenic in Drinking Water, National Academy Press, Washington, DC, 1999.
[11] A.N. Jha, M. Noditi, R. Nilsson, A.T. Natarajan, Genotoxic effects of sodium arsenite on human cells, Mutat. Res. 284 (1992) 215–221.
[12] M.E. Gonsebatt, L. Vega, A.M. Salazar, R. Montero, P. Guzman, J. Blas, L.M. Del Razo, G. Garcia-Vargas, A. Albores, M.E. Cebrian, M. Kelsh, P. Ostrosky-Wegman, Cytogenetic effects in human exposure to arsenic, Mutat. Res. 386 (1997) 219–228.
[13] L.E. Moore, A.H. Smith, C. Hopenhayn-Rich, M.L. Biggs, D.A. Kalman, M.T. Smith, Decreased in bladder cell micronucleus prevalence after intervention to lower the concentration of arsenic in drinking water, Cancer Epidemiol. Biomarkers Prev. 12 (1997) 1051–1056.
[14] T.K. Hei, S.X. Liu, C. Waldren, Mutagenicity of arsenic in mammalian cells: role of reactive species, Proc. Natl. Acad. Sci. U.S.A. 95 (1998) 8103–8107.
[15] D.R. Germolec, J. Spalding, G.A. Boorman, J.L. Wilmer, T. Yoshida, P.P. Simeonova, A. Bruccoleri, F. Kayama, K. Gaido, R. Tennant, F. Burleson, W. Dong, R.W. Lang, M.I. Luster, Arsenic can mediate skin neoplasia by chronic stimulation of keratinocyte-derived growth factors, Mutat. Res. 386 (1997) 209–218.
[16] D.R. Germolec, J. Spalding, H.S. Yu, G.S. Chen, P.P. Simeonova, M.C. Humble, A. Bruccoleri, G.A. Boorman, J.F. Foley, T. Yoshida, M.I. Luster, Arsenic enhancement of skin neoplasia by chronic stimulation of growth factors, Am. J. Pathol. 153 (1998) 1775–1785.
[17] P.P. Simeonova, S. Wang, W. Toriuma, V. Kommineni, J. Matheson, N. Unimye, F. Kayama, D. Harki, M. Ding, V. Vallyathan, M.I. Luster, Arsenic-mediated cell proliferation and gene expression in the bladder epithelium: association with activating protein-1 transactivation, Cancer Res. 60 (2000) 2445–2453.
[18] K.J. Trouba, E.M. Wauson, R.L. Vorce, Sodium arsenite-induced dysregulation of proteins involved in proliferative signaling, Toxicol. Appl. Pharmacol. 164 (2000) 161–179.
[19] P.L. Chen, P. Scully, J.Y. Shew, J.Y. Wang, W.H. Lee, Phosphorylation of the retinoblastoma gene product is modulated during the cell cycle and cellular differentiation, Cell 58 (1989) 1193–1198.
[20] S.S. Yuan, S.Y. Lee, G. Chen, M. Song, G.E. Tomlinson, E.Y. Lee, BRCA2 is required for ionizing radiation-induced assembly of Rad51 complex in vivo, Cancer Res. 59 (1999) 3547–3551.
[21] G.K. Dasika, S.C. Lin, S. Zhao, P. Sung, A. Tomkinson, E.Y. Lee, DNA damage-induced cell cycle checkpoints and DNA strand break repair in development and tumorigenesis, Oncogene 18 (1999) 7883–7899.
[22] W.H. Park, J.G. Seol, E.S. Kim, J.M. Hyun, C.W. Jung, C.C. Lee, B.K. Kim, Y.Y. Lee, Arsenic trioxide-mediated growth inhibition in MC/CAR myeloma cells via cell cycle arrest in association with induction of cyclin-dependent kinase inhibitor, p21, and apoptosis, Cancer Res. 60 (2000) 3065–3071.
[23] S.C. Huang, C.Y. Huang, T.C. Lee, Induction of mitosis-mediated apoptosis by sodium arsenite in HeLa S3 cells, Biochem. Pharmacol. 60 (2000) 771–780.
[24] G.S. Stewart, J.I. Last, T. Stankovic, N. Haites, A.M. Kidd, P.J. Byrd, A.M. Taylor, Residual ataxia-telangiectasia mutated protein function in cells from ataxia-telangiectasia patients, with 5762ins137 and 7271T → G mutations, showing a less severe phenotype, J. Biol. Chem. 276 (2001) 30133–30141.

Elimination of Mcl-1 is required for the initiation of apoptosis following ultraviolet irradiation

Deepak Nijhawan,[1] Min Fang,[1] Elie Traer, Qing Zhong, Wenhua Gao, Fenghe Du, and Xiaodong Wang[2]

Howard Hughes Medical Institute & Department of Biochemistry, University of Texas Southwestern Medical Center at Dallas, Dallas, Texas 75390, USA

Ultraviolet (UV) irradiation of HeLa cells triggers an apoptotic response mediated by mitochondria. Biochemical analysis of this response revealed that the elimination of cytosolic inhibitors is required for mitochondrial release of cytochrome *c* and subsequent caspase activation. These inhibitors were found to be Mcl-1 and Bcl-x_L, two antiapoptotic members of the Bcl-2 family. Following UV treatment, Mcl-1 protein synthesis is blocked, the existing pool of Mcl-1 protein is rapidly degraded by the proteasome, and cytosolic Bcl-x_L translocates to the mitochondria. These events are sequential; the elimination of Mcl-1 is required for the translocation of Bcl-x_L. The disappearance of Mcl-1 is also required for other mitochondrial apoptotic events including Bax translocation, cytochrome *c* release, and caspase activation.

[*Keywords*: Apoptosis; cytochrome *c*; mitochondria; Mcl-1; Bcl-x_L; proteasome]

Received March 17, 2003; revised version accepted April 18, 2003.

Apoptosis provides a powerful protection mechanism to eliminate harmful cells that have suffered a lethal dose of DNA damage. Failure to die results in the survival of cells harboring genetic mutations that may become cancerous (Johnstone et al. 2002). Therefore, molecular dissection of the cellular apoptotic response to DNA damage is of both theoretical and practical significance.

DNA-damaging reagents such as ultraviolet (UV) light and genotoxic chemotherapeutical agents induce apoptosis through a mitochondrial pathway (Kim et al. 1997; Kluck et al. 1997; Bossy-Wetzel et al. 1998). In response to these treatments, cytochrome *c* is released from the mitochondrial intermembrane space to the cytoplasm, where it binds to Apaf-1. Cytochrome *c* binding to Apaf-1 triggers the formation of the apoptosome, which activates procaspase-9 (Li et al. 1997; Acehan et al. 2002). Activated caspase-9 cleaves and activates caspase-3 and caspase-7, which subsequently cleave many intracellular substrates, leading to the characteristic morphological changes associated with apoptosis (Rodriguez and Lazebnik 1999; Hengartner 2000).

In addition to cytochrome *c*, several other apoptogenic proteins are also released from the mitochondrial intermembrane space. These include Smac/Diablo and Omi/HtrA2, which antagonize the caspase-inhibitory IAP proteins, and AIF and EndoG, which cause apoptotic changes independent of caspase activity (Susin et al. 1999; Du et al. 2000; Verhagen et al. 2000; Li et al. 2001; Suzuki et al. 2001; Hegde et al. 2002; Martins et al. 2002).

The balance between pro- and antiapoptotic Bcl-2 family members determines the mitochondrial response to apoptotic stimuli (Gross et al. 1999; Martinou and Green 2001). Antiapoptotic proteins such as Bcl-2, Bcl-x_L, and Mcl-1 protect mitochondrial integrity, whereas the proapoptotic members of the family promote the release of apoptogenic proteins from mitochondria. The function of these proapoptotic proteins can be further divided into the BH3-only proteins including Bid, Bad, and Bim and their effectors Bak and Bax (Cheng et al. 2001; Wei et al. 2001; Zong et al. 2001). Activated BH3-only proteins induce the formation of mitochondrial oligomeric Bax/Bak complexes either directly or indirectly by binding and inactivating antiapoptotic Bcl-2 family members (Korsmeyer et al. 2000; Letai et al. 2002). These complexes may function as protein pores for cytochrome *c* and other proteins to pass through, or cause mitochondrial outer membrane destabilization (Vander Heiden et al. 1997; Kuwana et al. 2002).

The essential question of how the Bcl-2 family of proteins translates genotoxic stress into mitochondrial damage remains unaddressed. In the present report, we used classic biochemical fractionation and reconstitution to map a sequential signaling pathway composed of

[1]These authors contributed equally to this work.
[2]Corresponding author.
E-MAIL xwang@biochem.swmed.edu; FAX (214) 648-9729.
Article published online ahead of print. Article and publication date are at http://www.genesdev.org/cgi/doi/10.1101/gad.1093903.

Bcl-2 family members that leads to cytochrome *c* release after UV treatment.

Results

Activation of a mitochondrial apoptotic pathway in response to UV irradiation

After receiving a strong dose of UV irradiation, cultured HeLa cells exhibit synchronized characteristic apoptotic changes beginning 2 h after irradiation. After 4 h, most cells die by apoptosis. As shown in Figure 1A (lanes 1–4), these changes include the oligomerization of Bak, the appearance of cytochrome *c* in the cytosol, and the activation of caspase-9 and caspase-2.

When cells were irradiated in the presence of a pan-caspase inhibitor, z-VAD-fmk, caspase-9 activation was completely blocked (Fig. 1A, lanes 5–8). However, the oligomerization of Bak and release of cytochrome *c* remained intact, indicating that these two events are upstream of caspase activation. Caspase-2 activation was also blocked by zVAD-fmk, suggesting that caspase-2 activation is not required for UV-induced cytochrome *c* release in HeLa cells as it is in oncogene transformed human fibroblasts (Lassus et al. 2002).

The mitochondria from UV-irradiated cells were primed to release cytochrome c *in vitro*

In vivo, mitochondria from UV-irradiated cells start to release cytochrome *c* 120 min after UV irradiation; however, mitochondria isolated from cells just 30–60 min after UV irradiation readily formed oligomerized Bak and released cytochrome *c* when incubated in vitro (Fig. 1B, lanes 2–3). In contrast, mitochondria from untreated cells did not form oligomerized Bak or release cytochrome *c* under the same conditions (Fig. 1B, lane 1). Mitochondria from cells 30–60 min after UV are therefore "primed" to release cytochrome *c* in vitro, at least 1 h before cytochrome *c* release can be detected in vivo.

Inhibitors in normal cytosol prevent cytochrome c *release from primed mitochondria*

Our finding that cytochrome *c* release is delayed in vivo compared with in vitro is consistent with a previous report predicting that cytoplasm contains inhibitors of cy-

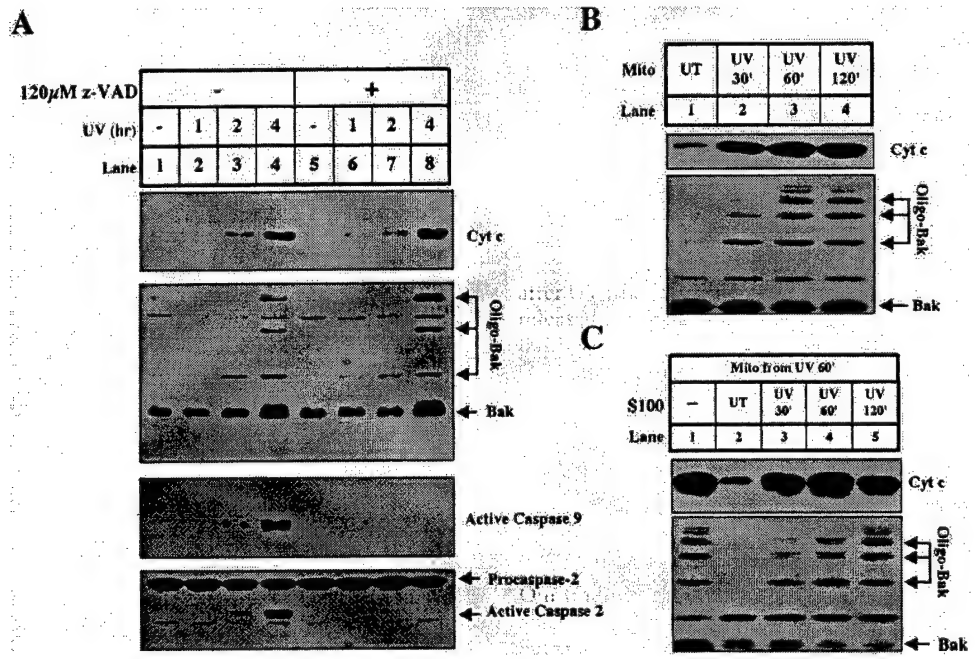

Figure 1. UV induces cytochrome *c* release from HeLa cells in vivo and in vitro. (*A*) Mitochondria and S100 were harvested from HeLa cells treated with UV for different amounts of time as described in Materials and Methods. In lanes *5–8*, we preincubated the cells in the presence of Z-VAD.fmk, a broad-spectrum caspase inhibitor as indicated. Cytochrome *c*, caspase-9, and caspase-2 were analyzed in S100. Bak oligomerization was analyzed in mitochondrial fractions as described (Wei et al. 2000). (*B*) Mitochondria from UV-treated cells release cytochrome *c* in vitro. Mitochondria (0.67 mg/mL) from untreated cells (lane *1*) or cells that were UV-treated for 30 min (lane *2*), 60 min (lane 3), or 120 min (lane *4*) were incubated in vitro at 37°C for 30 min. Following incubation, the mitochondria were pelleted and analyzed as described in Materials and Methods. (*C*) S100 inhibits cytochrome *c* release from primed mitochondria. Mitochondria (0.67 mg/mL) from cells treated with UV for 1 h were coincubated (lanes *1–5*) at 37°C for 30 min with only buffer (lane *1*) or HeLa S100 (4 mg/mL) from untreated cells (lane *2*) or cells that were UV-treated for 30 min (lane 3), 60 min (lane *4*), or 120 min (lane *5*). Mitochondria and supernatants were analyzed for Bak oligomerization and cytochrome *c* release, respectively.

tochrome *c* release (Duelli and Lazebnik 2000). To test this hypothesis in our system, primed mitochondria isolated from cells 60 min after UV irradiation were incubated with cytosol (S100) from untreated cells (naive), or cells 30–120 min after UV irradiation. As shown in Figure 1C, cytosol from naive cells efficiently inhibited cytochrome *c* release from UV-primed mitochondria (Fig. 1C, lane 2). The ability of cytosol to inhibit release was gradually lost with increasing time after UV irradiation (Fig. 1C, lanes 3–5).

Purification and identification of Mcl-1 and Bcl-x_L as the cytosolic inhibitors of cytochrome c *release*

We used biochemical fractionation in concert with a candidate protein approach to identify the inhibitors present in the cytosol of naive cells. The cytosol from naive HeLa cells was fractionated by ammonium sulfate precipitation, ion exchange Mono Q column chromatography, gel-filtration column chromatography (data not shown), and hydroxyapatite chromatography (data not shown), and assayed for inhibition of cytochrome *c* release from UV-primed mitochondria. As shown in the upper panel of Figure 2A, 30% ammonium sulfate precipitated the activity (Fig. 2A, lanes 4,6). The precipitated activity was subsequently loaded onto a Mono Q column, and an activity peak was eluted from the column by ~200 mM NaCl (Fig. 2B, upper panel, lane 9).

Because antiapoptotic members of the Bcl-2 family of proteins are likely candidates for such an activity, we probed the column fractions using antibodies against these proteins. As shown in the middle and lower panels of Figure 2A and B, we found that Bcl-x_L and Mcl-1 copurified with the inhibitory activity.

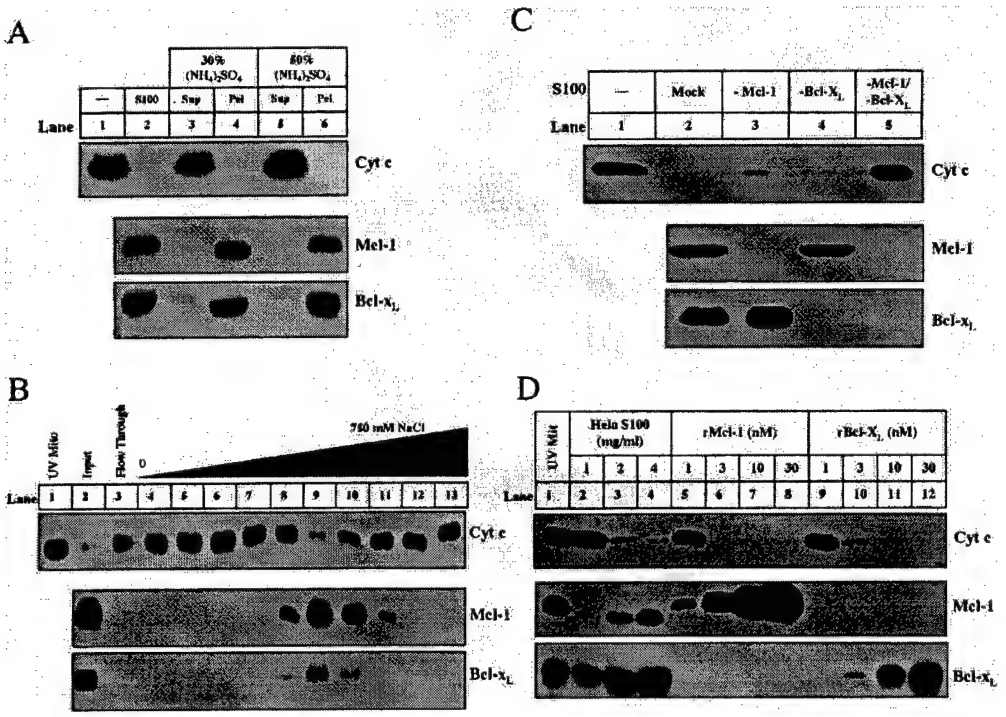

Figure 2. Mcl-1 and Bcl-x_L are necessary and sufficient for cytosolic inhibitory activity. (*A*) Mcl-1 and Bcl-x_L correlate with inhibitory activity after ammonium sulfate fractionation. Ammonium sulfate was added to 1 mL of S100 (5 mg/mL) up to 30% (lanes *3,4*) or 50% (lanes *5,6*). Following incubation at 4°C for 1 h, the supernatant (Sup) and pellet (Pel) were separated by centrifugation (20,000*g*). The pellet was resuspended in 1 mL of Buffer A. Both the supernatants and pellets were dialyzed in Buffer A overnight. All fractions were assayed for inhibitory activity (as described in Materials and Methods) and evaluated for Mcl-1 and Bcl-x_L. (*B*) HeLa S100 (36 mg) was first precipitated with 30% ammonium sulfate. The resulting pellet (7.5 mg) was resuspended and dialyzed in Buffer A and then loaded onto a 1-mL Hi-trap Q Sepharose column (Amersham) equilibrated in Buffer A. The protein was eluted with a gradient from 0 to 750 mM NaCl (in Buffer A) over 14 mL. Inhibitory activity was assayed for buffer alone (lane *1*), input (lane *2*), Q flow through (lane *3*), and fractions eluting from Q sepharose (lanes *4–13*). The amount of Mcl-1 and Bcl-x_L in each sample and the mitochondria (lane *1*) was measured by Western blot. (*C*) HeLa S100 was immunodepleted as described in Materials and Methods. Inhibitory activity was assayed in buffer alone (lane *1*), S100 mock-immunodepleted (lane *2*), depleted of Mcl-1 (lane *3*), Bcl-x_L (lane *4*), or both (lane *5*). The amount of Mcl-1 and Bcl-x_L was determined by Western blot for each S100 sample. (*D*) Recombinant Mcl-1 (rMcl-1) and Bcl-x_L (rBcl-x_L) were prepared as described in Materials and Methods. S100, rMcl-1, and rBcl-x_L were analyzed for inhibitory activity. The levels of Mcl-1 and Bcl-x_L in recombinant fractions were compared with those in S100. Mitochondria solubilized in Buffer A with 1% NP-40 were analyzed for Mcl-1 and Bcl-x_L to compare the levels of these proteins in mitochondria to those in the fractions.

We tested whether the inhibitory activity in naive cytosol was due to Mcl-1 and Bcl-x_L by immunodepleting these two proteins either individually or in combination from naive S100. As shown in the middle and lower panels of Figure 2C, antibodies against Mcl-1 and Bcl-x_L efficiently depleted these proteins from naive cytosol (Fig. 2C, lanes 3–5). Cytosol depleted of Mcl-1 (Fig. 2C, lane 3) or Bcl-x_L (Fig. 2C, lane 4) lost some activity whereas cytosol depleted of both (Fig. 2C, lane 5) completely lost the ability to inhibit cytochrome *c* release, indicating that both Mcl-1 and Bcl-x_L are necessary for full activity (Fig. 2C, upper panel).

To confirm that Bcl-x_L and Mcl-1 are sufficient to inhibit cytochrome *c* release from UV-treated mitochondria, purified recombinant Bcl-x_L or Mcl-1 was incubated with UV-primed mitochondria. As shown in the upper panel of Figure 2D, 3 nM Mcl-1 or 10 nM Bcl-x_L was able to completely block cytochrome *c* when added directly to UV-primed mitochondria (Fig. 2D, lanes 6,11). The concentration of recombinant Bcl-x_L and Mcl-1 in the reactions is comparable with that of Bcl-x_L and Mcl-1 present on the mitochondria and in naive cytosol (Fig. 2D, middle and lower panels, lanes 1–4).

UV irradiation triggers a decrease in Mcl-1 levels and the translocation of Bcl-x_L to the mitochondria

The inhibition of cytochrome *c* release in naive cytosol is removed by UV irradiation (Fig. 1C, lanes 3–5). We therefore examined the levels of Mcl-1 and Bcl-x_L in cytosol and mitochondria isolated from naive and UV-treated cells. As shown in Figure 3A, the total amount of Mcl-1 was markedly decreased 1 h after UV treatment and completely disappeared after 2 h (Fig. 3A, lanes 1–4). On the other hand, the total amount of Bcl-x_L in cells did not change even 4 h after UV irradiation. However, cytosolic Bcl-x_L started to decrease 1 h after UV irradiation and disappeared by 4 h, when robust apoptosis is observed (Fig. 3A, middle panel, lanes 5–8). Unlike Mcl-1, there was a corresponding increase of Bcl-x_L on mitochondria, indicating that Bcl-x_L translocates from cytosol to mitochondria after UV irradiation (Fig. 3A, middle panel, lanes 9–12). As a loading control, the levels of cytochrome *c* oxidase, a mitochondrial inner membrane protein, and a cross-reactive cytosolic protein remained unchanged (Fig. 3A, lower panel). The translocation of Bcl-x_L from the cytosol to the mitochondria was previously described in thymocytes undergoing apoptosis (Hsu et al. 1997). In that study, the authors also showed that Bax, a proapoptotic Bcl-2 family member, similarly translocated from the cytosol to the mitochondria. Bax translocation, along with cytochrome *c* release and caspase activation, is commonly used as a marker for apoptosis.

To test whether the disappearance of Mcl-1 and translocation of Bcl-x_L is specific to HeLa cells, we treated human fibroblasts with UV and tracked the levels of

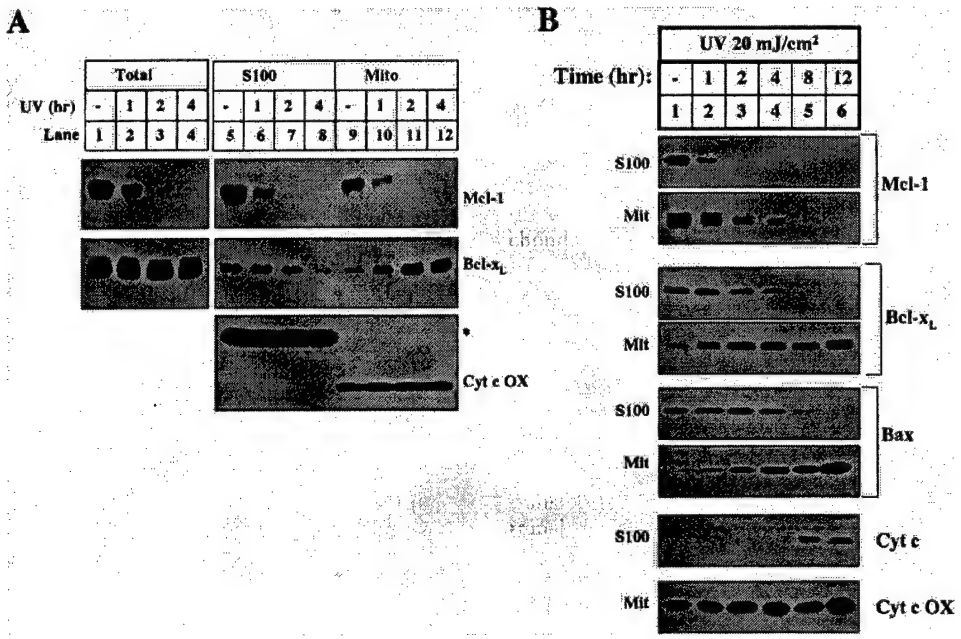

Figure 3. UV treatment induces the disappearance of Mcl-1 and the translocation of Bcl-x_L. (*A*) HeLa cells left untreated or treated with UV for different amounts of time were either harvested for 1% CHAPS total cell lysate or fractionated into mitochondria (Mito) and S100. The levels of Mcl-1, Bcl-x_L, and cytochrome *c* oxidase were determined in total cell lysate (lanes *1–4*), S100 (lanes *5–8*), and Mito (lanes *9–12*). (*B*) Human fibroblast cells were treated (as described in Materials and Methods) with UV at different time points before harvest. Mcl-1, Bcl-x_L, Bax, and cytochrome *c* levels were compared in the S100. Mcl-1, Bcl-x_L, Bax, and cytochrome *c* oxidase were compared in the mitochondria.

Mcl-1, Bcl-x_L, and Bax in the mitochondria and cytosol. Following UV treatment, both the disappearance of Mcl-1 and the translocation of Bax and Bcl-x_L precede cytochrome *c* release (Fig. 3B). These data demonstrate that following UV treatment the disappearance of Mcl-1 and translocation of Bcl-x_L are not restricted to HeLa cells. Additionally, this experiment demonstrates that the translocation of Bax and Bcl-x_L occurs with similar kinetics.

To determine if the disappearance of Mcl-1 is a general response to genotoxic stress, we analyzed the levels of Mcl-1 in cells treated with etoposide and γ-irradiation. In both cases, Mcl-1 disappears from the cytosol and mitochondria well before cytochrome *c* is released and caspases are activated (Fig. 4A). To evaluate the importance of the disappearance of Mcl-1 during UV-induced apoptosis, we used RNA interference (RNAi) to specifically knock down the levels of Mcl-1 (Fig. 4B; Elbashir et al. 2001). The levels of Mcl-1 were decreased in cells transfected with Mcl-1 siRNA, whereas the levels of Bcl-x_L remained unchanged (Fig. 4B, lane 5). When Mcl-1 was eliminated by siRNA treatment, UV-induced caspase-3 activation was accelerated, suggesting that the disappearance of Mcl-1 is an important early event in apoptosis (Fig. 4B, lower panel). However, Mcl-1 siRNA-treated cells did not activate caspase-3 in the absence of UV, indicating that the elimination of Mcl-1 is not sufficient to activate caspase-3.

Mcl-1 elimination is caused by a lack of synthesis

UV-induced Mcl-1 elimination could be caused by accelerated protein degradation or inhibition of synthesis. To distinguish between these possibilities, we pulse-labeled cells with ^{35}S methionine and chased with or without UV irradiation. Newly synthesized Mcl-1 was analyzed by immunoprecipitation. As shown in Figure 5A and B, Mcl-1 is a short-lived protein with a half-life of ~40 min. Interestingly, the half-life of Mcl-1 was the same with or without UV irradiation, even though the total amount of Mcl-1 protein was dramatically decreased after UV irradiation (Fig. 5A, lower panel).

The above experiment suggests that Mcl-1 protein synthesis must be blocked after UV irradiation. To demonstrate that directly, we pulse-labeled the cells with ^{35}S methionine at the same time as UV irradiation (Fig. 5C, lanes 1,2). After a 60-min pulse, newly synthesized Mcl-1 was dramatically decreased if cells were exposed to UV irradiation. This decrease was not affected by blocking degradation with the proteasome inhibitor, MG132 (Fig. 5C, lanes 3,4; Palombella et al. 1994). To verify that the disappearance of Mcl-1 protein is consis-

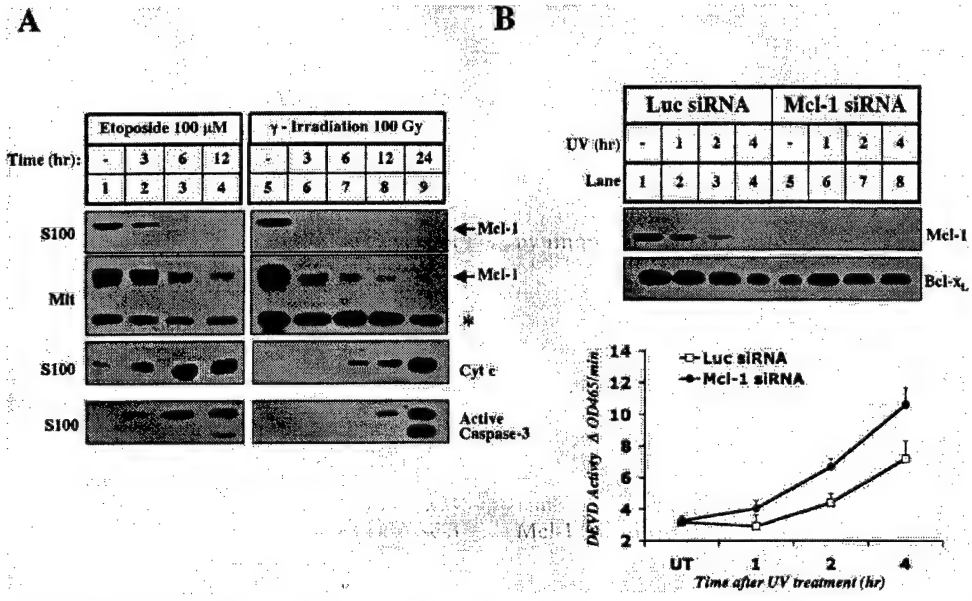

Figure 4. Mcl-1 disappears in the early stages of apoptosis induced by other DNA-damaging agents. (*A*) Mitochondria and S100 were isolated from HeLa cells that were left untreated (lanes *1,5*), treated with 100 μM Etoposide (Sigma; lanes *2–4*), or treated with 100 Gy of γ-irradiation (lanes *6–9*) and harvested for cytosol and mitochondria at the indicated times. The levels of cleaved caspase-3, cytochrome *c* and Mcl-1 were measured in S100. Mcl-1 mitochondrial levels were compared between the samples. The asterisk denotes a cross-reactive band that indicates equal loading. (*B*) Elimination of Mcl-1 by RNAi accelerates UV-induced apoptosis. HeLa cells were pretreated with Luciferase or Mcl-1 siRNA as described in Materials and Methods. Triplicate samples were harvested without treatment (UT) or at different time points after UV treatment. Whole-cell lysate prepared with 0.5% CHAPS was used to determine the levels of Mcl-1 and Bcl-x_L by Western blot and caspase-3 activity by a fluorogenic assay as described in Materials and Methods.

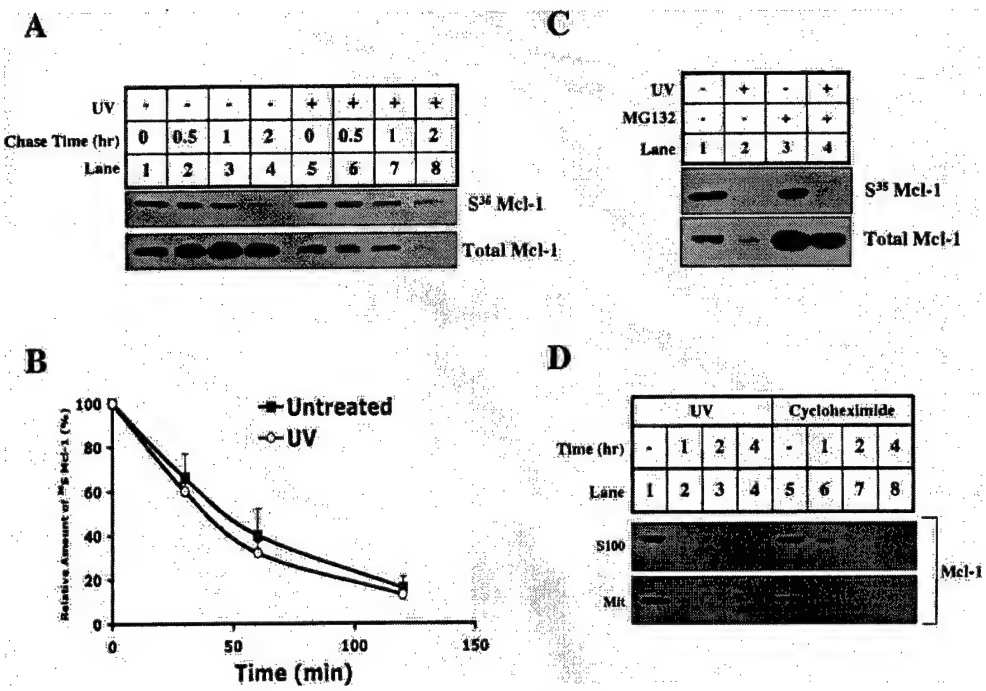

Figure 5. The synthesis of Mcl-1 is blocked by UV, and the protein half-life is unchanged. (*A*,*B*) HeLa cells were incubated in methionine starvation medium for 30 min before adding [^{35}S]methionine to pulse for 1 h. Following the pulse, cells were either UV-treated (lanes *5–8*) or untreated (lanes *1–4*), and then immediately chased by complete medium for 0 (lanes *1,5*), 30 min (lanes *2,6*), 60 min (lanes *3,7*), or 120 min (lanes *4,8*). Mcl-1 was immunoprecipitated and analyzed by SDS-PAGE. (*B*) The amount of ^{35}S-labeled Mcl-1 was quantified by PhosphorImager analysis and plotted with respect to time. Values are representative of three independent experiments. (*C*) HeLa cells were either left untreated (lanes *1,3*) or UV-treated (lanes *2,4*), and pretreated with DMSO (lanes *1,2*) or 10 μM MG132 (lanes *3,4*), and then methionine-starved for 30 min followed by 1 h of labeling with [^{35}S]methionine. After labeling, the synthesis of new Mcl-1 was measured by Mcl-1 immunoprecipitation, and total Mcl-1 levels were determined by Western blot. (*D*) HeLa cells were left untreated (lanes *1,5*), UV-treated (lanes *2–4*), or treated with 20 μM cycloheximide (lanes *6–8*). At the indicated times after treatment, the cells were harvested for S100 and mitochondria. The levels of Mcl-1 were determined by Western blotting both fractions.

tent with the inhibition of its synthesis, we treated HeLa cells with an inhibitor of protein synthesis, cycloheximide, and checked the fate of Mcl-1 protein in the same time course as UV irradiation. As shown in Figure 5D, Mcl-1 disappeared after UV or cycloheximide treatment at a similar rate.

Proteasome-mediated degradation of Mcl-1 is required for UV-induced apoptosis

The short half-life of Mcl-1 is due to constitutive polyubiquitination and subsequent degradation by the proteasome (data not shown). Hence, to test whether the elimination of Mcl-1 is necessary for apoptosis, we incubated UV-treated cells in the presence of MG132 or another structurally unrelated proteasome inhibitor, epoxomicin (Meng et al. 1999). As shown in Figure 6A, both inhibitors efficiently block the degradation of Mcl-1 (Fig. 6A, lanes 5–12). Concomitantly, they also block other biochemical markers of apoptosis including Bcl-x_L and Bax translocation, Bak oligomerization (data not shown), cytochrome *c* release, and caspase-3 activation.

To ensure that the antiapoptotic effect of the proteasome inhibitors was due specifically to the accumulation of Mcl-1, we first eliminated Mcl-1 using RNAi and then tested the effect of the proteasome inhibitors. As shown in Figure 6B, pretreatment of HeLa cells with Mcl-1 siRNA completely blocked the ability of MG132 or epoxomicin (data not shown) to prevent Bcl-x_L and Bax translocation, cytochrome *c* release, and caspase-3 activation (Fig. 6B, lanes 4–6, and bar graph). However, in control siRNA-treated cells, proteasome inhibitors efficiently blocked all of these events (Fig. 6B, lanes 1–3, and bar graph).

Mcl-1 is upstream of Bcl-x_L and Bax translocation

The ability of proteasome inhibitors to block Bcl-x_L/Bax translocation, Bak oligomerization, cytochrome *c* release, and caspase-3 activation indicates that proteasome-mediated degradation of Mcl-1 is an upstream step in this apoptotic pathway. This hypothesis predicts that if the levels of Mcl-1 are artificially elevated, downstream events such as Bax and Bcl-x_L translocation will

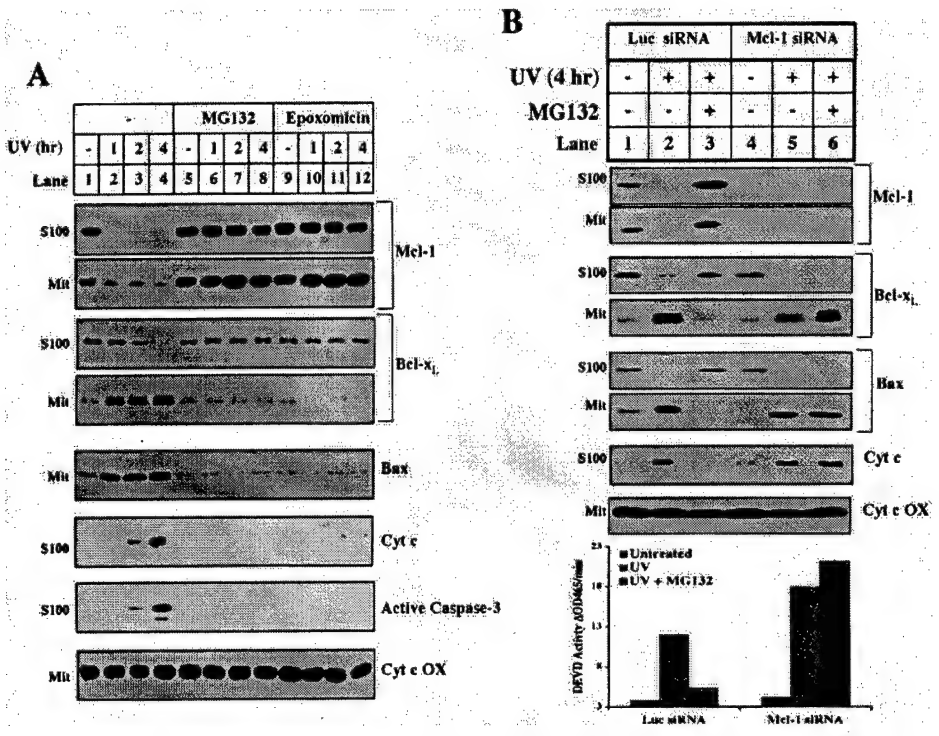

Figure 6. Proteasome inhibitors block the decrease of Mcl-1, the translocation of Bcl-x_L, and other apoptotic events after UV treatment. (*A*) Mitochondria and S100 were fractionated from HeLa cells treated with UV for different amounts of time and pretreated for 1 h with DMSO (lanes *1–4*), 10 µM MG132 (lanes *5–8*), or 10 µM epoxomicin (lanes *9–12*). The levels of Mcl-1, Bcl-x_L, Bax, and cytochrome *c* oxidase were measured in the mitochondria. The levels of Mcl-1, Bcl-x_L, cytochrome *c*, and cleaved caspase-3 were measured in the cytosol. (*B*) Six 6-well dishes of HeLa cells were transfected with Luciferase or Mcl-1 siRNA as described in Materials and Methods. For each sample, two dishes were pretreated (30 min) 24 h later with DMSO (lanes *1,2,4,5*) or 10 µM MG132 (lanes *3,6*). Cells were either left untreated (lanes *1,4*) or UV-treated (lanes *2,3,5,6*) and harvested 4 h later. A small aliquot of the cell pellet was used to make whole cell lysate in 0.5% CHAPS for the caspase assay. The remaining cells were fractionated for mitochondria and S100. The levels of Mcl-1, Bcl-x_L, Bax, and cytochrome *c* oxidase were measured in the mitochondria. The levels of Mcl-1, Bcl-x_L, Bax, and cytochrome *c* were measured in the cytosol.

be delayed. We tested this hypothesis by developing two independent HeLa cell lines that stably express Flag-tagged Mcl-1 under a CMV promoter. In response to UV irradiation, both the levels of endogenous Mcl-1 and the tagged Mcl-1 expressed from the transgene decreased (Fig. 7A, lanes 5–12). Nevertheless, 4 h after UV irradiation, there was still some Flag-tagged Mcl-1 protein in the cytosol and mitochondria (Fig. 7A, lanes 8,12). When the levels of Mcl-1 are artificially elevated in Mcl-1 transgenic cells, cytochrome *c*, Bcl-x_L, and Bax do not translocate 4 h after UV irradiation in contrast to a control HeLa cell line that expresses the Neo vector (Fig. 7A, lanes 1–4), indicating that the elimination of Mcl-1 is a required upstream event for Bcl-x_L and Bax translocation.

To verify that Mcl-1 degradation and Bax/Bcl-x_L translocation are sequential events and not merely a product of antiapoptotic protein overexpression, we examined a Bcl-x_L-overexpressing HeLa cell line, which also does not release cytochrome *c* after UV treatment (data not shown). After UV treatment, despite extremely high levels of exogenous Bcl-x_L expression, Mcl-1 is eliminated at the same rate (Fig. 7B, lanes 4–6). Moreover, in contrast to Mcl-1 overexpression, exogenous expression of Bcl-x_L does not inhibit the translocation of Bax or Bcl-x_L to the mitochondria (Fig. 7C, lanes 6–10). Bcl-x_L overexpression does, however, block the oligomerization of Bax on the mitochondria (Fig. 7C, bottom panel) suggesting the following sequence of events: Mcl-1 degradation, Bcl-x_L/Bax translocation to the mitochondria, Bax oligomerization, and cytochrome *c* release.

Discussion

Mcl-1 and Bcl-x_L function at different steps in a UV-induced apoptotic pathway

The Bcl-2 family is composed of both pro- and antiapoptotic proteins that share sequence and structural homology (Cory and Adams 2002). Most of the initial studies of the Bcl-2 family used overexpression as a means of characterizing the apoptotic nature of the proteins (Vaux et

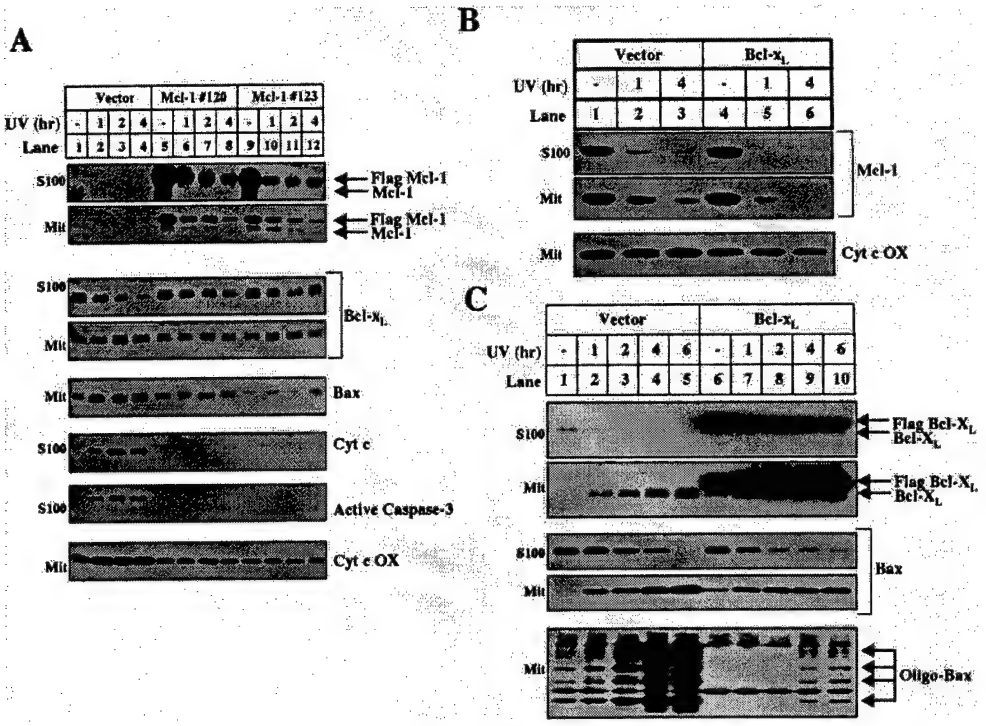

Figure 7. The disappearance of Mcl-1 is a required upstream event for UV-induced apoptosis. (*A*) After UV treatment, mitochondria and S100 were isolated from vector control (lanes *1–4*) and two independent Flag-Mcl-1-overexpressing lines: line 120 (lanes *5–8*) and line 123 (lanes *9–12*). The levels of Mcl-1, Bcl-x_L, Bax, and cytochrome *c* oxidase were measured in the mitochondria. The levels of Mcl-1, Bcl-x_L, cytochrome *c*, and cleaved caspase-3 were measured in the cytosol. (*B*) Mcl-1 levels were analyzed in mitochondria and S100 fractionated from Vector (lanes *1–3*) or Flag-Bcl-x_L-overexpressing (lanes *4–6*) cells treated with UV for 1 h (lanes *2,5*) or 4 h (lanes *3,6*). (*C*) HeLa cells that stably express the Neo vector (lanes *1–5*) or Flag-Bcl-x_L (lanes *6–10*) were left untreated or UV-treated and harvested between 1 and 6 h later for mitochondria and S100. The levels of Flag-Bcl-x_L, Bcl-x_L, and Bax were determined in the S100 and mitochondria. Mitochondria were also used to evaluate Bax oligomerization.

al. 1988; Oltvai et al. 1993). Although effective at separating pro- and antiapoptotic characteristics, overexpression studies do not differentiate specific functions within the pro- or antiapoptotic groups.

Recently, genetic experiments separated the proapoptotic members of the Bcl-2 family into two functional classes: Bax/Bak and BH3-only proteins. BH3-only proteins are upstream of Bax/Bak because BH3-only proteins fail to trigger cytochrome *c* release in Bax/Bak-deficient cells (Cheng et al. 2001; Wei et al. 2001; Zong et al. 2001). On the other hand, mouse knock'out models have proven less effective at sorting out the functions of the antiapoptotic Bcl-2 family members. Mcl-1-null embryos have a preimplantation lethal phenotype, revealing only that Mcl-1 has an important and early role in development (Rinkenberger et al. 2000). The knockout of Bcl-x_L was also early embryonic lethal; the embryo displayed widespread apoptosis, indicating that this gene also functions early in development (Motoyama et al. 1995).

Using a biochemical approach, this study demonstrates that the antiapoptotic members of the Bcl-2 family also function at distinct steps. Mcl-1 is at the apical point in the pathway. The disappearance of Mcl-1 is required for downstream events including Bcl-x_L and Bax translocation, Bak and Bax oligomerization, cytochrome *c* release, and caspase activation. Mcl-1 may regulate downstream events by sequestering proapoptotic BH3 proteins that activate downstream events such as Bax/Bcl-x_L translocation and Bax/Bak oligomerization (Letai et al. 2002).

The cytosol-to-membrane translocation of both proapoptotic Bax and antiapoptotic Bcl-x_L is counterintuitive and seemingly counterproductive. However, because the levels of Bax are in excess of Bcl-x_L in HeLa cells (M. Fang and X. Wang, unpubl.), continuous translocation of Bax may eventually result in excess free Bax on the mitochondria, leading to oligomerization. Consistent with this model, Bcl-x_L overexpression blocks oligomerization but does not affect Bcl-x_L or Bax translocation (Fig. 7C). The effect of Bcl-2 overexpression on Bax translocation when apoptosis is induced by growth factor deprivation is variable. Bcl-2 overexpression blocks Bax translocation in B-cells after IL-3 withdrawal but not in primary neurons after NGF withdrawal (Gross et al. 1998; Putcha et al. 1999).

Mcl-1 is an apical sensor for apoptotic stimuli

The elimination of Mcl-1 is not limited to UV irradiation. Genotoxic stress induced by etoposide or γ-irradiation also efficiently induces Mcl-1 elimination (Fig. 4A), suggesting that the disappearance of Mcl-1 may be initiated through a common pathway. Previous studies have shown that UV irradiation, γ-irradiation, and etoposide treatment induce an arrest in protein synthesis (Clemens et al. 2000). UV light treatment triggers the ubiquitination and subsequent degradation of RNA polymerase II and the GCN2-mediated phosphorylation of eIF2α to arrest transcription and translation, respectively (Bregman et al. 1996; Deng et al. 2002). Because Mcl-1 protein and mRNA both have short half-lives (Yang et al. 1996), Mcl-1 can serve as a sensor of acute changes in the rate of mRNA and protein synthesis after genotoxic stress. On the other hand, increased Mcl-1 synthesis may enhance the general well being of the cell. Growth factor pathways that promote cell survival through the AKT/PI3 kinase pathway up-regulate Mcl-1 mRNA levels (Wang et al. 1999; Huang et al. 2000; Liu et al. 2001). Our study predicts that this up-regulation of Mcl-1 may explain how growth factors render cells less sensitive to apoptotic stimuli (Datta et al. 1999).

Although the elimination of Mcl-1 by an arrest in synthesis is required, this event is not sufficient for activation of the mitochondrial apoptosis pathway. The elimination of Mcl-1 by RNAi did not induce Bax/Bcl-x_L translocation, Bax/Bak oligomerization (data not shown), cytochrome *c* release, and caspase activation (Figs. 4B, 6B). Therefore, another UV-induced event in addition to the elimination of Mcl-1 must be required to promote this pathway. In other systems, it appears that Mcl-1 disappearance is both necessary and sufficient for apoptosis. For example, it is possible to induce apoptosis in a multiple myeloma cell line merely by treating it with inhibitors of protein synthesis or by specifically removing Mcl-1 with anti-sense oligonucleotides (Zhang et al. 2002). In this system, depletion of Mcl-1 is the only hit needed for apoptosis.

Stress-activated pathways have also been implicated in UV-induced cytochrome *c* release. Fibroblasts deficient in JNK1/JNK2 kinases fail to release cytochrome *c* in response to UV treatment (Tournier et al. 2000). JNK kinases might activate the Mcl-1 pathway by directly phosphorylating and inactivating Mcl-1 as they do after oxidative stress (Inoshita et al. 2002). Alternatively, JNK activity might regulate pathways leading to a stop in Mcl-1 synthesis or initiate a separate required pathway. All of these possibilities can now be tested in JNK-deficient cells.

The quest to delineate the apoptosis pathway upstream of cytochrome *c* release is partly motivated by data suggesting that mitochondrial damage from pro-apoptotic Bcl-2 family members is toxic to cells even in the absence of caspase activation (Xiang et al. 1996). Hence, potential therapies that inhibit apoptosis before the onset of mitochondrial dysfunction are likely to be more effective than direct caspase inhibitors. The sequential nature of the apoptotic signal transduction pathway revealed by this study offers several points for potential intervention. Novel therapies that block Mcl-1 degradation may effectively prevent apoptosis and cell death.

Materials and methods

Reagents

The following antibodies were used for Western blots: monoclonal Bak Ab-1 (Oncogene), monoclonal cytochrome *c* (Pharmingen), polyclonal Bcl-x_L (Cell signaling), monoclonal Mcl-1 (Pharmingen), monoclonal caspase-2 (Pharmingen), polyclonal caspase-3 (cell signaling), monoclonal caspase-9 (Cell Signaling), and polyclonal Bax N-20 (Santa Cruz). Immunoprecipitations or immunodepletions for Mcl-1 and Bcl-x_L were performed with polyclonal antibodies to Mcl-1 (Pharmingen) and Bcl-x_L (Cell Signaling). Z-VAD.fmk, cycloheximide, MG132, epoxomicin, caspase-3 fluorogenic II substrate, phosphatase inhibitor cocktail II, and λ Protein Phosphatase were all obtained from Calbiochem.

UV treatment and cellular fractionation

HeLa cells were plated at a density of 2×10^7 cells in a 15-cm dish with DMEM medium supplemented with 10% FBS. Several hours before treatment, each dish was replaced with 13 mL of fresh medium. The cover of each dish was removed before the cells were treated in a Stratagene stratalinker with 200 mJ/cm^2 of UV irradiation (254 nm). At the indicated times after treatment, cells were scraped, collected, and washed once in PBS. The cell pellet was resuspended in 5 times the volume of Buffer A (20 mM HEPES, 10 mM KCl, 1.5 mM $MgCl_2$, 1 mM EDTA, 1 mM EGTA, 1 mM DTT, 0.1 mM PMSF, and Complete Protease Inhibitor, Roche) supplemented with 250 mM sucrose. The resuspended cell pellet was incubated on ice for 15 min before the cells were broken by passing them through a 22-gauge needle 25 times. The resulting broken cell mixture was centrifuged in three sequential steps: 1000*g*, 10,000*g*, and 100,000*g*. The 10,000*g* pellet was considered the "mitochondrial" fraction and the 100,000*g* supernatant (S100) the cytosol. Mitochondrial pellets were lysed in SDS loading buffer, and equal volumes were analyzed by SDS-PAGE. S100 protein concentrations were normalized using the Bio-Rad Bradford reagent.

Recombinant Mcl-1 and Bcl-x_L

The cDNA of full-length human Mcl-1 was subcloned into *NdeI* and *SapI* sites of the pTYB1 vector (New England Biolabs). Full-length Bcl-x_L cDNA was cloned into *NdeI* and *XhoI* sites of the pet15B vector (Novagen). BL21 (DE3) cells were transformed with these constructs, and the recombinant proteins were purified according to the manufacturer's protocol (New England Biolabs and QIAGEN, respectively). The eluted recombinant Mcl-1 protein was purified in two additional steps: Hitrap Q sepharose and Superdex 200 size exclusion chromatography. The eluted recombinant Bcl-x_L was further purified on a Hitrap Q sepharose column.

In vitro assays for mitochondrial priming and inhibitory activity

Mitochondria (0.67 mg/mL) alone or with S100 (4 mg/mL) were incubated in Buffer A with 250 mM sucrose and 150 mM NaCl

at 37°C for 15 min. Following incubation, the mitochondria were pelleted, and the supernatant was tested for cytochrome *c* release. The mitochondria pellet was tested for Bak oligomerization (Wei et al. 2000).

During biochemical fractionation, to increase our yield we made S100 from HeLa cells using Buffer A without sucrose. Hypotonic buffers cause mitochondrial rupture and cytochrome *c* contamination in the S100. Contaminating cytochrome *c* was removed from the S100 by incubating with SP-sepharose XL resin (Amersham) at 4°C for 1 h. Cytochrome *c* binds SP resin, but our activity does not (data not shown).

Mcl-1 RNA interference

Annealed, purified, and desalted double-stranded siRNA, Luciferase (AACGUACGCGGAAUACUUCGA), and Mcl-1 (AAGAAACGCGGUAAUCGGACU) were ordered from Dharmacon Research. Then 1.5×10^5 HeLa cells were plated in a 6-well dish on day 0. On day 1, cells were transfected with 200 nM siRNA in Opti-MEM medium (Invitrogen) without FBS using Oligofectamine reagent (Invitrogen) according to the manufacturer's transfection protocol. After 4 h, FBS was added to a final concentration of 10%. On day 2, the medium over the cells was adjusted to 1 mL before treatment.

Fluorogenic assay for caspase-3 activity

In a 20-µL system, 10 µg of whole cell lysate was incubated in Buffer A containing 0.125% CHAPS and 10 µM fluorogenic DEVD substrate. Samples were applied to a 384-well microplate, and the reaction was carried out at 30°C. Every 10 min, the samples were excited at 360 nM and the $OD_{465\ nM}$ was measured by the SpectraFluor4 spectrometry reader (TECAN).

Mcl-1 pulse-chase experiments

HeLa suspension cells were plated at a density of 5×10^6 cells per 10-cm dish. For the pulse chase, the cells were washed with phosphate-buffered saline (PBS), starved in methionine/cysteine-free DMEM (GIBCO-BRL) at 37°C for 30 min, then labeled with 200–500 µCi of [^{35}S]cysteine/methionine (ICN) per plate at 37°C for 60 min. After labeling, the cells were chased with complete DMEM containing 10% FBS and 2 M cold methionine at 37°C for the indicated amount of time. A total of 10^7 cells were collected at each time point. Cells were subsequently subjected to immunoprecipitation analysis as described below.

Immunoprecipitation

For immunodepletion and Mcl-1 immunoprecipitation experiments, samples were incubated with beads precoupled to antibody. Protein A agarose beads (Santa Cruz; 0.5-mL bed volume) were incubated in 1 mL of PBS with 1 mg/mL of BSA at 4°C alone overnight, with 100 µg of polyclonal antibodies to Mcl-1 or Bcl-x_L. After incubation, the beads were pelleted by centrifugation and washed at least 5 times with Buffer A. For immunodepletion reactions, 50 µL of beads were incubated with 500 µL of S100 (5 mg/mL) with rotation at 4°C overnight. After incubation, the beads were pelleted, and the supernatant was collected as immunodepleted S100.

For pulse-chase experiments, radiolabeled cells were lysed in cold RIPA lysis buffer (10 mM Tris-HCl at pH 7.4, 1% NP-40, 1 mM EDTA, 0.1% SDS, 150 mM NaCl) with fresh proteinase inhibitors, followed by breaking through a 25-gauge syringe 20 times. Equivalent amounts of cell extract were adjusted to equal volumes with RIPA buffer, precleared with protein A agarose beads, and clarified by centrifugation. Lysates were then incubated with polyclonal antibodies to Mcl-1 at 4°C overnight, and the immune complexes were precipitated with protein A agarose beads for 4–6 h. The immunoprecipitates were washed five times with RIPA buffer and incubated at 95°C for 5 min in SDS sample buffer. Samples were subjected to (SDS-PAGE) followed by autoradiography.

Mcl-1- and Bcl-x_L-overexpressing stable cell lines

Full-length Mcl-1 cDNA was cloned into *Hin*dIII and *Bam*HI sites of p3XFLAG-CMV-10 (Sigma). The resulting fusion protein was full-length Mcl-1 with three Flag epitopes at the N terminus followed by a two-amino-acid linker. The full-length Bcl-x_L was cloned into *Xho*I and *Nde*I sites of pCDNA 3.1(–) (Invitrogen) with a single Flag tag at the N terminus followed by a short linker sequence. Empty vector or subcloned plasmids were transfected into 5×10^5 attached HeLa cells grown in DMEM with 10% FBS using Lipofectamine Plus transfection reagent (Invitrogen) according to the manufacturer's protocol. Then, 2 d later, the cells were transferred to 20 100-mm dishes in DMEM with 10% FBS and 0.5 mg/mL of G418. After several weeks, individual clones were lifted and tested for expression of the transgene.

Acknowledgments

We thank X. Luo for Bcl-x_L expression constructs. X. Jiang and I. Alibhai gave us critical insight and helpful advice. Michael Brown, Joseph Goldstein, and A. Shulman offered helpful advice in the preparation of our manuscript. R. Harold provided valuable technical assistance. This work was also supported by NIH (GMR01-57158) and the Welch foundation (2-1412). D.N. and E.T. are medical scientist training fellows supported by the Perot Family foundation.

The publication costs of this article were defrayed in part by payment of page charges. This article must therefore be hereby marked "advertisement" in accordance with 18 USC section 1734 solely to indicate this fact.

References

Acehan, D., Jiang, X., Morgan, D.G., Heuser, J.E., Wang, X., and Akey, C.W. 2002. Three-dimensional structure of the apoptosome: Implications for assembly, procaspase-9 binding, and activation. *Mol. Cell* **9:** 423–432.

Bossy-Wetzel, E., Newmeyer, D.D., and Green, D.R. 1998. Mitochondrial cytochrome *c* release in apoptosis occurs upstream of DEVD-specific caspase activation and independently of mitochondrial transmembrane depolarization. *EMBO J.* **17:** 37–49.

Bregman, D.B., Halaban, R., van Gool, A.J., Henning, K.A., Friedberg, E.C., and Warren, S.L. 1996. UV-induced ubiquitination of RNA polymerase II: A novel modification deficient in Cockayne syndrome cells. *Proc. Natl. Acad. Sci.* **93:** 11586–11590.

Cheng, E.H., Wei, M.C., Weiler, S., Flavell, R.A., Mak, T.W., Lindsten, T., and Korsmeyer, S.J. 2001. BCL-2, BCL-X_L sequester BH3 domain-only molecules preventing BAX- and BAK-mediated mitochondrial apoptosis. *Mol. Cell* **8:** 705–711.

Clemens, M.J., Bushell, M., Jeffrey, I.W., Pain, V.M., and Morley, S.J. 2000. Translation initiation factor modifications and the regulation of protein synthesis in apoptotic cells. *Cell Death Differ.* **7:** 603–615.

Cory, S. and Adams, J.M. 2002. The Bcl2 family: Regulators of the cellular life-or-death switch. *Nat. Rev. Cancer* **2:** 647–656.

Datta, S.R., Brunet, A., and Greenberg, M.E. 1999. Cellular survival: A play in three Akts. *Genes & Dev.* **13:** 2905–2927.

Deng, J., Harding, H.P., Raught, B., Gingras, A.C., Berlanga, J.J., Scheuner, D., Kaufman, R.J., Ron, D., and Sonenberg, N. 2002. Activation of GCN2 in UV-irradiated cells inhibits translation. *Curr. Biol.* **12:** 1279–1286.

Du, C., Fang, M., Li, Y., Li, L., and Wang, X. 2000. Smac, a mitochondrial protein that promotes cytochrome *c*-dependent caspase activation by eliminating IAP inhibition. *Cell* **102:** 33–42.

Duelli, D.M. and Lazebnik, Y.A. 2000. Primary cells suppress oncogene-dependent apoptosis. *Nat. Cell Biol.* **2:** 859–862.

Elbashir, S.M., Harborth, J., Lendeckel, W., Yalcin, A., Weber, K., and Tuschl, T. 2001. Duplexes of 21-nucleotide RNAs mediate RNA interference in cultured mammalian cells. *Nature* **411:** 494–498.

Gross, A., Jockel, J., Wei, M.C., and Korsmeyer, S.J. 1998. Enforced dimerization of BAX results in its translocation, mitochondrial dysfunction and apoptosis. *EMBO J.* **17:** 3878–3885.

Gross, A., McDonnell, J.M., and Korsmeyer, S.J. 1999. BCL-2 family members and the mitochondria in apoptosis. *Genes & Dev.* **13:** 1899–1911.

Hegde, R., Srinivasula, S.M., Zhang, Z., Wassell, R., Mukattash, R., Cilenti, L., DuBois, G., Lazebnik, Y., Zervos, A.S., Fernandes-Alnemri, T., et al. 2002. Identification of Omi/HtrA2 as a mitochondrial apoptotic serine protease that disrupts inhibitor of apoptosis protein–caspase interaction. *J. Biol. Chem.* **277:** 432–438.

Hengartner, M.O. 2000. The biochemistry of apoptosis. *Nature* **407:** 770–776.

Hsu, Y.T., Wolter, K.G., and Youle, R.J. 1997. Cytosol-to-membrane redistribution of Bax and Bcl-X_L during apoptosis. *Proc. Natl. Acad. Sci.* **94:** 3668–3672.

Huang, H.M., Huang, C.J., and Yen, J.J. 2000. Mcl-1 is a common target of stem cell factor and interleukin-5 for apoptosis prevention activity via MEK/MAPK and PI-3K/Akt pathways. *Blood* **96:** 1764–1771.

Inoshita, S., Takeda, K., Hatai, T., Terada, Y., Sano, M., Hata, J., Umezawa, A., and Ichijo, H. 2002. Phosphorylation and inactivation of myeloid cell leukemia 1 by JNK in response to oxidative stress. *J. Biol. Chem.* **277:** 43730–43734.

Johnstone, R.W., Ruefli, A.A., and Lowe, S.W. 2002. Apoptosis: A link between cancer genetics and chemotherapy. *Cell* **108:** 153–164.

Kim, C.N., Wang, X., Huang, Y., Ibrado, A.M., Liu, L., Fang, G., and Bhalla, K. 1997. Overexpression of Bcl-X_L inhibits Ara-C-induced mitochondrial loss of cytochrome *c* and other perturbations that activate the molecular cascade of apoptosis. *Cancer Res.* **57:** 3115–3120.

Kluck, R.M., Bossy-Wetzel, E., Green, D.R., and Newmeyer, D.D. 1997. The release of cytochrome *c* from mitochondria: A primary site for Bcl-2 regulation of apoptosis. *Science* **275:** 1132–1136.

Korsmeyer, S.J., Wei, M.C., Saito, M., Weiler, S., Oh, K.J., and Schlesinger, P.H. 2000. Pro-apoptotic cascade activates BID, which oligomerizes BAK or BAX into pores that result in the release of cytochrome *c*. *Cell Death Differ.* **7:** 1166–1173.

Kuwana, T., Mackey, M.R., Perkins, G., Ellisman, M.H., Latterich, M., Schneiter, R., and Newmeyer, D.D. 2002. Bid, Bax, and lipids cooperate to form supramolecular openings in the outer mitochondrial membrane. *Cell* **111:** 331–342.

Lassus, P., Opitz-Araya, X., and Lazebnik, Y. 2002. Requirement for caspase-2 in stress-induced apoptosis before mitochondrial permeabilization. *Science* **297:** 1352–1354.

Letai, A., Bassik, M.C., Walensky, L.D., Sorcinelli, M.D., Weiler, S., and Korsmeyer, S.J. 2002. Distinct BH3 domains either sensitize or activate mitochondrial apoptosis, serving as prototype cancer therapeutics. *Cancer Cell* **2:** 183–192.

Li, L.Y., Luo, X., and Wang, X. 2001. Endonuclease G is an apoptotic DNase when released from mitochondria. *Nature* **412:** 95–99.

Li, P., Nijhawan, D., Budihardjo, I., Srinivasula, S.M., Ahmad, M., Alnemri, E.S., and Wang, X. 1997. Cytochrome *c* and dATP-dependent formation of Apaf-1/caspase-9 complex initiates an apoptotic protease cascade. *Cell* **91:** 479–489.

Liu, H., Perlman, H., Pagliari, L.J., and Pope, R.M. 2001. Constitutively activated Akt-1 is vital for the survival of human monocyte-differentiated macrophages. Role of Mcl-1, independent of nuclear factor (NF)-κB, Bad, or caspase activation. *J. Exp. Med.* **194:** 113–126.

Martinou, J.C. and Green, D.R. 2001. Breaking the mitochondrial barrier. *Nat. Rev. Mol. Cell. Biol.* **2:** 63–67.

Martins, L.M., Iaccarino, I., Tenev, T., Gschmeissner, S., Totty, N.F., Lemoine, N.R., Savopoulos, J., Gray, C.W., Creasy, C.L., Dingwall, C., et al. 2002. The serine protease Omi/HtrA2 regulates apoptosis by binding XIAP through a reaper-like motif. *J. Biol. Chem.* **277:** 439–444.

Meng, L., Mohan, R., Kwok, B.H., Elofsson, M., Sin, N., and Crews, C.M. 1999. Epoxomicin, a potent and selective proteasome inhibitor, exhibits in vivo antiinflammatory activity. *Proc. Natl. Acad. Sci.* **96:** 10403–10408.

Motoyama, N., Wang, F., Roth, K.A., Sawa, H., Nakayama, K., Nakayama, K., Negishi, I., Senju, S., Zhang, Q., Fujii, S., et al. 1995. Massive cell death of immature hematopoietic cells and neurons in Bcl-x-deficient mice. *Science* **267:** 1506–1510.

Oltvai, Z.N., Milliman, C.L., and Korsmeyer, S.J. 1993. Bcl-2 heterodimerizes in vivo with a conserved homolog, Bax, that accelerates programmed cell death. *Cell* **74:** 609–619.

Palombella, V.J., Rando, O.J., Goldberg, A.L., and Maniatis, T. 1994. The ubiquitin–proteasome pathway is required for processing the NF-κ B1 precursor protein and the activation of NF-κ B. *Cell* **78:** 773–785.

Putcha, G.V., Deshmukh, M., and Johnson Jr., E.M. 1999. BAX translocation is a critical event in neuronal apoptosis: Regulation by neuroprotectants, BCL-2, and caspases. *J. Neurosci.* **19:** 7476–7485.

Rinkenberger, J.L., Horning, S., Klocke, B., Roth, K., and Korsmeyer, S.J. 2000. Mcl-1 deficiency results in peri-implantation embryonic lethality. *Genes & Dev.* **14:** 23–27.

Rodriguez, J. and Lazebnik, Y. 1999. Caspase-9 and APAF-1 form an active holoenzyme. *Genes & Dev.* **13:** 3179–3184.

Susin, S.A., Lorenzo, H.K., Zamzami, N., Marzo, I., Snow, B.E., Brothers, G.M., Mangion, J., Jacotot, E., Costantini, P., Loeffler, M., et al. 1999. Molecular characterization of mitochondrial apoptosis-inducing factor. *Nature* **397:** 441–446.

Suzuki, Y., Imai, Y., Nakayama, H., Takahashi, K., Takio, K., and Takahashi, R. 2001. A serine protease, HtrA2, is released from the mitochondria and interacts with XIAP, inducing cell death. *Mol. Cell* **8:** 613–621.

Tournier, C., Hess, P., Yang, D.D., Xu, J., Turner, T.K., Nimnual, A., Bar-Sagi, D., Jones, S.N., Flavell, R.A., and Davis, R.J. 2000. Requirement of JNK for stress-induced activation of the cytochrome *c*-mediated death pathway. *Science* **288:** 870–874.

Vander Heiden, M.G., Chandel, N.S., Williamson, E.K., Schumacker, P.T., and Thompson, C.B. 1997. Bcl-xL regulates the membrane potential and volume homeostasis of

mitochondria. *Cell* **91:** 627–637.
Vaux, D.L., Cory, S., and Adams, J.M. 1988. Bcl-2 gene promotes haemopoietic cell survival and cooperates with c-myc to immortalize pre-B cells. *Nature* **335:** 440–442.
Verhagen, A.M., Ekert, P.G., Pakusch, M., Silke, J., Connolly, L.M., Reid, G.E., Moritz, R.L., Simpson, R.J., and Vaux, D.L. 2000. Identification of DIABLO, a mammalian protein that promotes apoptosis by binding to and antagonizing IAP proteins. *Cell* **102:** 43–53.
Wang, J.M., Chao, J.R., Chen, W., Kuo, M.L., Yen, J.J., and Yang-Yen, H.F. 1999. The antiapoptotic gene mcl-1 is up-regulated by the phosphatidylinositol 3-kinase/Akt signaling pathway through a transcription factor complex containing CREB. *Mol. Cell. Biol.* **19:** 6195–6206.
Wei, M.C., Lindsten, T., Mootha, V.K., Weiler, S., Gross, A., Ashiya, M., Thompson, C.B., and Korsmeyer, S.J. 2000. tBID, a membrane-targeted death ligand, oligomerizes BAK to release cytochrome *c*. *Genes & Dev.* **14:** 2060–2071.
Wei, M.C., Zong, W.X., Cheng, E.H., Lindsten, T., Panoutsakopoulou, V., Ross, A.J., Roth, K.A., MacGregor, G.R., Thompson, C.B., and Korsmeyer, S.J. 2001. Proapoptotic BAX and BAK: A requisite gateway to mitochondrial dysfunction and death. *Science* **292:** 727–730.
Xiang, J., Chao, D.T., and Korsmeyer, S.J. 1996. BAX-induced cell death may not require interleukin 1 β-converting enzyme-like proteases. *Proc. Natl. Acad. Sci.* **93:** 14559–14563.
Yang, T., Buchan, H.L., Townsend, K.J., and Craig, R.W. 1996. MCL-1, a member of the BLC-2 family, is induced rapidly in response to signals for cell differentiation or death, but not to signals for cell proliferation. *J. Cell Physiol.* **166:** 523–536.
Zhang, B., Gojo, I., and Fenton, R.G. 2002. Myeloid cell factor-1 is a critical survival factor for multiple myeloma. *Blood* **99:** 1885–1893.
Zong, W.X., Lindsten, T., Ross, A.J., MacGregor, G.R., and Thompson, C.B. 2001. BH3-only proteins that bind pro-survival Bcl-2 family members fail to induce apoptosis in the absence of Bax and Bak. *Genes & Dev.* **15:** 1481–1486.

Cell, Vol. 114, 255–266, July 25, 2003, Copyright ©2003 by Cell Press

S Phase Activation of the Histone H2B Promoter by OCA-S, a Coactivator Complex that Contains GAPDH as a Key Component

Lei Zheng, Robert G. Roeder,* and Yan Luo*
Laboratory of Biochemistry and Molecular Biology
The Rockefeller University
1230 York Avenue
New York, New York 10021

Summary

We have isolated and functionally characterized a multicomponent Oct-1 coactivator, OCA-S which is essential for S phase-dependent histone H2B transcription. The p38 component of OCA-S binds directly to Oct-1, exhibits potent transactivation potential, is selectively recruited to the H2B promoter in S phase, and is essential for S phase-specific H2B transcription in vivo and in vitro. Surprisingly, p38 represents a nuclear form of glyceraldehyde-3-phosphate dehydrogenase, and binding to Oct-1, as well as OCA-S function, is stimulated by NAD^+ but inhibited by NADH. OCA-S also interacts with NPAT, a cyclin E/cdk2 substrate that is broadly involved in histone gene transcription. These studies thus link the H2B transcriptional machinery to cell cycle regulators, and possibly to cellular metabolic state (redox status), and set the stage for studies of the underlying mechanisms and the basis for coordinated histone gene expression and coupling to DNA replication.

Introduction

Histones are essential components of eukaryotic chromosomes and play key roles in their maintenance, replication, and function. The genes that encode the various histone subtypes (H1, H2A, H2B, H3, and H4) are present in multiple copies, regulated at both transcriptional and posttranscriptional levels, and expressed predominantly in an S phase- and DNA replication-dependent fashion. Earlier studies on transcriptional mechanisms identified essential subtype-specific regulatory elements (SSREs) in the promoters of the S phase-inducible histone genes, as well as transcription factors that bind directly to these elements (reviewed in Osley, 1991). The cognate SSRE binding factors, however, seem not to account for the S phase regulation of histone gene transcription. For example, the SSRE of the human H2B gene contains a conserved octamer sequence, 5′-ATG CAAAT-3′, that, along with the TATA box, is necessary and sufficient for S phase-dependent H2B transcription (LaBella et al., 1988). However, the ubiquitous octamer binding protein (Oct-1) that acts through this element (Fletcher et al., 1987) cannot account for the S phase regulation since it shows no variation in expression level, DNA binding activity, or modification during the G1 to S and S to G2 phases of the cell cycle (Segil et al., 1991). These studies suggested the possible involvement of an S phase-specific cofactor(s) or modification of the general transcription machinery in conferring S phase-specific H2B transcription.

Transcriptional cofactors facilitate functional communication between sequence-specific transcriptional activators bound to distal regulatory elements and the basal transcription machinery assembled on proximal core promoter elements (reviewed in Malik and Roeder, 2000). While most cofactors are ubiquitous and mediate the function of diverse activators on a variety of genes, a subset play more specialized roles in gene activation and thus provide a paradigm for cell- and gene-specific transcriptional regulation. This was exemplified by the biochemical identification of the B cell-specific coactivator OCA-B (*O*ct *C*o-*A*ctivator from *B* cells; Luo et al., 1992), which mediates B cell-specific immunoglobulin (Ig) promoter activation in conjunction with either the ubiquitously expressed Oct-1 or the B-cell-enriched Oct-2. OCA-B binds to the POU domains of the Oct factors and is the major determinant of B cell-restricted, octamer-dependent Ig promoter activity (reviewed in Luo and Roeder, 1999). Purified Oct-1 and OCA-B were shown to fully stimulate Ig promoters in a system reconstituted with highly purified general initiation factors and a general coactivator fraction termed USA; however, the failure of Oct-1 to stimulate transcription from an octamer-containing H2B promoter in this assay system led us to postulate the existence of an *O*ct-1 *C*o*A*ctivator in *S* phase (OCA-S) that confers high-level H2B promoter activation (Luo and Roeder, 1995).

More recent studies of cyclin E/cdk2, a kinase known to regulate the G1/S transition and multiple S phase events including histone synthesis (reviewed in Ewen, 2000), have identified a substrate (NPAT) that has been implicated in histone gene regulation. Thus, overexpression of NPAT stimulates H2B, H3, and H4 promoter activities in a manner that is dependent on the SSREs within each promoter and that requires phosphorylation of NPAT by cyclin E/cdk2 (Ma et al., 2000; Zhao et al., 2000). Chromatin immunoprecipitation (ChIP) assays further indicated an association of NPAT, as well as cyclin E, with the H2B, H3, and H4 promoters (Zhao et al., 2000). These studies demonstrated an apparently global role for NPAT in the regulation of histone transcription, although its mechanism of action on individual histone genes, and whether it acts directly or indirectly, is not yet known.

Here, we describe the functional identification and purification of the OCA-S activity. Further characterization of this multicomponent cofactor has established a key role(s) for the p38 subunit, identical to glyceraldehyde-3-phosphate dehydrogenase (GAPDH), in mediating S phase-inducible H2B promoter activation, as well as a link between OCA-S and NPAT.

Results

OCA-S Copurifies with Seven Polypeptides

Although high level octamer-dependent transcription of the H2B promoter was observed in nuclear extracts from

*Correspondence: luoy@mail.rockefeller.edu (Y.L.); roeder@mail.rockefeller.edu (R.G.R.).

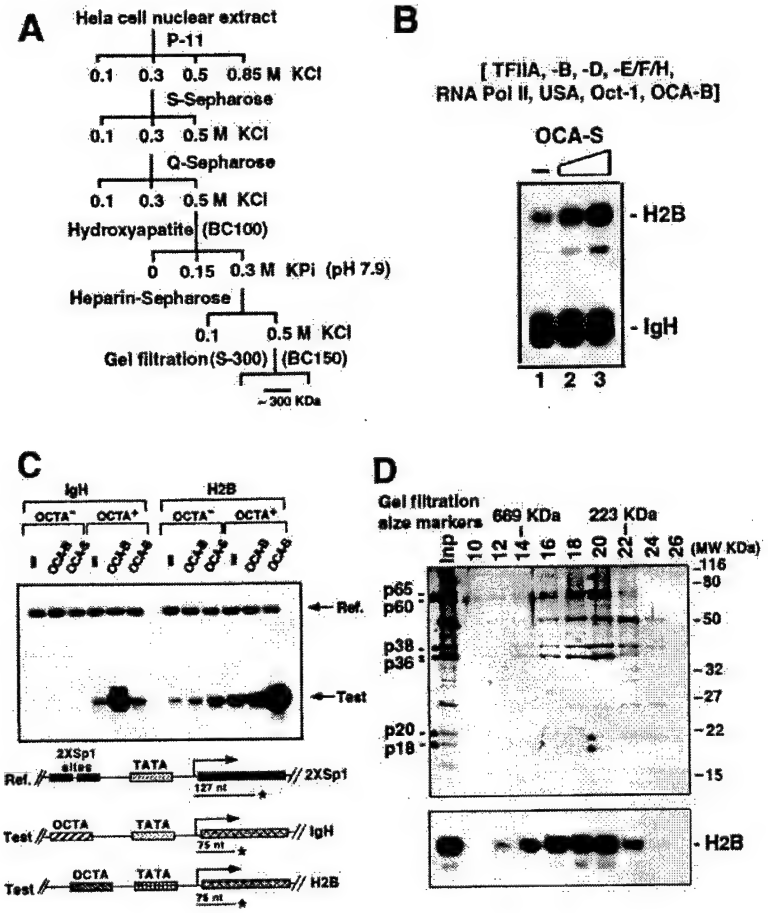

Figure 1. Identification and Purification of the OCA-S Activity

(A) Purification scheme.

(B) Identification of the OCA-S activity. Reactions contained the purified components indicated at the top of the image and 0 (lane 1), 6 (lane 2), or 15 (lane 3) μg of P11 0.3 M KCl OCA-S fraction. Transcription levels were measured by primer extension with 75 nt (IgH) and 110 nt (H2B) signals.

(C) Differential functions of OCA-B and OCA-S on IgH and H2B promoters. Templates containing promoter sequences with an intact (OCTA$^+$) or mutated (OCTA$^-$) octamer element were assayed in the presence of a reference Sp1-dependent template. The system contained the same components as in (B) except for the addition of Sp1 and omission of OCA-B. Coactivators OCA-B (recombinant) and OCA-S (hydroxyapatite fraction) were added as indicated.

(D) Polypeptide composition of the purified OCA-S activity. Upper image, protein profiles revealed by SDS-PAGE analysis. The Input (Inp) lane corresponds to the OCA-S fraction prior to S300 chromatography and the remaining lanes correspond to S300 column fractions (indicated by numbers). Lower image, OCA-S activity examined for the above-described fractions in the assay system described in (B). The upper image also highlights (by dots) the activity peak (#20) along with polypeptides that correlate with the OCA-S activity, with their molecular weights in kDa indicated on the left. The positions of molecular weight (MW) markers for the gel are shown on the right.

dividing HeLa cells, only basal transcription was observed in an assay system that contained purified general transcription factors, the USA coactivator fraction, purified Oct-1, and the B-cell coactivator OCA-B (Luo and Roeder, 1995). However, transcription of the H2B promoter in this assay system was markedly and selectively stimulated by a HeLa nuclear extract-derived 0.3 M KCl phosphocellulose (P11) fraction (Figure 1A) that contained most of this OCA-S activity (Figure 1B). The OCA-S activity in the P11 fraction was further enriched by S-Sepharose, Q-Sepharose, and hydroxyapatite steps, resulting in an overall purification of ~16,000-fold (Figure 1A).

To investigate the promoter specificity of OCA-B versus OCA-S, we compared the functions of recombinant OCA-B and highly purified OCA-S (hydroxyapatite fraction) on wild-type or octamer mutant H2B and immunoglobulin heavy chain (IgH) promoters cloned upstream of the same reporter gene (Figure 1C). OCA-S stimulated octamer-/Oct-1-dependent transcription from the H2B promoter, but not from the IgH promoter, whereas the reverse was true for OCA-B. A weak stimulatory effect of OCA-S on the octamer-independent transcription from the H2B promoter was also observed (Figure 1C), suggesting a potential role of OCA-S in a core promoter interaction.

The OCA-S enriched hydroxyapatite fraction was further purified by chromatography on heparin-Sepharose and then subjected to gel filtration on Sephacryl 300 (S300). Fractions were analyzed by SDS-PAGE (Figure 1D, upper image) and for OCA-S activity (lower image). This step resulted in an overall purification of ~30,000-fold and an estimated native size of ~300 kDa for OCA-S. The OCA-S activity coeluted with seven polypeptides, whose identities were revealed by peptide sequencing. p20 and p18 were identified as nm23-H1 and nm23-H2, respectively, and are thought to possess nucleoside diphosphate (NDP) kinase activity (reviewed in Freije et al., 1998). One polypeptide in the p36 doublet band was identified as uracil-DNA glycosylase (UNG), whereas the other was identified as LDH (lactate dehydrogenase). The 38 kDa protein was identified as glyceraldehyde-3-phosphate dehydrogenase (GAPDH). Although well-characterized glycolytic enzymes are localized predominantly in the cytoplasm, nuclear localization and DNA binding activities of GAPDH and LDH have been documented (reviewed in Ronai, 1993). The p65 and p60 proteins were identified as Hsp70 and Sti1, which are components of molecular chaperones (reviewed in Frydman and Hohfeld, 1997).

p38/GAPDH Interacts Directly with Oct-1

In view of the interaction of OCA-B with Oct-1/-2 POU domains (Luo and Roeder, 1995), we examined the seven OCA-S-associated polypeptides for similar interaction(s). When in vitro translated proteins were tested in GST pull-down assays, only p38/GAPDH bound to GST-fused POU-1 and POU-2 (Figure 2A). Moreover,

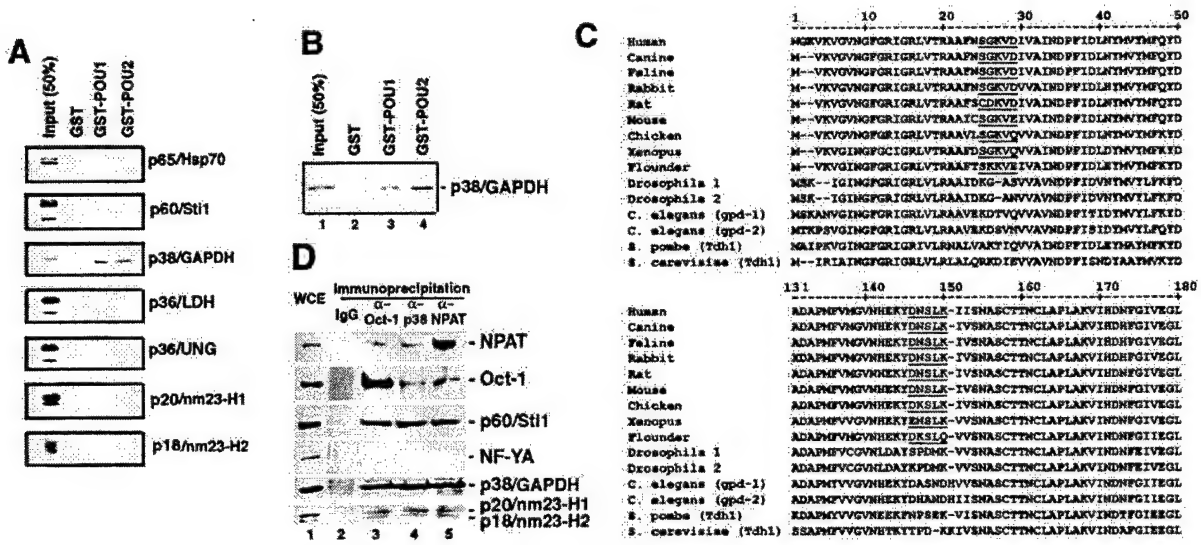

Figure 2. In Vitro and In Vivo Interactions between OCA-S Components and Oct-1/-2 POU Domains and between Oct-1, OCA-S, and NPAT

(A) Interactions of in vitro translated OCA-S components with Oct-1/-2 POU domains.

(B) Interaction of homogeneously purified p38/GAPDH with Oct-1/-2 POU domains.

(C) Alignment of relevant vertebrate and nonvertebrate GAPDH protein sequences. The residues in the two small regions that display significant divergence from vertebrate GAPDHs to nonvertebrate ones are underlined. Numbers indicate amino acid positions. The GenBank accession numbers for these GAPDH sequences from human to *S. cerevisiae* on the list are CAA25833, BAA90817, BAA90818, P51469, P46406, CAA26150, NP_032110, P00356, BAA88638, NP_525108 and NP_542445, CAA888170 and AAB53874, P78958, and NP_012483, respectively.

(D) Coimmunoprecipitation of Oct-1, OCA-S, and NPAT. A T24 whole-cell extract (WCE) was immunoprecipitated with antibodies against Oct-1 (lane 3), p38/GAPDH (lane 4), NPAT (lane 5), or control IgG (lane 2) under salt conditions equivalent to 150 mM NaCl. The intact WCE (lane 1) and immunoprecipitates were subjected to immunoblot with antibodies against NPAT, Oct-1, p60/Sti1, p38/GAPDH, p20/nm23-H1, p18/nm23-H2, or NF-YA.

homogeneous purified recombinant p38/GAPDH also bound to the POU domains (Figure 2B), indicating a direct interaction. p38/GAPDH thus becomes a new member of the Oct-1 POU domain interacting protein family, which includes OCA-B (Luo and Roeder, 1995), VP16 (reviewed in Babb et al., 1997), and SNAP190 (reviewed in Ford et al., 1998).

An alignment of p38/GAPDH protein sequences from a number of vertebrate and nonvertebrate species revealed protein sequence conservation throughout the entire length, except for two small regions (underlined in Figure 2C) where the conservation is restricted to vertebrates. These vertebrate-specific sequences might provide the basis for Oct-1 interactions and transcriptional activation functions (see below) on H2B genes, although the involvement of p38/GAPDH and Oct-1-related POU domain proteins in the regulation of nonvertebrate H2B transcription, via the octamer element, is not yet excluded.

We then employed coimmunoprecipitation assays to examine possible in vivo interactions among OCA-S-associated proteins, as well as interactions between these proteins and Oct-1. Since NPAT has been implicated in the transcription of multiple histone subtypes (Ma et al., 2000; Zhao et al., 2000), and thus likely acts upstream of OCA-S during H2B promoter activation, we also explored possible interactions of OCA-S proteins with NPAT. To this end, a whole-cell extract of human T24 bladder carcinoma cells was subjected to immunoprecipitation with anti-Oct-1, anti-p38/GAPDH, anti-NPAT, or control IgG antibodies, and the immunoprecipitates were analyzed by immunoblotting. Anti-Oct-1, anti-p38/GAPDH, and anti-NPAT antibodies all coimmunoprecipitated Oct-1, p18/nm23-H2, p20/nm23-H1, p38/GAPDH, p60/Sti1, and NPAT (Figure 2D), as well as p36/LDH, p36/UNG, and p65/Hsp70 (data not shown). The native H2B promoter also contains a CCAAT box that does not contribute to its cell cycle regulation (Labella et al., 1988). NF-YA, the factor that binds to this element (Fan et al., 2002), served as a control here and was not immunoprecipitated by any of the antibodies (Figure 2D). These results, together with the observed copurification of seven OCA-S-associated proteins, strongly support the notion that these seven proteins form a complex, hereafter designated OCA-S, and that this complex interacts with Oct-1 in vivo, most likely via p38/GAPDH. The observed NPAT-OCA-S interaction further suggests a physical link between NPAT and the H2B transcriptional regulatory machinery, possibly via a transient mechanism (see Figure 6I, Figure 8E, and Discussion).

p38/GAPDH Has an Intrinsic Transactivation Potential

To test whether one or more subunits of the OCA-S complex might possess an intrinsic transactivation potential (activation domain), p18/nm23-H2, p20/nm23-H1, p38/GAPDH, and p60/Sti1, as well as OCA-B as a positive control (Luo and Roeder, 1999), were individually fused to LexA and cotransfected into 293T human kidney cells with a reporter bearing LexA binding sites. The reporter was activated by both LexA-OCA-B and LexA-p38, but not by LexA alone or LexA fused to other

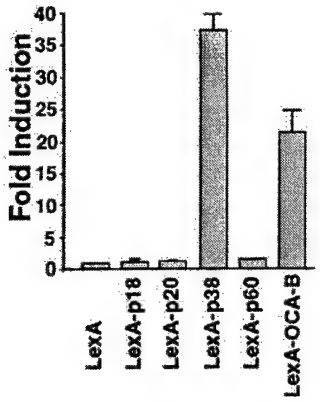

Figure 3. p38/GAPDH Has an Intrinsic Activation Domain

The indicated LexA or LexA fusion proteins were assayed by co-transfection of cognate expression vectors with a luciferase reporter bearing four LexA binding sites in front of an E1B minimal promoter, and values were normalized to activity with LexA alone.

proteins (Figure 3). This result indicates that p38/GAPDH has a transactivation potential that might account for most, if not all, of the OCA-S transcription activity. A prominent role of p38/GAPDH in the OCA-S complex thus prompted focus on p38/GAPDH in further studies of the transcription function of the complex.

p38/GAPDH Is Essential for Octamer-/ Oct-1-Dependent H2B Transcription In Vitro

To study the transcription function of the OCA-S complex, we first attempted to immunodeplete OCA-S proteins from HeLa cell nuclear extracts with specific antibodies. Of the available antibodies tested, anti-p38/GAPDH and anti-p60/Sti1 quantitatively removed corresponding proteins under high salt conditions (500 mM KCl; Figure 4A). Depletion of p38/GAPDH, but not p60/Sti1, reduced octamer-dependent H2B transcription by ~4-fold (Figure 4B). Consistent with a role for OCA-S in the core promoter interaction (Figure 1C), depletion of p38/GAPDH and p60/Sti1 also reduced, albeit marginally, transcription from the octamer mutant H2B promoter (Figure 4C). Indicative of promoter specificity, OCA-B-dependent activation of the IgH promoter was intact in either p38/GAPDH- or p60/Sti1-depleted extracts (Figure 4D).

Altogether, these results suggest that p38/GAPDH is an essential nuclear factor for H2B transcription and, further, that it plays the central role in the coactivator function of the OCA-S complex. The apparent dispensability of p60/Sti1 for H2B transcription in vitro (Figure 4B) suggests a functional redundancy for p60/Sti1 in the p60/Sti1-deficient nuclear extract, which contained normal levels of other OCA-S-associated proteins (Figure 4A); however, it is also possible that p60/Sti1 and other untested OCA-S proteins might be required for the transcription of natural (chromatin) templates or for another function(s) of the OCA-S complex (see Discussion).

To verify that the reduction of H2B transcription in p38/GAPDH-depleted nuclear extracts is due directly to a missing p38/GAPDH function, the ability of homogeneous-purified p38/GAPDH to rescue this deficiency was examined. To this end, a HeLa cell line that stably expresses f-p38-HA (p38/GAPDH doubly tagged by Flag and HA epitopes) was established. f-p38-HA protein was purified to homogeneity on anti-Flag agarose followed by anti-HA agarose under high salt (500 mM KCl) conditions, from either nuclear or cytoplasmic (S100) extracts of the cell line (Figures 4E and 4F). The f-p38-HA in these preparations is predominantly monomeric since the endogenous p38/GAPDH did not copurify (compare Figure 4F with 4G). Addition of purified nuclear f-p38-HA to the p38/GAPDH-deficient extracts restored high-level H2B transcription (Figure 4H), thus confirming a transcription coactivation function for nuclear p38/GAPDH. In marked contrast, addition of monomeric cytoplasmic f-p38-HA (Figure 4H) or commercial tetrameric GAPDH from erythrocyte cytoplasm (data not shown), failed to effectively restore the H2B transcription. These results suggest that conformational changes and modifications of p38/GAPDH may be important for its nuclear function in H2B transcription.

Immunodepletion of endogenous p38/GAPDH and affinity purification of f-p38-HA were very inefficient under physiological salt conditions (data not shown). It is conceivable that endogenous p38/GAPDH and tagged f-p38-HA epitopes are blocked by other proteins of the OCA-S complex, thus making p38/GAPDH poorly accessible to antibodies under these conditions. Consistent with this possibility, as well as a high salt-induced dissociation of p38/GAPDH from other OCA-S subunits that remained intact in the p38/GAPDH-depleted extract (Figure 4A), the optimal salt condition either for immunodepletion of endogenous p38/GAPDH or for affinity purification of f-p38-HA on M2 agarose was 500 mM KCl.

p38/GAPDH Is Essential for H2B Transcription In Vivo

To test the role of p38/GAPDH in H2B transcription in vivo, we used the RNA interference (RNAi) method (Elbashir et al., 2001) to block p38/GAPDH expression in human U2OS osteosarcoma cells. As these cells and other cells used throughout this study were routinely passaged and maintained in pyruvate-containing medium, any requirement for p38/GAPDH in the glycolytic pathway could be bypassed. Immunoblot analysis revealed a time-dependent reduction in the nuclear p38/GAPDH protein level, which was already significant at 24 hr and reached ~90% reduction at 60 hr, whereas the levels of Oct-1 and other OCA-S components were unaltered (Figure 5A). RT-PCR analysis showed a reduction, already apparent at 24 hr, in the level of endogenous H2B mRNA in concert with the decline of the nuclear p38/GAPDH level, while the level of β-actin mRNA remained constant (Figure 5C). A second p38/GAPDH-specific short interfering double-strand RNA (siRNA) that targets a different mRNA region was also employed and produced similar results (data not shown). Interestingly, the level of H4 mRNA was also decreased, but this was apparent only at a relatively late time (60 hr) after RNAi treatment (Figure 5D). We reason that inhibition of H4 mRNA expression is secondary to the cell cycle effect caused by inhibition of H2B mRNA expression. This is consistent with previous reports showing that expres-

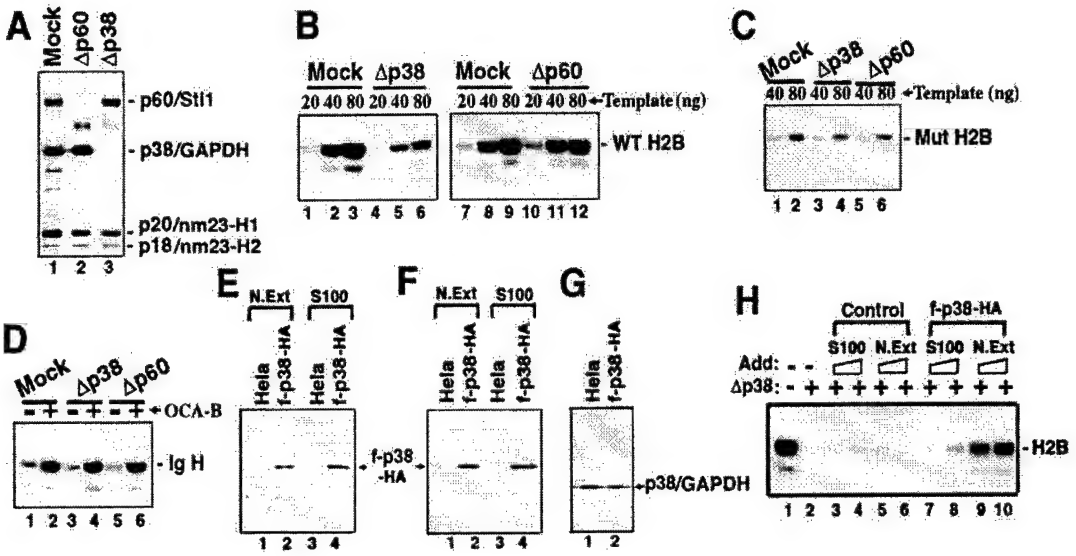

Figure 4. Purified Nuclear f-p38-HA Restores H2B Transcription in a p38/GAPDH-Deficient Nuclear Extract

(A) Immunodepletion of p38/GAPDH or p60/Sti1 from HeLa cell nuclear extracts. Mock- (lane 1), p60/Sti1- (lane 2) or p38/GAPDH- (lane 3) depleted nuclear extracts were examined by immunoblot.

(B–D) H2B or IgH promoter activities in depleted nuclear extracts. Variable doses of H2B promoter templates were used as indicated.

(B) Wild-type H2B promoter activity in p38/GAPDH-depleted nuclear extract (left image, lanes 4–6) or p60/Sti1-depleted nuclear extract (right image, lanes 10–12) in comparison with mock-depleted extract (lane 1–3, 7–9).

(C) Octamer mutant H2B promoter activity in mock- (lanes 1–2), p38/GAPDH- (lanes 3–4), or p60/Sti1- (lanes 5–6) depleted nuclear extracts.

(D) IgH promoter activity in mock- (lanes 1–2), p38/GAPDH- (lanes 3–4), or p60/Sti1- (lanes 5–6) depleted nuclear extracts in the presence (lanes 2, 4, and 6) or absence (lanes 1, 3, and 5) of purified recombinant OCA-B.

(E and F) f-p38-HA purified from either nuclear (N. Ext) or cytoplasmic (S100) extracts of f-p38-HA-expressing Hela cells. M2- and anti-HA-agarose-purified f-p38-HA (lanes 2 and 4) and the eluate from control extracts (lanes 1 and 3) were analyzed by SDS/PAGE-silver staining (E) or by immunoblot with anti-p38/GAPDH antibodies (F).

(G) Position of endogenous p38/GAPDH in the SDS protein gel. Control (lane 1) and f-p38-HA-expressing (lane 2) cell nuclear extracts were analyzed directly by Western blot with anti-p38/GAPDH antibodies. Due to its low expression, f-p38-HA was not observed in the analysis (lane 2), the input (0.2 μl nuclear extract) of which was optimized for detection of endogenous p38/GAPDH. The eluate loaded in (F) corresponds to ~0.2 ml nuclear extract.

(H) H2B promoter activity in normal (lane 1) or p38/GAPDH-depleted nuclear extracts without (lane 2) or with control S100 (lanes 3–4) or nuclear extract (lanes 5–6) eluates, or with f-p38-HA from S100 (lanes 7–8) or nuclear (lanes 9–10) extracts. The two doses of f-p38-HA used were ~10 and 20 ng, respectively.

sion of H3 and H4 was decreased upon deletion of H2B loci in yeast, presumably due to cell cycle arrest in H2B-defective cells (Han et al., 1987).

We thus expected that a block in p38/GAPDH expression would inhibit cell cycle progression into S phase. Indeed, the percentage of S phase cells, monitored by BrdU incorporation, was found to decrease in U2OS cells treated with p38/GAPDH siRNA for 48 hr (Figure 5B). Nevertheless, at an earlier time when the S phase progression was only marginally affected, i.e., at 24 hr after RNAi treatment (Figure 5B), a significant reduction in the level of H2B mRNA was already obvious (Figure 5C). This suggests that this reduction is not due to a nonspecific effect of cell cycle arrest. Conversely, the lag in the reduction of the H4 mRNA synthesis most likely results from a blockage of S phase progression. Therefore, as in yeast, expression of histone genes in mammalian cells is highly coordinated and essential for S phase progression.

To further assess whether the removal of p38/GAPDH has a direct effect on H2B transcription, we examined the effect of p38/GAPDH RNAi on wild-type and octamer-mutated H2B promoter reporters in transfected U2OS cells. The activity of the wild-type promoter was reduced 4- to 5-fold by RNAi treatment, whereas the basal octamer-independent activity of the mutant promoter was unaffected (Figure 5E). These results confirm a p38/GAPDH coactivation function for octamer-/Oct-1-dependent transcription of the H2B promoter.

S Phase-Specific Recruitment of OCA-S/p38/GAPDH to the H2B Promoter

It is expected that a cell cycle-dependent modulation of OCA-S protein abundance and/or activity underlies S phase-specific H2B promoter activation. To investigate possible changes in protein levels, cells were synchronized at various stages by aphidicolin treatment, density arrest (data not shown), or centrifugal elutriation (Figure 6A). Regardless of which approach was used for synchronization, immunoblot analyses of either whole-cell (data not shown) or nuclear (Figure 6B) extracts with available antibodies showed that the protein levels of the OCA-S proteins do not change significantly throughout the cell cycle.

We thus explored another possible modulation, i.e., recruitment of p38/GAPDH and/or other OCA-S proteins to the H2B promoter. As revealed by ChIP assays, the H2B promoter in unsynchronized HeLa cells is occupied

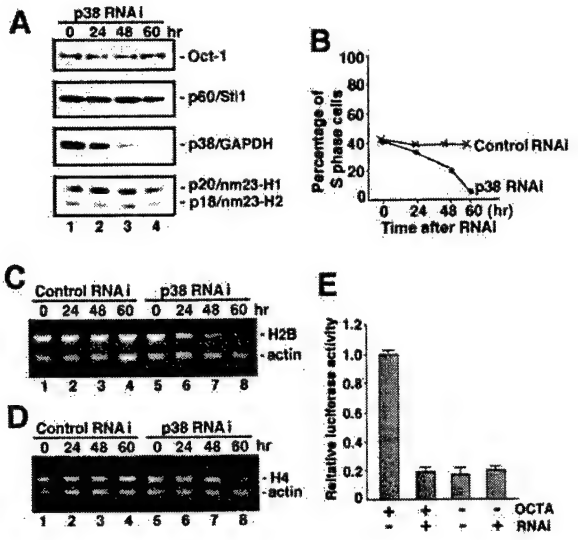

Figure 5. Inhibition of H2B Transcription by p38/GAPDH RNAi

(A) Expression of p38/GAPDH in U2OS cells treated with p38/GAPDH siRNA for 0 to 60 hr was monitored by anti-p38/GAPDH immunoblot analyses of nuclear extracts. Immunoblots with anti-Oct-1, −p60/Sti1, −p18/nm23-H2, and −p20/nm23-H1 antibodies served as controls.

(B) Effect of p38/GAPDH siRNA on S phase progression/DNA synthesis was monitored by BrdU incorporation.

(C and D) RT-PCR analysis of expression levels of H2B (C), H4 (D), and β-actin mRNAs in cells treated with p38/GAPDH-specific siRNA (lanes 5–8) or Ambion's control siRNA (lanes 1–4) for 0 to 60 hr.

(E) Effects of p38/GAPDH siRNA on expression of ectopic wild-type ($OCTA^+$) or mutant ($OCTA^-$) H2B promoters in U2OS cells. Activity was measured at 24 hr posttransfection.

both by Oct-1 and by OCA-S proteins including p18/nm23-H2, p20/nm23-H1, p38/GAPDH, and p60/Sti1 (data not shown). We next focused on the recruitment of Oct-1, p60/Sti1, and p38/GAPDH proteins to the H2B promoter in cells synchronized by centrifugal elutriation. DNA derived from antibody-precipitated chromatin was subjected to PCR using primers for the indicated promoter/DNA regions (Figures 6C-6H). In the assays where 30 cycle PCR was used for amplification, occupancy of the H2B promoter by p38/GAPDH was detected only in S phase, whereas occupancy by Oct-1 was detected in G1, S, and G2 phases (Figure 6C). Importantly, and as strong evidence for its promoter specificity, p38/GAPDH was not detected on the H4 promoter (Figure 6E). By contrast, the Rb family protein Rb2/p130 was selectively recruited to the E2F-recognized H4 promoter in G1, but not S or G2, phase (Figure 6E), as was E2F-4 (data not shown). This is consistent with the suggestion that Rb2/p130 represses E2F-regulated promoter activity at G1 phase via members (mainly E2F-4) of the E2F family (Takahashi et al., 2000). As an additional control, microsatellite DNA was not amplified from any precipitated chromatin DNA (Figures 6G or 6H). These results indicate that p38/GAPDH is recruited specifically to the H2B promoter in an S phase-dependent manner and, in view of a direct p38/GAPDH-Oct-1 interaction (Figure 2), further suggest that this recruitment is central to the S phase regulation of H2B transcription.

The presence of p60/Sti1 on the H2B promoter, but not on the H4 promoter or microsatellite DNA, was detected when 40-cycle PCR was used (Figure 6D versus 6F or 6H). This suggests a specific, albeit possibly more indirect, association of p60/Sti1 with the H2B promoter. Apparently, this association is also S phase-dependent (Figure 6D). Similarly, 40-cycle PCR, but not 30-cycle PCR, revealed an association (possibly more indirect) of NPAT with both H2B and H4 promoters (Figures 6D and 6F). This is in line with an upstream and broader role of NPAT in regulating the transcription of all histone subtypes (Zhao et al., 2000; Ma et al., 2000).

The S phase-specific association of NPAT with the H2B promoter (Figure 6D) suggests a cell cycle-dependent NPAT-OCA-S interaction. To test this possibility, we monitored interactions between ectopic Flag- and HA-tagged NPAT (f-NPAT-HA) and endogenous OCA-S components by coimmunoprecipitation of extracts from U2OS cells that were synchronized at G1 or S phase following transfection. Although the expression of endogenous NPAT is induced at the G1/S transition (Zhao et al., 2000), ectopic f-NPAT-HA expression was similar at G1 and S phases (Figure 6I, lanes 4 and 5). Nonetheless, OCA-S proteins (p60/Sti1, p38/GAPDH, p20/nm23-H1, and p18/nm23-H2) were found in f-NPAT-HA coimmunoprecipitates from S phase cells but not those from G1 phase cells (Figure 6I), suggesting an S phase-dependent NPAT-OCA-S interaction in vivo.

Requirement of p38/GAPDH for S Phase-Specific H2B Promoter Activation In Vitro

To provide more direct evidence that p38/GAPDH is involved specifically in S phase H2B transcription, we first attempted to recapitulate cell cycle dependent H2B transcription in vitro using nuclear extracts of HeLa cells separated by elutriation at various stages (Figure 6A). In line with in vivo results (LaBella et al., 1988), an S phase nuclear extract supported high-level H2B transcription, whereas G1 and G2 phase nuclear extracts supported only low-level H2B transcription (Figure 7A, lanes 1–4). In contrast, OCA-B-dependent IgH promoter activity was equally active in random or staged extracts (Figure 7A, lanes 5–8).

This assay system thus offered an opportunity to assess the OCA-S dependency of H2B activities in both S phase and G1 or G2 phase. To this end, we used a direct antibody inhibition assay in which nuclear extracts were incubated with anti-p38/GAPDH or anti-p60/Sti1 antibodies prior to being used for transcription. In an initial test of this approach and consistent with the immunodepletion data (Figure 4), anti-p38/GAPDH, but not anti-p60/Sti1, antibodies inhibited H2B transcription in an extract from unsynchronized cells (Figure 7B). Similarly, anti-p38/GAPDH, but not anti-p60/Sti1, antibodies inhibited H2B transcription in S phase extract (Figure 7C, lane 7 versus lane 3; Figure 7D). In marked contrast, neither of the antibodies had any effect on H2B transcription in either G1 or G2 phase extracts (Figure 7C, lanes 6 and 8 versus lanes 2 and 4; Figure 7D). That the inhibitory effect is specific for the in vitro-recapitulated S phase H2B transcription clearly strengthens the notion that p38/GAPDH, as a key component of a bona fide Oct-1 coactivator, is indeed responsible for S phase-inducible transcription of the H2B gene.

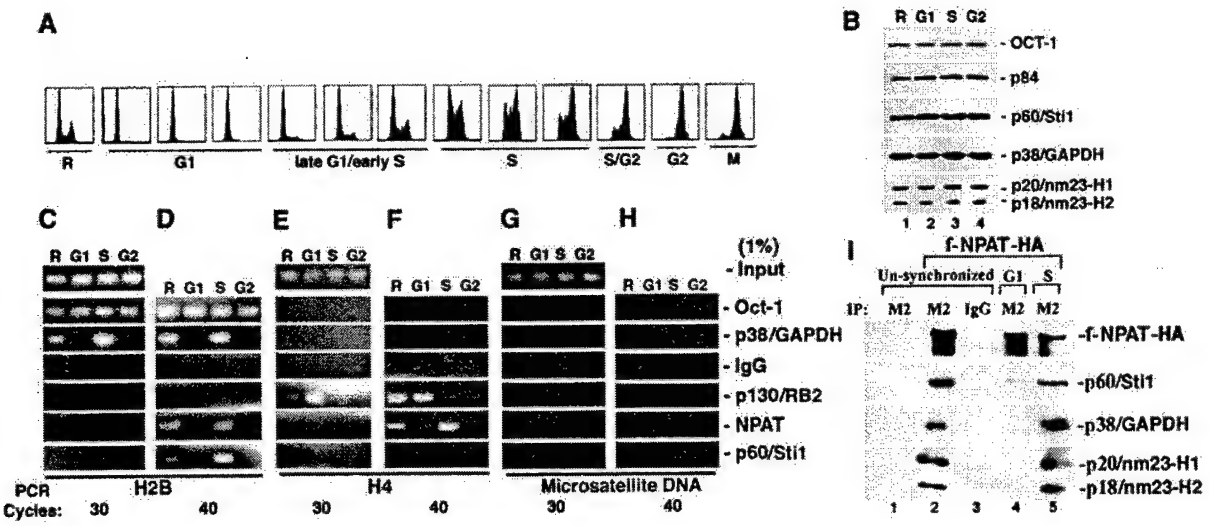

Figure 6. S Phase-Specific Association of OCA-S Components with the H2B Promoter and with NPAT

(A) FACS analyses of HeLa cells synchronized at different stages by elutriation. R, unsynchronized cells.

(B) Immunoblot of p18/nm23-H2, p20/nm23-H1, p38/GAPDH, p60/Sti1, Oct-1, and p84 in nuclear extracts of HeLa cells separated by centrifugal elutriation at different cell cycle stages. The p84 control is a nuclear matrix protein that is not cell cycle regulated.

(C–H) ChIP assays on elutriation-synchronized cells with antibodies against Oct-1, p38/GAPDH, p60/Sti1, NPAT, Rb2/p130, or normal IgG. Precipitated chromatin DNA was amplified by PCR, for either 30 or 40 cycles, with primers specific for H2B (C and D) or H4 (E and F) promoter or microsatellite DNA (G and H).

(I) An S phase-dependent OCA-S-NPAT interaction. Whole-cell extracts were made from cells transfected with empty (lane 1) or f-NPAT-HA-expressing (lanes 2–5) vectors. Cells were either unsynchronized (lanes 1–3) or synchronized at either G1 or S phase (lanes 4 and 5). Immunoprecipitation was carried out with either anti-Flag (M2) (lanes 1, 2, 4, and 5) or control IgG (lane 3) antibodies conjugated to agarose. Immunocomplexes were blotted with anti-p60/Sti1, −p38/GAPDH, −p20/nm23-H1, and −p18/nm23-H2 antibodies and by an anti-HA antibody (to detect tagged NPAT).

Modulation of OCA-S Function by NAD^+/NADH

NAD^+ and NADH are essential coenzymes for the enzymatic activities of cytosolic GAPDH and LDH and, further, have been shown to modulate the functions of several factors involved in transcriptional regulation (see below). Hence, our findings that p38/GAPDH is an essential OCA-S component, and that p36/LDH is also part of the OCA-S complex, make it important to determine whether there is a link between the OCA-S activity and the cellular metabolic state/redox status. To this end, we first employed a GST pull-down assay to test the effects of NAD^+/NADH on the binding of purified recombinant human p38/GAPDH to the Oct-1 POU domain. As shown in Figure 8A, NAD^+ significantly enhanced this interaction in a dose-dependent manner (lower image, compare lane 1 with lanes 2–6). On the other hand, increasing concentrations of NADH inhibited the interaction between POU-1 and p38/GAPDH (lower image, compare lane 1 with lanes 7–11). As a control, the interaction between POU-1 and OCA-B was not affected by either NAD^+ or NADH (upper image). This suggests that both the stimulatory and the inhibitory effects are specific for p38/GAPDH.

We next measured the influence of NAD^+/NADH on the association of p38/GAPDH (via Oct-1) with an H2B promoter (containing both octamer and CAAT box elements) in the context of a nuclear extract fraction. In an initial test of the specificity of such an association, HeLa nuclear extract was mixed with streptavidin agarose-immobilized DNA fragments bearing either wild-type or mutant H2B promoter sequences (Figure 8B), and H2B promoter-associated proteins were analyzed by immunoblotting with corresponding antibodies. As indicated (Figure 8B), p38/GAPDH and Oct-1 bound to promoter fragments in an octamer-dependent manner, whereas NF-YA bound to promoter fragments in a CAAT-box-dependent manner, and little or no cooperative binding was observed. We then explored the effects of NAD^+/NADH on the association of p38/GAPDH with the wild-type H2B promoter. To avoid the influence of possible endogenous (free) NAD^+/NADH, we analyzed such an association in a nuclear extract-derived chromatographic fraction (P11, 0.3 M KCl) that was enriched for OCA-S (Figure 1A) and Oct-1 (data not shown) but depleted of free NAD^+/NADH. We observed stimulatory (NAD^+) and inhibitory (NADH) effects on p38/GAPDH promoter association (Figure 8C, lower image) that were nearly identical to those observed for binding of purified p38/GAPDH to the Oct-1 POU domain (Figure 8A, lower image). By contrast, the direct association of Oct-1 with the H2B promoter was unaffected by either NAD^+ or NADH (Figure 8C, upper image).

To test the effects of NAD^+/NADH in a more physiological setting, we asked whether H2B transcription in a nuclear extract could be modulated by NAD^+/NADH. To reduce the possible influence of endogenous NAD^+/NADH and other redox system(s) in HeLa nuclear extracts, we employed a partially purified reconstituted transcription system consisting of three nuclear extract-derived P11 chromatographic fractions (0.3, 0.5, and 0.85 M KCl; Figure 1A) and highly purified native TFIIA. This system is capable of supporting both H2B and

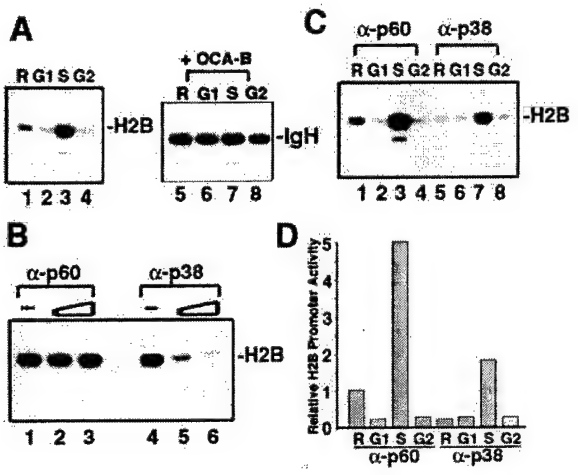

Figure 7. Antibody-Mediated Inhibition of S Phase H2B Transcription

(A) H2B (lanes 1–4) and OCA-B-dependent IgH (lanes 5–8) promoter transcription in nuclear extracts from random (R) or HeLa cells synchronized at G1, S, or G2 phase by elutriation.

(B) Antibody-mediated inhibition of H2B transcription in nuclear extracts of unsynchronized HeLa cells following preincubation with buffer (lanes 1 and 4) or two doses (2 μl and 5 μl) of anti-p60/Sti1 (lanes 2–3) or anti-p38/GAPDH (lanes 5–6) antibodies.

(C) Antibody-mediated inhibition of H2B transcription in nuclear extracts from randomly growing cells (R) or from cells synchronized at G1, S, or G2 phase. Extracts were preincubated with 5 μl of either anti-p60/Sti1 (lanes 1–4) or anti-p38/GAPDH (lanes 5–8) antibodies before being assayed for H2B transcription.

(D) Quantitation of H2B transcription inhibition data from (C). Data in all lanes are normalized to that in lane 1 (as 1).

OCA-B-dependent IgH transcription (Figure 8D). Consistent with the coenzyme effects on the p38/GAPDH-Oct-1 interaction, H2B transcription was stimulated by increasing concentrations of NAD^+ (Figure 8D, upper image, lanes 2–6) and inhibited by increasing concentrations of NADH (Figure 8D, upper image, lanes 7–11). In contrast, the OCA-B-dependent IgH promoter activity was unaffected by either NAD^+ or NADH (Figure 8D, lower image). The concentrations of NAD^+ or NADH required for their stimulatory or inhibitory effects on H2B transcription (Figure 8D) are considerably higher than those that modulate the Oct-1-p38/GAPDH interactions (Figures 8A and 8C). This could be due to persistence of endogenous redox system(s) in the partially purified transcription system and/or other complications associated with the reactions. Nevertheless, the results from all three approaches lead us to conclude that the redox status of NAD^+/NADH can significantly modulate the interaction of Oct-1 with p38/GAPDH, as well as H2B transcription.

Discussion

In an extension of our previous studies that defined the key H2B promoter regulatory element (e.g., LaBella et al., 1988) and the interacting transcriptional activator Oct-1 (Fletcher et al., 1987), we report the biochemical purification of a multicomponent transcriptional coactivator, OCA-S, which appears to be the major determinant for S phase activation of the H2B promoter. We also show that the p38 subunit provides the key Oct-1 recognition and coactivation functions and, remarkably, that it represents a nuclear form of glyceraldehyde-3-phosphate dehydrogenase (GAPDH). Furthermore, the transcription function of OCA-S is modulated by NAD^+ and NADH. Along with a demonstrated interaction of the OCA-S complex with NPAT, a cyclin E/cdk2 kinase substrate and global regulator of histone gene transcription (reviewed in Ewen, 2000), these results offer new insights into the regulation of histone gene transcription and set the stage for further analysis of the basis, possibly involving other OCA-S subunits, of coordinate histone gene transcription and linkages to both DNA replication and cellular metabolic state.

Key Role for p38/GAPDH in OCA-S Function

That p38/GAPDH is an essential OCA-S component specific for H2B transcription was clearly established by functional studies involving RNAi-mediated depletion in cells and immunodepletion, followed by complementation with purified p38/GAPDH, in nuclear extracts. Strongly supporting these conclusions, p38/GAPDH showed S phase-specific function in vitro and S phase-specific association with the H2B promoter in vivo. Further indicative of its essential role in OCA-S coactivator function, p38/GAPDH interacts directly with Oct-1, thus providing the main anchor for the OCA-S complex to promoter bound Oct-1, and has an intrinsic activation domain that likely interacts with the general transcription machinery. Finally, while the finding of a nuclear form of GAPDH as a key component of OCA-S was surprising, it is important to note that there are previous reports of diverse cytoplasmic and nuclear GAPDH functions that include apoptosis and DNA replication/repair (reviewed in Sirover, 1999).

Possible Modes for the Modulation of OCA-S Coactivation Function

The S phase-specific recruitment of p38/GAPDH/OCA-S to the H2B promoter is probably central to the regulation of the OCA-S activity. Since we observed no changes in the levels of OCA-S subunits throughout the cell cycle, the most likely scenarios for the modulation of OCA-S activity include posttranslational modifications by, or interactions with, other S phase-specific factors that facilitate intracellular translocations and/or promoter occupancy (including Oct-1 interactions) of one or more OCA-S subunits. In this regard, the selective function of affinity purified nuclear p38/GAPDH, relative to the cytoplasmic form, clearly points to some modification(s).

Also of note is the modulation of p38/GAPDH-Oct-1 interactions and OCA-S transcription activity by NAD^+/NADH redox status. NAD^+ and NADH were earlier shown to influence the functions of several transcription (co)-factors (Imai et al., 2000; Rutter et al., 2001; Zhang et al., 2002), including one (CtBP) that proved to be an NAD^+-dependent dehydrogenase (Kumar et al., 2002). Our study shows that the OCA-S transcriptional coactivator complex contains two classical dehydrogenases, p38/GAPDH and p36/LDH, at least one of which is essential for the activity of the coactivator complex on

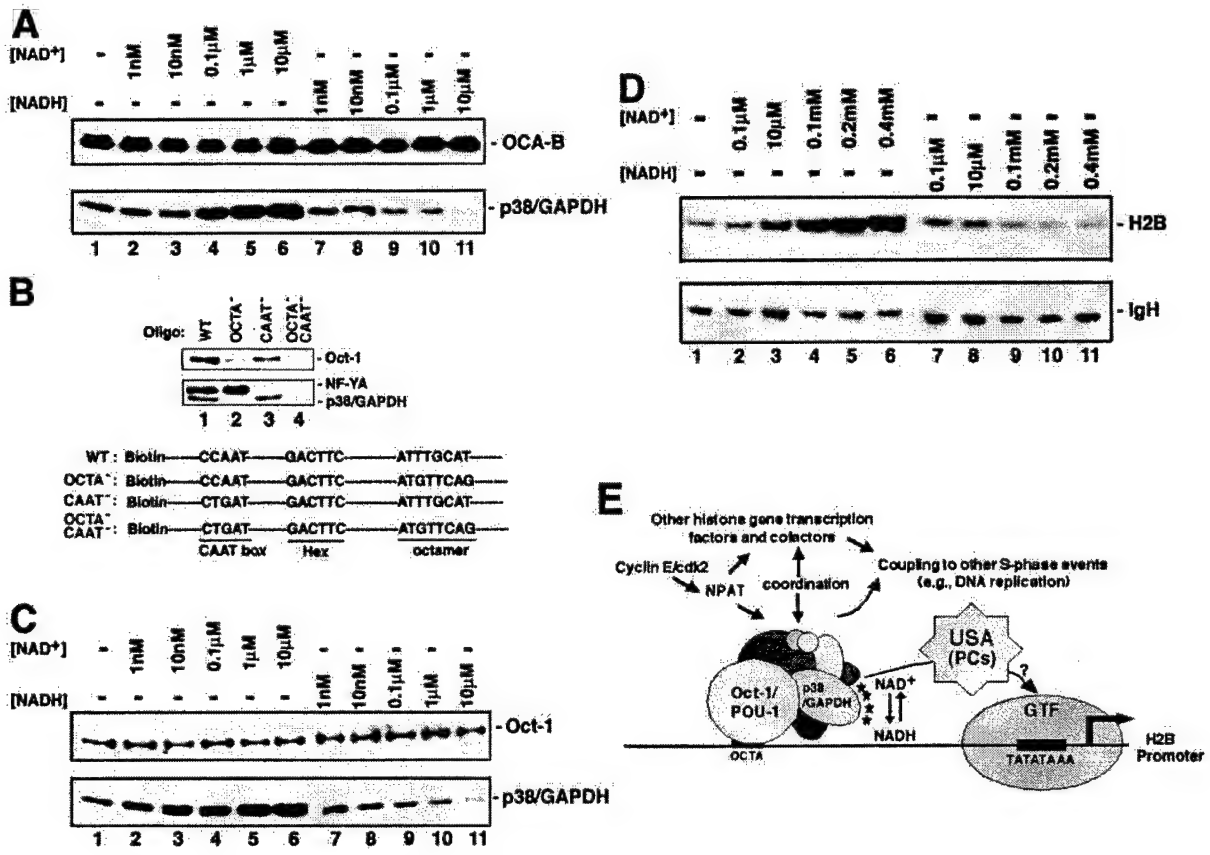

Figure 8. Modulation of POU Domain Binding Activity of p38/GAPDH and H2B Transcription by NAD^+/NADH and a Model for OCA-S-Mediated Coactivation

(A) Effects of NAD^+/NADH on the interaction between purified p38/GAPDH and the Oct-1 POU domain. The interaction between GST-fused POU domain and either recombinant p38/GAPDH or OCA-B was analyzed in a buffer containing either no (lane 1) or increasing concentrations (lanes 2–11) of NAD^+ or NADH, as indicated, by GST pull-down assays as described in Figure 2B. Bound proteins were detected by anti-OCA-B or anti-p38/GAPDH immunoblots.

(B) Octamer-dependent association of p38/GAPDH with an H2B promoter fragment in biotin-streptavidin pull-down assays. HeLa nuclear extract was incubated with biotin-labeled, streptavidin-agarose-immobilized oligonucleotides that contained either the wild-type (lane 1, WT), octamer-mutated (lane 2, $OCTA^-$), CAAT box-mutated (lane 3, $CAAT^-$), or octamer/CAAT box double-mutated (lane 4, $OCTA^-CAAT^-$) H2B promoter sequences. Proteins bound to these oligonucleotides were detected by immunoblotting with anti-Oct-1, −NF-YA, and −p38/GAPDH antibodies. Schematic structures of the oligonucleotides are shown in the lower image.

(C) Effects of NAD^+/NADH on octamer-dependent association of p38/GAPDH with the H2B promoter. Using the same pull-down assays described in (B), the P11 0.3 M KCl fraction of HeLa nuclear extract was incubated with the wild-type oligonucleotides in the absence (lane 1) or presence (lanes 2–11) of the indicated concentrations of NAD^+ or NADH. Bound p38/GAPDH and Oct-1 (as a control) were detected by immunoblots with corresponding antibodies.

(D) Effects of NAD^+/NADH on H2B transcription in vitro. Transcription reactions were carried out in the absence (lane 1) or in the presence (lanes 2–11) of indicated concentrations of NAD^+ or NADH in the system specified in the text. The reactions with the IgH promoter template, as a control, also contained purified OCA-B.

(E) Model for OCA-S-mediated coactivation of the H2B promoter. See text for a detailed explanation.

S phase-specific H2B transcription. Further, our intriguing demonstration of significant NAD^+/NADH-dependent modulations of p38/GAPDH interactions (with free and promoter bound Oct-1) and function (via OCA-S) in H2B transcription prompts speculation regarding two scenarios: (1) that NAD^+/NADH binding and/or dehydrogenase activities associated with p38/GAPDH and/or p36/LDH play important roles in the transcription coactivation function of OCA-S and (2) that histone transcription and cell cycle (S phase) progression may be linked, in part, to overall cellular (or nuclear) metabolic state/redox status. Further studies of the structural basis for the NAD^+/NADH-modulated Oct-1-p38/GAPDH interaction, the mechanisms by which the coenzymes modulate H2B transcription, and the physiological role(s) played by these modulations, promise to be of great interest.

OCA-S: a Multisubunit Transcription Cofactor Complex

That the OCA-S activity resides within a multicomponent complex is evidenced by copurification of the activity with seven stoichiometric polypeptides over a 30,000-fold range, by coelution of the activity with these polypeptides as a high molecular weight entity in gel filtration, and by coimmunoprecipitation of those components (p60/Sti1, p38/GAPDH, p20/nm23-H1, and p18/nm23-

H2) for which antibodies are available. Furthermore, as revealed by ChIP assays, these proteins also occupy the H2B promoter in an S phase-dependent manner, presumably as part of a cognate H2B promoter binding complex. The fact that a single homogeneous f-p38-HA protein can restore H2B transcription to p38/GAPDH-deficient nuclear extracts probably reflects a scenario in which f-p38-HA can reassociate with other OCA-S components in nuclear extracts to acquire transcription competency.

While p38/GAPDH is a key OCA-S component for H2B promoter coactivation, the roles of other subunits and other functions of the complex remain unknown. p20/nm23-H1 and p18/nm23-H2 are members of the nm23 family that have been variably associated with cancer metastasis (reviewed in Freije et al., 1998) and, as revealed by ChIP assays (data not shown), also occupy active H2B promoters, thus suggesting some function(s) related to H2B transcription. Another OCA-S component, p36/UNG, has been shown to play a role in removing dUMP from U:A pairs during DNA replication (Nilsen et al., 2000), raising the possibility of crosstalk, via p36/UNG, between the S phase events of histone transcription and DNA replication/repair. The indication, from its presence in OCA-S, that p36/LDH is associated with transcriptional regulation is consistent with a reported nuclear localization and general DNA binding activity of p36/LDH (Ronai, 1993). As previously suggested, the NAD^+/NADH binding and dehydrogenase activities of p36/LDH, possibly in conjunction with p38/GAPDH, could also participate in the modulation of OCA-S-mediated H2B transcription. The OCA-S components p65/Hsp70 and p60/Sti1/Hop are also subunits of a chaperone complex capable of promoting maturation of certain transcription factors (reviewed in Kimmins and MacRae, 2000). It is thus conceivable that nuclear p65/Hsp70 and p60/Sti1 may help maintain a transcriptionally potent form of the OCA-S complex.

An OCA-S-NPAT Interaction Links Cell Cycle Regulators and H2B Transcription Machinery

Importantly, our results show that Oct-1 occupies the H2B promoter at G1, S, and G2 phases of the cell cycle, whereas OCA-S (notably p38/GAPDH) does so in an S phase-specific manner and is indeed critical for S phase-inducible coactivation. Promoter bound OCA-S likely acts to facilitate recruitment and/or function of general transcription factors and positive cofactors (PCs), including Mediator (Malik and Roeder, 2000), in the USA fraction (Figure 8E). The cyclinE/cdk2 substrate NPAT could also play a role in these processes; however, its demonstrated role in regulating multiple histone subtype genes makes it more likely that NPAT functions at an upstream level, perhaps in the recruitment/activation of individual histone gene-specific (co)factors like OCA-S (Figure 8E). In support of an indirect role of NPAT in H2B transcription, NPAT was not detected in our purified transcriptionally active OCA-S fraction but, instead, was observed to associate in a more dynamic and S phase-dependent manner with OCA-S (Figure 6I). Therefore, it is most likely that OCA-S is a submodule of a larger dynamic complex containing NPAT, OCA-S, and Oct-1.

Consistent with the notion that transcription of histone subtypes is tightly coordinated and coupled to DNA replication in concert with S phase progression (reviewed in Osley, 1991), inhibition of H2B transcription by RNAi-mediated depletion of p38/GAPDH led to blockage of cell cycle progression and an eventual inhibition of transcription of H4 (Figure 5). Although cyclin E/cdk2 is known to be essential for initiation of both DNA replication and histone biosynthesis in concert with S phase entry (reviewed in Ewen, 2000), the mechanisms by which the above-described coordination and coupling throughout the S phase are not yet fully understood. A recent report suggests that the coupling of histone expression to DNA synthesis following S phase entry is not regulated at the level of cyclin E/cdk2, but rather by other (unknown) factors (Nelson et al., 2002). We speculate that OCA-S, a multisubunit and potentially multifunctional complex harboring a transcription cofactor activity, could provide an efficient way to achieve this concerted regulation. Thus, functions that mediate the coordination of multiple histone subtypes, couple histone synthesis to DNA replication, and transmit the S phase cell cycle regulatory signals, could be exerted through additional subunits of OCA-S either directly or via NPAT (Figure 8E). Our biochemical identification of the multisubunit OCA-S complex and cell cycle study of H2B transcription thus provides a paradigm for further exploring the mechanisms underlying this complex regulation.

Experimental Procedures

Plasmids and Antibodies

Mammalian expression vectors for OCA-S-associated proteins are pCIN4-based (Fondell et al., 1996) and involve CMV promoter-driven transcription of in-frame inserted cDNAs encoding f-p38-HA, LexA alone, and LexA fusions with p18/nm23-H2, p20/nm23-H1, p38/GAPDH, and p60/Sti1. The mammalian expression vector for NPAT (pcDNA3.1-f-NPAT-ha) is pcDNA3.1-based (Invitrogen) and encodes an NPAT that is both Flag- and HA-tagged. Antibodies against p38/GAPDH, p20/nm23-H1, p18/nm23-H2, p60/Sti1, and NPAT were raised in rabbits. Rabbit antibodies against Oct-1, Rb2/p130, NF-YA, and E2F-4 were purchased from Santa Cruz Biotechnologies, and mouse antibodies against p84 were from Novus Biologicals.

Protein Purification

The BC buffer system (Luo et al., 1992) was used in all chromatographic steps for OCA-S purification. The nuclear extract-derived P11 OCA-S fraction was enriched on S-Sepharose, Q-Sepharose, and hydroxyapatite. For the latter step, the indicated potassium phosphate salt concentrations in BC100 (100 mM KCl) were used to step-elute proteins. The activity was then concentrated by heparin-Sepharose and by Amicon centricon. This preparation was equilibrated in BC150 (150 mM KCl) and subjected to gel filtration on Sephacryl 300 (S300).

f-p38-HA was affinity-purified from nuclear or cytoplasmic (S100) extracts of a stable f-p38-HA-expressing HeLa cell line, using anti-Flag (mouse MAb M2, Sigma) and anti-HA (rat MAb 3F10, Roche) agarose affinity resins.

Homogeneous recombinant p38/GAPDH was obtained through successive steps of bacterial expression as a GST fusion protein, purification on an affinity column, removal of GST by thrombin digestion, and repurification by Q-Sepharose.

Cell Synchronization

Synchronization of transfected U2OS cells followed a procedure described in Zhao et al. (1998). Separation of suspension HeLa-S cells by centrifugal elutriation was carried out as described in Mendez and Stillman (2000).

GST Pull-Down Assays

OCA-S-associated proteins were in vitro translated and ^{35}S-labeled by the TNT system (Promega). GST, GST-POU1, and GST-POU2 were bacterially expressed (Luo and Roeder, 1995). Each fusion protein (10 μg), immobilized on glutathione-Sepharose beads, was mixed either with 2.5 μl of each in vitro translated OCA-S-associated protein or with 30 ng p38/GAPDH (Figure 2B), 100 ng p38/GAPDH (Figure 8A), or 250 ng OCA-B (Figure 8A) in the binding buffer (50 mM Tris, [pH 7.5], 150 mM NaCl, 4 mM EDTA, 0.5% NP40, 0.5% BSA, proteinase inhibitor cocktail, and, when appropriate, NAD^+/NADH). The binding reactions were incubated for 1 hr at room temperature.

Biotin-Streptavidin Pull-Down Assay

Biotin-streptavidin pull-down assays were performed as described (Fan et al., 2002). In brief, double-stranded oligonucleotides, corresponding to positions −91 to −30 of the human H2B promoter, were end-labeled by biotin and bound to streptavidin-agarose beads. The resultant beads were incubated, in the presence or absence of NAD^+/NADH, with either HeLa nuclear extract or a derived P11 0.3 M KCl column fraction for 20 min at room temperature. The protein-DNA-streptavidin-agarose complexes were washed, and the eluted proteins resolved by SDS-PAGE and detected by immunoblotting.

Chromatin Immunoprecipitation (ChIP) Assays

The ChIP assays were performed as described in Shang et al. (2000), using 1×10^6 HeLa cells synchronized by centrifugal elutriation for each antibody. Primers for histone promoters and microsatellite sequences were described in Zhao et al. (2000).

RNA Interference and RT-PCR Assays

Two duplexes of siRNAs that target two distinct regions on the p38/GAPDH mRNA (AUUCCAUGGCACCGUCAAG and GUCAACGGAU UUGGUCGUA) were designed (Dharmacon). RNAi assays were carried out in U2OS cells as described in Elbashir et al. (2001).

BrdU Incorporation Assays

RNAi-treated cells were grown on glass coverslips in 24-well plates. BrdU (10 μg/ml) was added to the medium for 1 hr before anti-BrdU immunostaining was conducted as described (Ma et al., 2000). One hundred cells were randomly picked and the numbers of BrdU-positive cells were counted for each sample. The percentage of S phase cells was averaged from three counts.

Transfection Assays

To assess the transactivation potential of OCA-S proteins, vectors expressing LexA or LexA fusions to p18/nm23-H2, p20/nm23-H1, p38/GAPDH, p60/Sti1, or OCA-B were each cotransfected into 293T cells with a luciferase reporter bearing LexA binding sites. At 48 hr posttransfection, cells were harvested for luciferase activity measurement. To assess H2B promoter activity in vivo, U2OS cells were cotransfected with wild-type or octamer-mutated reporters (Zhao et al., 2000) and, when appropriate, p38/GAPDH siRNA. At 24 hr posttransfection/RNAi treatment, cells were harvested for analysis of luciferase activity. For all transfections, a Renilla luciferase reporter was cotransfected for the normalization of transfection efficiency.

Immunodepletion and Direct Antibody Inhibition

Antigens were crosslinked to CNBr-activated Sepharose and the resultant resins used to affinity-purify specific antibodies (IgGs). For immunodepletion of p38/GAPDH and p60/Sti1, the corresponding affinity-purified IgGs were crosslinked to protein-A-Sepharose to generate antibody-affinity resins. The depleted nuclear extracts in BC500 (Luo and Roeder, 1995) were dialyzed to BC100 for in vitro transcription assays. For direct antibody inhibition, the affinity-purified anti-p38/GAPDH or anti–p60/Sti1 IgGs in BC500 were incubated with nuclear extracts for 3 hr at 4°C. The treated nuclear extracts were then dialyzed to BC100.

In Vitro Transcription

Conditions for both crude and purified assay systems, as well as DNA templates, were described in Luo and Roeder (1995). For the reconstituted transcription systems described in Figure 1, RNA pol II, general initiation factors, and the USA cofactor fraction were purified as in Ge et al. (1996), Oct-1 and Sp1 as in Luo et al. (1992), recombinant OCA-B as mentioned in Luo and Roeder (1999), and OCA-S as described above.

Peptide Sequencing

Identities of the polypeptides that copurified with OCA-S were revealed by protein sequence analyses following resolution by SDS/PAGE. Derived sequences include: PEELVDYK (p18/nm23-H2); TFI AIKPDGVQR (p20/nm23-H1); SADTLWGIQK (p36/LDH M chain) and SADTLWDIQK (p36/LDH H chain); GSAIDRK (p36/UNG); VVDLMAH MASK (p38/GAPDH); AAALEAMK (p60/Sti1); and LQDFFNGRDLNK (p65/Hsp70).

Acknowledgments

We thank Mr. Z. Fu for technical help, Drs. S. Malik, J. Zhang, and X. Zhang for critical reading of the manuscript, and Drs. T. de Lange, A. Koff, and J. Ye for invaluable help with centrifugal elutriation. This work was supported by an NIH grant and a Johnson and Johnson's Focused Giving Award to R.G.R. and by an American Cancer Society grant and Investigator Awards from New York Community Trust and Academic Medicine Development to Y.L. L.Z. is an American Cancer Society postdoctoral fellow. Rockefeller University DNA/Protein Technology Center carried out the peptide sequencing analyses.

Received: March 19, 2003
Revised: June 30, 2003
Accepted: July 1, 2003
Published: July 24, 2003

References

Babb, R., Cleary, M.A., and Herr, W. (1997). OCA-B is a functional analog of VP16 but targets a separate surface of the Oct-1 POU domain. Mol. Cell. Biol. *17*, 7295–7305.

Elbashir, S.M., Harborth, J., Lendeckel, W., Yalcin, A., Weber, K., and Tuschl, T. (2001). Duplexes of 21-nucleotide RNAs mediate RNA interference in cultured mammalian cells. Nature *411*, 494–498.

Ewen, M.E. (2000). Where the cell cycle and histones meet. Genes Dev. *14*, 2265–2270.

Fan, W., Jin, S., Tong, T., Zhao, H., Fan, F., Antinore, M.J., Rajasekaran, B., Wu, M., and Zhan, Q. (2002). BRCA1 regulates GADD45 through its interactions with the OCT-1 and CAAT motifs. J. Biol. Chem. *277*, 8061–8067.

Fletcher, C., Heintz, N., and Roeder, R.G. (1987). Purification and characterization of OTF-1, a transcription factor regulating cell cycle expression of a human histone H2b gene. Cell *51*, 773–781.

Fondell, J.D., Ge, H., and Roeder, R.G. (1996). Ligand induction of a transcriptionally active thyroid hormone receptor coactivator complex. Proc. Natl. Acad. Sci. USA *93*, 8329–8333.

Ford, E., Strubin, M., and Hernandez, N. (1998). The Oct-1 POU domain activates snRNA gene transcription by contacting a region in the SNAPc largest subunit that bears sequence similarities to the Oct-1 coactivator OBF-1. Genes Dev. *12*, 3528–3540.

Freije, J.M., MacDonald, N.J., and Steeg, P.S. (1998). Nm23 and tumour metastasis: basic and translational advances. Biochem. Soc. Symp. *63*, 261–271.

Frydman, J., and Hohfeld, J. (1997). Chaperones get in touch: the Hip-Hop connection. Trends Biochem. Sci. *22*, 87–92.

Ge, H., Martinez, E., Chiang, C.M., and Roeder, R.G. (1996). Activator-dependent transcription by mammalian RNA polymerase II: in vitro reconstitution with general transcription factors and cofactors. Meth. Enzymol. *274*, 57–71.

Han, M., Chang, M., Kim, U.J., and Grunstein, M. (1987). Histone H2B repression causes cell-cycle-specific arrest in yeast: effects on chromosomal segregation, replication, and transcription. Cell *48*, 589–597.

Imai, S., Armstrong, C.M., Kaeberlein, M., and Guarente, L. (2000).

Transcriptional silencing and longevity protein Sir2 is an NAD-dependent histone deacetylase. Nature *403*, 795–800.

Kimmins, S., and MacRae, T.H. (2000). Maturation of steroid receptors: an example of functional cooperation among molecular chaperones and their associated proteins. Cell Stress Chaperones *5*, 76–86.

Kumar, V., Carlson, J.E., Ohgi, K.A., Edwards, T.A., Rose, D.W., Escalante, C.R., Rosenfeld, M.G., and Aggarwal, A.K. (2002). Transcription corepressor CtBP is an NAD(+)-regulated dehydrogenase. Mol. Cell *10*, 857–869.

LaBella, F., Sive, H.L., Roeder, R.G., and Heintz, N. (1988). Cell-cycle regulation of a human histone H2B gene is mediated by the H2B subtype-specific consensus element. Genes Dev. *2*, 32–39.

Luo, Y., and Roeder, R.G. (1995). Cloning, functional characterization, and mechanism of action of the B-cell-specific transcriptional coactivator OCA-B. Mol. Cell. Biol. *15*, 4115–4124.

Luo, Y., and Roeder, R.G. (1999). B Cell-specific coactivator OCA-B: biochemical aspects, role in B cell development and beyond. Cold Spring Harb. Symp. Quant. Biol. *63*, 119–131.

Luo, Y., Fujii, H., Gerster, T., and Roeder, R.G. (1992). A novel B cell-derived coactivator potentiates the activation of immunoglobulin promoters by octamer-binding transcription factors. Cell *71*, 231–241.

Ma, T., van Tine, B.A., Wei, Y., Garrett, M.D., Nelson, D., Adams, P.D., Wang, J., Qin, J., Chow, L.T., and Harper, J.W. (2000). Cell cycle-regulated phosphorylation of p220(NPAT) by cyclin E/Cdk2 in Cajal bodies promotes histone gene transcription. Genes Dev. *14*, 2298–2313.

Malik, S., and Roeder, R.G. (2000). Transcriptional regulation through mediator-like coactivators in yeast and metazoan cells. Trends Biochem. Sci. *25*, 277–283.

Mendez, J., and Stillman, B. (2000). Chromatin association of human origin recognition complex, cdc6, and minichromosome maintenance proteins during the cell cycle: assembly of prereplication complexes in late mitosis. Mol. Cell. Biol. *20*, 8602–8612.

Nelson, D.M., Ye, X., Hall, C., Santos, H., Ma, T., Kao, G.D., Yen, T.J., Harper, J.W., and Adams, P.D. (2002). Coupling of DNA synthesis and histone synthesis in S phase independent of cyclin/cdk2 activity. Mol. Cell. Biol. *22*, 7459–7472.

Nilsen, H., Rosewell, I., Robins, P., Skjelbred, C.F., Andersen, S., Slupphaug, G., Daly, G., Krokan, H.E., Lindahl, T., and Barnes, D.E. (2000). Uracil-DNA glycosylase (UNG)-deficient mice reveal a primary role of the enzyme during DNA replication. Mol. Cell *5*, 1059–1065.

Osley, M.A. (1991). The regulation of histone synthesis in the cell cycle. Annu. Rev. Biochem. *60*, 827–861.

Ronai, Z. (1993). Glycolytic enzymes as DNA binding proteins. Int. J. Biochem. *25*, 1073–1076.

Rutter, J., Reick, M., Wu, L.C., and McKnight, S.L. (2001). Regulation of clock and NPAS2 DNA binding by the redox state of NAD cofactors. Science *293*, 510–514.

Segil, N., Roberts, S.B., and Heintz, N. (1991). Mitotic phosphorylation of the Oct-1 homeodomain and regulation of Oct-1 DNA binding activity. Science *254*, 1814–1816.

Shang, Y., Hu, X., DiRenzo, J., Lazar, M.A., and Brown, M. (2000). Cofactor dynamics and sufficiency in estrogen receptor-regulated transcription. Cell *103*, 843–852.

Sirover, M.A. (1999). New insights into an old protein: the functional diversity of mammalian glyceraldehyde-3-phosphate dehydrogenase. Biochim. Biophys. Acta *1432*, 159–184.

Takahashi, Y., Rayman, J.B., and Dynlacht, B.D. (2000). Analysis of promoter binding by the E2F and pRB families in vivo: distinct E2F proteins mediate activation and repression. Genes Dev. *14*, 804–816.

Zhang, Q., Piston, D.W., and Goodman, R.H. (2002). Regulation of corepressor function by nuclear NADH. Science *295*, 1895–1897.

Zhao, J., Dynlacht, B., Imai, T., Hori, T., and Harlow, E. (1998). Expression of NPAT, a novel substrate of cyclin E-CDK2, promotes S-phase entry. Genes Dev. *12*, 456–461.

Zhao, J., Kennedy, B.K., Lawrence, B.D., Barbie, D.A., Matera, A.G., Fletcher, J.A., and Harlow, E. (2000). NPAT links cyclin E-Cdk2 to the regulation of replication-dependent histone gene transcription. Genes Dev. *14*, 2283–2297.

JBC Papers in Press. Published on June 17, 2003 as Manuscript M210659200

M-phase specific phosphorylation of BRCA2 by Polo-like Kinase 1 correlates with the dissociation of the BRCA2-P/CAF complex.

Horng-Ru Lin[1], Nicholas S.Y. Ting[1], Jun Qin[2] and Wen-Hwa Lee[1]*

1 Department of Molecular Medicine, Institute of Biotechnology, University of Texas Health Science Center, 15355 Lambda Drive, San Antonio, Texas 78245, USA

2 Verna and Marrs Mclean Department of Biochemistry and Molecular Biology , Department of Cell Biology, Baylor College of Medicine, Houston, Texas 77030, USA

Running title: M-phase specific phosphorylation of BRCA2

*To whom correspondence should be addressed. Phone: 210-567-7353; Fax: 210-567-7377; Email: leew@uthscsa.edu

H-R. L is supported by pre-doctoral training grant DAMD 17-99-1-9402 from the U.S. Army Medical Research and Materiel Command. N. T. is a recipient of a post-doctoral fellowship from the Susan G. Komen Breast Cancer Foundation. This research was supported by grants from the National Institutes of Health (CA 81020 and CA 94170) to W-H. L.

Abbreviations: HR - homologous recombination; P/CAF - p300/CBP associated factor; DTT - dithiothreitol; hr - hour; MOI - multiplicity of infection; PMSF - Phenylmethyl-sulfonyl Flouride; GFP - green fluorescence protein; SDS-PAGE - sodium dodecyl sulfate – polyacrlamide gel electrophoresis.

Copyright 2003 by The American Society for Biochemistry and Molecular Biology, Inc.

SUMMARY

BRCA2 is a breast tumor susceptibility gene encoding a 390 kDa protein with functions in maintaining genomic stability and cell cycle progression. Evidence has been accumulated to support the concept that BRCA2 has a critical role in homologous recombination of DNA double stranded breaks by interacting with Rad51. In addition, BRCA2 may have chromatin modifying activity through interaction with a histone acetyltransferase protein, p300/CBP-associated factor, P/CAF. To explore how the functions of BRCA2 may be regulated, the post-translational modifications of BRCA2 throughout the cell cycle were examined. We found that BRCA2 is hyperphosphorylated specifically in M-phase, and becomes dephosphorylated as cells exit M-phase and enter into interphase. This specific phosphorylation of BRCA2 was not observed in cells treated with DNA damaging agents. Systematic mapping of the potential mitosis specific phosphorylation sites revealed the N-terminal 284 amino acids of BRCA2 (BR-N1) as the major region of phosphorylation and mass spectrometric analysis identified two phosphopeptides which contained "phosphorylation consensus motifs" for Polo-like kinase 1 (Plk1). Phosphorylation of BR-N1 with Plk1, recapitulated the electrophoretic mobility change as seen in BR-N1 isolated from M-phase cells. Moreover, mutation of Ser193 to Ala in BR-N1 showed reduced phosphorylation, while a deletion mutant of BR-N1 (amino acids 193-207) abolished Plk1 phosphorylation, suggesting that, at least, Ser193 of BRCA2 is phosphorylated by Plk1. Furthermore, RAD51 binds to both the hyperphosphorylated and hypophosphorylated form of BRCA2 while the M-phase hyperphosphorylated form of BRCA2 no longer associates with the P/CAF, suggesting that the dissociation of P/CAF-BRCA2 complex is regulated by phosphorylation. Taken together, these results implicate a potential role of BRCA2 in modulating

M phase progression.

INTRODUCTION

Mutations in the breast cancer susceptibility gene *BRCA2* are responsible for about 45% of hereditary early-onset breast cancer (1,2). Inheritance of one defective allele confers cancer predisposition and tumor cells from predisposed individuals exhibit loss of heterozygosity (3,4). Expression of the wild type BRCA2 in a human pancreatic cell line, Capan 1, which contains a truncated BRCA2, suppresses its neoplastic phenotypes (5). These results indicated that BRCA2 is a bona fide tumor suppressor protein (6,7). In addition, biallelic hypomorphic mutations in BRCA2 have recently been found in cell lines derived from patients in the B and D1 subgroups of Fanconi anemia, a recessive cancer susceptibility disorder (8).

Inactivation of Brca2, a murine homologue, leads to embryonic lethality at an early stage of embryo development (9-12). Brca2-null mouse embryonic fibroblasts show increased sensitivity to genotoxic agents (12,13), spontaneous accumulation of chromosomal abnormalities, including aberrant chromatid exchanges, triradial and quadriradial chromosome structures, and gross chromosomal rearrangements (13,14), and frequently develop micronuclei, chromosome missegregation, and centrosome amplification (15). These observations implicate a requirement for BRCA2 in maintaining chromosome stability. Similar aberrant chromosome configurations are observed in cells mutant for proteins involved in homologous recombination (16,17), suggesting that BRCA2 is needed for this error-free repair process. Homologous recombination (HR) involves the repair of DNA strand breaks by using an adjacent sister chromatid as template (18). Loss of BRCA2 reduces the efficiency of HR-mediated double stranded break (DSB) repair, resulting in the repair of these lesions through error-prone mechanisms such as

nonhomologous end joining (NHEJ) (19-21).

The role of BRCA2 in HR is mediated through an interaction with Rad51, the evolutionary conserved homologue of bacteria RecA, which plays an essential role in DNA double strand pairing and exchange during HR (22). RAD51 interacts with the BRC repeats, a stretch of unique amino acid sequences that is repeated eight times within the central region of BRCA2 (23-25). Disruption of the endogenous interaction between RAD51 and BRCA2 by ectopic expression of the BRC repeats leads to radiation sensitivity and G2/M checkpoint failure (26). Recently, x-ray crystallographic studies of the highly conserved C-terminal domain of murine Brca2 (Brca2CTD) indicated that this domain binds to single and double stranded DNA hybrid structures. Moreover, purified Brca2CTD is able to stimulate RAD51-mediated DNA strand pairing and exchange *in vitro* (27). Taken together, the DNA binding activities of the BRCA2CTD, in conjunction with the RAD51 binding activities of the eight BRC repeats, BRCA2 may have a direct role in facilitating crucial steps of RAD51-mediated HR.

Besides roles in HR, BRCA2 has been linked to transcription regulation. The region encoded by exon 3 in the N-terminus of BRCA2 when fused to a DNA-binding domain, has the ability to activate transcription in yeast and mammalian cells, and this transactivation activity is severely compromised by a cancer predisposing mutation, tyrosine 42 to cysteine (28). This ability of BRCA2 to activate transcription may be explained via the recruitment of chromatin modifying activity in the form of P/CAF (29). P/CAF, which is classified as a transcriptional co-activator because of its intrinsic histone acetyltransferase (HAT) activity (30), interacts with the N-terminal region of BRCA2 (29). The exact mechanism of how P/CAF or other HATs act as co-activators remains unclear, but it is believed that the transfer of acetyl groups to histone tails may act either as a "flag" for recruitment, or "loosen" chromatin structure to create an "activated-

state" by making nucleosomal DNA more accessible to transcription factors and polymerases (31,32). To date, BRCA2 has not been shown to directly activate the transcription of a specific gene; therefore, it is possible that the association of P/CAF may be required for other chromosomal metabolic functions.

The chromosome aberrations seen in BRCA2 deficient cells cannot be solely attributed to an absence of BRCA2 mediated HR. We therefore postulate that BRCA2 must be involved in chromosome metabolism throughout the cell cycle, and predict that this function must be regulated. A common mechanism for regulation is by post-translational modifications such as phosphorylation, acetylation or ubiquitination. Thus, we explored whether or not BRCA2 may be regulated through some form of post-translational modifications during the cell cycle. Here, we report that endogenous human BRCA2 protein is hyperphosphorylated specifically in M phase, and show at least Ser193 in the extreme N-terminus of BRCA2 is targeted by the mitotic kinase, Plk1. Moreover, we found that RAD51 associates with both hyperphosphorylated (M-phase form) and hypophosphorylated (interphase form) BRCA2 *in vivo*. On the other hand, P/CAF associates only with the hypophosphorylated form rather than the hyperphosphorylated form of BRCA2 *in vivo*. These results suggest that the phosphorylation of BRCA2 in M phase, at least by Plk, regulates the dissociation of the BRCA2-P/CAF complex, implying a potential role of BRCA2 in modulating M phase progression.

EXPERIMENTAL PROCEDURES

Cell culture, synchronization, and traansfection

Human bladder carcinoma T24 cell line and osteocarcinoma U2OS cell line (American Type Culture Collection) were cultured in Dulbecco's modified Eagle's medium (DMEM, Life

Technologies, Inc., Rockville, MD) supplemented with 10 % of fetal bovine serum, 2 mM of L-glutamine and 50 units of penicillin/streptomycin at 37 °C with 10 % CO_2.

T24 cells, synchronized at G0/G1 by contact inhibition (33), were seeded at low density to release them back into the cell cycle and thereafter harvested at 0, 12, 18, and 24 hrs after seeding. M-phase cells were enriched by treatment with 0.3 μg/ml nocodazole (Sigma, Saint Louis, MO) for 18 hrs starting at 24 hrs after release. To further isolate a distinct M-phase population of cells, the slightly detached nocodazole-treated cells were shaken off (shake-off method). In order to enrich for M-phase cells without nocodazole treatment, cells first were synchronized at S phase by double-thymidine block, and then released back into the cell cycle. Briefly, the cells were treated with 2mM thymidine for 18-24 hrs, released for 8-10 hrs, and then treated with the same concentration of thymidine for another 16-18 hrs; the cells were released for another 8-10 hrs before being harvested. Lastly, to release cells from nocodazole block (prometaphase or metaphase), arrested cells were collected using the mitotic shake-off method and washed with phosphate-buffered saline (PBS), before being plated to allow reentry into the cell cycle.

Transfections were performed with Lipofectin reagents (Invitrogen, Carlsbad, CA), according to the manufacturer's instructions. U2OS cells (1×10^6 cells/10-cm dish) were seeded one day before transfection, and fresh medium was added 18 hrs after transfection. Cells were incubated either in the absence or presence of nocodazole (0.3 μg/ml) 30 hrs after transfection for another 18 hrs and then harvested for analyses.

Cell treatment with DNA damaging agents

Cycling T24 cells were exposed to 4000 Rads ionizing radiation (IR), 10 Jm^{-2} ultraviolet

light (UV), and then harvested 1 hr later. The time of treatment of 20 μg/ml mitomycin C (Sigma), 10 mM hydroxyurea (Sigma), or 0.3 μg/ml nocodazole was 1 hr, 2 hrs, or 18 hrs, respectively. IR was delivered using a ^{137} Cs source. UV was delivered using a Stratalinker (Stratagene, La Jolla, CA) without culture medium.

Construction of plasmids

Full length human BRCA2 cDNA flanked with *Not* I and *Xho* I linkers at its 5' and 3' ends, respectively, and then subcloned in pcDNA3.1(+) (Invitrogen). Various fragments of BRCA2 cDNA obtained using polymerase chain reactions were subcloned in pUGN, a pUHD10-3-based vector (Strategene), or pCHPL-GFP2 (24). Both of the vectors were engineered for gene fragments as N-terminal fusion with Myc-GFP.

To generate FLAG-mGST-BR-N1, the BR-N1 fragment was subcloned in FLAG-mGST, an engineered plasmid created by assembling mammalian GST cDNA in p3×FLAG-CMV-10 (Sigma).

GST-BR-N1 (WT) was generated by subcloning the BR-N1 fragment in pGEX-4T-1 (Amersham Pharmacia Biotech, Piscataway, NJ). GST-BR-N1 mutants (MTs), S183A, S193A, S239A, and Δ193-207, were created using a QuickChange site-directed mutagenesis kit (Stratagene), and the results were verified by sequencing.

The murine HA-Plk1WT (wild-type) and HA-Plk1K82M (kinase-inactive) cDNAs were kindly provided by Dr. Eisuke Nishida (Kyoto University, Japan) and Dr. Kyung S. Lee (NIH, Bethesda). The pCI-FLAG-P/CAF construct was kindly provided by Dr. Yoshihiro Nakatani (Dana Farber Cancer Institute, Boston).

Preparation of whole-cell extracts

Whole-cell extracts were prepared as described previously (34). Briefly, cells were resuspended in ice-cold NETN buffer (250 mM NaCl , 5 mM EDTA, 50 mM Tris-HCl, pH 7.4, 0.1 % NP-40, 10 μg/ml aprotinin, 10 μg/ml leupeptin, 10 μg/ml pepstain, 5 μg/ml antipain, 1 mM PMSF, 50 mM NaF, 2 mM Na_3Vo_4, and 10 mM glycerophosphate), and then subjected to 3 freeze/thaw cycles. Insoluble debris was removed by centrifugation at 14,000 × g for 10 min. at 4 °C. Total protein concentrations were determined by the Bradford assay (Bio-Rad, Hercules, CA).

Immunoprecipitation, phosphatase treatment of immunoprecipitates, and Western blot

Immunoprecipitations were carried out with modification from Chen et al. (24). Briefly, whole-cell extracts (about 3 mg) were first pre-cleared by incubating with 40 μl of protein A-Sepharose beads (1:1 slurry) (Amersham Pharmacia Biotech) at 4 °C for 30 min. The supernatants were then incubated with 3 μg of murine IgG or anti-BRCA2 (BBA) monoclonal antibody (24) at 4 °C for 1.5 hr and then incubated with 40 μl of a mixture of protein A- and G-Sepharose beads at 4 °C for 1.5 hr. Finally, beads were washed in ice-cold NETN buffer.

Co-immunoprecipitation of RAD51 and BRCA2 or FLAG-P/CAF and Myc-GFP-BR-NL, were carried out using anti-RAD51 (14B4) monoclonal antibody (35) or anti-FLAG (M2) antibody (Sigma), respectively.

For phosphatase treatment, BRCA2 immune complexes were washed in NETN buffer in the absence of phosphatase inhibitors, and resuspended in phosphatase buffer (100 mM NaCl, 50 mM Tris-HCl, pH 7.9, 10 mM $MgCl_2$, 1 mM DTT). Parallel samples were incubated with or without calf intestinal alkaline phosphatase (New England Biolabs, Beverly, MA) at 30 °C for 30

min.

Western blots were developed by standard colorimetric procedures using the appropriate alkaline phosphatase conjugated secondary antibodies (Promega, Madison, WI) or ECL (Amersham Pharmacia Biotech). The BRCA2 immunoprecipitates were analyzed by 6.5 % SDS-PAGE and Western with anti-BRCA2 (Ab2) polyclonal antibody (Oncogene Research Products, Boston, MA). Ectopically expressed Myc-GFP fusion proteins in U2OS cells were probed with anti-GFP monoclonal antibody (Roche Applied Science, Indianapolis, IN).

In vitro kinase assays

Plk1 kinase assay was adapted from Lee et al. (36); briefly, nocodazole-treated U2OS whole-cell extracts (500 μg) in NETN buffer were immunoprecipitated with 1.5 μg of murine IgG, anti-Plk monoclonal antibody (Zymed Laboratotries Inc., South San Francisco, CA), or anti-HA (12CA5) monoclonal antibody at 4 °C for 1.5 hrs and then incubated with 20 μl of a mixture of protein A- and protein G- Sepharose beads at 4°C for another 1.5 hrs. Following extensive washing of the immune complexes with NETN buffer, kinase reactions were initiated by adding 50 μM cold ATP and 5 μCi [γ-^{32}P]-ATP (Amersham Pharmacia Biotech) in the presence of 12 μl of Plk1 kinase buffer (50 mM Tris-HCl, pH 7.4, 2 mM EDTA, pH 8.0, 2 mM DTT, 10 mM $MgCl_2$, 50 mM NaF, 2 mM Na_3Vo_4, and 10 mM glycerophosphate), using 6 μg of unphosphorylated casein (Sigma), GST, or GST-BRN1 as substrates.

Cdk1 kinase assay was adapted from Park et al. (37); briefly, cycling U2OS whole-cell extracts (500 μg) in NETN buffer were immunoprecipitated with 1.5 μg of anti-Cdc2 (p34) monoclonal antibody (Santa Cruz Biotechnology, Santa Cruz, CA) and washed as described above. Kinase reactions were initiated by adding 50 μM cold ATP and 5 μCi [γ-^{32}P]-ATP in the presence of 12

μl of Cdk1 kinase buffer (50 mM Tris-HCl, pH 7.4, 1 mM DTT, and 10 mM $MgCl_2$), using 2 μg of histone H1 (Roche Applied Science) and 6 μg of GST or GST-BRN1 as substrates.

The kinase reactions were carried out at 30 °C for 30 min. and stopped by SDS protein sample buffer. One-third of the total volume were fractionated on SDS-PAGE and analyzed by Coomassie blue staining, autoradiography, or Western blot.

Recombinant proteins

Recombinant BRCA2 protein was expressed using the baculovirus expression system according to manufacturer's guide (Pharmingen, San Diego, CA). Briefly, approximately 1 x 10^6 sf9 cells were infected with baculovirus expressing full length His-tagged BRCA2 at the appropriate MOI (multiplicity of infection); infected cells were then harvested 48 hrs later, and lysed in NETN buffer.

For partial purification of recombinant FLAG-mGST-BR-N1 proteins, nocodazole-treated whole-cell extracts (200 10-cm dishes of U2OS) prepared in NETN buffer 48 hrs after transient transfection with FLAG-mGST-BR-N1 were subjected to immunoaffinity purification using anti-FLAG (M2) resins. The FLAG-mGST-BR-N1 immune complexes were eluted using SDS protein sample buffer, fractioned on 8.5 % SDS-PAGE and analyzed by Coomassie blue staining and Western blot with anti-BRCA2 (I-17) polyclonal antibody (Santa Cruz Biotechnology).

To purify GST fusion proteins, all the recombinant GST-BR-N1 proteins expressed in BL21 Star (DE3) (Invitrogen), were purified using glutathione agarose resins according to manufacturer's instructions (Amersham Pharmacia Biotech).

Mass spectrometry for the identification of phosphorylation sites

Identification of phosphorylation sites using mass spectrometry was performed as described previously (38).

RESULTS

BRCA2 is hyperphosphorylated specifically in M phase.

The BRCA2 mRNA and protein levels have been shown to be present at high levels at late G1/early S phase in rapidly proliferating cells (39,40). However, the precise expression profile of BRCA2 throughout the cell cycle remains unclear. We re-examined the expression of BRCA2 in synchronized human bladder carcinoma T24 cells following previously established protocols (33). As shown in Fig. 1A, BRCA2 was expressed once cells enter S phase (lane 3, upper panel). Conspicuously, we observed the appearance of several slower migrating forms of BRCA2 in extracts from cells enriched for M phase by nocodazole treatment (lane 6, Fig. 1A, upper panel). This unique migration pattern was not observed in cell extracts from interphase cells or sf9 insect cells expressing recombinant BRCA2 (compare lane 6 with lanes 1-5, upper panel, Fig. 1A). The phosphorylation pattern of RB (Fig. 1A, middle panel) was used as an indicator for the cell cycle phase as previously described (33).

To rule out the possibility that the slower migrating forms of BRCA2 resulted from the treatment of cells with nocodazole, M-phase enriched cell extracts were prepared from T24 cells released from double thymidine block without nocodazole (referred to as M-SN for M-phase-Synchronized extracts, Fig. 1B). Consistently, BRCA2 displayed similar slower migrating forms (Fig. 1B, lane 4, upper panel). Furthermore, the slower migrating forms of BRCA2 were more distinct and prominent using highly purified M-phase cells, which were collected by shaking off slightly detached mitotic cells ("Mitotic Shake-Off" extracts were referred as M-SO) (Fig. 1B,

lane 2, upper panel). Based on these observations, we conclude that the slower migrating pattern seen with BRCA2 is M-phase specific. Similar results were seen with another microtubule depolymerizing drug, vinblastine (41), which is known to arrest cells in M phase (data not shown).

To determine whether the alteration in electrophoretic mobility of BRCA2 was attributed to phosphorylation, immune complexes of BRCA2 from M-phase and interphase cells were treated with phosphatase. As shown in Fig. 1C, the slower migrating forms of BRCA2 from mitotic cells converted to a faster migrating form, which co-migrated with the form of BRCA2 from interphase cells, suggesting that BRCA2 becomes hyperphosphorylated as cells enter M phase (compare lane 3 to 6, Fig. 1C).

DNA damage does not induce similar M-phase phosphorylation pattern of BRCA2.

DNA damage-induced phosphorylation of BRCA1 by ATM (Ataxia Telangiecstasia-Mutated), ATR (Ataxia Telangiecstasia and Rad3-Related), and CHK2 kinases has been shown (42-45). However, it is currently unknown whether DNA damage also induces phosphorylation of BRCA2. To test this possibility, asynchronous T24 cells were exposed to various DNA damaging agents, such as ionizing radiation (IR), ultraviolet light (UV), mitomycin C (MMC), and hydroxyurea (HU). All of these genotoxic agents, except for nocodazole, induced dramatic alterations in electrophoretic mobility of BRCA1 (Fig. 2, compare lane 2 to lanes 3-6, middle panel); in contrast, the genotoxic agents failed to induce the conspicuous slower migrating forms of BRCA2 as observed in M phase (Fig. 2, upper panel). We do, however, note that these genotoxic agents did elicit slight but not distinctive changes in the mobility of BRCA2.

BRCA2 becomes dephosphorylated upon exit from M phase.

The fate of hyperphosphorylated BRCA2 in M phase was further examined in T24 cells released from nocodazole arrest. After the release from nocodazole block for 0.6 to 1 hour, the slower migrating forms of BRCA2 were gradually converted to faster migrating forms of BRCA2 (Fig. 3, top panel). At this time point, the fastest migrating form of RB had emerged, signifying the beginning of G1 (Fig. 3, middle panel, 0.6 and 1 hr time points). This observation revealed that BRCA2 becomes dephosphorylated as cells exit M phase and enter interphase. It appears that the dephosphorylation of the slowest migrating form of BRCA2 is gradual, with the appearance of "intermediate" migrating forms (at 0.6 and 1 hr post-release), before the appearance of the fastest migrating form of BRCA2 (at 1.5 hrs post-release). In light of these data, we speculate that one of the biological functions of BRCA2 may, in part, be modulated by phosphorylation and dephosphorylation events as cells enter and exit M phase.

Mapping the M-phase specific phosphorylation regions of BRCA2.

As an initial step towards defining a role for M-phase phosphorylation in the function of BRCA2, we sought to map the regions of BRCA2 that become hyperphosphorylated. Since the hyperphosphorylated form of full length BRCA2 showed such a dramatic alteration of gel mobility, we predicted that smaller fragments of BRCA2 that harbored the M-phase specific phosphorylation sites would have similar alteration in gel mobility, and used this as a basis for a strategy to identify these sites. We initially generated four mammalian expression constructs that express fusion proteins containing Myc-green fluorescent protein (GFP) with overlapping fragments of BRCA2 (Myc-GFP-BR-CR, -BRC4-CR, -BRC1-5, and -BR-N, Fig. 4A) and transiently transfected them into U2OS cells. The transfected cells were then treated with

nocodazole and harvested for Western blot analyses with anti-GFP (or anti-Myc) antibodies. Of the four fusion proteins, only Myc-GFP-BR-N (which constituted the first 923 amino acids of BRCA2), exhibited a clear electrophoretic mobility shift following nocodazole treatment (Fig. 4B, compare lane 4 to lanes 6, 8 and 10). This finding directed us to focus on the N-terminal region of BRCA2 (designated as BR-N).

Three other derivatives of the BR-N construct were generated (Myc-GFP-BR-NS, -BR-NC, and -BR-NL, Fig. 4A). All the fusion proteins exhibited different migration patterns after nocodazole treatment (Fig. 4B, lanes 12, 14, and 16). BR-NL showed a more distinct change in mobility shift compared to BR-NC, which only showed a slight change (Fig. 4B, compare lane 12 to 14). Interestingly, BR-NS showed two distinctive slower migrating forms, but the slowest migrating form appeared only after nocodazole treatment (Fig. 4B, lanes 15 and 16). These findings suggest that BR-NC contains at least one M-phase specific phosphorylation site, while BR-NS contains at least two phosphorylation sites (one that is phosphorylated in a nocodazole-independent manner, and the other in a nocodazole-dependent manner). Furthermore, the dramatic conformational change of BR-NL that leads to electrophoretic mobility shift in the presence of nocodazole may require the extreme N-terminal region of BRCA2 (amino acids 1-190).

To further define the region of BR-NL (amino acids 1-672) that harbors the potential M-phase specific phosphorylation sites, we generated four other constructs that were serial deletions from the C-terminus of BR-NL and designated them as Myc-GFP-BR-N4, -BR-N3, -BR-N2, and -BR-N1 (Fig. 4A). All four fragments of BR-NL displayed prominent changes in mobility after nocodazole treatment (Fig. 4B, lanes 18, 20, 22 and 24). Phosphatase treatment of immunoprecipitates with anti-GFP antibody confirmed that the BR-NL and BR-N1 fragments

were phosphorylated (data not shown). Taken together, these studies suggest that the major M-phase specific phosphorylation sites contributing to the electrophoretic mobility shift of full length BRCA2 reside within BR-N1 (amino acids 1-284), although we cannot exclude the possibility that other M-phase specific phosphorylation sites exist in other portions of BRCA2.

Identification of M-phase specific phosphorylation sites in the BR-N1 fragment.

To identify the M-phase specific phosphorylation sites within BR-N1, we generated a construct expressing BR-N1 translationally fused with mammalian Glutathione S-transferase (mGST) and FLAG epitope and transfected the construct into U2OS cells. The ectopically expressed FLAG-mGST-BR-N1 fusion protein was then purified using anti-FLAG affinity resins from non-treated and nocodazole-treated cells (Fig. 5A, left panel). Western blot with anti-BRCA2 antibodies specific for the N-terminal region confirmed the identity of the purified polypeptides (Fig. 5A, right panel). Both the hyperphosphorylated (ppFLAG-mGST-BRN1, Fig. 5A) and hypophosphorylated (pFLAG-mGST-BRN1, Fig. 5A) polypeptides were excised from the Coomassie blue stained gel for sequencing using microcapillary reverse-phase HPLC nanoelectrospray tandem mass spectrometry (on a Finnigan LCQ DECA quadrupole ion trap mass spectrometer). Two major M-phase specific phosphopeptides corresponding to the sequences shown in Fig. 5B (open and shaded boxes) were recovered after tryptic digestion of the hyperphosphorylated form of FLAG-mGST-BR-N1. Sequence analyses were able to confirm Ser239 of phosphopeptide B (PP-B) was phosphorylated, but only predicted 3 sites in phosphopeptide A (PP-A) were phosphorylated (Fig. 5B). Nevertheless, alignment of the phosphopeptide sequences revealed that PP-A is highly conserved among chicken, mouse, and human, while PP-B is only conserved between mouse and human (Fig. 5C) (46), suggesting that

the M-phase specific phosphorylation within this region may be vital for the overall function of BRCA2.

Plk1 and Cdk1 phosphorylate the BR-N1 fragment of BRCA2 in vitro.

The amino acid sequence surrounding the serine/threonine residues in the identified phosphopeptides (Fig. 5C) appears to show some resemblance to the predicted "consensus phosphorylation motif" for the highly conserved mitotic kinase, Polo-like kinase 1 (Plk1). This consensus motif, which is two negatively charged/uncharged amino acid residues preceding the Ser or Thr, followed by a hydrophobic/uncharged residue (for example, DE-**S/T**-L), is deduced from the sites identified in Plk1 phosphorylation of Cyclin B1 (47,48), Cdc25C (49), and TCTP (50). In addition, 4 potential phosphorylation sites for Cdk kinases were also found within BR-N1 (Fig. 5B), although they were not identified by mass spectrometric analysis. Cdk kinases display substrate specificity toward proteins containing the motif (**S/T**)-P-(X)-(K/R) (X stands for any amino acid) or (S/T)-P-(K/R) (51-53). Furthermore, it has been shown that during the cell cycle, the kinase activity of Plk1 and Cdk1 reaches maximum levels at the G2/M transition and gradually decreases as M phase proceeds, and both proteins play crucial roles in the entry and exit from mitosis (36,54-56). In light of this information, we performed *in-vitro* kinase assays using Plk1 and Cdk1 immunoprecipated from U2OS cells with GST-BR-N1 as the substrate. As shown in Fig. 6A, phosphorylation of BR-N1 by Plk1, but not by Cdk1, resulted in a dramatic mobility change of GST-BR-N1 which was comparable to BR-N1 isolated from M-phase cells (Fig. 6A, top panel, compare lane 3 with 7).

To confirm that Plk1 directly phosphorylates BR-N1, kinase active or inactive forms of HA-tagged Plk1 were transfected into U2OS, and extracts were subsequently prepared for

immunoprecipitation with anti-HA for *in-vitro* kinase assays. Significantly, only the active HA-Plk1 kinase was able to phosphorylate and induce a mobility change in GST-BR-N1 as detected by the ^{32}P signal (Fig. 6B, lane 3, indicated by PP) and by comparing protein position in the Coomassie blue stained gel (Fig. 6B, lane 6, indicated by two diamonds). The presence of HA-Plk1 in the assays was confirmed by Western blots (Fig. 6B, lanes 7-9). The phosphoproteins with lower molecular weight indicated by arrowheads likely represent Plk1 associated substrates (Fig. 6A, lane 3).

To determine which residues on BR-N1 are targeted by Plk1, various GST-BR-N1 mutants were generated (Fig. 6C) based on the mass spectrometric results, to serve as substrates in the Plk1 immunoprecipitation-kinase assays. Fig. 6D showed that phosphorylation of the GST-BR-N1S193A mutant was reduced, while phosphorylation of GST-BR-N1Δ193-207 was abolished (lanes 5 and 7, top panel). Together, these data suggest that Plk1 targets Ser193 and possibly two other sites between amino acids 193 and 207 on BRCA2 in an M-phase specific manner.

M-phase specific phosphorylation of BRCA2 does not affect its association with RAD51.

Several BRCA2-interacting proteins, including RAD51 (11,23,24) and P/CAF (29), and their minimal interacting motifs on BRCA2 have been identified (Fig. 7A). The interaction with RAD51 is central to the function of BRCA2 in HR. To investigate whether this M-phase specific phosphorylation influences the interaction between BRCA2 and RAD51, co-immunoprecipitation experiments using anti-human RAD51 antibody and extracts from interphase and M-phase T24 cells were performed. As shown in Fig. 7B (lanes 5 and 6), both of the hyperphosphorylated and hypophosphorylated forms of BRCA2 were co-immunoprecipitated with RAD51, suggesting that the association between BRCA2 and RAD51 is independent of the

M-phase specific phosphorylation event of BRCA2.

The hyperphosphorylated M-phase form of BRCA2 dissociates from P/CAF.

It has been shown that the N-terminus of BRCA2 associates with acetyltransferase activity when bound to P/CAF (29). By means of an *in-vitro* GST pull-down assay, the amino acid residues 290-453 of BRCA2 were determined to be sufficient for interaction with P/CAF. This interaction was also confirmed *in vivo* by co-immunoprecipitation of FLAG-tagged P/CAF with HA-tagged N-terminal region of BRCA2 (amino acid residues 1-1963). Because the major M-phase specific phosphorylation region of BRCA2 resides in its N-terminal region, we examined whether the association of P/CAF with BRCA2 is influenced by the M-phase hyperphosphorylation. A co-immunoprecipitation experiment was performed using cell extracts prepared from asynchronous, adriamycin-treated (G2 arrest), nocodazole-treated (M-phase-enriched), or mitotic shake-off (highly purified M-phase cells) U2OS cells, transiently transfected with a Myc-GFP-tagged BRCA2 N-terminal fragment (Myc-GFP-BRNL 1-672) as well as a FLAG-tagged P/CAF (FLAG-P/CAF). Fig. 7C showed that only the hypophosphorylated but not the hyperphosphorylated form of Myc-GFP-BRNL 1-672 could be co-immunoprecipitated with FLAG-P/CAF using anti-FLAG (M2) antibody (lanes 8-11). As previously shown in Fig. 2B, the predominant form of BRCA2 in M phase is the hyperphosphorylated form. Collectively, these observations suggest the interaction between BRCA2 and P/CAF is regulated by phosphorylation in a cell cycle dependent manner.

DISCUSSION

In the present study, we showed that (i) BRCA2 is hyperphosphorylated specifically in M

phase and becomes dephosphorylated as cells exit mitosis or enter interphase *in vivo*; (ii) the N-terminus of BRCA2 is the major M-phase specific phosphorylation region that contributes to the alterations in electrophoretic mobility of BRCA2. Furthermore, we demonstrated that (iii) the mitotic kinase Plk1 targets at least Ser193 within amino acids 193-204 of BRCA2 and (iv) dissociation of BRCA2 from P/CAF, but not from RAD51, correlates with M-phase specific phosphorylation of BRCA2. Taken together these data suggest that Plk1 may regulate a number of potential functions of BRCA2 during mitosis (Fig. 8).

The phenotypes of mice harboring various truncation mutations 5' of the BRC repeats in *Brca2*, range from embryonic lethality between E6 and E9, to survival until birth (9-12). Mouse embryonic cells derived from these mice show radiation sensitivity, defects in HR and pronounced chromosomal aberrations (57,58). These phenotypes can be attributed, in part, to the loss of RAD51 interacting function within the BRC repeats and conserved CTD and possibly the absence of nuclear localization (NLS) sequences in the extreme C-terminus (Fig. 7A) (57). Moreover, many cancer predisposing point mutations have also been identified within the BRC repeats (for example, D1420Y, G1529R) or clustered within the highly conserved C-terminal domain (for example, A2466V, A2951T) (Breast Cancer Information Core). Besides the potential involvement in transcription regulation, the function of the N-terminus of BRCA2 remains relatively unknown (28). Cancer predisposing point mutations have also been found within exon 3 (amino acids 23-105, Y42C) and in frame deletion of BRCA2 exon 3 has been identified in a Swedish family with a history of breast and ovarian cancer (59), suggesting that the N-terminus of BRCA2 must provide an important contribution to its overall functions.

Interestingly, it has been shown that the N-terminal region of BRCA2 (amino acids 18-141) associates with and is phosphorylated by a yet to be identified cellular kinase and removal of the

exon 3 region (amino acids 23-105) disrupted this interaction (60). Consistently, we found the extreme N-terminus of BRCA2 (amino acids 1-284, BR-N1), which includes the region encoded by exon 3, is phosphorylated specifically in M phase. More precisely, at least 4 phosphorylation sites within two stretches of amino acids (PP-A and PP-B, Fig 5C) within this region were identified to be targeted *in vivo*. Mutation of highly conserved Ser193 leads to a reduction in the phosphorylation of BR-N1 by Plk1, while elimination of one of these stretches of amino acid (193-207), abolishes BR-N1 phosphorylation by Plk1, suggesting that Plk1 targets at least Ser193 within this region of BRCA2 *in vivo*. Plk1, the mammalian ortholog of Drosophila Polo, has been implicated in the regulation of a number of mitotic events including entry into mitosis, centrosome separation and maturation, metaphase to anaphase transition and cytokinesis (55,56,61-63). These roles coincide with the potential roles of BRCA2 during the transition of G2 to M phase (to be discussed later). Although Cdk1 is able to phosphorylate BR-N1 *in vitro*, it does not induce the mobility change as seen with Plk1; however, we cannot eliminate the possibility that Cdk1 also targets BRCA2 *in vivo*. Moreover, since Ser239 is identified by the mass spectrometric analysis as another *in vivo* phosphorylation site, there are likely many kinases that target this region of BRCA2, implicating the potential for a very complex and intricate network of regulation for the N-terminus of BRCA2.

What is the consequence of M-phase specific phosphorylation of BRCA2? Our results suggest that RAD51 associates with both the hyperphosphorylated and hypophosphorylated forms of BRCA2 during mitosis; therefore, the M-phase specific phosphorylation of BRCA2 may have little influence on the function of the BRCA2/RAD51 complex. Our data however do suggest that P/CAF associates with the N-terminal region of BRCA2 and this association becomes disrupted following phosphorylation of BRCA2 during M phase. One potential function

of the intact BRCA2-P/CAF complex in G2 is to prevent premature entry into mitosis. This is consistent with our finding that BRCA2 is a substrate of Plk1, a kinase intimately linked to regulating entry into mitosis (54). It has been shown that phosphorylation of Ser133 and Ser147 on the Cyclin B1 and Ser198 on the Cdc25C phosphatase by Plk1 is required for their nuclear localization and cell mitotic entry (47-49). It is possible that Plk1 may also regulate BRCA2 in a similar manner. Furthermore, the dissociation of P/CAF from BRCA2 at pre-metaphase, may be necessary for proper chromosome segregation events (Fig. 8), which are monitored by mitotic checkpoints. Supporting this notion, BRCA2 has been reported to associate with BubR1, a spindle checkpoint kinase (64). Similarly, inactivation of another spindle protein, Bub1, is sufficient to overcome growth arrest and promote transformation of Brca2-deficient cells (65). Moreover, BRCA2 has been found to associate with a cruciform-DNA binding protein, BRAF35, in a supramolecular protein complex that associates with chromatin during mitosis. Microinjection of BRCA2 or BRAF35 antibodies results in a delayed entry into M phase (66). Deregulation of the potential BRCA2 function during mitosis may lead to major chromosomal alterations as seen in BRCA2-deficient cells. However, the precise role of the BRCA2-P/CAF complex during mitosis remains to be elucidated.

The observation that BRCA2 becomes hyperphosphorylated during M phase is significant in that it reveals a novel regulatory mechanism for BRCA2 functions. Further identification of other kinases responsible for phosphorylating BRCA2 at M-phase will enhance the understanding of the role of BRCA2 during mitosis.

ACKNOWLEDGEMENTS

We thank Eisuke Nishida and Kyung S. Lee for HA-Plk1 (WT and K82M) cDNAs, Yoshihiro Nakatani for FLAG-P/CAF cDNA, Phang-Lang Chen for GFP-BR-CR and mammalian GST cDNAs. We are grateful to Chi-Fen Chen, Diane Jones and Paula Garza for antibody production and to Jeanho Yun, Yong-Lei Shang and Ahmad R. H. Utomo for helpful discussions.

REFRENCES

1. Wooster, R., Bignell, G., Lancaster, J., Swift, S., Seal, S., Mangion, J., Collins, N., Gregory, S., Gumbs, C., and Micklem, G. (1995) *Nature* **378**, 789-792.
2. Tavtigian, S. V., Simard, J., Rommens, J., Couch, F., Shattuck-Eidens, D., Neuhausen, S., Merajver, S., Thorlacius, S., Offit, K., Stoppa-Lyonnet, D., Belanger, C., Bell, R., Berry, S., Bogden, R., Chen, Q., Davis, T., Dumont, M., Frye, C., Hattier, T., Jammulapati, S., Janecki, T., Jiang, P., Kehrer, R., Leblanc, J. F., Goldgar, D. E., and et al. (1996) *Nat Genet* **12**, 333-337.
3. Collins, N., McManus, R., Wooster, R., Mangion, J., Seal, S., Lakhani, S. R., Ormiston, W., Daly, P. A., Ford, D., Easton, D. F., and et al. (1995) *Oncogene* **10**, 1673-1675.
4. Gudmundsson, J., Johannesdottir, G., Bergthorsson, J. T., Arason, A., Ingvarsson, S., Egilsson, V., and Barkardottir, R. B. (1995) *Cancer Res* **55**, 4830-4832.
5. Wang, S. C., Shao, R., Pao, A. Y., Zhang, S., Hung, M. C., and Su, L. K. (2002) *Cancer Res* **62**, 1311-1314.
6. Zheng, L., Li, S., Boyer, T. G., and Lee, W. H. (2000) *Oncogene* **19**, 6159-6175.
7. Zheng, L., and Lee, W. H. (2001) *Exp Cell Res* **264**, 2-18.
8. Howlett, N. G., Taniguchi, T., Olson, S., Cox, B., Waisfisz, Q., De Die-Smulders, C., Persky, N., Grompe, M., Joenje, H., Pals, G., Ikeda, H., Fox, E. A., and D'Andrea, A. D.

(2002) *Science* **297**, 606-609.

9. Ludwig, T., Chapman, D. L., Papaioannou, V. E., and Efstratiadis, A. (1997) *Genes Dev* **11**, 1226-1241.

10. Suzuki, A., de la Pompa, J. L., Hakem, R., Elia, A., Yoshida, R., Mo, R., Nishina, H., Chuang, T., Wakeham, A., Itie, A., Koo, W., Billia, P., Ho, A., Fukumoto, M., Hui, C. C., and Mak, T. W. (1997) *Genes Dev* **11**, 1242-1252.

11. Sharan, S. K., Morimatsu, M., Albrecht, U., Lim, D. S., Regel, E., Dinh, C., Sands, A., Eichele, G., Hasty, P., and Bradley, A. (1997) *Nature* **386**, 804-810.

12. Connor, F., Bertwistle, D., Mee, P. J., Ross, G. M., Swift, S., Grigorieva, E., Tybulewicz, V. L., and Ashworth, A. (1997) *Nat Genet* **17**, 423-430.

13. Patel, K. J., Yu, V. P., Lee, H., Corcoran, A., Thistlethwaite, F. C., Evans, M. J., Colledge, W. H., Friedman, L. S., Ponder, B. A., and Venkitaraman, A. R. (1998) *Mol Cell* **1**, 347-357.

14. Yu, V. P., Koehler, M., Steinlein, C., Schmid, M., Hanakahi, L. A., van Gool, A. J., West, S. C., and Venkitaraman, A. R. (2000) *Genes Dev* **14**, 1400-1406.

15. Tutt, A., Gabriel, A., Bertwistle, D., Connor, F., Paterson, H., Peacock, J., Ross, G., and Ashworth, A. (1999) *Curr Biol* **9**, 1107-1110.

16. Liu, N., Lamerdin, J. E., Tebbs, R. S., Schild, D., Tucker, J. D., Shen, M. R., Brookman, K. W., Siciliano, M. J., Walter, C. A., Fan, W., Narayana, L. S., Zhou, Z. Q., Adamson, A. W., Sorensen, K. J., Chen, D. J., Jones, N. J., and Thompson, L. H. (1998) *Mol Cell* **1**, 783-793.

17. Takata, M., Sasaki, M. S., Tachiiri, S., Fukushima, T., Sonoda, E., Schild, D., Thompson, L. H., and Takeda, S. (2001) *Mol Cell Biol* **21**, 2858-2866.

18. Thompson, L. H., and Schild, D. (2001) *Mutat Res* **477**, 131-153.

19. Moynahan, M. E., Pierce, A. J., and Jasin, M. (2001) *Mol Cell* **7**, 263-272.

20. Tutt, A., Bertwistle, D., Valentine, J., Gabriel, A., Swift, S., Ross, G., Griffin, C., Thacker, J., and Ashworth, A. (2001) *Embo J* **20**, 4704-4716.

21. Xia, F., Taghian, D. G., DeFrank, J. S., Zeng, Z. C., Willers, H., Iliakis, G., and Powell, S. N. (2001) *Proc Natl Acad Sci U S A* **98**, 8644-8649.

22. Sung, P. (1994) *Science* **265**, 1241-1243.

23. Wong, A. K., Pero, R., Ormonde, P. A., Tavtigian, S. V., and Bartel, P. L. (1997) *J Biol Chem* **272**, 31941-31944.

24. Chen, P. L., Chen, C. F., Chen, Y., Xiao, J., Sharp, Z. D., and Lee, W. H. (1998) *Proc Natl Acad Sci U S A* **95**, 5287-5292.

25. Pellegrini, L., Yu, D. S., Lo, T., Anand, S., Lee, M., Blundell, T. L., and Venkitaraman, A. R. (2002) *Nature* **420**, 287-293.

26. Chen, C. F., Chen, P. L., Zhong, Q., Sharp, Z. D., and Lee, W. H. (1999) *J Biol Chem* **274**, 32931-32935.

27. Yang, H., Jeffrey, P. D., Miller, J., Kinnucan, E., Sun, Y., Thoma, N. H., Zheng, N., Chen, P. L., Lee, W. H., and Pavletich, N. P. (2002) *Science* **297**, 1837-1848.

28. Milner, J., Ponder, B., Hughes-Davies, L., Seltmann, M., and Kouzarides, T. (1997) *Nature* **386**, 772-773.

29. Fuks, F., Milner, J., and Kouzarides, T. (1998) *Oncogene* **17**, 2531-2534.

30. Yang, X. J., Ogryzko, V. V., Nishikawa, J., Howard, B. H., and Nakatani, Y. (1996) *Nature* **382**, 319-324.

31. Nakatani, Y. (2001) *Genes Cells* **6**, 79-86.

32. Narlikar, G. J., Fan, H. Y., and Kingston, R. E. (2002) *Cell* **108**, 475-487.

33. Chen, P. L., Scully, P., Shew, J. Y., Wang, J. Y., and Lee, W. H. (1989) *Cell* **58**, 1193-1198.

34. Kumar, V., and Chambon, P. (1988) *Cell* **55**, 145-156.

35. Zhong, Q., Chen, C. F., Li, S., Chen, Y., Wang, C. C., Xiao, J., Chen, P. L., Sharp, Z. D., and Lee, W. H. (1999) *Science* **285**, 747-750.

36. Lee, K. S., Yuan, Y. L., Kuriyama, R., and Erikson, R. L. (1995) *Mol Cell Biol* **15**, 7143-7151.

37. Park, M., Chae, H. D., Yun, J., Jung, M., Kim, Y. S., Kim, S. H., Han, M. H., and Shin, D. Y. (2000) *Cancer Res* **60**, 542-545.

38. Zhang, X., Herring, C. J., Romano, P. R., Szczepanowska, J., Brzeska, H., Hinnebusch, A. G., and Qin, J. (1998) *Anal Chem* **70**, 2050-2059.

39. Vaughn, J. P., Cirisano, F. D., Huper, G., Berchuck, A., Futreal, P. A., Marks, J. R., and Iglehart, J. D. (1996) *Cancer Res* **56**, 4590-4594.

40. Bertwistle, D., Swift, S., Marston, N. J., Jackson, L. E., Crossland, S., Crompton, M. R., Marshall, C. J., and Ashworth, A. (1997) *Cancer Res* **57**, 5485-5488.

41. Clarke, D. J., and Gimenez-Abian, J. F. (2000) *Bioessays* **22**, 351-363.

42. Khanna, K. K., and Jackson, S. P. (2001) *Nat Genet* **27**, 247-254.

43. Cortez, D., Wang, Y., Qin, J., and Elledge, S. J. (1999) *Science* **286**, 1162-1166.

44. Lee, J. S., Collins, K. M., Brown, A. L., Lee, C. H., and Chung, J. H. (2000) *Nature* **404**, 201-204.

45. Tibbetts, R. S., Cortez, D., Brumbaugh, K. M., Scully, R., Livingston, D., Elledge, S. J., and Abraham, R. T. (2000) *Genes Dev* **14**, 2989-3002.

46. Takata, M., Tachiiri, S., Fujimori, A., Thompson, L. H., Miki, Y., Hiraoka, M., Takeda, S., and Yamazoe, M. (2002) *Oncogene* **21**, 1130-1134.

47. Toyoshima-Morimoto, F., Taniguchi, E., Shinya, N., Iwamatsu, A., and Nishida, E. (2001) *Nature* **410**, 215-220.

48. Jackman, M., Lindon, C., Nigg, E. A., and Pines, J. (2003) *Nat Cell Biol* **5**, 143-148.

49. Toyoshima-Morimoto, F., Taniguchi, E., and Nishida, E. (2002) *EMBO Rep* **3**, 341-348.

50. Yarm, F. R. (2002) *Mol Cell Biol* **22**, 6209-6221.

51. Peter, M., Nakagawa, J., Doree, M., Labbe, J. C., and Nigg, E. A. (1990) *Cell* **61**, 591-602.

52. Holmes, J. K., and Solomon, M. J. (1996) *J Biol Chem* **271**, 25240-25246.

53. Nigg, E. A. (1993) *Curr Opin Cell Biol* **5**, 187-193.

54. Nigg, E. A. (1998) *Curr Opin Cell Biol* **10**, 776-783.

55. Nigg, E. A. (2001) *Nat Rev Mol Cell Biol* **2**, 21-32.

56. Donaldson, M. M., Tavares, A. A., Hagan, I. M., Nigg, E. A., and Glover, D. M. (2001) *J Cell Sci* **114**, 2357-2358.

57. Venkitaraman, A. R. (2001) *Curr Opin Cell Biol* **13**, 338-343.

58. Venkitaraman, A. R. (2002) *Cell* **108**, 171-182.

59. Nordling, M., Karlsson, P., Wahlstrom, J., Engwall, Y., Wallgren, A., and Martinsson, T. (1998) *Cancer Res* **58**, 1372-1375.

60. Milner, J., Fuks, F., Hughes-Davies, L., and Kouzarides, T. (2000) *Oncogene* **19**, 4441-4445.

61. Glover, D. M., Hagan, I. M., and Tavares, A. A. (1998) *Genes Dev* **12**, 3777-3787.

62. Weitzer, S., and Uhlmann, F. (2002) *Dev Cell* **2**, 381-382.

63. Seong, Y. S., Kamijo, K., Lee, J. S., Fernandez, E., Kuriyama, R., Miki, T., and Lee, K. S. (2002) *J Biol Chem* **277**, 32282-32293.

64. Futamura, M., Arakawa, H., Matsuda, K., Katagiri, T., Saji, S., Miki, Y., and Nakamura, Y. (2000) *Cancer Res* **60**, 1531-1535.

65. Lee, H., Trainer, A. H., Friedman, L. S., Thistlethwaite, F. C., Evans, M. J., Ponder, B. A., and Venkitaraman, A. R. (1999) *Mol Cell* **4**, 1-10.

66. Marmorstein, L. Y., Kinev, A. V., Chan, G. K., Bochar, D. A., Beniya, H., Epstein, J. A., Yen, T. J., and Shiekhattar, R. (2001) *Cell* **104**, 247-257.

67. Marston, N. J., Richards, W. J., Hughes, D., Bertwistle, D., Marshall, C. J., and Ashworth, A. (1999) *Mol Cell Biol* **19**, 4633-4642.

68. Liu, J., Yuan, Y., Huan, J., and Shen, Z. (2001) *Oncogene* **20**, 336-345.

69. Yuan, Y., and Shen, Z. (2001) *J Biol Chem* **276**, 48318-48324.

FIGURE LEGENDS

Fig. 1. BRCA2 is hyperphosphorylated specifically in M phase of the cell cycle *in vivo*.

(A) *The expression profile of BRCA2 protein during the cell cycle.* T24 cells were arrested in a quiescent state using contact inhibition and then released to grow. Cultures were harvested at 0, 12, 18, and 24 hrs following release (G0, G12, G18, and G24, lane 2-5), and M-phase cells (M, lane 6) were enriched by treatment of nocodazole. Recombinant BRCA2 expressed in sf9 cells was used as a control (Cntl, lane 1) for positioning of endogenous BRCA2. The whole-cell extracts were immunoblotted for BRCA2 (top), RB (middle), or p84 (bottom), a component of the nuclear matrix which was used as an internal control for equal loading.

(B) *The slower migrating forms of BRCA2 appear only in M phase.* Asynchronously growing

T24 cells were either untreated (ASN, lanes 1 and 5) or exposed to nocodazole for obtaining M-phase-Enriched cells (M-EN, lane 3). To obtain the Mitotic Shake-Off cells (M-SO, lane 2), cells were collected by shaking off the nocodazole-treated cells. To obtain M-phase-Synchronized cells (M-SN, lane 4) in the absence of nocodazole, cells were released from double thymidine block and then harvested once cells showed an increase in mitotic indices. The whole-cell extracts were immunoblotted for BRCA2 (top) or p84 (bottom).

(C) *Alteration in electrophoretic mobility of BRCA2 is due to phosphorylation.* Equal amounts of asynchronous (ASN, lane 1) or nocodazole-treated (NOC, lane 2) T24 whole-cell extracts were immunoprecipitated using anti-BRCA2 (BBA) monoclonal antibody. Endogenous BRCA2 immune complexes were either untreated (lanes 3 and 4) or treated (lanes 5 and 6) with alkaline phosphatase (PPase) and then immunoblotted with anti-BRCA2 (Ab-2) polyclonal antibody.

Fig. 2. DNA damage does not induce similar M-phase phosphorylation of BRCA2.

Asynchronous T24 cells were either untreated (ASN, lane 1), or exposed to nocodazole (NOC, lane 2), ionizing radiation (IR, lane 3), ultraviolet light (UV, lane 4), mitomycin C (MMC, lane 5), or hydroxyurea (HU, lane 6) as described in experimental procedures. The whole-cell extracts were immunoblotted for BRCA2 (top), BRCA1 (middle), or p84 (bottom).

Fig. 3. BRCA2 becomes dephosphorylated as cells exit from M phase.

Nocodazole-arrested T24 cells collected by the mitotic shake-off method were re-plated in fresh media to allow re-entry into the cell cycle. Whole-cell extracts were prepared at 0, 0.3, 0.6, 1, 1.5, 2, 4, 8, and 14 hr(s) after removal of nocodazole, and immunoblotted for BRCA2 (top), RB (middle), or p84 (bottom). The phases of the cell cycle, M, G1, and S, are indicated below the

bottom panel.

Fig. 4. Mapping the region of BRCA2 that is hyperphosphorylated during M phase.

(A) *A schematic diagram of full length BRCA2 and the various BRCA2 fragments used in identifying the M-phase specific phosphorylation sites.* The size and location of the various Myc-GFP-BRCA2 fragments used in the transient transfection assays are shown below the full length schematic of BRCA2. EX3 and CTD stand for exon 3 and the conserved C-terminal domain of BRCA2, respectively. The various degrees of electrophoretic mobility shift of the BRCA2 fragments seen in cells exposed to nocodazole are indicated by minus signs (-, no change), single plus signs (+, slight change), or double plus signs (++, distinct change).

(B) *Identification of the major M-phase specific phosphorylation regions of BRCA2, which contribute to the distinct shift in electrophoretic mobility.* U2OS cells were transiently transfected with Myc-GFP-BRCA2 expression constructs (lanes 1-24), which contain various fragments of BRCA2 as shown in **(A)**. Equal amounts of whole-cell extracts from untransfected asynchronous parental (UN, lane 0), transfected asynchronous (all of the odd numbered lanes), or nocodazole-treated (all of the even numbered lanes except lane 0) U2OS cells were analyzed by immunoblotting with anti-GFP antibody.

Fig. 5. Identification of M-phase specific phosphorylation sites on the BR-N1 fragment of BRCA2.

(A) *Purification of FLAG-mGST-BR-N1 for mass spectrometric analysis.* Whole-cell extracts made from untransfected parental (UN, lanes 1 and 4) and untreated (ASN, lanes 2 and 5) or nocodazole-treated (NOC, lanes 3 and 6) U2OS cells transfected with the construct expressing

BR-N1 fused with FLAG and mGST were subjected to immunoaffinity purification using anti-FLAG resins. Bound proteins were resolved on SDS-PAGE and stained with Coomassie blue (lanes 1-3) or analyzed by Western blot using anti-BRCA2 polyclonal antibody (lanes 4-6). The polypeptides corresponding to FlAG-mGST-BRN1-p and -pp were excised for mass spectrometric analysis. IgG HC and LC stand for IgG heavy and light chains, respectively.

(B) *The amino acid sequence of BR-N1 (1-284) and the phosphopeptides identified by mass spectrometric analysis.* BR-N1 constitutes the first 284 amino acids of the N-terminus of BRCA2. The M-phase specific phosphopeptides, PP-A and PP-B, and phosphorylation site, Ser239, identified by mass spectrometric analysis are indicated as an open box, shaded box and a star symbol, respectively. The potential Cdk phosphorylation motifs are underlined.

(C) *The identified M-phase specific phosphopeptides of BRCA2 are highly conserved.* Amino acid sequence alignment of the identified M-phase specific phosphopeptides (PP-A and PP-B) from human (H) BRCA2 with its mouse (M) and chicken (C) counterparts. The highly conserved residues Ser181, Ser183, Ser193, Ser196, Ser197, Thr200, Thr203, and Thr207 within PP-A are boxed; Ser239 is conserved between mouse and human.

Fig. 6. Polo-like kinase1 (Plk1) phosphorylates BR-N1 fragment of BRCA2.

(A) *In vitro Plk1 and Cdk1 kinase assays with GST-BR-N1.* Whole-cell extracts prepared from U2OS cells were immunoprecipitated with control IgG, (lane 4) anti-Plk (lanes 1 to 3) or anti-Cdk1 antibody (lanes 5 to 7); immune complexes were incubated with [γ-^{32}P]-ATP in the presence of 2 μg of the indicated substrates for the kinase reaction. Casein and histone H1 were used as controls for the kinase assays. Following the reaction, the samples were divided equally for SDS-PAGE and Coomassie blue staining (middle panel), autoradiography (top panel) and

Western blot analysis with anti-Plk and Cdk1 antibodies (bottom panel). IgG HC stands for IgG heavy chain.

(B) *BR-N1 is phosphorylated specifically by Plk1*. Extracts prepared from U2OS cells transfected with kinase inactive (KD, lanes 2, 5 and 8) or active (WT, lanes 3, 6, and 9), and from untransfected parental cells (UN, lanes 1, 4 and 7). HA-Plk1 was immunoprecipitated with anti-HA antibody for *in-vitro* kinase assays with 2 μg of GST-BR-N1 and [γ–^{32}P]-ATP. The reactions were divided equally and fractionated on SDS-PAGE for Coomassie blue staining (middle panel), autoradiography (left panel) and Western Blot analysis with anti-HA antibodies (right panel). Hypo- and hyperphosphorylated GST-BR-N1 (lane 6) in the Comassie blue stained gel are indicated by single and double diamond(s), respectively. Potential Plk1 associated substrates (lane 3) are indicated by arrow heads. IgG HC stands for IgG heavy chain.

(C) *Phosphorylation mutants of GST-BR-N1*. The specific serine to alanine (S to A) and deletion (Δ, boxed) mutants of BR-N1 are shown.

(D) *In-vitro kinase assay of Plk1 with various GST-BR-N1 phosphorylation mutants*. Plk1 immune-complexes were incubated with 2 μg of the various substrates indicated and [γ–^{32}P]-ATP as described in Methods and Materials. The samples were divided equally for SDS-PAGE and Coomassie blue staining (middle panel), autoradiography (top panel) and Western blot analysis with anti-Plk antibody (bottom panel). IgG HC stands for IgG heavy chain.

Fig. 7. M-phase phosphorylated BRCA2 associates with RAD51 but not with P/CAF *in vivo*.

(A) *Schematic diagram showing BRCA2 interacting proteins*. The minimal amino acid region on BRCA2 required for association with P/CAF, RAD51, BRAF35, DSS1, BUBR1, BCCIP and FLNa, are indicated by short bars and shown above the schematic for full length BRCA2

(11,23,24,29,64,66-69). Exon 3 (EX3), 8 BRC repeats, and conserved C-terminal domain (CTD) are shown below BRCA2. The size and location of the BRCA2 N-terminal fragment (BR-NL) harboring the potential M-phase specific phosphorylation sites used for the co-immunoprecipitation studies with FLAG-P/CAF are also presented.

(B) *Endogenous hyperphosphorylated (M-phase form) and hypophosphorylated (interphase form) BRCA2 both associate with RAD51 in vivo.* Equal amounts of asynchronous (ASN, lane 1) or nocodazole-treated (NOC, lane 2) T24 whole-cell extracts were immunoprecipitated using murine IgG (lanes 3 and 4) as a control or anti-RAD51 antibody (lanes 5 and 6), fractioned on 5-10 % gradient SDS-PAGE and subjected to Western blot analysis for BRCA2 (top) or RAD51 (bottom).

(C) *M-phase hyperphosphorylated N-terminus of BRCA2 dissociates from P/CAF.* U2OS cells were transiently co-transfected with GFP-tagged BRCA2 N-terminus (GFP-BR-NL) and FLAG-tagged P/CAF (FLAG-P/CAF) and the transfected cells were either untreated (ASN, lanes 2, 7, and 8; lane 1 and 6 referred as untransfected parental cells), or treated with adriamycin (ADM, lanes 3 and 9), or nocodazole (NOC, lanes 4 and 10, referred as M-phase-enriched cells); the highly purified M-phase cells (M-SO, lanes 5 and 11) were collected using the mitotic shake-off method. The whole-cell extracts were immunoprecipitated with murine IgG (lane 7) as a control or anti-FLAG antibody (M2, lanes 6 and 8-11). The resulting immune complexes were immunoblotted with anti-GFP (top) or anti-FLAG antibody (bottom). Hyperphosphorylated and hypophosphorylated GFP-BR-NL are indicated with PP and P, respectively.

Fig. 8. Model for the possible roles of M-phase specific phosphorylation event of BRCA2. The intact BRCA2-P/CAF complex in G2 may have roles related to preventing premature entry

of cells into mitosis. Since Plk1 is important for cellular mitotic entry, phosphorylation of BRCA2 by Plk1 and possibly by Cdk1 and other M-phase kinase may regulate this potential function of the BRCA2-P/CAF complex. Furthermore, one of the consequences of the hyperphosphorylation event of BRCA2 is the dissociation of P/CAF, which may allow BRCA2 and its associated proteins to participate in modulating chromatin structure for proper transition of cells through mitosis. Once cells exit mitosis and re-enter G1, hyperphosphorylated BRCA2 becomes dephosphorylated, perhaps to re-establish association with P/CAF for interphase functions.

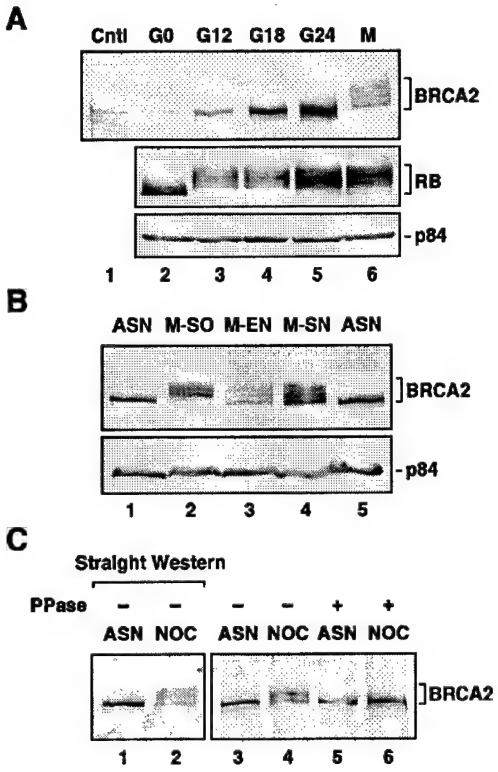

Fig. 1A. 1B. 1C.
(Lin,H.R. *et al.*)

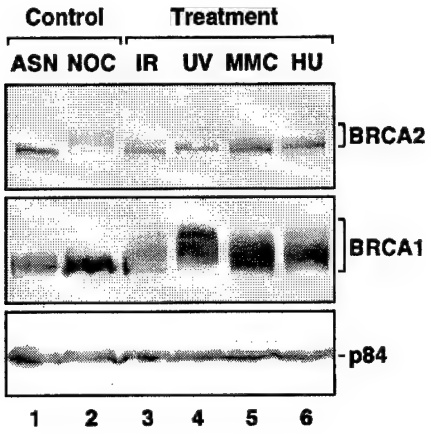

Fig. 2.
(Lin,H.R. *et al.*)

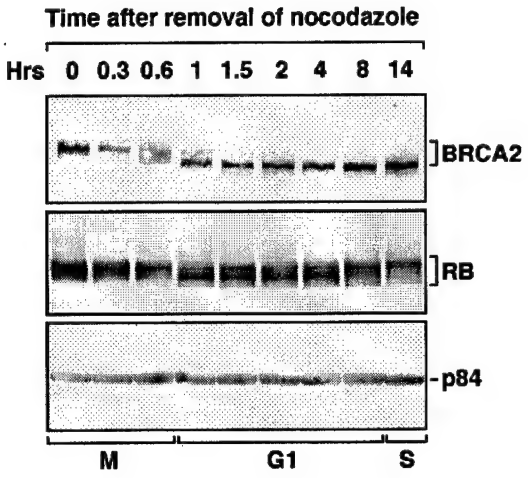

Fig. 3.
(Lin,H.R. *et al.*)

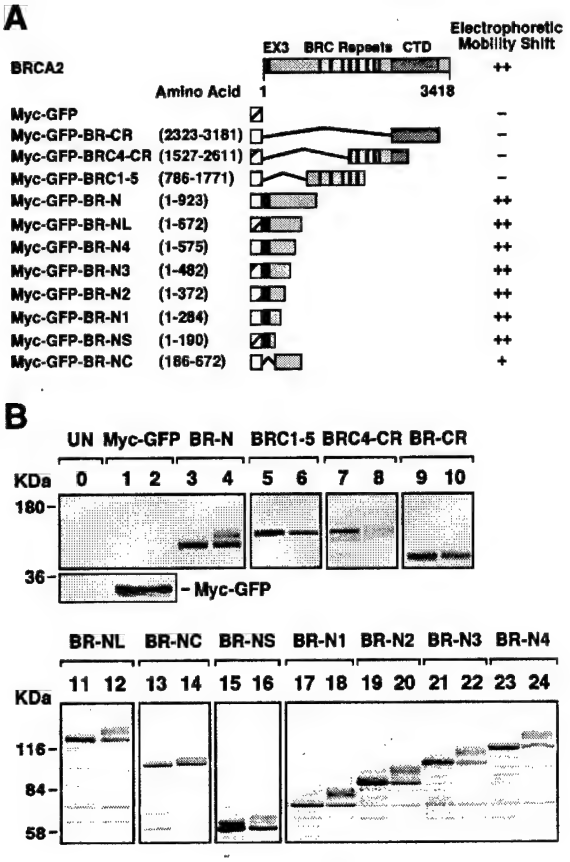

Fig. 4A. 4B.
(Lin,H.R. *et al.*)

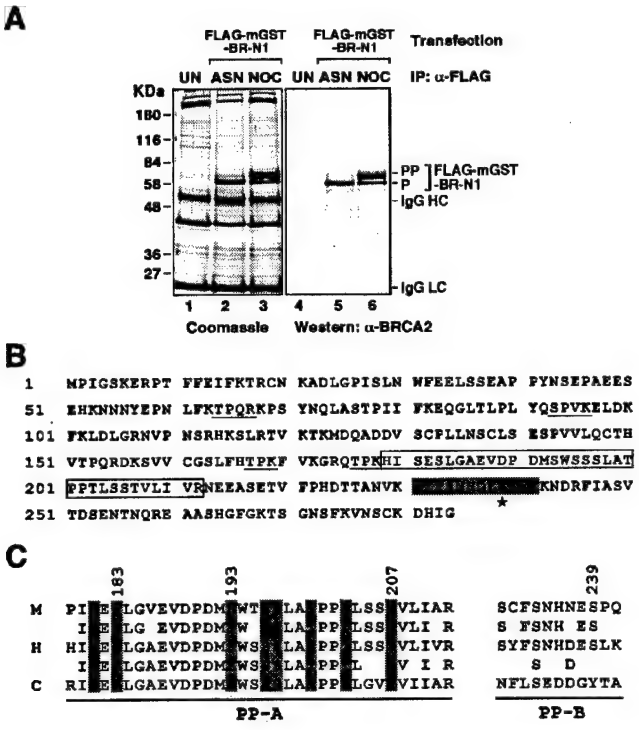

Fig. 5A. 5B. 5C
(Lin,H.R. *et al.*)

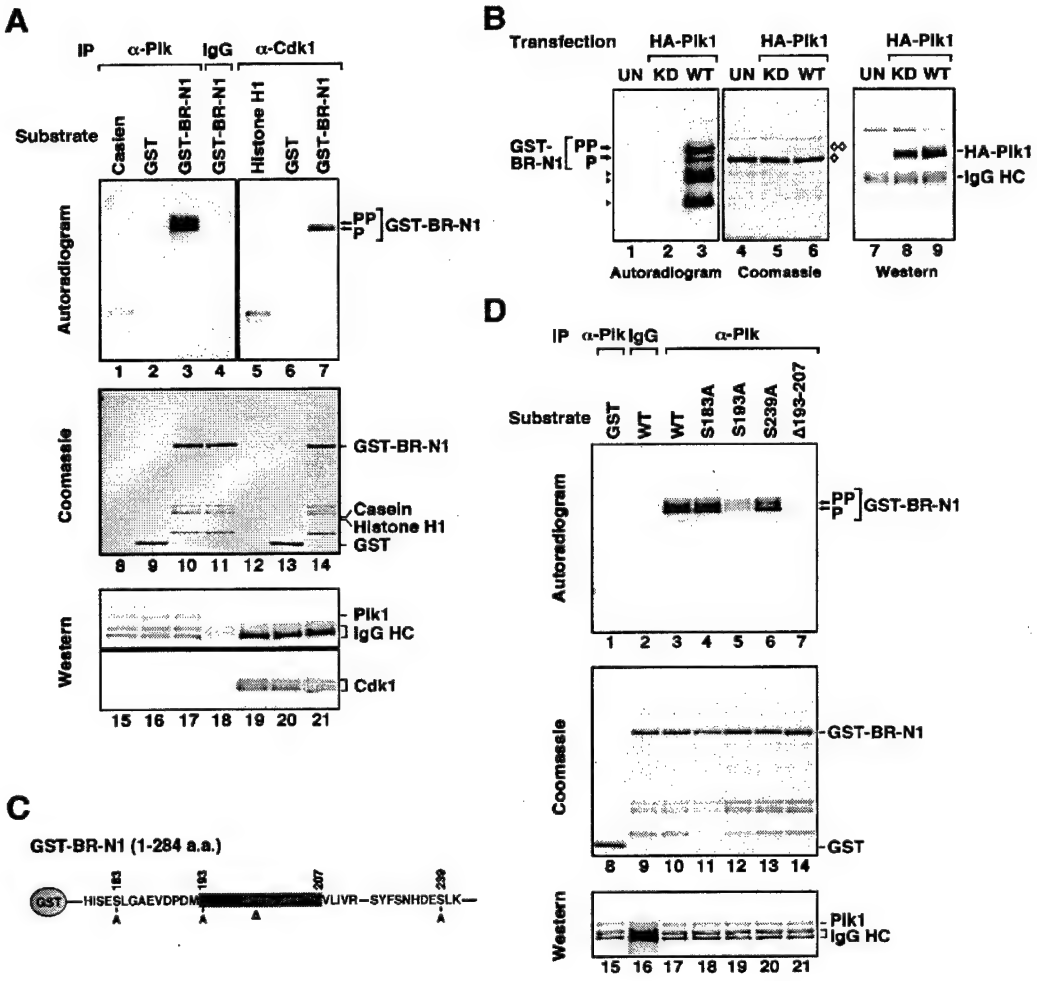

Fig. 6A. 6B. 6C. 6D
(Lin,H.R. *et al.*)

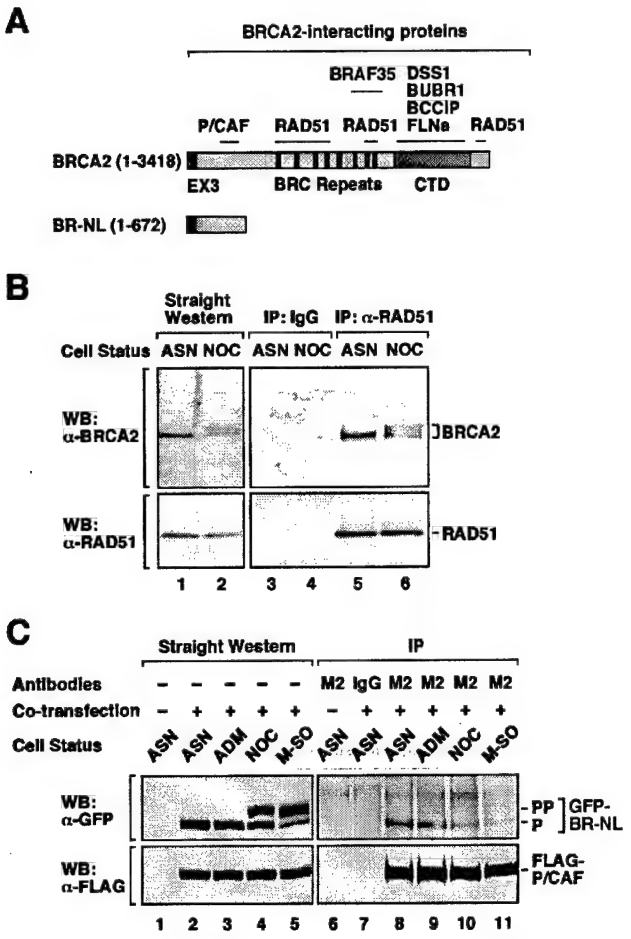

Fig. 7A. 7B. 7C.
(Lin,H.R. *et al.*)

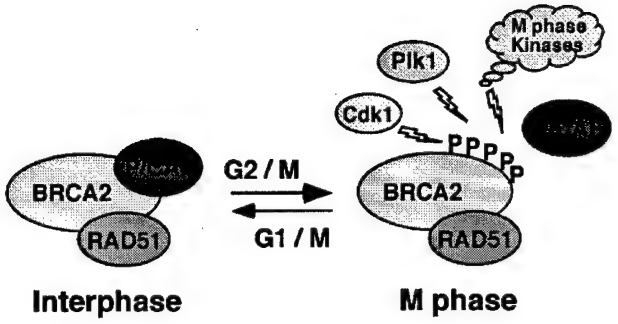

Fig. 8.
(Lin,H.R. *et al*)

Molecular Cell, Vol. 12, 221–232, July, 2003, Copyright ©2003 by Cell Press

Recruitment of the Recombinational Repair Machinery to a DNA Double-Strand Break in Yeast

Branden Wolner,[1] Stephen van Komen,[2] Patrick Sung,[2] and Craig L. Peterson[1,*]
[1]Program in Molecular Medicine
University of Massachusetts Medical School
Worcester, Massachusetts 01605
[2]Institute of Biotechnology and
Department of Molecular Medicine
University of Texas Health
Science Center at San Antonio
San Antonio, Texas 78245

Summary

Repair of DNA double-strand breaks (DSBs) by homologous recombination requires members of the *RAD52* epistasis group. Here we use chromatin immunoprecipitation (ChIP) to examine the temporal order of recruitment of Rad51p, Rad52p, Rad54p, Rad55p, and RPA to a single, induced DSB in yeast. Our results suggest a sequential, interdependent assembly of Rad proteins adjacent to the DSB initiated by binding of Rad51p. ChIP time courses from various mutant strains and additional biochemical studies suggest that Rad52p, Rad55p, and Rad54p each help promote the formation and/or stabilization of the Rad51p nucleoprotein filament. We also find that all four Rad proteins associate with homologous donor sequences during strand invasion. These studies provide a near comprehensive view of the molecular events required for the in vivo assembly of a functional Rad51p presynaptic filament.

Introduction

DNA double-strand breaks (DSBs) arise in DNA due to environmental insults such as ionizing radiation or chemical exposure. DSBs also play an important role as intermediates in DNA replication, immunoglobulin V(D)J recombination, meiotic and mitotic crossing-over, and yeast mating-type switching. Failure to correctly process these DSBs can result in deletion or insertion of genetic information, chromosomal fragmentation, translocation, and chromosome loss.

Homologous recombination (HR) is a major pathway of DSB repair in all eukaryotes and has a distinct advantage over other mechanisms in that it is mostly error free. Repair of DSBs by HR requires the *RAD52* epistasis group, defined by the yeast *RAD50, RAD51, RAD52, RAD54, RAD55, RAD57, RAD59, MRE11*, and *XRS2* genes. These genes are highly conserved among all eukaryotes (Cromie et al., 2001; Pâques and Haber, 1999; Sung et al., 2000), highlighting the importance of these proteins for cell survival. In yeast, loss-of-function mutations in these *RAD* genes disrupt HR, leading to extreme sensitivity to radiation and chemical mutagens, as well as a vastly reduced capacity for mating-type switching (reviewed in Pâques and Haber, 1999; Sung et al., 2000). In the mouse, a homozygous null allele of *RAD51* leads to embryonic lethality (Tsuzuki et al., 1996), and mutations in *RAD* genes are associated with a spectrum of diseases, including cancer (reviewed in Ivanov and Haber, 1997; Jasin, 2000; Michelson and Weinert, 2000).

Studies in yeast have suggested a sequence of molecular events that occur following formation of a DSB (reviewed in Haber, 1998, 2000; Pâques and Haber, 1999; Sung et al., 2000). First, the 5′ ends of DNA that flank the break are resected by an exonuclease. Rad51p, a functional homolog of the *E. coli* RecA recombinase, then binds the exposed single-stranded tails forming a right-handed helical nucleoprotein filament. In vitro, Rad52p (Sung, 1997a) and a Rad55p/Rad57p heterodimer (Sung, 1997b) can promote this early step by overcoming the inhibitory effects of the heterotrimeric single-stranded DNA binding protein, RPA. The Rad51p nucleoprotein filament is then believed to function in cooperation with Rad54p to search the genome for a homologous pairing partner and to form a heteroduplex "joint molecule" (Petukhova et al., 1998, 2000). Joint molecule formation is followed by extension of the incoming strand by DNA polymerases and branch migration, ultimately leading to restoration of the genetic information spanning the break (reviewed in Pâques and Haber, 1999).

Much less is known about how Rad proteins functionally cooperate during DSB repair in vivo. Immunofluorescence studies have shown that Rad51p, Rad52p, and Rad54p colocalize to "foci" in response to DNA damage in vivo (Haaf et al., 1995; Tan et al., 1999), suggesting that Rad proteins might function together within a larger, multiprotein complex. Consistent with this view, coimmunoprecipitation and yeast two-hybrid assays have shown that many members of the *RAD52* group can interact with each other (Golub et al., 1997; Hays et al., 1995; Johnson and Symington, 1995; Krejci et al., 2001). In contrast, recent studies indicate that the composition of the damage-induced foci are dynamic, and photobleaching studies indicate that several Rad proteins have very different diffusion coefficients, suggesting that they may not exist together in a preassembled protein complex (Essers et al., 2002).

We wished to dissect how Rad proteins are recruited and function at a DSB in vivo. Here we use chromatin immunoprecipitation (ChIP) analyses to examine the temporal order of Rad protein recruitment to a single, induced DSB in yeast. Our results suggest a sequential pathway, where Rad51p binds first, followed by Rad52p, Rad55p, and finally Rad54p. Each of these Rad proteins also associates with the homologous donor sequences during strand invasion. We further examined the functional interdependencies among these proteins by performing ChIP analyses in each single *rad* mutant. These results demonstrate key roles for Rad52p, Rad55p, and Rad54p in facilitating the formation of the Rad51p nucleoprotein filament. The unexpected requirement for *RAD54* during this early step in HR is explained by its mediator function as revealed in biochemical experiments.

*Correspondence: craig.peterson@umassmed.edu

Results

To facilitate analysis of Rad protein recruitment to a DSB in vivo, we generated an isogenic set of yeast strains. Each strain contains a *GAL10-HO* fusion gene that provides rapid expression of the HO endonuclease when cells are transferred to galactose media. Expression of HO leads to a single DSB at the *MAT* locus. For chromatin immunoprecipitation analyses, 13Myc epitope-tagged alleles of Rad51p, Rad54p, Rad55p, and Rfa1p (the 70 kDa subunit of RPA) were generated by homologous recombination at their C-terminal, genomic locations. The Rad54p-13Myc and Rad55p-13Myc proteins were fully functional for DNA repair, as each of these epitope-tagged alleles fully complemented the MMS sensitivity characteristic of the *rad54Δ* and *rad55Δ* null mutants at 30°C (data not shown). Likewise, the Rfa1p-13Myc allele showed no growth defects or MMS sensitivity at 30°C (data not shown). The *RAD51-13Myc* allele exhibited a weak MMS sensitivity, and thus key observations made with this strain were verified using polyclonal antibodies to Rad51p and strains that lacked the 13Myc epitope tag. Polyclonal antibodies to Rad52p were used to monitor Rad52p recruitment in each strain.

Sequential Binding of RAD52 Group Proteins in Cells that Lack Homologous Donors

First, we investigated the recruitment of Rad proteins to a single DSB in strains that lacked homologous donor sequences (*hmlΔ hmrΔ*). In such strains the DSB cannot be repaired efficiently, and we anticipated that recruitment events might be more easily detected. In all ChIP experiments, strains were grown at 30°C in YEP media with raffinose as the sole carbon source until mid-log phase. Galactose was then added in order to induce expression of the HO endonuclease. At various times after galactose addition, cell aliquots were removed and treated with formaldehyde to induce crosslinking of proteins to DNA, and samples were processed for chromatin immunoprecipitation. In every time course, samples were also analyzed for the formation of a DSB at the *MAT* locus using a PCR assay (Figure 1A, upper). Loss of a PCR product spanning the site of the break is detectable as early as 10 min after galactose induction and proceeds with roughly first-order kinetics until the reaction reaches completion about 50 min after induction. Approximately 10% of the original signal remains at this point and persists for as long as 4 hr in strains that lack homologous donor sequences (data not shown). These kinetics were highly reproducible and taken as a measure of correct DSB formation in each experiment. Each time point in the chart (Figure 1A, lower) represents the average of at least four experiments.

Figure 1B shows a typical ChIP from the *RAD51-13Myc* strain that lacks homologous donors, using either an antibody to the Myc tag or a polyclonal antibody to Rad52p. Immunoprecipitated DNA was analyzed by PCR for the presence of *MAT* locus DNA from both sides of the induced DSB. The *MAT*-Z side of the DSB is the normal substrate for HR, whereas the *MAT*-Y side of the break contains mating-type specific DNA sequences and is not believed to participate in homology searching. PCR primers specific to the *PHO5* promoter (which is on a different chromosome from MAT) were included as a control. These raw data were quantified and the amounts of immunoprecipitated DNA were divided by the input amounts resulting in a "percent IP" value at each time point. Since the initial percent IP for each amplicon was different, each set was normalized to its time zero value (relative percent IP), and these data are presented in Figure 1C. Figure 1D represents averages of several long time courses.

Rad51p-13Myc was detected at both sides of the *HO*-induced DSB as early as 20 min after induction of *HO* expression (Figure 1B). At this time roughly 45% of the cells contain a DSB at *MAT* (Figure 1A). Similar results were observed when polyclonal antibodies to Rad51p and an untagged strain were used in the analysis (data not shown). In contrast, immunoprecipitation of Rad52p from these same extracts indicated that Rad52p was not detectable until 40 min after galactose addition, when 80% of the cells harbor a DSB (Figure 1B, compare middle and bottom panels). Similar kinetics of Rad52p recruitment was also observed in strains that lack a Myc-tagged allele of Rad51p (for example, see Figure 1D). The *PHO5* signals seen in Figure 1B represent background, genome-wide binding of Rad proteins. These signals were not observed (nor were the *MAT*-Y or *MAT*-Z signals) when a mock immunoprecipitation was performed without antibody or when anti-Myc antibody was used with an untagged strain (data not shown). In both sets of immunoprecipitates, the relative percent IP of the *PHO5* promoter remained unchanged (Figure 1C, diamonds), verifying that Rad51p-13Myc and Rad52p were specifically recruited to the *MAT* locus.

While recruitment of both Rad51p-13Myc and Rad52p appears to increase in a linear fashion over the first 90 min (Figure 1C), there is a rapid and large increase in recruitment detected by ChIP between 90 and 120 min (Figure 1D). At these time points, DSB induction has reached its maximum, but in strains that contain the silent mating-type information, homologous recombination would not yet be completed (Connolly et al., 1988; White and Haber, 1990). We also observe a clear polarity in the recruitment of these proteins, with a 2- to 3-fold preference for *MAT*-Z (triangles) over *MAT*-Y (squares) at the 2 hr time point, but at 4 hr, recruitment to both sides is nearly equal.

We next performed ChIP assays using donorless strains harboring either a Rad54p-13Myc or Rad55p-13Myc allele. A typical set of raw data is shown in Figure 2A and quantified in Figure 2B. A clear increase in Rad55p-13Myc binding (at least 50% over background) is detected on the *MAT*-Z side of the DSB as early as 40 min after induction (Figure 2B, lower panel, triangles), while comparable binding to the *MAT*-Y side of the DSB (squares) is not detectable until the 60 min time point. On the longer time scale (Figure 2C), we see an abrupt and dramatic increase in binding of Rad55p-13Myc to both sides of the break at the 2 hr time point, and there is a roughly 2-fold preference for *MAT*-Z (Figure 2C, lower chart). This result is similar to the recruitment seen for Rad51p-13Myc and Rad52p (Figure 1D). Since Rad55p and Rad57p are thought to form a heterodimer

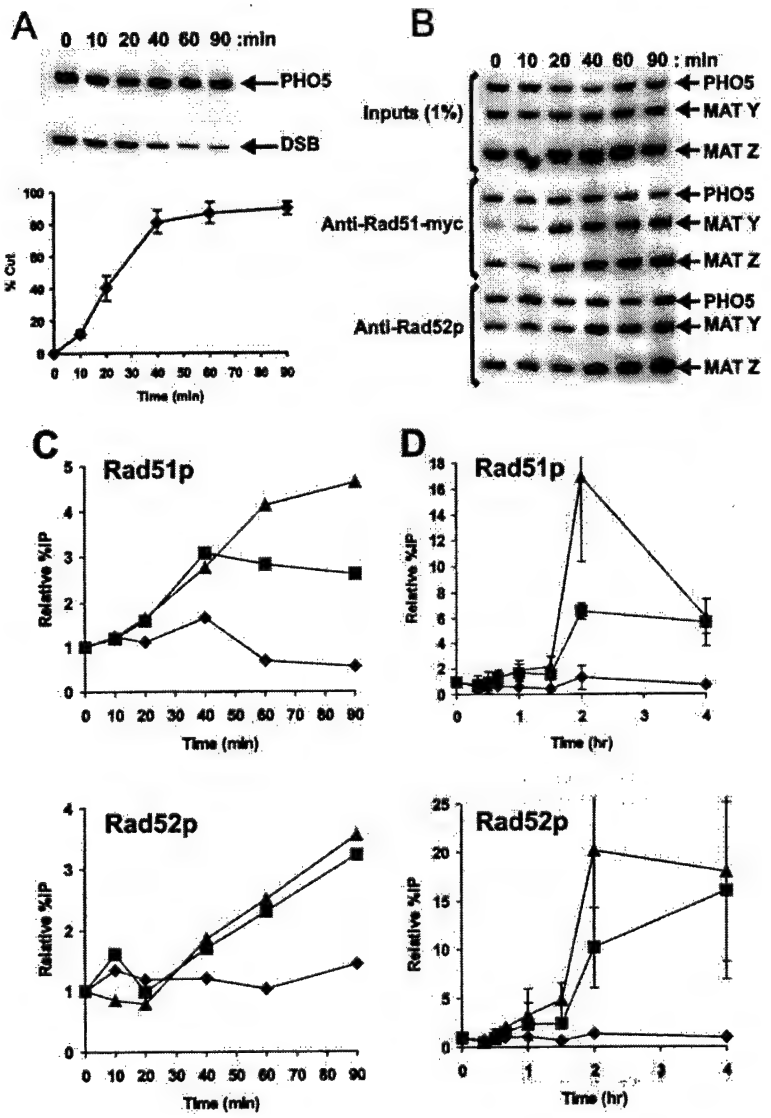

Figure 1. Recruitment of Rad51p-13Myc and Rad52p to an Induced DSB In Vivo

(A) Double-strand break induction kinetics. Galactose (2%, w/v) was added to cells in mid-log phase in order to induce HO endonuclease expression. Genomic DNA was purified at various time points, and PCR was performed using primers that flank the HO cut site from 96 bp CEN proximal of the HO cut site to 91 bp CEN distal. Appearance of the DSB is detected as a loss of PCR product (labeled DSB in the upper panel). Primers specific to the *PHO5* promoter region (Krebs et al., 2000) were included in the PCR as a control. DSB bands were quantified using a phosphorimager and the ImageQuant software, normalized to the *PHO5* bands, and plotted as the percentage of starting signal lost ("% Cut"). The chart in the lower panel represents the averages of at least four experiments per time point.

(B) Representative gels of ChIP assays performed using the same extracts as in (A). This strain lacked homologous donors sequences and harbored a 13Myc-tagged allele of *RAD51*. ChIPs were performed as described in the Experimental Procedures. "Input" DNA represents 1% of the total DNA used for the immunoprecipitations. DNA purified from the immunoprecipitations was subjected to PCR using primers specific to the *PHO5* promoter region, as well as the *MAT*-Y (from 78 bp to 361 bp CEN proximal of the HO cut site) and the *MAT*-Z (from 18 bp to 257 bp CEN distal of the HO cut site) regions of the *MAT* locus. Note that both the anti-Rad51p-13Myc and anti-Rad52p IPs were performed using the same extracts.

(C) The bands in (B) were quantified. For each locus, the amount of signal in the IP was divided by the amount of signal in the corresponding input and then normalized to the time zero value giving a "relative % IP." The results from the anti-Rad51p-13Myc IPs are plotted in the upper chart and those from the anti-Rad52p IP in the lower chart (*PHO5*, diamonds; *MAT*-Y, squares; *MAT*-Z, triangles). These data are representative of at least three independent short time course experiments.

(D) Long time courses of anti-Rad51p-13Myc (upper) and anti-Rad52p (lower) ChIP assays. These curves represent averages of three experiments for Rad51p-13Myc and five experiments for Rad52p. Error bars represent one standard deviation from the mean. Data obtained for Rad51p and Rad51p-13Myc using a polyclonal anti-Rad51p antibody were qualitatively comparable (data not shown). Note that the Rad52p ChIP dataset includes experiments from untagged Rad51 strains.

in vivo, we predict that the kinetics of Rad57p binding would parallel Rad55p-13Myc.

The time course for Rad54p binding is markedly different than other Rad proteins. We see no detectable binding of Rad54p-13Myc over background (i.e., the *PHO5* control) until 90 min after galactose addition. There is then an abrupt increase in the binding of Rad54p-13Myc between 90 min and 2 hr after galactose addition, similar to what was seen for Rad51p-13Myc, Rad52p, and Rad55p-13Myc. However, in the case of Rad54p-13Myc, the 2 hr time point does not represent the peak level of recruitment (Figure 2C, upper); Rad54p-13Myc binding continues to increase over the next 2 hr to a peak at roughly 12-fold over baseline. Rad54p binding, as detected by ChIP, also shows a dramatic preference for *MAT*-Z, with no detectable binding to *MAT*-Y.

Recruitment of RAD52 Group Proteins in Switching-Competent Strains

The results of the ChIP time courses in strains that lack homologous donors suggest a temporal sequence of recruitment events, where initial recruitment of Rad51p appears to be followed by Rad52p, Rad55p, and Rad54p. To investigate whether this sequence of events is influenced by the presence of homologous donors, we performed ChIP assays in strains that harbored an intact *HML* locus that serves as a donor for repair of the DSB at MATa.

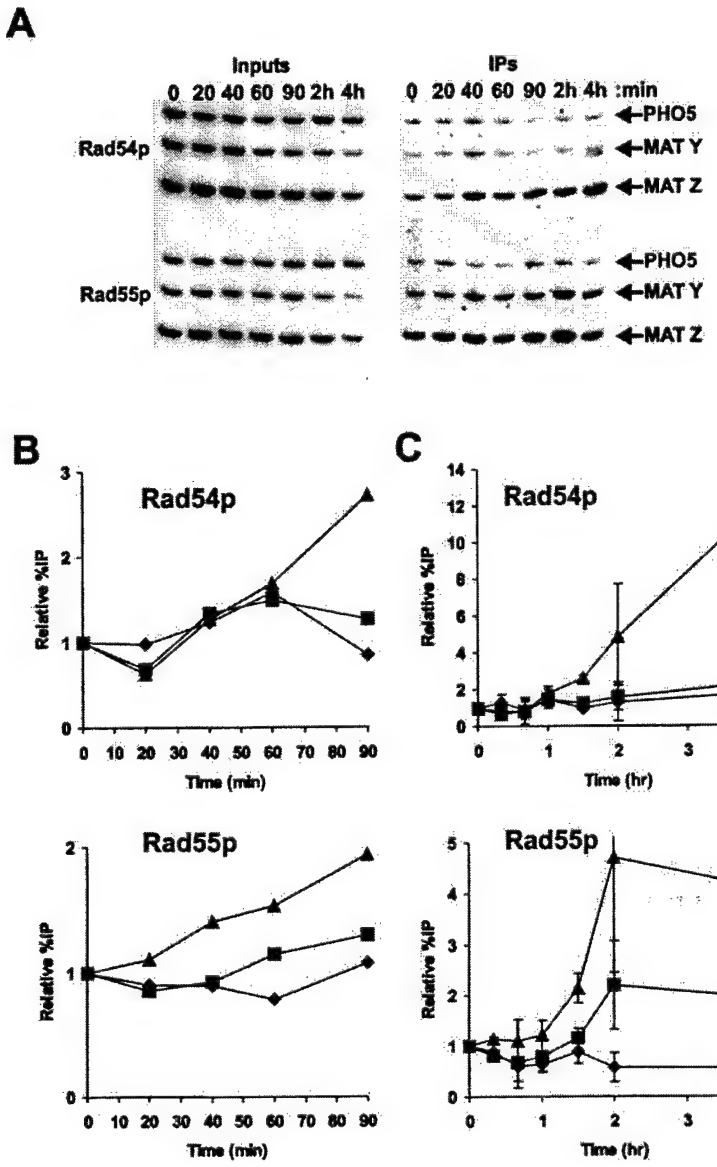

Figure 2. Recruitment of Myc-Tagged Rad54p and Rad55p to an Induced DSB

(A) Representative gels of PCR products from Rad54p-13Myc (upper) and Rad55p-13Myc (lower) ChIP assays in strains that lack homologous donor sequences.

(B) The bands in (A) were quantified and plotted as described in Figure 1 (*PHO5*, diamonds; *MAT*-Y, squares; *MAT*-Z, triangles). These data are representative of three independent time courses each.

(C) Long time courses for Rad54p-13Myc (upper) and Rad55p-13Myc (lower) ChIP assays. These curves represent the averages of three experiments each. Error bars represent one standard deviation from the mean.

Figure 3A shows typical PCR assays that monitor the kinetics of DSB formation and of invasion of the *MAT* recipient strand into the repair donor site (*HML*α). The schematic represents the postsynaptic complex and illustrates the design of PCR primers used in these experiments. Note that the "strand invasion" PCR product cannot be detected until the incoming, recipient strand is extended at least 30 bp into the Yα sequences at *HML* (White and Haber, 1990). We also note that break induction kinetics in these strains are virtually identical to what was seen in the donorless strains used above (Figure 1A).

ChIP time courses were performed in *MAT*a *HML*α strains that harbored either a Rad54-13Myc or a Rad55-13Myc allele. We then used polyclonal anti-Rad51p or anti-Rad52p antibodies to detect the binding of these proteins at both *MAT*-Z and *HML*α (Figure 3B). In these experiments the *ENA1* UAS was used as a specificity control. As in the experiments with the donorless strain, Rad51p is detectable at *MAT*-Z within 20 min after break induction (Figures 3B and 3C). Interestingly, in these same extracts, Rad52p is also detectable at *MAT*-Z by the 20 min time point. These experiments were repeated three times with similar results (data not shown). Binding of Rad51p and Rad52p is roughly linear for the first 90 min, and binding at *MAT*-Z precedes recruitment to *HML*, as expected.

We also followed the recruitment of Rad54p and Rad55p in these extracts, using antibodies to their 13Myc epitope tags. Rad55p-13Myc is detectable at *MAT*-Z at 20 min following DSB formation, and recruitment to *HML* is detected subsequently. In contrast, Rad54p-13Myc is first detected simultaneously at both *MAT*-Z and *HML* at the 40 min time point. Thus, although the kinetics of Rad protein binding is noticeably faster in the switching strains, much of the timing aspects are preserved. Rad51p, Rad52p, and Rad55p each appear to bind at *MAT*-Z before Rad54p. Once Rad54p is de-

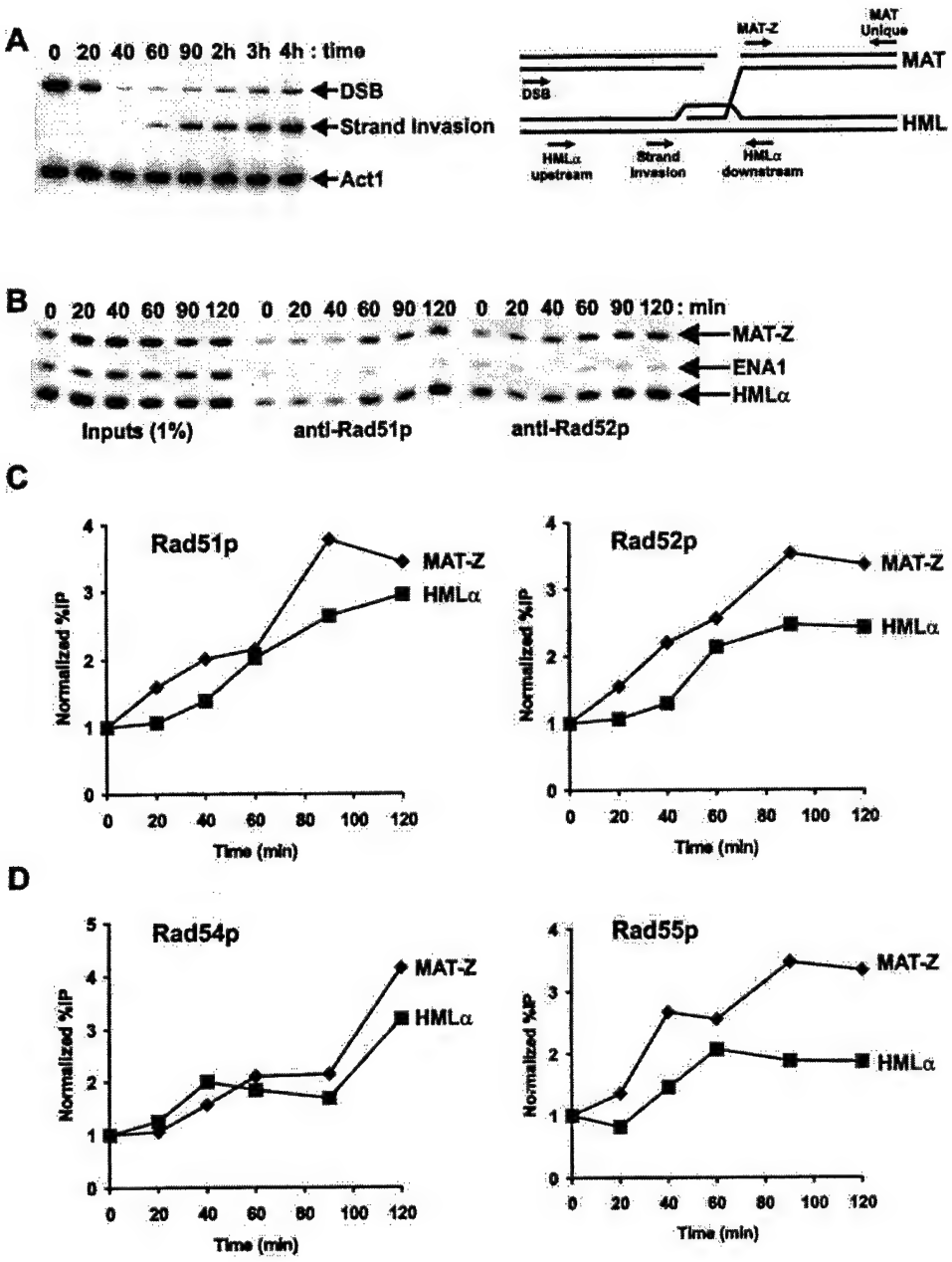

Figure 3. Recruitment of Rad Proteins in Switching Strains

ChIP experiments were performed exactly as in Figure 1 but using strains that contain homologous donor sequences (silent mating-type loci). In order to assure only one round of switching, HO expression was repressed after 30 min by addition of glucose (2% w/v) to the medium.

(A) Kinetics of DSB formation and strand invasion. The formation of the synaptic complex is illustrated in the schematic, and the locations of the primers used in these assays are shown. The "strand invasion" product is not detectable until the incoming strand is extended at least 30 bp into the Yα-specific region of *HML*. PCR products are labeled as: DSB, from 192 bp upstream to 428 bp downstream of the HO cut site; Strand Invasion, from 30 bp upstream of the HO recognition site in HML to 428 bp downstream of the HO site in MAT; Act1, 254 bp of the ACT1 ORF.

(B) Representative ChIP experiment using polyclonal antibodies to Rad51p and Rad52p. PCR products: *MAT-Z*, from 18 bp to 428 bp downstream of the HO site; HMLα, from 257 bp upstream of the HO recognition site at *HML* to 10 bp downstream. ENA1, 290 bp of the *ENA1* UAS on chromosome 4.

(C) Raw data from (B) were quantified, and relative percent IP was normalized to the percent IP of the *ENA1* UAS to control for immunoprecipitation efficiency as described in Experimental Procedures. These results are representative of three trials each.

(D) Representative data from ChIP experiments using anti-myc antibodies and extracts from strains harboring either a 13Myc-tagged *RAD54* or 13Myc-tagged *RAD55* allele. Data were quantified as in (C) and are representative of two experiments each.

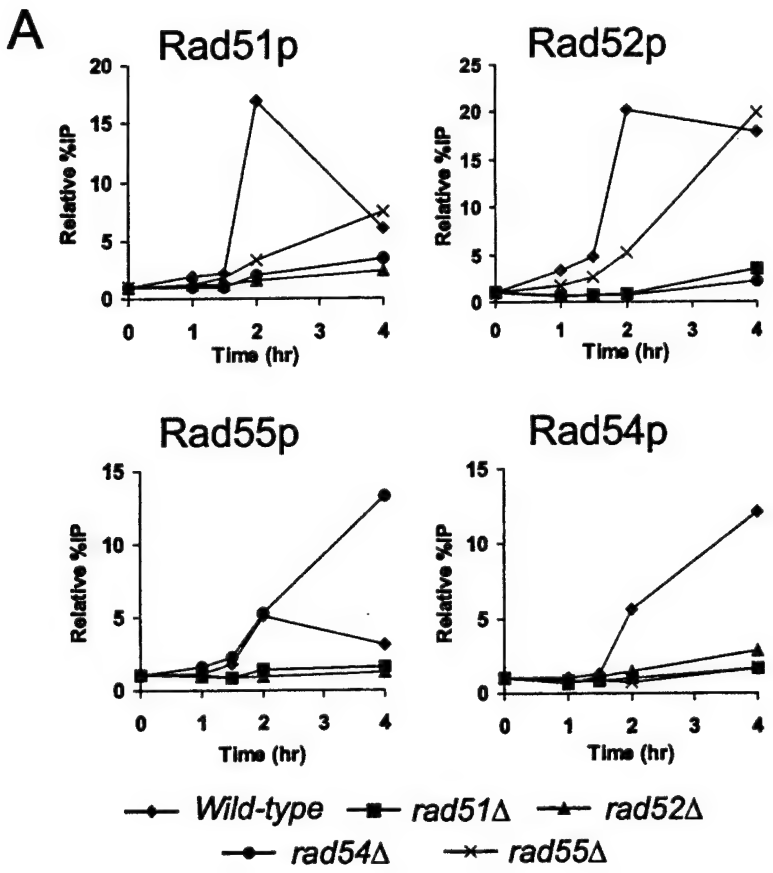

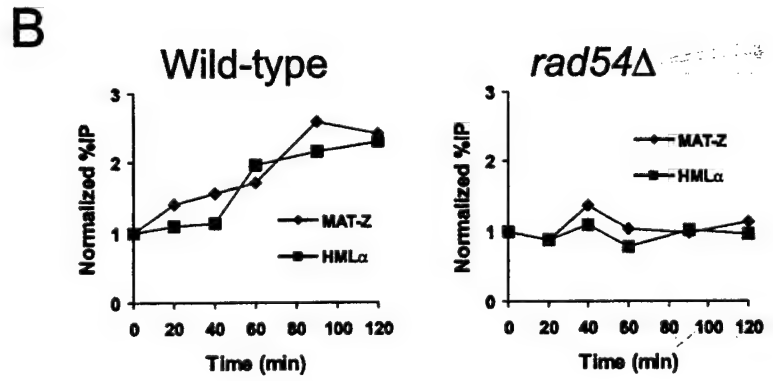

Figure 4. ChIP Assays in *rad* Mutant Strains

(A) Each chip assay was repeated at least twice in a strain harboring a complete deletion of one of the *RAD52* group genes. Relative percent IPs were calculated as in Figure 1. Only the results of *MAT*-Z PCRs (as in Figures 1 and 2) are shown. Wild-type curves (diamonds) are identical to those shown in Figures 1D and 2C. Deletion mutants used were: *rad51*Δ, squares; *rad52*Δ, triangles; *rad54*Δ, circles; *rad55*Δ, crosses. Curves from these mutants are representative of at least two experiments each and are not normalized to an internal control.

(B) ChIP assays performed with switching strains. Rad51p was immunoprecipitated using a polyclonal antibody and extracts from either *RAD54* or *rad54*Δ strains. (*MAT*-Z, diamonds; *HML*α, squares). These curves are representative of three experiments each and are normalized to the *ENA1* UAS control.

tected at *MAT*-Z, all four proteins can be crosslinked at *HML*, and shortly thereafter strand invasion and extension are detected.

Functional Interactions among RAD52 Group Proteins

In the absence of homologous donors, the ChIP studies are consistent with a sequential pathway for recruitment of RAD52 group proteins to a DSB in which Rad51p binds first, followed by Rad52p, Rad55p, and finally Rad54p. However, this simple model is not fully consistent with biochemical studies that have suggested key roles for Rad52p and Rad55p/57p in mediating the formation of the Rad51p filament. One possibility is that the ChIP assay only monitors stable binding of Rad proteins, and such "mediator" roles for Rad52p and Rad55p are not detectable. To test this idea, we monitored recruitment of RAD52 group proteins in each *rad* mutant strain. Each strain lacked homologous donors and was tested at least twice, and representative sets of data are shown in Figure 4A.

The functional interdependencies elucidated by ChIP correlate with both the sequential pathway as well as with previous in vitro data. For example, Rad51p-13Myc binding is severely impaired in a *rad52*Δ background (Figure 4A, upper left, triangles), consistent with biochemical studies indicating a requirement for Rad52p

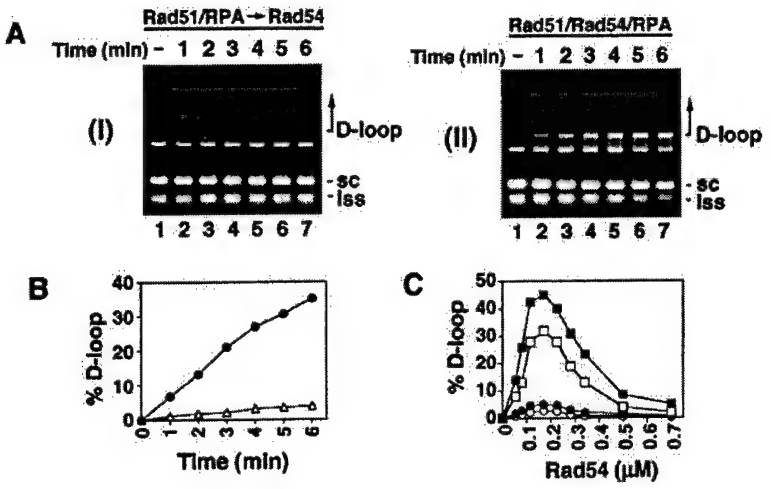

Figure 5. Rad54 Possesses a Mediator Function

(A) Effect of order of addition of reaction components on D loop formation. Presynaptic filaments were formed with or without Rad54p as described in Experimental Procedures. Rad54p was added in the initial incubation or after addition of ssDNA as indicated above the panels. The locations of DNA reactants and reaction products are indicated.

(B) Graphical representation of the results in (A). (Results from [AI], triangles; results from [AII], circles).

(C) Rad54p (0.05–0.7 μM) was either added with Rad51p and RPA to the ssDNA template (open squares, 6 min time point; closed squares, 9 min time point) or added after a preincubation of the ssDNA template with Rad51p and RPA (open circles, 6 min time point; closed circles, 9 min time point) as described in (A).

as a mediator. Inactivation of *RAD55* also decreases the recruitment of Rad51p (Figure 4A, upper left, crosses), although to a lesser extent than disruption of *RAD52*. The weaker effect of the *rad55Δ* mutant is consistent with previous studies indicating that this mutant has only a weak MMS sensitivity and only a partial defect in Rad51p focus formation and mating-type switching at 30°C (Gasior et al., 2001; Schmuckli-Maurer and Heyer, 1999). Similarly, recruitment of Rad52p requires Rad51p, but not Rad55p (Figure 4A, upper right). Binding of Rad55p-13Myc requires Rad51p and Rad52p but not Rad54p, which normally arrives at the DSB after Rad55p (Figure 4A, lower left). Rad54p-13Myc is the last protein to be recruited to the DSB, and its binding requires all other Rad proteins (Figure 4A, lower right panel).

We were surprised to find that deletion of *RAD54* nearly eliminates recruitment of Rad51p-13Myc (Figure 4A, upper left, circles). This suggests that Rad54p may also be a mediator of Rad51 nucleoprotein filament formation. Similar defects were also observed when a polyclonal antibody to Rad51p was used in ChIP analyses with a *rad54* mutant and an untagged allele of Rad51p (data not shown). Rad54p is also required for optimal Rad52p recruitment (Figure 4A, upper right, circles), although whether this effect is on Rad52p itself or indirectly through the Rad51p binding defect cannot be determined from these data.

In order to ensure that the mediator role for Rad54p is a general property and not due to the lack of homologous donors, we repeated the experiment using switching strains that contain either a wild-type *RAD54* allele or a *rad54* deletion. As we observed in donorless strains, Rad54p is strictly required for recruitment of Rad51p to *MAT*-Z and *HML* (Figure 4B). In addition, strains harboring *rad54Δ* failed to produce a "strand invasion" product (data not shown), consistent with a role for Rad54p in formation of the presynaptic complex.

Rad54p Has a Presynaptic Mediator Function

Recently, Mazin and colleagues (2003) reported that Rad54p can stabilize a Rad51p-ssDNA filament, suggesting that Rad54p may act in the latter stages of the presynaptic phase. In addition, our ChIP analyses suggest that Rad54p may act as a mediator for facilitating the actual assembly of the Rad51 nucleoprotein filament. We tested this hypothesis further by performing in vitro strand exchange and ssDNA binding assays previously devised to test the effects of various recombination mediator proteins on the efficiency of Rad51p presynaptic filament assembly. In one such scheme, a circular ssDNA template is incubated with a mixture of Rad51p and RPA. Due to competition between RPA and Rad51p for binding sites on the template (Sung, 1997a), little homologous pairing or D loop formation with a linear duplex is seen (Figure 5AI). When Rad54p was coincubated with Rad51p and RPA, a much higher level of D loop formation was seen (Figure 5AII). Specifically, whereas only 3% of the D loop was seen at the reaction endpoint of 6 min when Rad54p was omitted during preincubation, the level of D loop increases to ~35% when Rad54p was included in the preincubation (Figures 5A and 5B).

We examined the competition of RPA with Rad51p for binding to ϕX ssDNA immobilized on magnetic beads via a streptavidin-biotin linkage (see schematic in Figure 6A). Addition of an equimolar amount of RPA (2.2 μM) to Rad51p (2.3 μM) reduced the level of Rad51p that remained with the ssDNA to ≤10% of that seen in the absence of RPA (Figure 6BI, compare lanes 1 and 6, and Figure 6BIII). These results verified that RPA excludes Rad51p from ssDNA. By contrast, RPA (up to 2.2 μM) did not result in significant exclusion of Rad54p (0.8 μM) from the ssDNA (Figures 6BII and 6BIII). At Rad54p concentrations higher and lower than that used in Figure 6BII, we also did not observe significant exclusion of this factor from ssDNA by RPA (data not shown). These results and others (S.V.K. and P.S., unpublished data) suggest that Rad54p has high avidity for ssDNA.

We next questioned whether Rad54p could help overcome the effect of RPA on the binding of Rad51p to the ssDNA template. Indeed, substantially more Rad51p was found associated with the ssDNA template upon the inclusion of Rad54p (Figure 6C). Furthermore, amounts of Rad54p substoichiometric to that of Rad51p promoted significant restoration of Rad51p binding to the ssDNA.

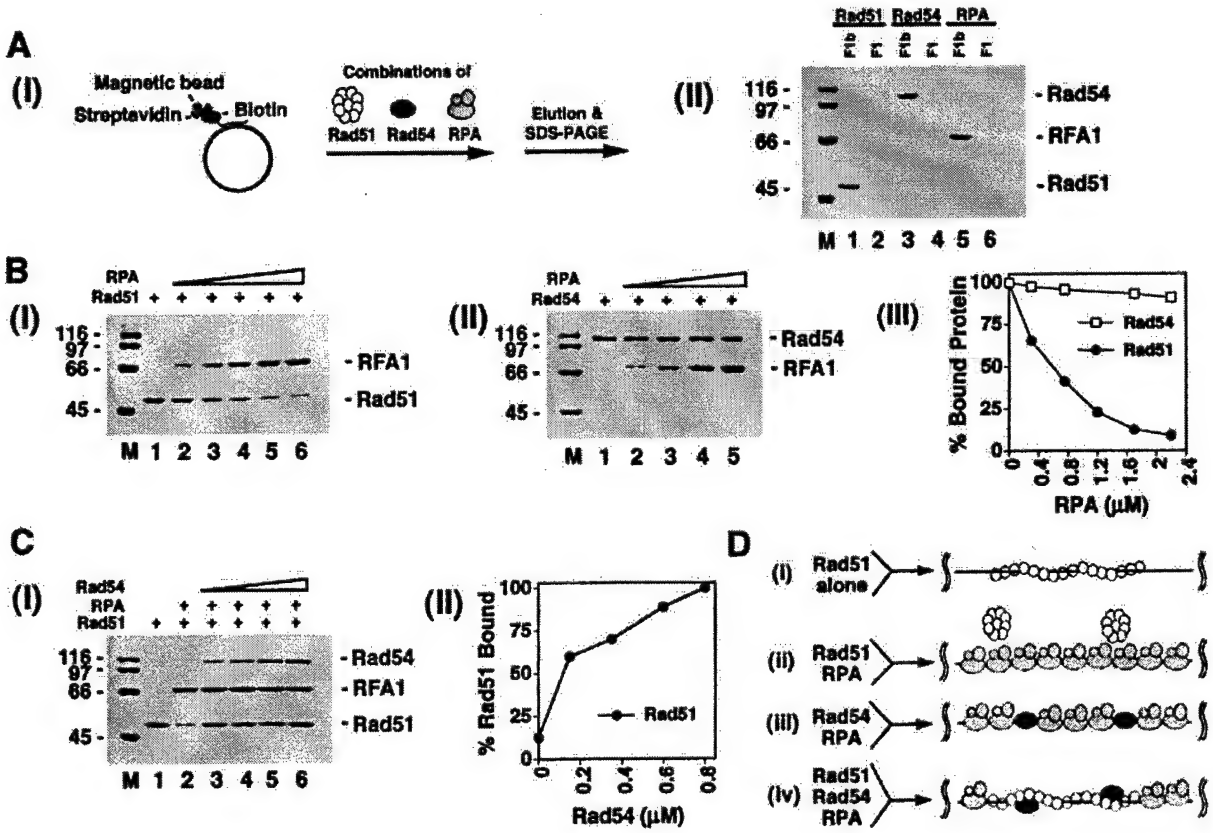

Figure 6. Rad54 Promotes Nucleation of Rad51 onto ssDNA

(A) (AI) shows the schematic for examining the contents of the presynaptic protein complexes formed on immobilized DNA templates. The magnetic beads preloaded with the F1b/ϕX hybrid were used to bind Rad51p, Rad54p, and RPA, or combinations of these proteins. (AII) DNA-bound proteins were stripped from the magnetic beads with SDS and analyzed by electrophoresis in a 10% SDS-PAGE gel and staining with Coomassie blue. Only the Rfa1p subunit of the heterotrimeric RPA is shown.

(B) (BI) Rad51p (2.3 μM) and increasing concentrations of RPA (0.3, 0.8, 1.2, 1.7, and 2.2 μM in lanes 2–6, respectively) were mixed with the immobilized ϕX (+) strand. (BII) Rad54p (0.8 μM) and increasing concentrations of RPA (0.3, 0.8, 1.7, and 2.2 μM in lanes 2–5, respectively) were mixed with the immobilized ϕX (+) strand DNA. Proteins were eluted from the magnetic beads and analyzed as described in (A). The results from (BI) and (BII) are graphed in (BIII).

(C) (CI) Rad51p (2.3 μM), RPA (1.7 μM), and increasing concentrations of Rad54p (0.15, 0.35, 0.6, and 0.8 μM in lanes 3–6, respectively) were mixed with immobilized ϕX (+) strand DNA. Proteins were eluted from the magnetic beads and analyzed as in (A). The results in (CI) are graphed in (CII).

(D) Diagrammatic summary of the results. Rad51p forms a nucleoprotein-filament on ssDNA (Di) but is excluded from the ssDNA template by RPA (Dii). Binding of Rad54p to the ssDNA is much less prone to competition by RPA (Diii). Coincubation of Rad51p and Rad54p results in targeting of the former to the ssDNA template (Div).

Binding of RPA Is *RAD54* Independent

From the in vitro data above, we predicted that the in vivo recruitment of RPA to a DSB would be independent of Rad54p. To investigate this possibility, we created *RAD54* and *rad54*Δ strains that each contained a 13Myc-tagged allele of *RFA1*, which encodes the 70 kDa subunit of RPA. Figure 7 shows a representative ChIP time course that follows the temporal recruitment of Rfa1-13Myc to an HO-induced DSB. We find that RPA is recruited to both sides of the break, with initial binding being detectable over background at the 45 min time point (Figure 7B). Thus, in these donorless strains, Rfa1p recruitment appears to be slightly later that Rad51p and similar to the kinetics of Rad52p (Figure 1C). In contrast to Rad51p and Rad52p, recruitment of RPA does not require *RAD54* (Figure 7B).

Discussion

Ordered Recruitment of RAD Proteins to a DSB

Several studies have demonstrated physical and functional interactions among various members of the *RAD52* epistasis group (Golub et al., 1997; Hays et al., 1995; Johnson and Symington, 1995; Krejci et al., 2001). One interpretation is that multiple members of this group exist within a cell as a preassembled, multiprotein complex that can be recruited in a single step to a DSB (the "recombinosome" model). Alternatively, Rad proteins could assemble in a step-wise fashion to facilitate homologous recombination. Here we used chromatin immunoprecipitations to follow the assembly of Rad51p, Rad52p, Rad54p, and Rad55p at a unique DNA double-strand break in yeast cells. Whereas the simple recombi-

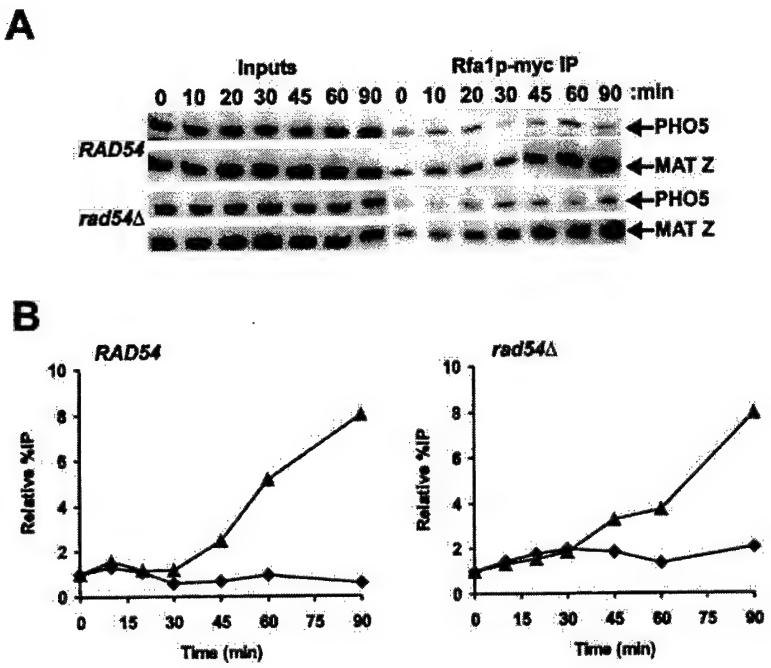

Figure 7. Recruitment of Rfa1p to a DSB

(A) Representative data from an Rfa1p-13Myc ChIP experiment using *RAD54* or *rad54Δ* strains that lacked homologous donors. Similar results were observed in three independent experiments. PCR products are as in Figure 1.

(B) The raw data in (A) were quantified and plotted as described for Figure 1 (*PHO5*, diamonds; *MAT*-Z, triangles).

nosome model predicts that each Rad protein would be recruited to a DSB with the same kinetics, our data in donorless strains support a stepwise, temporally distinct pathway for the assembly of Rad proteins at the DSB. Specifically, Rad51p appears to arrive soon after DSB formation, followed by Rad52p, Rad55p, and finally Rad54p. In strains that can repair the break, Rad51p, Rad52p, and Rad55p are recruited to the DSB quickly, but Rad54p is detected later. Thus in both cases, there are at least two temporally distinct steps of Rad protein recruitment required to form a functional presynaptic complex.

Our data indicate that Rad51p recruitment is impaired in *rad52Δ*, *rad54Δ*, or *rad55Δ* mutant strains. For instance, the rate and extent of Rad51p recruitment to the HO-induced DSB is dramatically reduced in the absence of Rad54p, even though Rad54p was not detectable by ChIP until 70 min after the initial binding of Rad51p in a donorless strain. These results suggest a level of interdependence among Rad proteins that is not entirely consistent with a simple stepwise assembly pathway. The steady-state levels of Rad51p-13Myc and untagged Rad51p are not altered in *rad* strains, which eliminates this trivial explanation (B.W., unpublished data). Rad52p, Rad55p, and Rad54p are all known to physically interact with Rad51p, and each of these proteins can facilitate assembly of the Rad51p nucleoprotein filament in vitro (Fortin and Symington, 2002; Sung, 1997a, 1997b; see Figure 4). In addition, our results indicate that substoichiometric amounts of Rad54p are optimal for D loop formation (1 to 10 ratio of Rad54p to Rad51p; see Figure 5C). This is similar to the result seen previously for Rad52p in strand exchange reactions (Song and Sung, 2000). These results taken together suggest that Rad54p and Rad52p may only transiently interact with the Rad51 nucleoprotein filament. Such transient interactions likely mediate enhanced assembly and stability of the Rad51p nucleoprotein filament. In this model, only the stable binding of Rad52p, Rad54p, and Rad55p is detectable by ChIP, reflecting the assembly of a nucleoprotein filament competent for strand invasion. Consistent with this model are recent cytological studies in mammalian cells which indicate that damage-induced nuclear foci have static levels of Rad51p, but that Rad52p and Rad54p are dynamic, rapidly entering and leaving the Rad51p-containing nuclear foci over time (Essers et al., 2002).

Asymmetry in Rad Protein Recruitment

In yeast strains that harbor the silent mating-type loci, *HML*α and *HMR*a, the HO-induced double-strand break at *MAT* leads to a highly efficient gene conversion event in which ~700 bp of a- or α-specific sequences are replaced by those of the opposite mating-type (reviewed in Haber, 1998). The HO cut site is located just downstream of the mating type-specific sequences and just upstream of a region of homology (called Z1) that is found at both the *MAT* and silent mating-type loci. During normal mating-type switching, only the downstream, Z1 side of the DSB participates in homology searching and strand invasion, which provides an opportunity for a switch in mating-type information. In our ChIP analyses, we found that each Rad protein was also preferentially recruited to the downstream (*MAT*-Z) side of the HO-induced DSB. This preference is most obvious for Rad54p, which can only be detected by ChIP at the downstream, *MAT*-Z side of the DSB (Figure 2). Previous studies have suggested that the recombinational inactivity of the upstream side of the HO-induced DSB is due at least in part to decreased 5′ to 3′ exonucleotytic digestion, which is required for formation of a presynaptic complex (White and Haber, 1990). It is currently not

clear if such a defect in resection is sufficient to account for the observed asymmetries in Rad protein recruitment as detected by ChIP.

Multiple Roles for Rad54p in Homologous Recombination

Rad54p is a member of the SWI2/SNF2 family of DNA-stimulated ATPases and DNA helicases (Eisen et al., 1995). Several members of this ATPase family use the energy of ATP hydrolysis to disrupt chromatin structure, and thus it has been suggested that Rad54p might facilitate repair of DSBs by contending with chromatin (Peterson, 1996). This hypothesis is supported by in vivo studies suggesting that the requirement for Rad54p function in the repair of DSBs is sensitive to chromosomal context (Sugawara et al., 1995). Likewise, our lab and others have recently found that Rad54p has bona fide chromatin remodeling activity in vitro and that this activity is essential for DNA strand invasion reactions in which chromatin substrates are used (Alexeev et al., 2003; Alexiadis and Kadonaga, 2002; Jaskelioff et al., 2003). However, it is clear that Rad54p also plays essential roles during HR that are unrelated to chromatin structure. In vitro, the ATPase activity of Rad54p plays an essential role in formation of DNA joint molecules even with naked DNA substrates. In fact, these in vitro studies led to the suggestion that Rad54p may be required for homologous pairing but not for presynaptic filament formation (Mazin et al., 2000; Solinger et al., 2001). Recently, Heyer and colleagues have also shown that Rad54p can promote the dissociation of Rad51p from the postsynaptic complex (Solinger et al., 2002). Thus, most in vitro studies have tended to focus on roles for Rad54p after formation of the presynaptic complex.

In contrast, our in vivo and in vitro studies provide compelling evidence for a key role of Rad54p in mediating formation of the Rad51 presynaptic filament (summarized in Figure 6D). Previous studies have shown that Rad54p physically interacts with Rad51p (Clever et al., 1997; Golub et al., 1997; Jiang et al., 1996; Petukhova et al., 1998), and our present study has indicated that Rad54p binds ssDNA avidly. Rad54p thus resembles Rad52p and the Rad55p/Rad57p heterodimer in being able to interact with Rad51p and in possessing a ssDNA binding function (reviewed in Sung et al., 2000). Coaddition of RPA with Rad51p in the presynaptic phase results in a marked reduction in homologous DNA pairing and strand exchange efficiency (Sung, 1997a), due to the exclusion of Rad51p from the ssDNA template (Sugiyama et al., 1997; Sung, 1997a). Addition of either Rad52p (New et al., 1998; Shinohara et al., 1997; Sung, 1997a) or the Rad55p/Rad57p complex (Sung, 1997b) helps alleviate this inhibitory effect of RPA. Likewise, we have shown here that coaddition of RPA with Rad51p to the circular ssDNA template results in pronounced suppression of D loop formation and decreased binding of Rad51p to the template. Importantly, the addition of Rad54p during the formation of the presynaptic complex restores D loop formation. Furthermore, we have shown that Rad54p helps to nucleate Rad51p onto the ssDNA template in vitro and in vivo, while binding of RPA is independent of Rad54p both in vitro and in vivo. Thus, our studies support an early role for Rad54p in enhancing the formation and stability of the Rad51p nucleoprotein filament.

Our biochemical and ChIP data are also in agreement with cytological observations of Tan and colleagues (Tan et al., 1999). These investigators found that mRad51 and mRad54 colocalize to the same nuclear foci in mouse embryonic stem (ES) cells after treatment with ionizing radiation. Furthermore, the assembly of the mRad51 nuclear foci were greatly diminished in isogenic ES cell lines deleted for the mRad54 protein, indicating that mRad54 is important for the delivery of mRad51 to the sites of DNA damage. Likewise, Shinohara and colleagues (Shinohara et al., 1997) have demonstrated that a Rad54p homolog, Rdh54p, is required for formation of Rad51p/Dmc1p foci during yeast meiosis. Taken together, these results suggest that Rad54p plays key roles during formation of the presynaptic complex and during the process of DNA homology searching and joint molecule formation. In the latter case, Rad54p may serve both as a general facilitator of Rad51p function as well as a chromatin-remodeling factor that overcomes the constraints on HR imposed by chromatin structure.

Experimental Procedures

Yeast Strains

All strains used in this study are isogenic to strain JKM179 that has the relevant genotype of *Δho Δhml::ADE1 MATα Δhmr::ADE1 ade1-110 leu2,3-112 lys5 trp1::hisG ura3-52 ade3::GAL10:HO*. All strains are *MATα* except for YSL53, which carries the *rad55::LEU2* knockout and is *MATa*. The "switching" strains are based on JKM154, which is isogenic to JKM179 except that it is *MATa HMLα HMRa*. All strains are based on the JKM series described by Moore and Haber (1996).

Epitope Tagging

Epitope tagging involved a PCR strategy using plasmid templates (Bahler et al., 1998). These plasmids carry 13 copies of the c-Myc epitope followed by a translation stop codon in tandem with the Kan-MX6 gene that confers resistance to the drug G418. Gene-specific recombination replaces the native stop codon with the epitope sequence, in frame, followed by a new stop codon and the KanMX6 gene. Recombinants were selected by plating on YEPD plates containing 250 μg/ml G418 and verified by patching on a second YEPD+G418 plate. Proper integration of the targeting vector was verified by genomic PCR, and expression of the tagged protein was verified by Western blotting.

Recombination Proteins

Rad51 and Rad54 proteins were overexpressed in yeast cells and purified to near homogeneity as described previously (Petukhova et al., 1998; Sung, 1994). RPA was overexpressed in yeast using three plasmids that code for the three subunits of RPA (Nakagawa et al., 2001) and purified to near homogeneity as described (Sung, 1997b).

DNA Substrates

The ϕX174 (+) strand and replicative form I DNA were purchased from New England Biolabs and GIBCO-BRL, respectively. Linearization of the viral (+) strand was done by hybridizing a 26-mer oligonucleotide to create a PstI site, followed by treatment with PstI (Petukhova et al., 1998).

Chromatin Immunoprecipitation

For ChIP assays, asynchronous cultures were grown at 30°C in YEP media containing 2% (w/v) raffinose as the sole carbon source. Under these conditions, HO is not expressed. When cultures had reached mid-log phase, HO expression was induced by the addition of galactose (2% w/v final). At various times after the addition of galactose, 5 ml samples of culture were taken, and the optical density at 600 nm was measured. The samples were cross-linked with

1% formaldehyde at room temperature for 15 min, after which the reaction was quenched by incubation in ice water. Extracts were prepared and processed for chromatin immunoprecipitation as previously described (Strahl-Bolsinger et al., 1997).

Radioactive semiquantitative PCR reactions were performed as described (Krebs et al., 2000) and verified for linearity of response by titrating template DNA (data not shown). PCR products were separated on 10% polyacrylamide (30:1 acrylamide:bis-acrylamide) gels (Bio-Rad mini protean 3). Gels were dried and exposed to phosphorimager screens overnight. Bands were quantified by volume analysis using ImageQuant software (Molecular Dynamics). Sequences of primers used in PCR are available on request.

Immunoprecipitation signals were divided by the corresponding "input" signals (representing 1% as much DNA as used in immunoprecipitations). Since the IP efficiencies of different loci were often very different, each series was normalized to its time zero value. In some cases, a further normalization to the control locus (*PHO5* or *ENA1*) was performed (Kuo et al., 1998). These are indicated as "normalized percent IP."

Measurement of Rad54 Mediator Function

Presynaptic filaments were formed as follows: Rad51p (1.4 μM added in 1.5 μl) and RPA (1.3 μM added in 1.5 μl) were preincubated on ice for 10 min in 27.6 μl buffer R (35 mM Tris-HCl [pH 7.2], 60 mM KCl, 2.5 mM ATP, 3 mM $MgCl_2$, 1 mM DTT, and an ATP regenerating system consisting of 20 mM creatine phosphate and 30 ng/μl creatine kinase) before the linear ssDNA (19.6 μM nucleotides in 3 μl) was added. Rad54p (150 nM in 0.9 μl) was added either during the initial 10 min incubation or after a 1 min incubation at 23°C, followed by 5 min at 23°C. The duplex substrate (12.3 μM bp added in 3 μl) and spermidine hydrochloride (3 μl of 50 mM stock) were then added to complete the reaction (final volume of 37.5 μl). After the indicated times at 23°C, a 5 μl aliquot of the reaction mixture was withdrawn for analysis. For Rad54p titrations, reactions were mixed as described above but scaled down to a final volume of 12.5 μl.

Binding of Recombination Proteins to ϕX174 ssDNA Immobilized on Magnetic Beads

Immobilized ϕX174 (+) strand was prepared as described previously (Sigurdsson et al., 2001). Ten microliters of the magnetic beads containing 200 ng ϕX (+) strand was mixed with the indicated amounts of each protein in 20 μl of buffer R containing 90 mM KCl and 0.012% Igepal (Sigma) for 5 min at 23°C by constant tapping. The beads were captured with the Magnetic Particle Separator (Boehringer Mannheim). After removing the supernatant, the bead-bound Rad51p, Rad54p, and RPA were eluted with 20 μl of SDS loading buffer, and 7 μl of the SDS eluates were analyzed by SDS-PAGE. Reproducibly, ~80% of the Rad51p, ~90% of the Rad54p, and ~90% on the RPA were retained on the magnetic beads. The proteins were bound to the F1b/ϕX (+) strand on the magnetic beads, as only ~3% of the Rad51p, Rad54p, and RPA were retained on magnetic beads that had not been mixed with any DNA. This low level of nonspecific retention of recombination proteins was seen with individual proteins or when combinations of the proteins were used, and it was taken into consideration when calculating the amounts of proteins specifically bound to the F1b/ϕX (+) strand hybrid.

Acknowledgments

We thank Jim Haber for communicating results prior to publication. This work was supported by grants from the NIH to C.L.P (GM49650) and to P.S. (GM57814) and by an NIH NRSA postdoctoral fellowship (GM64233) to B.W.

Received: October 1, 2002
Revised: April 23, 2003
Accepted: June 3, 2003
Published: July 24, 2003

References

Alexeev, A., Mazin, A., and Kowalczykowski, S.C. (2003). Rad54 protein possesses chromatin-remodeling activity stimulated by the Rad51-ssDNA nucleoprotein filament. Nat. Struct. Biol. *10*, 182–186.

Alexiadis, V., and Kadonaga, J.T. (2002). Strand pairing by Rad54 and Rad51 is enhanced by chromatin. Genes Dev. *16*, 2767–2771.

Bahler, J., Wu, J.Q., Longtine, M.S., Shah, N.G., McKenzie, A., 3rd, Steever, A.B., Wach, A., Philippsen, P., and Pringle, J.R. (1998). Heterologous modules for efficient and versatile PCR-based gene targeting in *Schizosaccharomyces pombe*. Yeast *14*, 943–951.

Clever, B., Interthal, H., Schmuckli-Maurer, J., King, J., Sigrist, M., and Heyer, W.-D. (1997). Recombinational repair in yeast: functional interactions between Rad51 and Rad54 proteins. EMBO J. *16*, 2535–2544.

Connolly, B., White, C.I., and Haber, J.E. (1988). Physical monitoring of mating type switching in *Saccharomyces cerevisiae*. Mol. Cell. Biol. *8*, 2342–2349.

Cromie, G.A., Connelly, J.C., and Leach, D.R. (2001). Recombination at double-strand breaks and DNA ends: conserved mechanisms from phage to humans. Mol. Cell *8*, 1163–1174.

Eisen, J.A., Sweder, K.S., and Hanawalt, P.C. (1995). Evolution of the SNF2 family of proteins: subfamilies with distinct sequences and functions. Nucleic Acids Res. *23*, 2715–2723.

Essers, J., Houtsmuller, A.B., van Veelen, L., Paulusma, C., Nigg, A.L., Pastink, A., Vermeulen, W., Hoeijmakers, J.H., and Kanaar, R. (2002). Nuclear dynamics of RAD52 group homologous recombination proteins in response to DNA damage. EMBO J. *21*, 2030–2037.

Fortin, G.S., and Symington, L.S. (2002). Mutations in yeast Rad51 that partially bypass the requirement for Rad55 and Rad57 in DNA repair by increasing the stability of Rad51-DNA complexes. EMBO J. *21*, 3160–3170.

Gasior, S.L., Olivares, H., Ear, U., Hari, D.M., Weichselbaum, R., and Bishop, D.K. (2001). Assembly of RecA-like recombinases: distinct roles for mediator proteins in mitosis and meiosis. Proc. Natl. Acad. Sci. USA *98*, 8411–8418.

Golub, E.I., Kovalenko, O.V., Gupta, R.C., Ward, D.C., and Radding, C.M. (1997). Interaction of human recombination proteins Rad51 and Rad54. Nucleic Acids Res. *25*, 4106–4110.

Haaf, T., Golub, E.I., Reddy, G., Radding, C.M., and Ward, D.C. (1995). Nuclear foci of mammalian Rad51 recombination protein in somatic cells after DNA damage and its localization in synaptonemal complexes. Proc. Natl. Acad. Sci. USA *92*, 2298–2302.

Haber, J.E. (1998). Mating-type gene switching in *Saccharomyces cerevisiae*. Annu. Rev. Genet. *32*, 561–599.

Haber, J.E. (2000). Lucky breaks: analysis of recombination in *Saccharomyces*. Mutat. Res. *451*, 53–69.

Hays, S.L., Firmenich, A.A., and Berg, P. (1995). Complex formation in yeast double-strand break repair: participation of Rad51, Rad52, Rad55, and Rad57 proteins. Proc. Natl. Acad. Sci. USA *92*, 6925–6929.

Ivanov, E.L., and Haber, J.E. (1997). DNA repair: RAD alert. Curr. Biol. *7*, R492–R495.

Jasin, M. (2000). Chromosome breaks and genomic instability. Cancer Invest. *18*, 78–86.

Jaskelioff, M., Van Komen, S., Krebs, J.E., Sung, P., and Peterson, C.L. (2003). Rad54p is a chromatin remodeling enzyme required for heteroduplex DNA joint formation with chromatin. J. Biol. Chem. *278*, 9212–9218.

Jiang, H., Xie, Y., Houston, P., Stemke-Hale, K., Mortensen, U.H., Rothstein, R., and Kodadek, T. (1996). Direct association between the yeast Rad51 and Rad54 recombination proteins. J. Biol. Chem. *271*, 33181–33186.

Johnson, R.D., and Symington, L.S. (1995). Functional differences and interactions among the putative RecA homologs Rad51, Rad55, and Rad57. Mol. Cell. Biol. *15*, 4843–4850.

Krebs, J.E., Fry, C.J., Samuels, M.L., and Peterson, C.L. (2000). Global role for chromatin remodeling enzymes in mitotic gene expression. Cell *102*, 587–598.

Krejci, L., Damborsky, J., Thomsen, B., Duno, M., and Bendixen, C. (2001). Molecular dissection of interactions between Rad51 and members of the recombination-repair group. Mol. Cell. Biol. *21*, 966–976.

Kuo, M.H., Zhou, J., Jambeck, P., Churchill, M.E., and Allis, C.D.

(1998). Histone acetyltransferase activity of yeast Gcn5p is required for the activation of target genes in vivo. Genes Dev. *12*, 627–639.

Mazin, A.V., Bornarth, C.J., Solinger, J.A., Heyer, W.-D., and Kowalczykowski, S.C. (2000). Rad54 protein is targeted to pairing loci by the Rad51 nucleoprotein filament. Mol. Cell *6*, 583–592.

Mazin, A.V., Alexeev, A.A., and Kowalczykowski, S.C. (2003). A novel function of Rad54 protein. Stabilization of the Rad51 nucleoprotein filament. J. Biol. Chem. *278*, 14029–14036.

Michelson, R.J., and Weinert, T. (2000). Closing the gaps among a web of DNA repair disorders. Bioessays *22*, 966–969.

Moore, J.K., and Haber, J.E. (1996). Cell cycle and genetic requirements of two pathways of nonhomologous end-joining repair of double-strand breaks in Saccharomyces cerevisiae. Mol. Cell. Biol. *16*, 2164–2173.

Nakagawa, T., Flores-Rozas, H., and Kolodner, R.D. (2001). The MER3 helicase involved in meiotic crossing over is stimulated by single-stranded DNA-binding proteins and unwinds DNA in the 3′ to 5′ direction. J. Biol. Chem. *276*, 31487–31493.

New, J.H., Sugiyama, T., Zaitseva, E., and Kowalczykowski, S.C. (1998). Rad52 protein stimulates DNA strand exchange by Rad51 and replication protein A. Nature *391*, 407–410.

Pâques, F., and Haber, J.E. (1999). Multiple pathways of recombination induced by double-strand breaks in *Saccharomyces cerevisiae*. Microbiol. Mol. Biol. Rev. *63*, 349–404.

Peterson, C.L. (1996). Multiple SWItches to turn on chromatin? Curr. Opin. Genet. Dev. *6*, 171–175.

Petukhova, G., Stratton, S., and Sung, P. (1998). Catalysis of homologous DNA pairing by yeast Rad51 and Rad54 proteins. Nature *393*, 91–94.

Petukhova, G., Sung, P., and Klein, H. (2000). Promotion of Rad51-dependent D-loop formation by yeast recombination factor Rdh54/Tid1. Genes Dev. *14*, 2206–2215.

Schmuckli-Maurer, J., and Heyer, W.-D. (1999). The *Saccharomyces cerevisiae RAD54* gene is important but not essential for natural homothallic mating-type switching. Mol. Gen. Genet. *260*, 551–558.

Shinohara, M., Shita-Yamaguchi, E., Buerstedde, J.M., Shinagawa, H., Ogawa, H., and Shinohara, A. (1997). Characterization of the roles of the *Saccharomyces cerevisiae RAD54* gene and a homologue of *RAD54*, *RDH54/TID1*, in mitosis and meiosis. Genetics *147*, 1545–1556.

Sigurdsson, S., Trujillo, K., Song, B., Stratton, S., and Sung, P. (2001). Basis for avid homologous DNA strand exchange by human Rad51 and RPA. J. Biol. Chem. *276*, 8798–8806.

Solinger, J.A., Lutz, G., Sugiyama, T., Kowalczykowski, S.C., and Heyer, W.-D. (2001). Rad54 protein stimulates heteroduplex DNA formation in the synaptic phase of DNA strand exchange via specific interactions with the presynaptic Rad51 nucleoprotein filament. J. Mol. Biol. *307*, 1207–1221.

Solinger, J.A., Kiianitsa, K., and Heyer, W.-D. (2002). Rad54, a Swi2/Snf2-like recombinational repair protein, disassembles Rad51:dsDNA filaments. Mol. Cell *10*, 1175–1188.

Song, B., and Sung, P. (2000). Functional interactions among yeast Rad51 recombinase, Rad52 mediator, and replication protein A in DNA strand exchange. J. Biol. Chem. *275*, 15895–15904.

Strahl-Bolsinger, S., Hecht, A., Luo, K., and Grunstein, M. (1997). SIR2 and SIR4 interactions differ in core and extended telomeric heterochromatin in yeast. Genes Dev. *11*, 83–93.

Sugawara, N., Ivanov, E.L., Fishman-Lobell, J., Ray, B.L., Wu, X., and Haber, J.E. (1995). DNA structure-dependent requirements for yeast RAD genes in gene conversion. Nature *373*, 84–86.

Sugiyama, T., Zaitseva, E.M., and Kowalczykowski, S.C. (1997). A single-stranded DNA-binding protein is needed for efficient presynaptic complex formation by the Saccharomyces cerevisiae Rad51 protein. J. Biol. Chem. *272*, 7940–7945.

Sung, P. (1994). Catalysis of ATP-dependent homologous DNA pairing and strand exchange by yeast RAD51 protein. Science *265*, 1241–1243.

Sung, P. (1997a). Function of yeast Rad52 protein as a mediator between replication protein A and the Rad51 recombinase. J. Biol. Chem. *272*, 28194–28197.

Sung, P. (1997b). Yeast Rad55 and Rad57 proteins form a heterodimer that functions with replication protein A to promote DNA strand exchange by Rad51 recombinase. Genes Dev. *11*, 1111–1121.

Sung, P., Trujillo, K.M., and Van Komen, S. (2000). Recombination factors of *Saccharomyces cerevisiae*. Mutat. Res. *451*, 257–275.

Tan, T.L., Essers, J., Citterio, E., Swagemakers, S.M., de Wit, J., Benson, F.E., Hoeijmakers, J.H., and Kanaar, R. (1999). Mouse Rad54 affects DNA conformation and DNA-damage-induced Rad51 foci formation. Curr. Biol. *9*, 325–328.

Tsuzuki, T., Fujii, Y., Sakumi, K., Tominaga, Y., Nakao, K., Sekiguchi, M., Matsushiro, A., Yoshimura, Y., and Morita, T. (1996). Targeted disruption of the *Rad51* gene leads to lethality in embryonic mice. Proc. Natl. Acad. Sci. USA *93*, 6236–6240.

White, C.I., and Haber, J.E. (1990). Intermediates of recombination during mating type switching in *Saccharomyces cerevisiae*. EMBO J. *9*, 663–673.

mice with or without the C57Bl/Ka-Ly5.2 recipient bone marrow cells[1]. Reconstitution of donor (Ly5.1) myeloid and lymphoid cells was monitored by staining blood cells with antibodies against Ly5.1, CD3, B220, Mac-1 and Gr-1. The secondary bone marrow transplant was performed with 10^7 whole bone marrow cells from mice reconstituted with *Bmi-1*$^{+/+}$ or *Bmi-1*$^{-/-}$ fetal liver cells.

Retroviral gene transfer of HSCs

Mouse stem cell viruses expressing mouse *p16*^{Ink4a} or *p19*^{Arf} cDNAs together with GFP were produced using Phoenix ecotropic packaging cells[28]. Infection of HSCs was done as described[29] except that three cycles of infections were performed. After 48 h, single GFP-positive cells were sorted into a 96-well plate containing 100 µl HSC medium[29] and grown for 7 days. Each well was scored for the presence of GFP-positive cells by observation with a fluorescence microscope.

Received 10 February; accepted 19 March 2003; doi:10.1038/nature01587.
Published online 20 April 2003.

1. Morrison, S. J. & Weissman, I. L. The long-term repopulating subset of hematopoietic stem cells is deterministic and isolatable by phenotype. *Immunity* **1**, 661–673 (1994).
2. van der Lugt, N. M. *et al.* Posterior transformation, neurological abnormalities, and severe hematopoietic defects in mice with a targeted deletion of the *bmi-1* proto-oncogene. *Genes Dev.* **8**, 757–769 (1994).
3. Ramalho-Santos, M. *et al.* 'Stemness': transcriptional profiling of embryonic and adult stem cells. *Science* **298**, 597–600 (2002).
4. Park, I.-K. *et al.* Molecular cloning and characterization of a novel regulator of G-protein signaling from mouse hematopoietic stem cells. *J. Biol. Chem.* **276**, 915–923 (2001).
5. Park, I. K. *et al.* Differential gene expression profiling of adult murine hematopoietic stem cells. *Blood* **99**, 488–498 (2002).
6. Lessard, J., Baban, S. & Sauvageau, G. Stage-specific expression of Polycomb group genes in human bone marrow cells. *Blood* **91**, 1216–1224 (1999).
7. Kiyono, T. *et al.* Both Rb/p16^{INK4a} inactivation and telomerase activity are required to immortalize human epithelial cells. *Nature* **396**, 84–88 (1998).
8. van der Lugt, N. M. T., Alkema, M., Berns, A. & Deschamps, J. The Polycomb-group homolog Bmi-1 is a regulator of murine Hox gene expression. *Mech. Dev.* **58**, 153–164 (1996).
9. Akashi, K. *et al.* Transcriptional accessibility for genes of multiple tissues and hematopoietic lineages is hierarchically controlled during early hematopoiesis. *Blood* **101**, 383–389 (2003).
10. Morrison, S., Hemmati, H., Wandycz, A. & Weissman, I. The purification and characterization of fetal liver hematopoietic stem cells. *Proc. Natl Acad. Sci. USA* **92**, 10302–10306 (1995).
11. Wright, D. E. *et al.* Hematopoietic stem cells are uniquely selective in their migratory reponse to chemokines. *J. Exp. Med.* **195**, 1145–1154 (2002).
12. Mahmoudi, T. & Verrijzer, C. P. Chromatin silencing and activation by Polycomb and trithorax group proteins. *Oncogene* **20**, 3055–3066 (2001).
13. Weber, J. D. *et al.* Nucleolar Arf sequesters Mdm2 and activates p53. *Nature Cell Biol.* **1**, 20–26 (1999).
14. Jacob, J. *et al.* The oncogene and Polycomb-group gene *bmi-1* regulates cell proliferation and senescence through the *ink4a* locus. *Nature* **397**, 164–168 (1999).
15. Quelle, D. E., Zindy, F., Ashmun, R. A. & Sherr, C. J. Alternative reading frames of the INK4a tumour suppressor gene encode two unrelated proteins capable of inducing cell cycle arrest. *Cell* **84**, 993–1000 (1995).
16. Antonchuk, J., Sauvageau, G. & Humphries, R. K. HOXB4 overexpression mediates very rapid stem cell regeneration and competitive hematopoietic repopulation. *Exp. Hematol.* **29**, 1125–1134 (2002).
17. Lawrence, H. J. *et al.* Mice bearing a targeted interruption of the homeobox gene HOXA9 have defects in myeloid, erythroid, and lymphoid hematopoiesis. *Blood* **89**, 1922–1930 (1997).
18. Christensen, J. L. & Weissman, I. L. Flk-2 is a marker in hematopoietic stem cell differentiation: a simple method to isolate long-term stem cells. *Proc. Natl Acad. Sci. USA* **98**, 14541–14546 (2001).
19. Zhang, Y., Xiong, Y. & Yarbrough, W. G. ARF promotes MDM2 degradation and stabilizes p53: ARF-INK4a locus deletion impairs both the Rb and p53 tumour suppression pathways. *Cell* **92**, 725–734 (1998).
20. Shivdasani, R., Mayer, E. & Orkin, S. Absence of blood formation in mice lacking the T-cell leukaemia oncoprotein tal-1/SCL. *Nature* **373**, 432–434 (1995).
21. Porcher, C. *et al.* The T cell leukemia oncoprotein SCL/tal-1 is essential for development of all hematopoietic lineages. *Cell* **86**, 47–57 (1996).
22. Antonchuk, J., Sauvageau, G. & Humphries, R. K. HOXB4-induced expansion of adult hematopoietic stem cells *ex vivo*. *Cell* **109**, 39–45 (2002).
23. Domen, J., Cheshier, S. H. & Weissman, I. L. The role of apoptosis in the regulation of hematopoietic stem cells: overexpression of BCL-2 increases both their number and repopulation potential. *J. Exp. Med.* **191**, 253–264 (2000).
24. Nichogiannopoulou, A. *et al.* Defects in hemopoietic stem cell activity in Ikaros mutant mice. *J. Exp. Med.* **190**, 1201–1214 (1999).
25. Fisher, R. C., Lovelock, J. D. & Scott, E. W. A critical role for PU.1 in homing and long-term engraftment by hematopoietic stem cells in the bone marrow. *Blood* **94**, 1283–1290 (1999).
26. Cheng, T. *et al.* Hematopoietic stem cell quiescence maintained by p21$^{cip1/waf1}$. *Science* **287**, 1804–1808 (2000).
27. Ohta, H. *et al.* Polycomb group gene *rae28* is required for sustaining activity of hematopoietic stem cells. *J. Exp. Med.* **195**, 759–770 (2002).
28. Pear, W., Nolan, G., Scott, M. & Baltimore, D. Production of high-titer helper-free retroviruses by transient transfection. *Proc. Natl Acad. Sci. U.S.A.* **90**, 8392–8396 (1993).
29. Cotta, C., Swindle, C., Weissman, I. L. & Klug, C. A. *Retroviral Transduction of FACS-Purified Hematopoietic Stem Cells* (eds Klug, C. A. & Jordan, C. T.) 243–252 (Humana Press, Totowa, New Jersey, 2001).
30. Lessard, J. & Sauvageau, G. *Bmi-1* determines the proliferative capacity of normal and leukaemic stem cells. *Nature* advance online publication, 20 April 2003 (doi: 10.1038/nature01572).

Supplementary Information accompanies the paper on **www.nature.com/nature**.

Acknowledgements We thank T. Magnuson and C. Klug for providing *Bmi-1*$^{+/-}$ mice and the MSCV plasmid, respectively; and the Flow Cytometry Core and the Microarray Core at the University of Michigan for their work. The Microarray Core is supported in part by a University of Michigan's Cancer Center Support Grant from the NIH. This work is supported by grants from the NIH.

Competing interests statement The authors declare that they have no competing financial interests.

Correspondence and requests for materials should be addressed to M.F.C. (mclarke@umich.edu).

DNA helicase Srs2 disrupts the Rad51 presynaptic filament

Lumir Krejci*†, Stephen Van Komen*†, Ying Li‡, Jana Villemain*, Mothe Sreedhar Reddy*, Hannah Klein§, Thomas Ellenberger‡ & Patrick Sung*

** Institute of Biotechnology and Department of Molecular Medicine, University of Texas Health Science Center at San Antonio, 15355 Lambda Drive, San Antonio, Texas 78245, USA*
‡ Department of Biological Chemistry and Molecular Pharmacology, Harvard Medical School, Boston, Massachusetts 02115, USA
§ Department of Biochemistry, New York University School of Medicine, New York, New York 10016, USA
† These authors contributed equally to the work

Mutations in the *Saccharomyces cerevisiae* gene *SRS2* result in the yeast's sensitivity to genotoxic agents, failure to recover or adapt from DNA damage checkpoint-mediated cell cycle arrest, slow growth, chromosome loss, and hyper-recombination[1,2]. Furthermore, double mutant strains, with mutations in DNA helicase genes *SRS2* and *SGS1*, show low viability that can be overcome by inactivating recombination, implying that untimely recombination is the cause of growth impairment[1,3,4]. Here we clarify the role of *SRS2* in recombination modulation by purifying its encoded product and examining its interactions with the Rad51 recombinase. Srs2 has a robust ATPase activity that is dependent on single-stranded DNA (ssDNA) and binds Rad51, but the addition of a catalytic quantity of Srs2 to Rad51-mediated recombination reactions causes severe inhibition of these reactions. We show that Srs2 acts by dislodging Rad51 from ssDNA. Thus, the attenuation of recombination efficiency by Srs2 stems primarily from its ability to dismantle the Rad51 presynaptic filament efficiently. Our findings have implications for the basis of Bloom's and Werner's syndromes, which are caused by mutations in DNA helicases and are characterized by increased frequencies of recombination and a predisposition to cancers and accelerated ageing[5].

We have been unable to overexpress Srs2 protein significantly in yeast, suggesting that this protein is unstable in, and/or toxic to, yeast cells. We therefore turned to *Escherichia coli* and an inducible T7 promoter as vehicle for Srs2 expression. Srs2 could be revealed by Coomassie Blue staining of *E. coli* extracts and by immunoblotting with antibodies against Srs2 (Fig. 1a). We subjected *E. coli* lysate to precipitation with ammonium sulphate and a five-step chromatographic fractionation scheme to purify Srs2 to near-homogeneity (Fig. 1b). Purified Srs2 has a robust ssDNA-dependent ATPase activity ($k_{cat} \geq 2{,}500\ min^{-1}$) and a DNA helicase activity[6] that is fuelled by ATP hydrolysis (Fig. 1c).

Previous studies have unveiled an anti-recombination function in *SRS2* and a genetic interaction with *RAD51* (refs 7–9). We investigated whether Srs2 protein interacts physically with Rad51 protein, and also tested its effect on the Rad51 recombinase activity[10]. To

© 2003 Nature Publishing Group

examine whether Srs2 associates with Rad51, we coupled the latter to Affi-gel 15 beads and used the resulting matrix to bind Srs2. As shown in Fig. 1d, Srs2 was retained on the Affi-Rad51 beads, but no binding of Srs2 to bovine serum albumin (BSA) immobilized on Affi-beads (Affi-BSA) was detected. An interaction between Rad51 and two carboxy-terminal fragments of Srs2 was seen in the two-hybrid assay in yeast (Fig. 1e). We were unable to detect significant interaction between Rad51 and full-length Srs2 in this assay, which could be the result of low expression of full-length Srs2.

We next tested the effect of Srs2 on the Rad51-mediated homologous pairing and strand exchange reaction that serves to join recombining DNA molecules[10,11]. For this, we employed a commonly used assay in which Rad51 and the heterotrimeric ssDNA-binding factor RPA are incubated with ssDNA and ATP to form a Rad51–ssDNA nucleoprotein filament[11–13]. Such a filament, often called the presynaptic filament[11–13], is then incubated with the homologous linear duplex (Fig. 2Aa). Pairing between the DNA substrates yields a joint molecule, which is further processed by DNA strand exchange to nicked circular duplex (Fig. 2Aa, b). As shown in Fig. 2Ac, d, the addition of a catalytic quantity of Srs2 strongly suppressed the homologous pairing and strand exchange reaction.

To characterize its anti-recombination activity further, Srs2 was added to D-loop reactions in which pairing of a ^{32}P-labelled 90-mer oligonucleotide with a homologous duplex target is mediated by the combination of Rad51 and Rad54 proteins[14,15] (Fig. 2Ba). As reported previously[14–16], efficient D-loop formation was catalysed by Rad51 and Rad54 (Fig. 2Bb, d). As expected, the inclusion of Srs2 decreased the level of D-loop formation (Fig. 2Bb, d). RPA enhanced D-loop formation in the absence of Srs2 (Fig. 2Bc, d), but the inhibitory effect of Srs2 became much more pronounced when RPA was present. We provide an explanation below for this observation.

We considered the possibility that suppression of recombination by Srs2 might result from the dissociation of DNA joints by its helicase activity. To address this, D-loop was formed with Rad51/Rad54 and then Srs2 was added. Srs2 was incapable of dissociating the preformed D-loop, regardless of the presence or absence of RPA (Fig. 3A), suggesting that suppression of the recombination reaction does not stem from the unwinding of DNA by Srs2.

Several approaches were used to test the idea that Srs2 inhibits Rad51 recombinase function by disrupting the presynaptic filament. In doing so, we reasoned that disruption of the presynaptic filament would yield free Rad51 molecules that could be trapped on duplex DNA (dsDNA). The binding of Rad51 to topologically relaxed dsDNA induces lengthening of the DNA[17,18] that can be monitored as a change in the DNA linking number on treatment with topoisomerase I (Fig. 3Ba). The product of this reaction is an underwound species referred to as form U (Fig. 3Bb, lane 4). RPA and Srs2 do not catalyse the formation of form U (Fig. 3Bb, lane 8), and these proteins have no effect on the formation of form U by Rad51 (Fig. 3Bb, compare lanes 6 and 4). The presynaptic filament consisting of Rad51–ssDNA does not make form U (Fig. 3Bc, lane 3). The addition of Srs2 to the Rad51–ssDNA presynaptic filament causes the generation of form U (Fig. 3Bc, lanes 4–6), indicating the transfer of Rad51 from the presynaptic filament to the dsDNA. The addition of RPA further stimulates the Srs2-mediated release of Rad51 from the presynaptic filament and the formation of form U (Fig. 3Bc, lanes 8–10). RPA has high affinity for ssDNA and it can compete with Rad51 for binding to ssDNA[10,19,20]. The enhanced production of form U was therefore probably due to the sequestering of ssDNA by RPA after Srs2 had released Rad51, thereby preventing the renucleation of Rad51 on the ssDNA. This premise was verified by electron microscopy and explains the

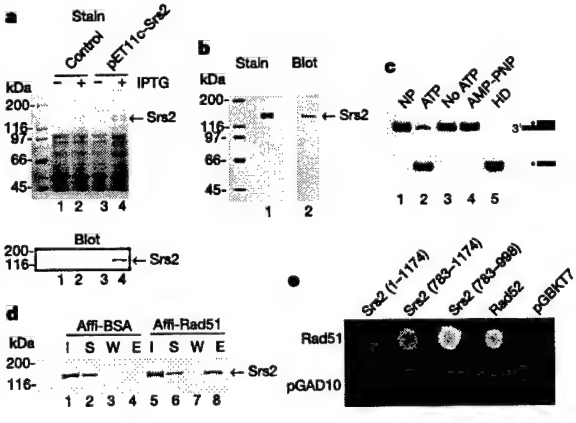

Figure 1 Purification and characterization of Srs2. **a**, Extracts from *E. coli* cells harbouring pET11c::Srs2 and the control vector pET11c grown with or without isopropyl β-D-thiogalactoside (IPTG) were analysed by SDS–PAGE and immunoblotting. **b**, Purified Srs2 was analysed by SDS–PAGE (2 μg) and immunoblotting (20 ng). **c**, DNA unwinding by Srs2 occurs with ATP but not without it or with AMP-PNP. The substrate was also incubated alone (NP) or boiled (HD) for 1 min. **d**, Srs2 was mixed with Affi-Rad51 and Affi-BSA beads. The input (I), supernatant (S), wash (W) and SDS eluate (E) were immunoblotted. **e**, Full-length and truncated versions of Srs2 were tested for two-hybrid interaction with Rad51. Empty vectors and Rad52 were included as controls.

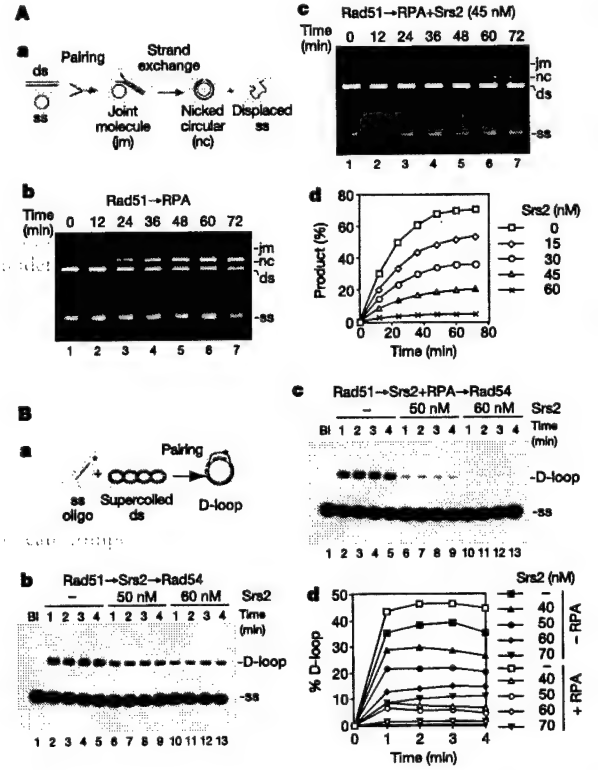

Figure 2 Srs2 inhibits Rad51-mediated DNA pairing and strand exchange. **A**, **a**, The DNA strand exchange scheme. In **b**, the DNA substrates were incubated with Rad51 and RPA. In **c**, Srs2 was also included. The results from **b** and **c** and from reactions with other Srs2 amounts are plotted in **d**. **B**, **a**, The D-loop reaction scheme. In **b**, Rad51, Srs2 and Rad54 were incubated with the DNA substrates. In **c**, RPA was also included. The results from **b** and **c** and from reactions with other Srs2 amounts are plotted in **d**. Filled symbols, reactions without RPA; open symbols, reactions with RPA.

© 2003 Nature Publishing Group

RPA-mediated enhancement of the inhibitory effect of Srs2 in the D-loop reaction (Fig. 2B).

The Srs2-mediated disruption of the Rad51 presynaptic filament was examined by a second approach. Here, Rad51 that had been dissociated from ssDNA by Srs2 was trapped on a DNA duplex bound to magnetic beads through a biotin–streptavidin linkage (Fig. 3Ca). Rad51 was eluted from the bead-bound DNA duplex by treatment with SDS and then analysed in a denaturing polyacrylamide gel. Consistent with results from the topoisomerase I-linked assay (Fig. 3B) was the observation that there was an Srs2-concentration-dependent transfer of Rad51 from the presynaptic filament to the bead-bound DNA duplex (Fig. 3Cb).

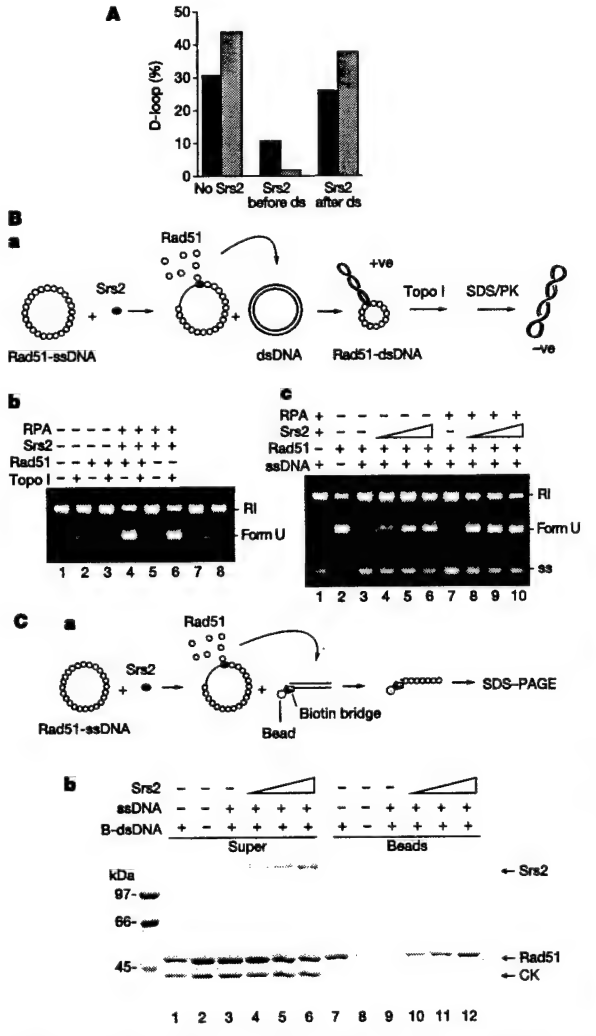

Figure 3 Srs2 disrupts the Rad51 presynaptic filament. **A**, D-loop reactions without and with Srs2 added before or after the duplex substrate were performed. The reactions were repeated with RPA present. Black bars, reactions without RPA; grey bars, reactions with RPA. **B**, **a**, The reaction scheme. PK, proteinase K. **b**, Only Rad51 makes form U. In **c**, Rad51 presynaptic filaments, assembled with or without RPA, were treated with Srs2 and topoisomerase. Lane 2 contained form U marker. RI, relaxed duplex; ss, single-stranded DNA. **C**, **a**, The reaction scheme. In **b**, Rad51 presynaptic filaments were incubated with Srs2 and then with beads containing dsDNA. Rad51 was also incubated with beads containing dsDNA (lanes 1 and 7) and beads without DNA (lanes 2 and 8). The supernatant and bead fractions were analysed. CK, creatine kinase.

Last, we used electron microscopy to characterize the action of Srs2 on the Rad51 presynaptic filament. After incubation of Rad51 with circular ssDNA, abundant presynaptic filaments[17,18] were seen (Fig. 4a). Under the same conditions, RPA formed complexes with ssDNA that appeared as compact structures with distinctive protein bulges (Fig. 4b). Although RPA alone was unable to disrupt the Rad51 presynaptic filaments (Fig. 4c), the addition of Srs2 with RPA to the presynaptic filaments caused a complete loss of the filaments, and the concomitant formation of RPA–ssDNA complexes (Fig. 4d). Previous biochemical experiments had shown transfer of Rad51 from the presynaptic filament to dsDNA promoted by Srs2 (Fig. 3B and C). This Srs2-mediated transfer of Rad51 to dsDNA could be observed directly by electron microscopy (Fig. 4e). The data from the electron microscopic analyses agree with results from the biochemical experiments (Figs 2 and 3), because they show that Srs2 disrupts the Rad51 presynaptic filament.

Even though homologous recombination is important for repairing DNA strand breaks induced by ionizing radiation and endogenous agents, and for restarting delinquent DNA replication forks, it can also generate deleterious genomic rearrangements and create DNA structures that cannot be properly resolved[1]. Cells have therefore evolved mechanisms to avoid untimely recombination[1,5]. Our studies provide evidence that Srs2 does this by disrupting the Rad51 presynaptic filament. The same conclusion has been reached independently[21]. Furthermore, even though RPA can function as a cofactor in the assembly of the Rad51 presynaptic filament[10,20], it might also promote the anti-recombination function of Srs2 by preventing reassembly of the presynaptic filament (Figs 3 and 4). That Srs2 uses the free energy from ATP hydrolysis to dislodge Rad51 from the presynaptic filament has been verified with mutant variants of Srs2 (srs2 K41A and srs2 K41R) defective for ATP hydrolysis. The physical interaction noted between Rad51 and Srs2 further suggests a mechanism for targeting the latter to the presynaptic filament. Taken together, the results presented here indicate that the motor activity of Srs2 driven by ATP hydrolysis is capable of dissociating not only DNA structures[6] but also DNA–protein complexes.

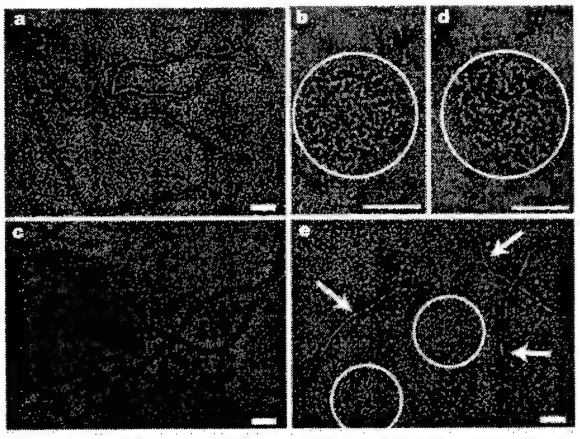

Figure 4 EM analysis of Rad51 filament disruption by Srs2. **a**, **b**, Rad51 (**a**) and RPA (**b**) were each incubated with ssDNA; examples of the nucleoprotein complexes that formed are shown. **c**, RPA was not able to disrupt preformed Rad51 filaments; an example of the Rad51 filaments present is shown. **d**, Incubation of preformed Rad51 filaments with Srs2 and RPA caused the loss of filaments and concomitant formation of RPA–ssDNA complexes, an example of which is shown. **e**, When preformed Rad51–ssDNA filaments were incubated with Srs2, RPA and linear duplex, RPA–ssDNA complexes were formed (circled) and transfer of Rad51 onto the linear duplex was visualized (arrows). Scale bars, 100 nm.

© 2003 Nature Publishing Group

The inhibitory effect of Srs2 on Rad51-mediated DNA strand exchange can be partly overcome by the inclusion of Rad52 protein, a recombination mediator that promotes Rad51 presynaptic filament assembly[11,12]. However, the Rad55–Rad57 complex, which also has recombination mediator activity[11,12], is much less effective in alleviating the inhibitory effect of Srs2. Furthermore, Rad52 and the Rad55–Rad57 complex do not seem to act synergistically. Interestingly, we have found that Srs2 can also dismantle presynaptic filaments of RecA and human Rad51 proteins. It therefore seems that the presynaptic filaments formed by the RecA/Rad51 class of general recombinases share a conserved feature that is recognized by Srs2, making them prone to disruption by the motor activity of Srs2.

The sensitivity of *srs2* mutants to DNA-damaging agents[6,22] is alleviated by deleting *RAD51* (ref. 23), and the inability to remove Rad51 from DNA in the *srs2* mutants most probably accounts for the hyper-recombination phenotype of these mutants[1]. Similarly, the cell cycle checkpoint recovery and adaptation defect in *srs2* mutants might be related to an inability to evict Rad51 from damaged DNA[2]. Cells mutated for *SRS2* grow slowly, exhibit an extended late S and/or G2 phase, and are defective in meiosis[25]. These defects could result from the generation of unresolvable recombination intermediates that trigger checkpoint activation and thereby compromise cell cycle progression. In addition to functioning as an anti-recombinase, Srs2 could conceivably prevent D-loop reversal by removing Rad51 bound to the displaced ssDNA strand. The various activities of Srs2 might be subject to modulation by phosphorylation[24].

Other DNA helicase enzymes are known to suppress recombination in eukaryotic cells, including the *S. cerevisiae* Sgs1 protein and the human BLM and WRN proteins, mutated in Bloom's syndrome and Werner's syndrome, respectively. Untimely and aberrant recombination events in Bloom's syndrome and Werner's syndrome cells could contribute to the genomic instability in these cells[26]. It has been suggested that BLM and WRN proteins control the level of recombination by dissociating recombination intermediates[5,27]. It will be of interest to test whether Sgs1, BLM and WRN proteins affect the integrity of the hRad51 presynaptic filament, as overexpression of Sgs1 protein can partly suppress some of the defects of *srs2* mutants[28]. □

Methods

Antibodies and Srs2 purification

Polyclonal antiserum was raised against residues 177–646 of Srs2 fused to glutathione *S* transferase. Antibodies were purified from the rabbit anti-serum by affinity chromatography on a column containing the antigen crosslinked to cyanogen bromide-activated sepharose 4B matrix (Amersham Biosciences). *SRS2* gene was placed under the T7 promoter in the vector pET11c to yield plasmid pET11c::Srs2, which was introduced into *E. coli* BL21 (DE3). Srs2 expression was induced by isopropyl β-D-thiogalactoside, and extract from 7 l of culture was subjected to precipitation with ammonium sulphate and chromatographic fractionation in columns of Q Sepharose, SP Sepharose, hydroxyapatite and Mono Q. The final Srs2 pool (300 μg at 2 mg ml^{-1}) was nearly homogeneous and stored in small portions at −80 °C.

DNA substrates

The φX circular (+) strand was from New England Biolabs. The φX replicative form I DNA (Gibco-BRL) was linearized by digestion with *Apa*LI. The pBluescript SK(−) replicative form I DNA was prepared as described[29]. Oligonucleotide D1 has the sequence: 5′-AAATCAATCTAAAGTATATATGAGTAAACTTGGTCTGACAGTTACCAATGCTTAATCAGTGAGGCACCTATCTCAGCGATCTGTCTATTT-3′, being complementary to positions 1932–2022 of the pBluescript replicative form I DNA. Oligonucleotide H2 has the sequence: 5′-GTAACTGTCAGACCAAGTTTACTCATATATACTTTAGATTGATTT-3′, being complementary to the first 45 residues of oligonucleotide D1. The two oligonucleotides were 5′ end-labelled with [γ-^{32}P]ATP and purified as described[29]. The DNA helicase substrate was obtained by hybridizing D1 to radiolabelled H2, as described[14].

Biotinylated dsDNA coupled to magnetic beads

The ends of a 769-base pair fragment derived from digesting φX174 replicative form I DNA with *Apa*LI and *Xho*I were filled in with the Klenow polymerase, using a mixture of dGTP, dTTP, Bio-7-dATP and Bio-11-dCTP (Enzo Diagnostics). The biotinylated DNA fragment was immobilized on streptavidin-coated magnetic beads (Roche Molecular Biochemicals) to give biotinylated DNA at 40 ng μl^{-1} packed volume.

Binding of Srs2 to beads containing Rad51

Rad51 and BSA were coupled to Affi-Gel 15 beads (Bio-Rad) at 5 and 12 mg ml^{-1}, respectively[14]. To examine Srs2 binding, 3 μg Srs2 was mixed with 7 μl Affi-Rad 51 or Affi-BSA beads in 30 μl PBS (10 mM KH_2PO_4 pH 7.2, 150 mM KCl, 1 mM dithiothreitol (DTT) and 0.01% Igepal) at 4 °C for 30 min. The beads were collected by centrifugation; after the supernatant had been decanted off, the beads were washed twice with 100 μl buffer, then treated for 5 min with 30 μl 2% SDS at 37 °C to elute bound Srs2. The various fractions—10 μl each—were analysed by immunoblotting to determine their Srs2 content.

Yeast two-hybrid assay

RAD51 was cloned into pGAD10, which contains the *GAL4* transcription activation domain, and the resulting plasmid was introduced into the haploid yeast strain PJ69-4a (ref. 30). *SRS2* (residues 1–1174), two C-terminal fragments of *SRS2* (residues 783–1174 and residues 738–998), and *RAD52* were cloned into pGBKT7, which contains the *GAL4* DNA-binding domain; the resulting plasmids were introduced into the haploid yeast strain PJ69-4α (ref. 30). Diploid strains obtained by mating plasmid-bearing PJ69-4a and PJ69-4α haploids were grown on synthetic medium lacking tryptophan and leucine. To select for two-hybrid interactions, which would result in the activation of the *ADE2* and *HIS3* reporter genes, diploid cells were replica-plated on synthetic medium lacking tryptophan, leucine and adenine, and also on synthetic medium lacking tryptophan, leucine and histidine[30]. Both platings gave identical results. Only the plating on the tryptophan, leucine and adenine dropout medium is shown in Fig. 1e.

DNA helicase assay

Srs2 (35 nM) was incubated at 30 °C for 10 min with the DNA substrate (300 nM nucleotides) in 10 μl buffer H (25 mM Tris-HCl pH 7.5, 2.5 mM $MgCl_2$, 1 mM DTT, 100 μg ml^{-1} BSA) containing 2 mM ATP or β-γ-imidoadenosine 5′-phosphate (AMP-PNP) and then analysed[14].

Homologous DNA pairing and strand exchange reaction

Buffer R (35 mM Tris-HCl pH 7.4, 2.0 mM ATP, 2.5 mM $MgCl_2$, 50 mM KCl, 1 mM DTT, containing an ATP-regenerating system consisting of 20 mM creatine phosphate and 20 μg ml^{-1} creatine kinase) was used for the reactions, and all the incubation steps were performed at 37 °C. Rad51 (10 μM) was mixed with φX circular (+) strand (30 μM nucleotides) in 30 μl for 5 min, followed by the incorporation of RPA (2 μM) in 1.5 μl and a 3 min incubation. The reaction was completed by adding 3 μl 50 mM spermidine hydrochloride and linear φX dsDNA (30 μM nucleotides) in 3 μl. Portions (4.5 μl) of the reaction mixtures were taken at the indicated times, deproteinized and resolved in agarose gels followed by ethidium bromide staining of the DNA species, as described previously[18]. Srs2 was added to the reactions in 0.9 μl at the time of RPA incorporation.

D-loop reaction

Buffer R was used for the D-loop reactions. The radiolabelled oligonucleotide D1 (3 μM nucleotides) was incubated with Rad51 (1 μM) in 22 μl for 5 min at 37 °C, followed by the incorporation of Rad54 (150 nM) in 1 μl and a 2-min incubation at 23 °C. The reaction was initiated by adding pBluescript replicative form I DNA (50 μM base pairs) in 2 μl. The reaction mixtures were incubated at 30 °C, and 5-μl aliquots were withdrawn at the indicated times and processed for electrophoresis as described above. The gels were dried and subjected to phosphorimaging analysis. The percentage of D-loop refers to the quantity of the replicative form substrate that had been converted into D-loop. When present, RPA (200 nM) and Srs2 (40–70 nM) were added to the preassembled Rad51 filament, followed by a 4-min incubation at 37 °C before Rad54 was incorporated. In Fig. 3A, Srs2 (45 nM) was added to the D-loop reactions before Rad54 as above, or 1 min after the incorporation of the duplex substrate. The reactions were terminated after 4 min of incubation.

Topoisomerase-I-linked DNA unwinding assay

Buffer R was used for the reactions and all the incubation steps were performed at 37 °C. Rad51 (4 μM) was incubated for 4 min with pBluescript (−) strand (20 μM nucleotides) in 7.8 μl. Srs2 (40, 60 or 80 nM) and RPA (1 μM) were added in 1 μl, followed by a 4-min incubation. Topologically relaxed φX174 DNA (12.5 μM nucleotides) in 0.8 μl and 2.5 U calf thymus topoisomerase I (Invitrogen) in 0.4 μl storage buffer were then incorporated to complete the reaction. The reaction mixtures were incubated for 8 min and then stopped by adding SDS to 0.5%. In reactions that did not contain the (−) strand, Rad51, with or without RPA (1 μM) and Srs2 (80 nM), was incubated for 8 min with topologically relaxed φX174 DNA and topoisomerase I in a final volume of 10 μl. The reaction mixtures were treated for 10 min with proteinase K (0.5 mg ml^{-1}) before being analysed in 0.9% agarose gels.

Transfer of Rad51 to bead-bound biotinylated dsDNA

M13mp18 circular (+) strand (7.2 μM nucleotides) was incubated for 5 min with Rad51 (2.4 μM) at 37 °C, followed by the addition of Srs2 (30, 60 or 90 nM) in a final volume of 20 μl buffer R containing 50 mM KCl and 0.01% Igepal. After 3 min at 37 °C, 4 μl magnetic beads containing dsDNA were added to the reaction, followed by constant mixing for 5 min at 23 °C. The beads were captured with the Magnetic Particle Separator (Boehringer Mannheim), washed twice with 50 μl buffer, and the bound Rad51 was eluted with 20 μl 1% SDS. The supernatant, which contained unbound Rad51, and the SDS eluate (10 μl each) were analysed by SDS–polyacrylamide-gel electrophoresis (SDS–PAGE).

© 2003 Nature Publishing Group

Electron microscopy

The reactions were performed in buffer R at 37 °C and had a final volume of 12.5 μl. To assemble the Rad51 presynaptic filament, M13mp18 (+) strand (7.2 μM nucleotides) and 1.3 μg Rad51 (2.4 μM) were incubated for 5 min. To test the effects of Srs2 and RPA, these proteins were added to the reaction mixtures containing the preassembled Rad51 presynaptic filament to final concentrations of 60 nM (Srs2) and 350 nM (RPA), followed by a 3-min incubation. In some cases, linear dsDNA (a 5.2-kilobase fragment derived from the pET24 vector) was also added with Srs2 and RPA to 7.2 μM base pairs, followed by a 5-min incubation. For electron microscopy, 3 μl of each reaction mixture was applied to copper grids coated with thin carbon film after glow-discharging the coated grids for 2 min. The grids were washed twice with buffer R and stained for 30 s with 0.75% uranyl formate. After air-drying, the grids were examined with a Philips Tecnai12 electron microscope under low-dose conditions. Images were recorded either with a charge-coupled device camera (Gatan) or on Kodak SO-163 films at × 30,000 magnification and then scanned on a SCAI scanner (Zeiss). The experiments shown in Fig. 4 were each independently repeated three or more times and at least 100 nucleoprotein complexes were examined in each experiment.

Received 3 February; accepted 20 March 2003; doi:10.1038/nature01577.

1. Klein, H. L. A radical solution to death. *Nature Genet.* **25,** 132–134 (2000).
2. Vaze, M. B. *et al.* Recovery from checkpoint-mediated arrest after repair of a double-strand break requires Srs2 helicase. *Mol. Cell* **10,** 373–385 (2002).
3. Lee, S. K., Johnson, R. E., Yu, S. L., Prakash, L. & Prakash, S. Requirement of yeast SGS1 and SRS2 genes for replication and transcription. *Science* **286,** 2339–2342 (1999).
4. Gangloff, S., Soustelle, C. & Fabre, F. Homologous recombination is responsible for cell death in the absence of the Sgs1 and Srs2 helicases. *Nature Genet.* **25,** 192–194 (2000).
5. Oakley, T. J. & Hickson, I. D. Defending genome integrity during S-phase: putative roles for RecQ helicases and topoisomerase III. *DNA Repair* **1,** 175–207 (2002).
6. Rong, L. & Klein, H. L. Purification and characterization of the SRS2 DNA helicase of the yeast *Saccharomyces cerevisiae*. *J. Biol. Chem.* **268,** 1252–1259 (1993).
7. Milne, G. T., Ho, T. & Weaver, D. T. Modulation of *Saccharomyces cerevisiae* DNA double-strand break repair by SRS2 and RAD51. *Genetics* **139,** 1189–1199 (1995).
8. Chanet, R., Heude, M., Adjiri, A., Maloisel, L. & Fabre, F. Semidominant mutations in the yeast Rad51 protein and their relationships with the Srs2 helicase. *Mol. Cell. Biol.* **16,** 4782–4789 (1996).
9. Schild, D. Suppression of a new allele of the yeast RAD52 gene by overexpression of RAD51, mutations in srs2 and ccr4, or mating-type heterozygosity. *Genetics* **140,** 115–127 (1995).
10. Sung, P. Catalysis of ATP-dependent homologous DNA pairing and strand exchange by yeast RAD51 protein. *Science* **265,** 1241–1243 (1994).
11. Sung, P., Trujillo, K. M. & Van Komen, S. Recombination factors of *Saccharomyces cerevisiae*. *Mutat. Res.* **451,** 257–275 (2000).
12. Cox, M. M. Recombinational DNA repair of damaged replication forks in *Escherichia coli*: questions. *Annu. Rev. Genet.* **35,** 53–82 (2001).
13. Bianco, P. R., Tracy, R. B. & Kowalczykowski, S. C. DNA strand exchange proteins: a biochemical and physical comparison. *Front. Biosci.* **3,** 570–603 (1998).
14. Petukhova, G., Stratton, S. & Sung, P. Catalysis of homologous DNA pairing by yeast Rad51 and Rad54 proteins. *Nature* **393,** 91–94 (1998).
15. Mazin, A. V., Zaitseva, E., Sung, P. & Kowalczykowski, S. C. Tailed duplex DNA is the preferred substrate for Rad51 protein-mediated homologous pairing. *EMBO J.* **19,** 1148–1156 (2000).
16. Van Komen, S., Petukhova, G., Sigurdsson, S. & Sung, P. Functional cross-talk among Rad51, Rad54, and replication protein A in heteroduplex DNA joint formation. *J. Biol. Chem.* **277,** 43578–43587 (2002).
17. Ogawa, T., Yu, X., Shinohara, A. & Egelman, E. H. Similarity of the yeast RAD51 filament to the bacterial RecA filament. *Science* **259,** 1896–1899 (1993).
18. Sung, P. & Robberson, D. L. DNA strand exchange mediated by a RAD51-ssDNA nucleoprotein filament with polarity opposite to that of RecA. *Cell* **82,** 453–461 (1995).
19. Sung, P. Yeast Rad55 and Rad57 proteins form a heterodimer that functions with replication protein A to promote DNA strand exchange by Rad51 recombinase. *Genes Dev.* **11,** 1111–1121 (1997).
20. Sugiyama, T., Zaitseva, E. M. & Kowalczykowski, S. C. A single-stranded DNA-binding protein is needed for efficient presynaptic complex formation by the *Saccharomyces cerevisiae* Rad51 protein. *J. Biol. Chem.* **272,** 7940–7945 (1997).
21. Veaute, X. *et al.* The Srs2 helicase prevents recombination by disrupting Rad51 nucleoprotein filaments. *Nature* **423,** 309–312 (2003).
22. Aboussekhra, A. *et al.* RADH, a gene of *Saccharomyces cerevisiae* encoding a putative DNA helicase involved in DNA repair. Characteristics of radH mutants and sequence of the gene. *Nucleic Acids Res.* **17,** 7211–7219 (1989).
23. Aboussekhra, A., Chanet, R., Adjiri, A. & Fabre, F. Semidominant suppressors of Srs2 helicase mutations of *Saccharomyces cerevisiae* map in the RAD51 gene, whose sequence predicts a protein with similarities to procaryotic RecA proteins. *Mol. Cell. Biol.* **12,** 3224–3234 (1992).
24. Liberi, G. *et al.* Srs2 DNA helicase is involved in checkpoint response and its regulation requires a functional Mec1-dependent pathway and Cdk1 activity. *EMBO J.* **19,** 5027–5038 (2000).
25. Palladino, F. & Klein, H. L. Analysis of mitotic and meiotic defects in *Saccharomyces cerevisiae* SRS2 DNA helicase mutants. *Genetics* **132,** 23–37 (1992).
26. Adams, M. D., McVey, M. & Sekelsky, J. J. *Drosophila* BLM in double-strand break repair by synthesis-dependent strand annealing. *Science* **299,** 265–267 (2003).
27. Wu, L., Davies, S. L., Levitt, N. C. & Hickson, I. D. Potential role for the BLM helicase in recombinational repair via a conserved interaction with RAD51. *J. Biol. Chem.* **276,** 19375–19381 (2001).
28. Mankouri, H. W., Craig, T. J. & Morgan, A. SGS1 is a multicopy suppressor of srs2: functional overlap between DNA helicases. *Nucleic Acids Res.* **30,** 1103–1113 (2002).
29. Petukhova, G., Stratton, S. A. & Sung, P. Single strand DNA binding and annealing activities in the yeast recombination factor Rad59. *J. Biol. Chem.* **274,** 33839–33842 (1999).
30. Krejci, L., Damborsky, J., Thomsen, B., Duno, M. & Bendixen, C. Molecular dissection of interactions between Rad51 and members of the recombination-repair group. *Mol. Cell. Biol.* **21,** 966–976 (2001).

Acknowledgements We thank M. Sehorn and K. Trujillo for reading the manuscript. This work was supported by research grants from the NIH (H.K., T.E. and P.S.). S.V.K. was supported in part by a predoctoral fellowship from the US Department of Defense, and Y.L. was supported by a NIH postdoctoral fellowship. The molecular electron microscopy facility at Harvard Medical School was established by a donation from the Giovanni Armeise Harvard Center for Structural Biology, and is maintained through a NIH grant.

Competing interests statement The authors declare that they have no competing financial interests.

Correspondence and requests for materials should be addressed to L.K. (krejci@uthscsa.edu) or P.S. (sung@uthscsa.edu).

The Srs2 helicase prevents recombination by disrupting Rad51 nucleoprotein filaments

Xavier Veaute*, Josette Jeusset†, Christine Soustelle*‡, Stephen C. Kowalczykowski§, Eric Le Cam† & Francis Fabre*

** CEA, DSV, Département de Radiobiologie et Radiopathologie, UMR217 CNRS/CEA, BP6, 92265 Fontenay aux Roses Cedex, France*
† Interactions Moléculaires et Cancer, UMR 81126 CNRS/IGR/UPS, Institut Gustave Roussy, Rue Camille Desmoulins, 94805 Villejuif Cedex, France
§ Sections of Microbiology and of Molecular and Cellular Biology, Center for Genetics and Development, University of California, Davis, California 95616-8665, USA

Homologous recombination is a ubiquitous process with key functions in meiotic and vegetative cells for the repair of DNA breaks. It is initiated by the formation of single-stranded DNA on which recombination proteins bind to form a nucleoprotein filament that is active in searching for homology, in the formation of joint molecules and in the exchange of DNA strands[1]. This process contributes to genome stability but it is also potentially dangerous to cells if intermediates are formed that cannot be processed normally and thus are toxic or generate genomic rearrangements. Cells must therefore have developed strategies to survey recombination and to prevent the occurrence of such deleterious events. In *Saccharomyces cerevisiae*, genetic data have shown that the Srs2 helicase negatively modulates recombination[2,3], and later experiments suggested that it reverses intermediate recombination structures[4–7]. Here we show that DNA strand exchange mediated *in vitro* by Rad51 is inhibited by Srs2, and that Srs2 disrupts Rad51 filaments formed on single-stranded DNA. These data provide an explanation for the anti-recombinogenic role of Srs2 *in vivo* and highlight a previously unknown mechanism for recombination control.

Several phenotypes (discussed below) conferred by the *srs2* deletion are suppressed by mutations that prevent formation of the Rad51 nucleofilaments[8,9]. Two hypotheses could explain this suppression: either Srs2 functions in replication and repair to prevent the formation of toxic recombination structures, or Srs2 disrupts dead-end recombination intermediates, possibly formed after the arrest of the replication fork, to allow repair through alternative pathways. This second proposition led us to ask whether purified Srs2 acts on preformed recombination structures.

Srs2 was expressed from a baculovirus vector in which *SRS2* was cloned in frame with a histidine tag at its amino terminus. We showed that the protein fusion expressed in yeast fully complements the sensitivity of *srs2*-deleted cells to radiation (data not shown).

‡ Present address: UMR2167 CNRS Centre de Génétique Moléculaire, Bâtiment 26, avenue de la Terrasse, 91198 Gif-sur-Yvette Cedex, France.

© 2003 Nature Publishing Group

THE JOURNAL OF BIOLOGICAL CHEMISTRY
© 2003 by The American Society for Biochemistry and Molecular Biology, Inc.
Vol. 278, No. 11, Issue of March 14, pp. 9212–9218, 2003
Printed in U.S.A.

Rad54p Is a Chromatin Remodeling Enzyme Required for Heteroduplex DNA Joint Formation with Chromatin*

Received for publication, November 12, 2002, and in revised form, January 2, 2003
Published, JBC Papers in Press, January 3, 2003, DOI 10.1074/jbc.M211545200

Mariela Jaskelioff‡§¶, Stephen Van Komen§‖, Jocelyn E. Krebs‡ ‡‡, Patrick Sung‖, and Craig L. Peterson‡§§**

From the ‡Interdisciplinary Graduate Program and Program in Molecular Medicine, University of Massachusetts Medical School, Worcester, Massachusetts 01605, and ‖Department of Molecular Medicine and Institute of Biotechnology, University of Texas Health Science Center at San Antonio, San Antonio, Texas 78245-3207

In eukaryotic cells, the repair of DNA double-strand breaks by homologous recombination requires a RecA-like recombinase, Rad51p, and a Swi2p/Snf2p-like ATPase, Rad54p. Here we find that yeast Rad51p and Rad54p support robust homologous pairing between single-stranded DNA and a chromatin donor. In contrast, bacterial RecA is incapable of catalyzing homologous pairing with a chromatin donor. We also show that Rad54p possesses many of the biochemical properties of *bona fide* ATP-dependent chromatin-remodeling enzymes, such as ySWI/SNF. Rad54p can enhance the accessibility of DNA within nucleosomal arrays, but it does not seem to disrupt nucleosome positioning. Taken together, our results indicate that Rad54p is a chromatin-remodeling enzyme that promotes homologous DNA pairing events within the context of chromatin.

Chromosomal DNA double-strand breaks (DSBs)[1] arise through exposure of cells to harmful environmental agents such as ionizing radiation or mutagenic chemicals (radiomimetics, alkylating agents, etc.). DSBs can also be caused by endogenously produced oxygen radicals, by errors in DNA replication, or as obligatory intermediates during programmed cellular processes, such as meiosis or V(D)J recombination (1–3). Cell survival and maintenance of genome integrity depend on efficient repair of DSBs, because unrepaired or misrepaired DSBs may lead to mutations, gene translocations, gross chromosomal rearrangements, or cellular lethality.

Several pathways for repairing DSBs have evolved and are highly conserved throughout eukaryotes. Homologous recombination (HR) is a major pathway of DSB repair in all eukaryotes and has a distinct advantage over other mechanisms in that it is mostly error-free. In organisms ranging from yeast to human, HR is mediated by members of the *RAD52* epistasis group (*RAD50*, *RAD51*, *RAD52*, *RAD54*, *RAD55*, *RAD57*, *RAD59*, *MRE11*, and *XRS2*). Accordingly, mutations in any one of these genes result in sensitivity to ionizing radiation and other DSB-inducing agents (2). The importance of the HR pathway in maintaining genome integrity is underscored by the fact that mutations in each one of its critical factors have been correlated with chromosomal instability-related ailments, including ataxia telangiectasia-like disease, Nijmegen breakage syndrome, Li Fraumeni syndrome, as well as various forms of cancer (4).

In vivo and *in vitro* studies have suggested the following sequence of molecular events that lead to the recombinational repair of a DSB. First, the 5′ ends of DNA that flank the break are resected by an exonuclease to create ssDNA tails (5). Next, Rad51p polymerizes onto these DNA tails to form a nucleoprotein filament that has the capability to search for a homologous duplex DNA molecule. After DNA homology has been located, the Rad51-ssDNA nucleoprotein filament catalyzes the formation of a heteroduplex DNA joint with the homolog. The process of DNA homology search and DNA joint molecule formation is called "homologous DNA pairing and strand exchange." Subsequent steps entail DNA synthesis to replace the missing information followed by resolution of DNA intermediates to yield two intact duplex DNA molecules (6).

The homologous DNA pairing activity of Rad51p is enhanced by Rad54p (7). Rad54p is a member of the Swi2p/Snf2p protein family (8) that has DNA-stimulated ATPase activity and physically interacts with Rad51p (7, 9, 10). Because of its relatedness to the Swi2p/Snf2p family of ATPases, Rad54p may have chromatin remodeling activities in addition to its established role in facilitating Rad51p-mediated homologous pairing reactions. In this study we show that Rad51p and Rad54p mediate robust D-loop formation with a chromatin donor, whereas the bacterial recombinase, RecA, can only function with naked DNA. Furthermore, we find that the ATPase activity of Rad54p is essential for D-loop formation on chromatin and that Rad54p can use the free energy from ATP hydrolysis to enhance the accessibility of nucleosomal DNA. Experiments are also presented to suggest that chromatin remodeling by Rad54p and yeast SWI/SNF involves DNA translocation.

EXPERIMENTAL PROCEDURES

DNA—All DNA manipulations were carried out using standard methods (11). Oligonucleotides were obtained from Operon Technologies (Alameda, CA). Plasmid pXG540 and T4 EndonucleaseVII used in the cruciform extrusion experiments were a kind gift of Dr. T. Owen-Hughes.

The oligonucleotide used for triplex formation was TFO (triplex-forming oligonucleotide) (5′-TTCTTTTCTTTCTTCTTTCTTT-3′). To

* This work was supported by grants from the National Institutes of Health to C. L. P. (GM49650) and P. S. (GM57814). The costs of publication of this article were defrayed in part by the payment of page charges. This article must therefore be hereby marked "*advertisement*" in accordance with 18 U.S.C. Section 1734 solely to indicate this fact.

§ Both authors contributed equally to this work.

¶ Supported by a U. S. Department of Defense Predoctoral Fellowship (DAMD17-02-1-0471).

** Supported by a U. S. Department of Defense Predoctoral Fellowship (DAMD17-01-1-0414).

‡‡ Current Address: Dept. of Biological Sciences, University of Alaska, 3211 Providence Dr., Anchorage, AK 99508.

§§ To whom correspondence should be addressed. Tel.: 508-856-5858; Fax: 508-856-5011; E-mail: Craig.Peterson@umassmed.edu.

[1] The abbreviations used are: DSB, double-strand break; HR, homologous recombination; ssDNA, single-stranded DNA; dsDNA, double-stranded DNA; TFO, triplex-forming oligonucleotide; DTT, dithiothreitol; BSA, bovine serum albumin; ATPγS, adenosine 5′-*O*-(thiotriphosphate); AMP-PNP, adenosine 5′-(β,γ-imino)triphosphate; Mnase, micrococcal nuclease.

This paper is available on line at http://www.jbc.org

generate pMJ5, the annealed oligonucleotides TFOB5 (5′-TCGAGAAGAAAAGAAAGAAGAAAGAAAC-3′) and TFOB3 (5′-TCGAGT TTCTTTCTTTCTTTTCTTC-3′) were ligated to the product of a *Xho*I digestion carried out on pCL7c (12). This yielded a pBluescript SKII (−) plasmid containing 5 head-to-tail repeats of the 208-bp *Lytechinus variegatus* 5S rDNA nucleosome positioning element flanked by a TFO-binding site. The DNA template (208–11) for reconstituting nucleosomal arrays for the ATPase, remodeling, and Mnase assays consists a *Not*I-*Hin*dIII fragment derived from pCL7b (12), containing 11 head-to-tail repeats of a 5S rRNA gene from *L. variegatus*, each one possessing a nucleosome positioning sequence. The sixth nucleosome is tagged by a unique *Sal*I restriction site.

Reagent Preparation—Recombinant yeast Rad51p, Rad54p, rad54K341Ap, and rad54K341Rp were overexpressed in yeast and purified as previously described (7). SWI/SNF purification was as described (13). Histone octamers were purified from chicken erythrocytes as described by Hansen *et al.* (14). Octamer concentrations were determined by measurements of A_{230} (15). Nucleosomal array DNA templates (pXG540, pMJ5, or 208–11) were labeled by the Klenow polymerase fill-in reaction using [α-^{32}P]dCTP (3000 μCi/mmol, Amersham Biosciences). Nucleosomal arrays were reconstituted by salt dialysis as previously described (13), and the nucleosome saturation was determined to be 60–80% by digestion analysis.

D-loop Reactions—Oligonucleotide D1 (90-mer) used in the D-loop experiments has the sequence: 5′-AAATCAATCTAAAGTATATATGAGTAAACTTGGTCTGACAGTTACCAATGCTTAATCAGTGAGGCACCTATCTCAGCGATCTGTCTATTT-3′, being complementary to positions 1932–2022 of pBluescript SK(−) replicative form I DNA. Oligonucleotide D1 was 5′ end-labeled with ^{32}P using [γ-^{32}P]dATP and polynucleotide kinase, as described (7). Buffer R (35 mM Tris-HCl, pH 7.4, 2.0 mM ATP, 2.5 mM $MgCl_2$, 30 mM KCl, 1 mM DTT, and an ATP-regenerating system consisting of 20 mM creatine phosphate and 30 μg/ml creatine kinase) was used for the reactions; all of the incubation steps were carried out at 30 °C. Rad51 (0.8 μM) and Rad54 (120 nM) were incubated with radiolabeled oligonucleotide D1 (2.4 μM nucleotides) for 5 min to assemble the presynaptic filament, which was then mixed with naked pBluescript replicative form I DNA (38 μM base pairs) or the same DNA assembled into chromatin (38 μM base pairs). Chromatin assembly was monitored by following topological changes as well as measuring the degree of occlusion of a unique *Eco*RI restriction site close to the D1 sequence. Substrates were estimated to be ~80% saturated with nucleosomes. The reactions containing RecA protein (0.8 μM) were assembled in the same manner, except that they were supplemented with an additional 12.5 mM $MgCl_2$ at the time of incorporation of the duplex substrates. At the indicated times, 4-μl portions of the reactions were withdrawn and mixed with an equal volume of 1% SDS containing 1 mg/ml proteinase K. After incubation at 37 °C for 5 min, the deproteinized samples were run in 1% agarose gels in TAE buffer (40 mM Tris-HCl, pH 7.4, 0.5 mM EDTA) at 4 °C. The gels were dried, and the radiolabeled DNA species were visualized and quantified by PhosphorImager analysis (Personal Molecular Imager FX, Bio-Rad).

ATPase Assay—Recombinant yeast Rad54p (1 nM) was incubated at 30 °C or 37 °C with 5 nM of either naked 208–11 dsDNA or reconstituted nucleosomal arrays in the presence of 100 μM ATP, 2.5μCi [γ-^{32}P]dATP (6000 μCi/mmol, Amersham Biosciences), 2.5% glycerol, 0.1% Tween 20, 20 mM Tris-HCl, pH 8.0, 200 μM DTT, 5 mM $MgCl_2$, 100 μg/ml BSA. For the DNA length-dependence assays, 5 nM Rad54p, 5 nM Rad51p, or 10 nM SWI/SNF were used. Oligonucleotides (random N-mers ranging from 10–100 nucleotides in length) were PAGE-purified to ensure length homogeneity (Integrated DNA Technologies, Inc., Coralville, IA). Samples were taken after 2, 5, 15, and 30 min and resolved by TLC. The proportion of liberated ^{32}P-pyrophosphate was determined using the Molecular Dynamics PhosphorImager and ImageQuant Software. ATPase assays were independently repeated 3 times, yielding very similar results.

Cruciform Formation Assay—Cruciform formation assays were performed as previously described (16). Briefly, 8 ng of *Ava*I-linearized pXG540 (either naked, N, or nucleosomal, C) were incubated with various concentrations of Rad54, Rad51, or rad54 K341A and 0.15 mg/ml EndoVII (except where noted), in the presence of 10 mM Hepes, pH 7.9, 50 mM NaCl, 3 mM $MgCl_2$, 5% glycerol, 0.1 mM DTT, 1 mM ATP (except where noted), 3 mM phosphoenolpyruvate, and 20 units/ml pyruvate kinase for 30 min at 30 °C. The products were resolved in 1.2% agarose gels and visualized with Sybr Gold staining (Molecular Probes, Eugene, OR) followed by analysis with ImageQuant software.

Chromatin-remodeling Reaction—For the coupled SWI/SNF-or Rad54-*Sal*I reactions, reconstituted 208–11 nucleosomal arrays (~1 nM final concentration) were preincubated at 37 °C for 20 min with 2.5units/μl *Sal*I in a buffer containing (final concentrations) 50 mM NaCl, 5 mM $MgCl_2$, 1 mM ATP, 3 mM phosphoenolpyruvate, 10 units/ml pyruvate kinase, 1 mM DTT, 10 mM Tris-HCl, pH 8.0, 100 μg/ml BSA, and 3% glycerol. Nucleosomal arrays were ~80% saturated with nucleosomes. Buffer, 2 nM SWI/SNF complex, or various concentrations of recombinant Rad51p and Rad54p were added and samples were taken at the indicated time points, vigorously mixed for 10s with 25 μl TE and 50 μl 1:1 solution of phenol/chloroform. The purified DNA fragments were resolved by electrophoresis in 1.2% agarose gels in the presence of 50 μg/ml ethidium bromide. The gels were then dried on 3MM Whatman paper. The fraction of cut and uncut DNA was determined by PhosphorImager analysis using a Molecular Dynamics PhosphorImager and ImageQuant software. Experiments were repeated independently at least 3 times, which yielded very similar results.

Micrococcal Nuclease Digestion—15 nM reconstituted 208–11 nucleosomal arrays were incubated at 37 °C with 2 nM SWI/SNF, 100 nM Rad54p, or buffer, in the presence of 2 mM ATP, 5 mM NaCl, 2.5 mM Tris-HCl, pH 8.0, 0.25 mM $MgCl_2$, 0.3 mM $CaCl_2$, 3 mM phosphoenolpyruvate, 10 units/ml pyruvate kinase, 1 mM DTT, 10 μg/ml BSA, 0.5% glycerol. After 20 min, 0.0005 units of Micrococcal Nuclease (Worthington) was added to the reaction, and aliquots were taken at the indicated time points and then treated for 20 min with 2 μg/μl proteinase K and extracted twice with a 1:1 solution of phenol:chloroform. The resulting digestion products were resolved by electrophoresis in 2% agarose gels, run at 2.5 volts/cm for 12 h. The gels were fixed, dried, and analyzed using a Molecular Dynamics PhosphorImager and ImageQuant Software.

Triple-helix Displacement Assay—Triple-helix formation was performed as described (17). Briefly, equimolar concentrations (100 nM) of *Ssp*I-linearized pMJ5 and ^{32}P-labeled TFO were mixed in buffer MM (25 mM MES, pH 5.5, 10 mM $MgCl_2$) at 57 °C for 15 min and left to cool to room temperature overnight. The resulting triplex was either used directly or reconstituted into nucleosomal arrays. To introduce nicks into the DNA, pMJ5 was exposed to various concentrations of DNaseI (Promega, Madison, WI) for 2 min at 37 °C, the reactions were stopped with 5 mM EDTA, vigorously mixed for 10 s with a 1:1 solution of phenol/chloroform, ethanol-precipitated, and resuspended in water. The degree of nicking introduced by DNaseI treatment was assessed by electrophoretic analysis of native and heat-denatured samples (in the presence of 15% formamide) on denaturing 1.3% agarose gels, followed by Sybr Gold Stain (Molecular Probes, Eugene, OR).

The triplex-containing substrates (5 nM) were incubated at 30 °C with 5 nM recombinant Rad54 protein or SWI/SNF complex, in a buffer containing 35 mM Tris-HCl, pH 7.2, 3 mM $MgCl_2$, 100 μg/ml BSA, 50 mM KCl, 1 mM DTT, 3 mM phosphocreatine, 28 μg/ml creatine phosphokinase, and where noted, 3 mM ATP. Samples were taken at the indicated time points, the reactions were quenched with GSMB buffer (15% (w/v) glucose, 3% (w/v) SDS, 250 mM 4-morpholinepropanesulfonic acid, pH 5.5, 0.4 mg/ml bromphenol blue), and analyzed in 1.2% agarose gels (40 mM Tris acetate, 5 mM sodium acetate, 1 mM $MgCl_2$, pH 5.5) at 10 volts/cm for 1.5 h at 4 °C. Gels were fixed in 5% acetic acid, 50% methanol for 1 h, and dried. The proportion of bound and free TFO was determined using a Molecular Dynamics PhosphorImager and ImageQuant Software.

RESULTS

Rad51p and Rad54p Promote DNA Pairing with a Chromatin Donor—Repair of a DSB by homologous recombination begins with the invasion of a double-stranded, homologous donor by a Rad51-ssDNA nucleoprotein filament, also referred to as the presynaptic filament. This strand invasion reaction is typically monitored *in vitro* by following the Rad51p-dependent formation of a D-loop between a radiolabeled oligonucleotide and a homologous double-stranded DNA donor (Fig. 1*A*). In this case, efficient D-loop formation also requires the ATPase activity of Rad54p. *In vivo*, however, the search for homology and strand invasion involves a homologous donor that is assembled into chromatin. Given that the Rad54p ATPase shows sequence relatedness to known chromatin remodeling enzymes, it was of considerable interest to examine the ability of Rad54p to promote Rad51p-dependent D-loop formation with a nucleosomal donor.

Fig. 1 shows the results of D-loop assays that use either a circular, naked DNA donor or this same circular DNA assembled into nucleosomes. Consistent with previous studies, the

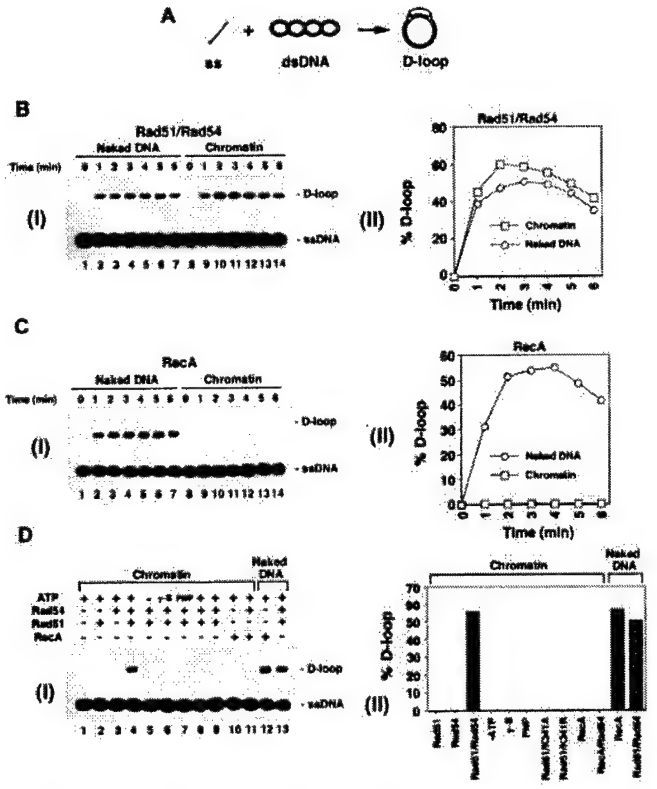

FIG. 1. **Rad51p and Rad54p promote efficient DNA strand invasion with chromatin.** *A*, schematic of the D-loop reaction. A radiolabeled oligonucleotide (*ss*) pairs with a homologous duplex target (*dsDNA*) to yield a D-loop, which, after separation from the free oligonucleotide on an agarose gel, is visualized and quantified by PhosphorImager analysis of the dried gel. *B, panel I* shows D-loop reactions mediated by Rad51p and Rad54p with the naked homologous duplex (*Naked DNA*) and the homologous duplex assembled into chromatin (*Chromatin*). The results from the experiments in *panel I* are graphed in *panel II*. The *ordinate* refers to the proportion of the homologous duplex converted into D-loop. *C, panel I* shows D-loop reactions mediated by RecA with the naked homologous duplex (*Naked DNA*) and the homologous duplex assembled into chromatin (*Chromatin*). The results from the experiments in *panel I* are graphed in *panel II*. *D, panel I* shows D-loop reactions in which Rad51p and RecA were used either alone or in conjunction with Rad54p or rad54 mutant variants with the naked homologous duplex (*Naked DNA*) and the homologous duplex assembled into chromatin (*Chromatin*), as indicated. ATP was omitted from the reaction in *lane 5*, and ATPγS (*γS*) and AMP-PNP (*PNP*) replaced ATP in *lanes 6* and *7*, respectively. The reactions in *lanes 8* and *9* contained ATP, but Rad54p was replaced with the ATPase-defective variants rad54 K341A (*KA*) and rad54 K341R (*KR*), respectively. The results from the experiments in *panel I* are summarized in the bar graph in *panel II*.

combination of yeast Rad51p and Rad54p led to rapid and highly efficient D-loop formation on the naked DNA donor (Fig. 1*B*). A similar level of D-loop formation was also obtained when the bacterial recombinase RecA was used in these assays with naked DNA (Fig. 1*C*). Surprisingly, assembly of the circular donor into chromatin had no effect on the efficiency of D-loop formation by Rad51p and Rad54p (Fig. 1*B*). D-loop formation on the chromatin donor required ATP hydrolysis by Rad54p, because nonhydrolyzable ATP analogs (ATPγS and AMP-PNP) were unable to substitute for ATP (Fig. 1*C*, *panel I*, *lanes 6* and *7*), and two ATPase-defective mutant variants of Rad54p, rad54K341Ap and rad54K341Rp (18), were inactive (Fig. 1*D*). In contrast to reactions that contained Rad51p/Rad54p, the activity of RecA was completely eliminated when the donor was assembled into nucleosomes (Fig. 1*C*). Furthermore, addition of Rad54p to the RecA reaction did not rescue D-loop formation on chromatin (Fig. 1*D*, *panel I*, *lane 11*). Thus, the eukaryotic recombination proteins have the unique capability of performing the DNA strand invasion reaction with a chromatin donor.

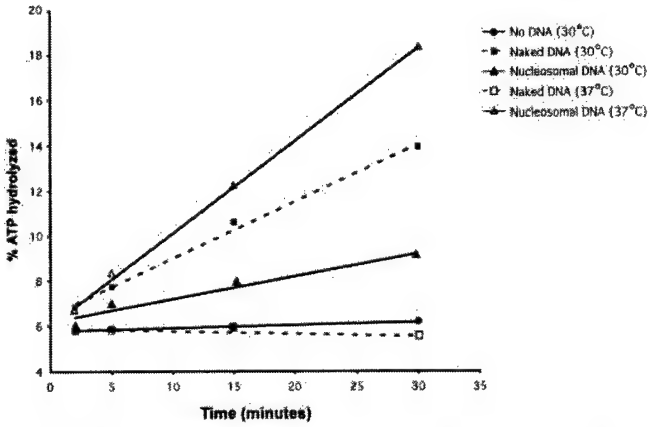

FIG. 2. **Nucleosomal DNA protects Rad54p from thermal inactivation.** ATPase assays. 1 nM Rad54p was incubated at 30 °C with no DNA (*circles*), 5 nM naked (*closed squares*) or nucleosomal dsDNA (*closed triangles*), or at 37 °C with 5 nM naked (*open squares*) or nucleosomal dsDNA (*open triangles*). Samples were taken after 2, 5, 15, and 30 min.

Nucleosomal DNA Protects Rad54p from Thermal Denaturation—The ATPase activity of Rad54p is required for many of its biological functions *in vivo* and for enhancing Rad51p-mediated homologous DNA pairing reactions *in vitro*, both on naked DNA (18) and on chromatin (Fig. 1*D*). Given the latter finding, we were interested in determining whether chromatin influences the ATPase activity of Rad54p.

As shown in Fig. 2, both naked DNA (*solid squares*) and chromatin (*solid triangles*) stimulated the ATPase activity of Rad54p at 30 °C, with naked DNA being somewhat more effective. At the low protein concentrations at which these assays were performed (1 nM), purified Rad54p is extremely temperature-labile and is rapidly inactivated at 37 °C (Fig. 2; Ref. 36). Thus, as expected, the ATPase activity of Rad54p was not detectable in the presence of naked DNA when the reactions were performed at 37 °C (Fig. 2, *open squares*). Importantly, when the reaction was carried out in the presence of chromatin (*open triangles*), the rate of ATP hydrolysis at 37 °C was even greater than the rate obtained in reactions conducted at 30 °C. Importantly, there was no measurable ATPase activity associated with the nucleosomal arrays in the absence of Rad54p, and BSA, free histones, and replication protein A were unable to stimulate the DNA-stimulated ATPase activity of Rad54p at 37 °C. These results indicate that nucleosomal DNA is uniquely able to protect Rad54p from thermal inactivation, and these data suggest that Rad54p may physically interact with nucleosomes.

Rad54 Generates Unconstrained Superhelical Torsion in Nucleosomal DNA—A number of chromatin remodeling complexes that contain Swi2/Snf2-related ATPases have been shown to alter chromatin structure by generating superhelical torsion in DNA and nucleosomal arrays (16). Indeed, the ability to introduce superhelical stress may represent a primary biomechanical activity of all Swi2/Snf2-like ATP-dependent DNA motors, and this activity is likely to be crucial for catalyzing alterations in chromatin structure. Previous studies have shown that Rad54p can also generate both negative and positive supercoiled domains in dsDNA, and it has been suggested that this activity reflects the tracking of Rad54p along DNA (19, 20).

We investigated whether Rad54p is able to introduce superhelical torsion on nucleosomal substrates, using a cruciform extrusion test that has been used for examining other chromatin remodeling enzymes (Fig. 3*A*). In this assay, superhelical

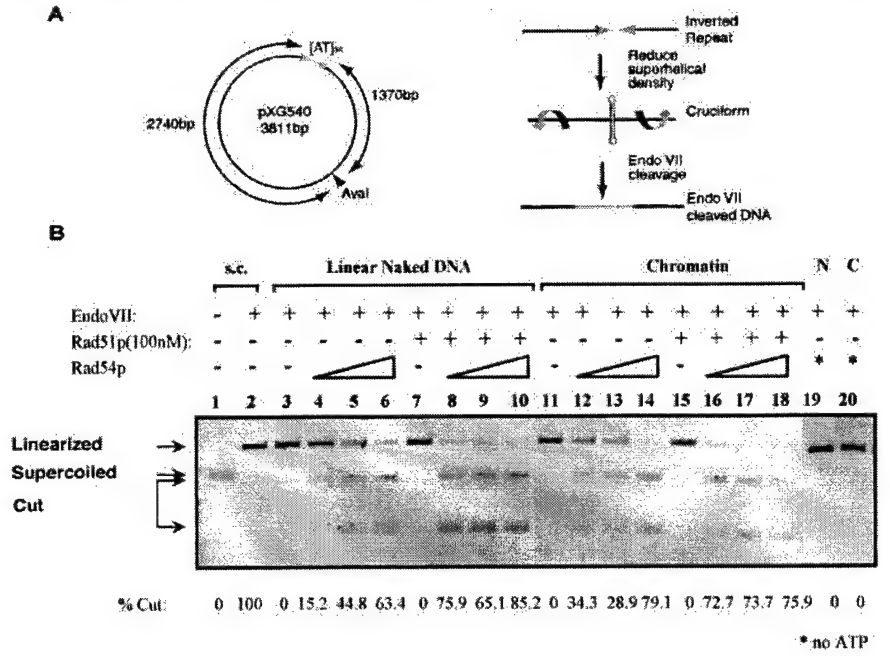

FIG. 3. **Rad54 generates superhelical torsion on nucleosomal DNA.** *A*, schematic illustration of the cruciform extrusion assay. A linearized plasmid (*pXG540*) containing an inverted repeat sequence is incubated with T4 Endonuclease VII, a highly selective junction resolving enzyme, and Rad54p, in the presence of ATP. Rad54p increases the local unconstrained superhelical density, resulting in the extrusion of a cruciform structure, which is recognized and cut by Endo VII. Adapted from Havas *et al.* (16). *B*, results of a typical cruciform formation assay. Supercoiled (*lanes 1, 2*), *Ava*I-linearized pXG540 DNA (*lanes 3–10, 19*), or nucleosomal pXG540 (*lanes 11–18, 20*) was incubated with 12.5, 25, or 50 nM Rad54p as indicated, in the presence or absence of 100 nM Rad51p. EndoVII was omitted in *lane 1*. ATP was omitted in *lanes 19* and *20*. The numbers below each lane (*% cut*) represent the percentage of pXG540 molecules cleaved by EndoVII. *s.c.*, supercoiled substrate; *C*, chromatin substrate; *N*, naked linear DNA substrate.

torsion leads to extrusion of a cruciform that is then recognized and cleaved by bacteriophage T4 endonuclease VII that has high specificity for this DNA structure (16). Consistent with previous studies (19), Rad54p action generates torsional stress on a linear, dsDNA substrate (*N*) which leads to cruciform extrusion (Fig. 3*B*, *lanes 4–6*). Importantly, Rad54p was able to generate torsional stress on the nucleosomal substrate (*C*) with comparable efficiency (*lanes 12–14*). The addition of 100 nM Rad51p greatly stimulated the ability of Rad54p to promote the formation of cruciform structures on both naked and nucleosomal substrates (compare *lanes 4* and *8*, and *12* and *16*, respectively. Also note the decreased levels of linear template in *lanes 16–18*). Importantly, Rad51p fails to support cruciform formation by itself (*lanes 7* and *15*). As expected, the generation of torsional stress required ATP (*lanes 19* and *20*). Furthermore, the ATP hydrolysis mutant variant rad54 K341A was inactive in these assays (data not shown). These data indicate that Rad54p, like other Swi2/Snf2 family members, uses the free energy from ATP hydrolysis to alter DNA topology and that nucleosomal arrays constitute excellent substrates for this activity.

Rad54p Can Disrupt a DNA Triple Helix—How Rad54p introduces topological stress in nucleosomal DNA is unclear. Previously, we suggested that superhelical torsion might result from translocation of Rad54p along the DNA double helix (19). Recently, chromatin remodeling by the yeast RSC complex (which contains the Swi2/Snf2-related ATPase, Sth1p) has been shown to involve ATP-dependent DNA translocation (21). To further evaluate the ability of Rad54p to translocate on DNA, we used a DNA triple-helix-displacement assay that was originally developed to follow the translocation of a type I restriction endonuclease along DNA (17). The substrate used (see Fig. 4*A*) consists of a radioactively labeled oligonucleotide (TFO*) bound via Hoogsteen hydrogen bonds to the major groove of a 2.5-kb linear dsDNA. Translocation of a protein along the DNA displaces the triplex, which can be detected as dissociation of the radioactive TFO* from the DNA triplex. Fig. 4*B* shows typical levels of triplex displacement in the absence or presence of Rad54p or yeast SWI/SNF. Both Rad54p and ySWI/SNF were able to efficiently displace a preformed triplex from both naked (*squares*) and nucleosomal (*triangles*) substrates in an ATP-dependent manner. Similar results were

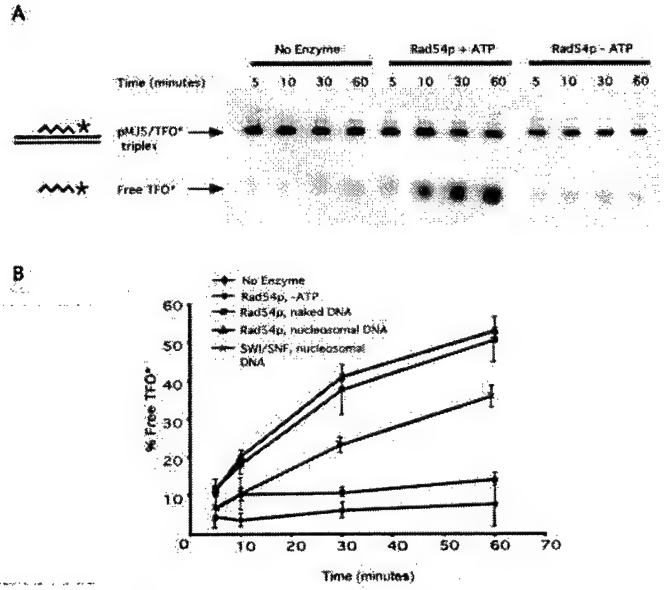

FIG. 4. **Rad54p action displaces a preformed triplex.** *A*, typical results obtained with naked triplex-containing substrate. The upper band corresponds to the duplex-bound TFO*; the lower band corresponds to free TFO*. Reactions contained 5 nM triplex substrate and 5 nM Rad54p. *B*, percentage of free TFO* in four or more experiments were averaged and plotted as a function of time. Note that triplex displacement from the nucleosomal template occurs at equal efficiency to that of naked DNA.

obtained when the TFO*-bound substrate contained single-strand nicks (data not shown), strongly suggesting that the displacement of the TFO* reflects translocation of Rad54p and ySWI/SNF and that it is not due simply to the generation of torsional stress. Thus, yeast RSC (21), ySWI/SNF, and Rad54p (Fig. 4) all share the ability to use the free energy from ATP hydrolysis to disrupt triplex DNA.

Rad54p Has ATPase Kinetics Diagnostic of a DNA-translocating Enzyme—The "inch-worm" model for DNA translocation, originally envisioned (22) for DNA helicases and later modified by Velankar *et al.* (23), proposes that the translocating enzyme progresses along the contour of the DNA in steps of

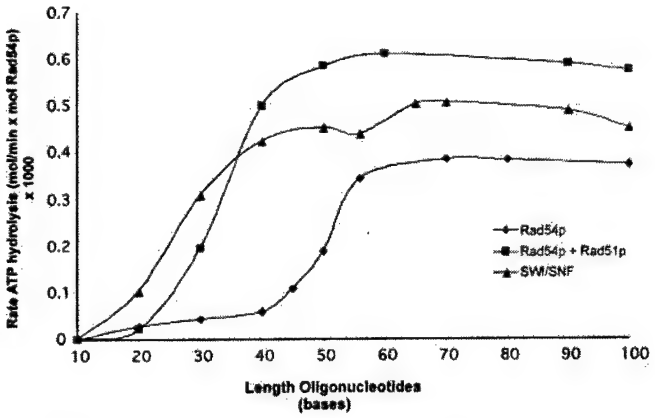

FIG. 5. **Rad54 has ATPase kinetics typical of a unidirectional DNA translocating enzyme.** The rate of ATP hydrolysis by 5 nM Rad54p (*diamonds*), 5 nM Rad54p + 5 nM Rad51p (*squares*), or 10 nM SWI/SNF (*triangles*) was measured in the presence of 50 μM ssDNA (n-mers) oligonucleotides of different lengths. The average values from 3 independent experiments were plotted. Rates were determined from experiments with at least four time points.

a single base, and each step requires the hydrolysis of one ATP molecule. This model predicts that the rate of ATP hydrolysis of a unidirectional DNA translocating enzyme will depend on the length of the DNA (24).

To investigate whether Rad54p has ATPase properties characteristic of a unidirectional DNA translocating enzyme, the rate of ATP hydrolysis was measured in the presence of saturating amounts of single-stranded oligonucleotides ranging from 10 to 100 nucleotides in length (Fig. 5). For comparison, we also monitored the ATPase activity of yeast SWI/SNF (*triangles*). In the case of Rad54p, oligonucleotides shorter than 40 bases failed to stimulate the ATPase activity of Rad54p (*diamonds*), whereas oligonucleotides between 40 and 70 bases led to a stimulation of ATPase activity that was proportional to DNA length. For oligonucleotides longer than 70 bases, the ATPase activity no longer increased with the DNA length. When Rad51p was added to these reactions (*squares*), shorter oligonucleotides became more effective in promoting ATP hydrolysis, and the overall activity was enhanced. Likewise, the ATPase activity of ySWI/SNF (*triangles*) was also proportional to the DNA length, with a plateau reached at 60 bases.

These results are fully consistent with both Rad54p and ySWI/SNF coupling ATP hydrolysis to unidirectional translocation, in which the rate of DNA binding is slower than the rate of DNA translocation (21). In this case, no ATP hydrolysis is observed with very short substrates, presumably because a minimum DNA length is required for Rad54p or ySWI/SNF to bind and to translocate before reaching an end and releasing the DNA. When the substrate is ~30–40 nucleotides in length, Rad54p and ySWI/SNF readily bind the substrate, and more extended translocation events take place. The rate of ATP hydrolysis is fairly constant with DNA substrates longer than 60–70 nucleotides, reflecting the possibility that Rad54p and ySWI/SNF have little processivity, and thus they release their substrate after ~60–70 bases regardless of the total length of the DNA molecule. Although the triphasic kinetics of ATPase activity are consistent with a DNA-translocation mechanism, it remains a possibility that the longer single-stranded oligonucleotides exhibit more extended secondary structures that are either more proficient at binding Rad54p (or SWI/SNF) or stimulating its ATPase activity.

Rad54 Is an ATP-dependent Chromatin Remodeling Enzyme—Cairns and colleagues (21) proposed that short-range translocation events may be the key feature of chromatin remodeling enzymes, leading to a "pumping" of DNA across the surface of the histone octamer, which then results in enhanced DNA accessibility and nucleosome movements. To investigate whether Rad54p might also enhance the accessibility of nucleosomal DNA, we used an assay in which nucleosome remodeling activity is coupled to restriction enzyme activity such that remodeling is revealed as an enhancement of restriction-enzyme cleavage rates (12). This assay uses a nucleosomal array substrate in which the central nucleosome of an 11-mer array contains a unique *Sal*I site located at the predicted dyad axis of symmetry (see Fig. 6*A*). In the absence of a remodeling enzyme, the rate of *Sal*I cleavage is very slow (Fig. 6*A*, *solid diamonds*), whereas addition of a remodeling enzyme, such as yeast SWI/SNF, leads to enhanced digestion (Fig. 6*A*, *solid squares*). When Rad54p was added to the remodeling reactions, *Sal*I digestion was also dramatically enhanced (*solid circles*, *triangles*), although a higher concentration of this protein (50 nM) was required to achieve a rate of digestion comparable with that of reactions that contained yeast SWI/SNF (2 nM, *squares*). However, when Rad51p (50 nM) and Rad54p (50 nM) were both present in the reaction, much higher levels of remodeling were attained (*open circles*). Note that Rad51p has no intrinsic chromatin remodeling activity (*open diamonds*). The stimulation of the Rad54p chromatin remodeling activity by Rad51p is congruent with previous studies showing that Rad51p enhances the rate of ATP hydrolysis and DNA supercoiling by Rad54p (19, 25, see Fig. 3). Thus, the above data indicate that Rad54p is sufficient for chromatin remodeling activity but that the combination of Rad51p and Rad54p constitutes a more potent remodeling machine.

Rad54p Does Not Induce Significant Nucleosome Mobilization—A number of chromatin remodeling complexes that contain a Swi2/Snf2-related ATPase (ySWI/SNF, dCHRAC, dNURF, and xMi-2) can use the energy of ATP hydrolysis to move nucleosomes in cis (26–30). To investigate whether Rad54p can also catalyze nucleosome mobilization, ^{32}P-end-labeled nucleosomal arrays were incubated with buffer, ySWI/SNF, or Rad54p, and nucleosome positions were mapped by micrococcal nuclease (Mnase) digestion (Fig. 6*B*). Mnase can only cleave DNA between nucleosomes, which leads to a periodic ladder of digestion products indicative of a positioned 11-mer nucleosomal array (Fig. 6*B*). Consistent with our previous studies, incubation with ySWI/SNF (2 nM) and ATP leads to a complete disruption of the Mnase digestion pattern, indicative of nucleosome sliding (Fig. 6*B*, *left panel*; also see Ref. 28). In contrast, addition of Rad54p (100 nM) and ATP had very little effect on the cleavage periodicity (Fig. 6*B*, *right panel*). Likewise, addition of both Rad51p and Rad54p (100 nM each) to these assays did not change the Mnase digestion profile (data not shown). Importantly, these experiments used concentrations of ySWI/SNF and Rad54p that yielded similar levels of chromatin remodeling in the restriction enzyme accessibility assay (Fig. 6*A*). Thus, although Rad54p can enhance the accessibility of nucleosomal DNA to restriction enzymes, this activity does not appear to reflect large scale rearrangement of nucleosome positions.

DISCUSSION

In eukaryotes, chromatin presents an accessibility dilemma for all DNA-mediated processes, including gene transcription and DNA repair. Although much progress has been made on identifying the enzymes that remodel chromatin structure to facilitate transcription, less is known of how the DNA-repair machinery gains access to damaged DNA within chromatin (reviewed in Ref. 31). In particular, it has not been clear how the recombinational repair machinery can locate short regions of DNA homology when those DNA donor sequences are assembled into chromatin. Here we have shown that the yeast re-

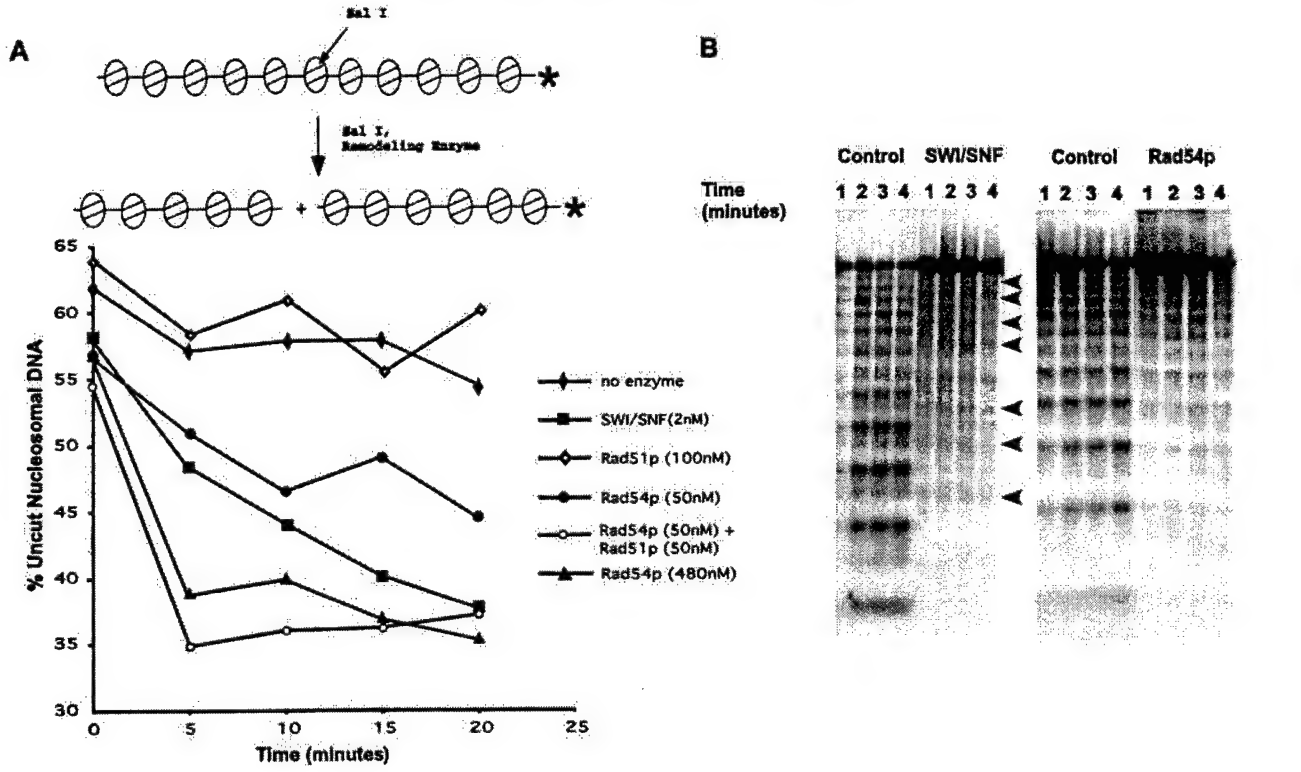

FIG. 6. **Rad54 is an ATP-dependent chromatin remodeling enzyme.** *A*, various concentrations of recombinant Rad54p were tested for chromatin-remodeling activity in a coupled remodeling-restriction enzyme cleavage assay. The nucleosomal substrate was incubated with 50 nM (*closed circles*) or 480 nM Rad54p (*triangles*), 100 nM Rad51p (*open diamonds*), 50 nM Rad54p + 50 nM Rad51p (*open circles*), 2 nM ySWI/SNF (*squares*), or buffer (*closed diamonds*). *B*, 208–11 reconstituted nucleosomal arrays were incubated at 37 °C with 2 nM SWI/SNF, 100 nM Rad54p, or buffer (control lanes). Aliquots were treated with Mnase for the indicated times. The *arrowheads* in the *left panel* indicate the alternate banding pattern as a result of SWI/SNF-induced nucleosome movement.

combination proteins, Rad51p and Rad54p, are sufficient to promote heteroduplex DNA joint formation with chromatin. In contrast, the bacterial recombinase RecA is completely inactive with a chromatin donor. The unique capacity of the eukaryotic machinery to contend with chromatin likely reflects the chromatin-remodeling activity of Rad54p, in which the free energy from ATP hydrolysis enhances the accessibility of nucleosomal DNA. Strand invasion with chromatin may also require a specific interaction between Rad51p and Rad54p because the chromatin remodeling activity of Rad54p does not facilitate RecA-dependent D-loop formation with chromatin (Fig. 1*D*). Recently, Alexiadis and Kadonaga have reported that the *Drosophila* Rad51 and Rad54 proteins can also facilitate strand invasion with chromatin (35).

How Does Rad54p Remodel Chromatin Structure?—Several studies have shown that SWI/SNF-like chromatin remodeling enzymes can perform two separable reactions: 1) they can use the free energy from ATP hydrolysis to enhance the accessibility of nucleosomal DNA and 2) they can use this free energy to mobilize nucleosomes in cis (reviewed in Ref. 32). Recent work from Cairns and colleagues have suggested that both of these activities may be caused by ATP-dependent "pumping" of DNA into the nucleosome (21). In this model, small amounts of DNA translocation might lead to transient exposure of small "loops" of DNA on the surface of the histone octamer, whereas larger quantities of DNA "pumped" into the nucleosome would lead to changes in nucleosome positions. Our data support this model, as we find that both yeast SWI/SNF and Rad54p, like yeast RSC (21), can disrupt a DNA triplex in an ATP-dependent reaction, presumably by translocation of DNA along the surface of the enzyme or by translocation of the enzyme along the DNA. Furthermore, the ATPase activities of ySWI/SNF and Rad54p are sensitive to DNA length, which is diagnostic of DNA-translocating enzymes (21).

Although ySWI/SNF and Rad54p can both enhance the accessibility of nucleosomal DNA, only ySWI/SNF appears to be proficient at changing nucleosome positioning. This result suggests that the precise mechanism of chromatin remodeling by Rad54p may be distinct from that of ySWI/SNF. For instance, Rad54p may only be able to pump small amounts of DNA across the histone octamer surface. Alternatively, Rad54p may translocate along DNA, rather than pumping DNA into the nucleosome. In this model, Rad54p may "pull" the Rad51-ssDNA nucleoprotein filament along the chromatin fiber, leading to changes in nucleosomal DNA topology and DNA accessibility. Such a DNA tracking mechanism might play a key role in facilitating both the search for homology as well as the strand invasion step.

Multiple Roles for Rad54p during Homologous Recombination—Our results suggest that Rad54p is an extremely versatile recombination protein that plays key roles in several steps of homologous recombination. Recently, we found that Rad54p is required for optimal recruitment of Rad51p to a double strand break *in vivo*, and likewise Rad54p can promote formation of the presynaptic filament *in vitro* by helping Rad51p contend with the inhibitory effects of the ssDNA-binding protein replication protein A.[2] Several studies over the past few years have also shown that the ATPase activity of Rad54p plays key roles subsequent to formation of the presynaptic filament. For instance, Rad54p is required for the Rad51p-nucleoprotein filament to form a heteroduplex joint DNA mol-

[2] B. Wolner, S. Van Komen, P. Sung, and C.L. Peterson, submitted for publication.

ecule, even when the homologous donor is naked DNA (Fig. 1*A*; see also Refs. 7, 18, 33). In this case, it has been proposed that Rad54p might use the free energy from ATP hydrolysis to translocate along DNA, which facilitates the homology search process. This DNA-translocation model is fully consistent with our findings that Rad54p can displace a DNA triplex and that the ATPase activity of Rad54p is proportional to DNA length. Rad54p also stimulates heteroduplex DNA extension of established joint molecules (34). Finally, we have shown that Rad54p is required for Rad51p-dependent heteroduplex joint molecule formation with a chromatin donor. In this case, our results suggest that the ATPase activity of Rad54p is used to translocate the enzyme along the nucleosomal fiber, generating superhelical torsion, which leads to enhanced nucleosomal DNA accessibility. It seems likely that this chromatin remodeling activity of Rad54p might also facilitate additional steps after heteroduplex joint formation. Future studies are now poised to reconstitute the complete homologous recombinational repair reaction that fully mimics each step in the repair of chromosomal DNA double strand breaks *in vivo*.

REFERENCES

1. Hiom, K. (2001) *Curr. Biol.* **11,** R278–R280
2. Pâques, F., and Haber, J. E. (1999) *Microbiol. Mol. Biol. Rev.* **63,** 349–404
3. Wood, R. D., Mitchell, M., Sgouros, J., and Lindhal, T. (2001) *Science* **291,** 1284–1289
4. Khanna, K. K., and Jackson, S. P. (2001) *Nat. Genet.* **27,** 247–254
5. Melo, J., and Toczyski, D. (2002) *Curr. Opin. Cell Biol.* **14,** 237–245
6. Kanaar, R., Hoeijmakers, J. H. J., and van Gent, D. C. (1998) *Trends Cell Biol.* **8,** 483–489
7. Petukhova, G., Stratton, S., and Sung, P. (1998) *Nature* **393,** 91–94
8. Eisen, J. A., Sweder, K. S., and Hanawalt, P. C. (1995) *Nucleic Acids Res.* **23,** 2715–2723
9. Jiang, H., Xie, Y., Houston, P., Stemke-Hale, K., Mortensen, U. H., Rothstein, R., and Kodadek, T. (1996) *J. Biol. Chem.* **271,** 33181–33186
10. Clever, B., Interthal, H., Schmuckli-Maurer, J., King, J., Sigrist, M., and Heyer, W. D. (1997) *EMBO J.* **16,** 2535–2544
11. Sambrook, J., Fritsch, E. F., and Maniatis, T. (1989) *Molecular Cloning: A Laboratory Manual*, Cold Spring Harbor Laboratory, Cold Spring Harbor, NY
12. Logie, C., and Peterson, C. L. (1997) *EMBO J.* **16,** 6772–6782
13. Logie, C., and Peterson, C. L. (1999) *Methods Enzymol.* **304,** 726–741
14. Hansen, J. C., Ausio, J., Stanik, V. H., and van Holde, K. E. (1989) *Biochemistry* **28,** 9129–9136
15. Stein, A. (1979) *J. Mol. Biol.* **130,** 103–134
16. Havas, K., Flaus, A., Phelan, M., Kingston, R., Wade, P. A., Lilley, D. M., and Owen-Hughes, T. (2000) *Cell* **103,** 1133–1142
17. Firman, K., and Szczelkun, M. D. (2000) *EMBO J.* **19,** 2094–2102
18. Petukhova, G., Van Komen, S., Vergano, S., Klein, H., and Sung, P. (1999) *J. Biol. Chem.* **274,** 29453–29462
19. Van Komen, S., Petukhova, G., Sigurdsson, S., Stratton, S., and Sung, P. (2000) *Mol. Cell.* **6,** 563–572
20. Ristic, D., Wyman, C., Paulusma, C., and Kanaar, R. (2001) *Proc. Natl. Acad. Sci. U. S. A.* **98,** 8454–8460
21. Saha, A., Wittmeyer, J., and Cairns, B. R. (2002) *Genes Dev.* **16,** 2120–2134
22. Yarranton, G. T., and Gefter, M. L. (1979) *Proc. Natl. Acad. Sci. U. S. A.* **76,** 1658–1662
23. Velankar, S. S., Soultanas, P., Dillingham, M. S., Subramanya, H. S., and Wigley, D. B. (1999) *Cell* **97,** 75–84
24. Dillingham, M. S., Wigley, D. B., and Webb, M. R. (2000) *Biochemistry* **39,** 205–212
25. Mazin, A. V., Zaitseva, E., Sung, P., and Kowalczykowski, S. C. (2000) *EMBO J.* **19,** 1148–1156
26. Guschin, D., Wade, P. A., Kikyo, N., and Wolffe, A. P. (2000) *Biochemistry* **39,** 5238–5245
27. Hamiche, A., Sandaltzopoulos, R., Gdula, D. A., and Wu, C. (1999) *Cell* **97,** 833–842
28. Jaskelioff, M., Gavin, I. M., Peterson, C. L., and Logie, C. (2000) *Mol. Cell. Biol.* **20,** 3058–3068
29. Langst, G., Bonte, E. J., Corona, D. F., and Becker, P. B. (1999) *Cell* **97,** 843–852
30. Whitehouse, I., Flaus, A., Cairns, B. R., White, M. F., Workman, J. L., and Owen-Hughes, T. (1999) *Nature* **400,** 784–787
31. Green, C. M., and Almouzni, G. (2002) *EMBO Rep.* **3,** 28–33
32. Peterson, C. L., and Workman, J. L. (2000) *Curr. Opin. Genet. Dev.* **10,** 187–192
33. Solinger, J. A., Lutz, G., Sugiyama, T., Kowalczykowski, S. C., and Heyer, W. D. (2001) *J. Mol. Biol.* **307,** 1207–1221
34. Solinger, J. A., and Heyer, W. D. (2001) *Proc. Natl. Acad. Sci. U. S. A.* **98,** 8447–8453
35. Alexiadis, V., and Kadonaga, J. T. (2002) *Genes Dev.* **16,** 2767–2771
36. Van Komen, S., Petukhova, G., Sigurdsson, S., and Sung, P. (2002) *J. Biol. Chem.* **277,** 43578–43587

[CANCER RESEARCH 63, 2589–2595, May 15, 2003]

Assembly of Functional ALT-associated Promyelocytic Leukemia Bodies Requires Nijmegen Breakage Syndrome 1[1]

Guikai Wu, Xianzhi Jiang, Wen-Hwa Lee, and Phang-Lang Chen[2]

Department of Molecular Medicine and Institute of Biotechnology, University of Texas Health Science Center at San Antonio, San Antonio, Texas 78245

ABSTRACT

Immortalized cells maintain telomere length through either a telomerase-dependent process or a telomerase-independent pathway termed alternative lengthening of telomeres (ALT). Homologous recombination is implicated in the ALT pathway in both yeast and human ALT cells. In ALT cells, two types of DNA double-strand break repair and homologous recombination factors, the Rad50/Mre11/NBS1 complex and Rad51/Rad52 along with replication factors (RPA) and telomere binding proteins (TRF1 and TRF2), are associated with the ALT-associated PML body (APB). DNA synthesis in late S-G_2 is associated with APBs, which contain telomeric DNA and, are therefore, potential sites for telomere length maintenance. Here, we show that the breast cancer susceptibility gene product, breast cancer susceptibility gene 1, and the human homologue of yeast Rap1, hRap1, are also associated with APBs specifically during late S-G_2 phase of the cell cycle. We additionally show that the localization of the double-strand break repair factors with APBs is distinct from their association with ionizing radiation-induced nuclear foci. To systematically explore the mechanism involved in the assembly of APBs, we examine the role of Nijmegen breakage syndrome 1 (NBS1) and TRF1 in this process, respectively. We demonstrated that NBS1 plays a key role in the assembly and/or recruitment of Rad50, Mre11, and breast cancer susceptibility gene 1, but not Rad51 or TRF1, to APBs. The NH_2 terminus of NBS1, specifically the BRCA1 COOH-terminal domain, is required for this activity. Although TRF1 interacts with NBS1 directly, it is dispensable for the association of either Rad50/Mre11/NBS1 or Rad51 with APBs. Perturbation of the interactions between NBS1/Mre11 and APBs correlates with reduced BrdUrd incorporation associated with APBs, consistent with decreased DNA synthesis at these sites. Taken together, these results support a model in which NBS1 has a vital role in the assembly of APBs, which function to maintain telomeres in human ALT cells.

INTRODUCTION

Telomeres, specialized structures at the ends of linear chromosomes, are comprised of GC-rich tandem repeats. The protection of telomere ends and maintenance of their length prevent chromosome degradation, end-to-end fusions, and rearrangements, events detrimental to chromosome stability and genome integrity. Yeast, germline cells, and the majority of cancer cells typically maintain telomere length by *de novo* addition of DNA by telomerase (1, 2). In addition to the standard mechanism, subsets of cells maintain telomere length through a telomerase-independent mechanism, termed the ALT[3] pathway (3).

Genetic studies in yeast have implicated a recombination-dependent mechanism in the ALT pathway. In this model, members of *RAD52* epistasis group, including the DNA recombination and DSB repair factors Rad52, Rad51, and the Rad50/Mre11/Xrs2 complex participate, along with a helicase, Sgs1, and mismatch repair factors (4–11). Two distinct ALT pathways have been proposed based on participation of either Rad50 or Rad51. Rad52, on the other hand, is required for both pathways (5, 7).

In humans, ~10–20% of tumors are telomerase negative and have been proposed to maintain telomere length by ALT pathways (3). Selection of the exact mechanism of ALT in the cells of these tumors, although not well understood, may be related to the germ layer of their origin (12). Evidence hints that homologous recombination plays a primary role in most of the mammalian ALT pathways, similar to the nonreciprocal recombination used by yeast that are telomerase defective (5, 7). Marker cassettes integrated into specific telomeres of mammalian cells can be copied to other short telomeres, presumably through a gene conversion-like recombination process (13). In mammalian ALT cells, recombination factors, including Rad51, Rad52, and the Rad50/Mre11/NBS1 complex (the human counterpart of yeast Rad50/Mre11/Xrs2), are specifically associated with a fraction of nuclear PML bodies. Also present are telomere binding factors TRF1, TRF2, replication factor RPA and telomere repetitive DNA (14–17). BrdUrd incorporation associated with the APBs in late S-G_2 phase indicates that the DNA synthesis associated with telomere lengthening may be an important function in these subnuclear compartments (16).

DNA recombination and DNA DSB repair involve a number of factors, defects in which are implicated in mammalian carcinogenesis. The product of the BRCA1 has essential roles in cellular responses to DNA damage, in checkpoint control, and in DSB repair (18–27). Consistent with these functions, BRCA1 associates with both the Rad50/Mre11/NBS1 complex and Rad51 *in vivo* (18, 20). In yeast, the Rad50/Mre11/Xrs2 complex participates in several processes, including homologous recombination and nonhomologous end-joining, S-phase replication, DNA damage response, and cell cycle checkpoint control (review in Ref. 28). Moreover, the Rad50/Mre11/Xrs2 complex is proposed to have a role in telomerase-dependent maintenance (5). Whether the Rad50/Mre11/NBS1 complex has a similar role in mammalian cells is unknown. Intriguingly, however, NBS1 physically interacts with TRF1, a telomere-specific binding protein, supporting a potential role for NBS1 complex in mammalian telomere homeostasis (16). Although the association of BRCA1 with Rad50/Mre11/NBS1 complex is critical for DNA damage response, it remains unclear whether BRCA1 plays a role in telomere length maintenance in mammalian cells. Furthermore, how the multiple repair/recombination factors with distinct function assembled in APBs during telomere elongation is also unknown.

Here, we present evidence that BRCA1 and hRap1 are new components of APBs. The association of repair proteins with IRIF is distinct from their association with APBs. Using overexpressed dominant-negative proteins, we show that NBS1 is required for recruitment and/or assembly of a subgroup of proteins into APBs, including Mre11, Rad50, and BRCA1 but not Rad51 or TRF1. The BRCT domain of NBS1 is required for this function. Although TRF1 interacts with NBS1, it is not critical for localization of either NBS1 or Rad51 within APBs. Finally, colocalization of Mre11, Rad50, and

Received 10/22/02; accepted 3/18/03.

The costs of publication of this article were defrayed in part by the payment of page charges. This article must therefore be hereby marked *advertisement* in accordance with 18 U.S.C. Section 1734 solely to indicate this fact.

[1] This work is supported by NIH Grants CA 85605 (to P-L. C.) and CA 94170 and CA 81020 (to W-H. L.). G. W. and X. J. are supported by Department of Defense Predoctoral Training Grant DAMD 17-99-1-9402.

[2] To whom requests for reprints should be addressed, at Department of Molecular Medicine and Institute of Biotechnology, University of Texas Health Science Center at San Antonio, 15355 Lambda Drive, San Antonio, Texas 78245. Phone: (210) 567-7353; Fax: (210) 567-7377; E-mail: chenp0@uthscsa.edu.

[3] The abbreviations used are: ALT, alternative lengthening of telomere; DSB, double-strand break; PML, promyelocytic leukemia; APB, ALT-associated PML body; BRCA1, breast cancer susceptibility gene 1; IRIF, ionizing radiation-induced foci; NBS, Nijmegen breakage syndrome; GST, glutathione *S*-transferase; GFP, green fluorescent protein; BrdUrd, bromodeoxyuridine; BRCT, BRCA1 COOH-terminal domain; CR, conserved region.

BRCA1 at APBs is important for BrdUrd incorporation at these subnuclear sites. These results suggest that NBS1 plays a critical role in mediating the assembly of functional APBs that is important for the propagation of human ALT cells.

MATERIALS AND METHODS

Cell Lines, Cell Synchronization, and BrdUrd Labeling. ALT cell lines, including SV40 large T-antigen-immortalized human fibroblasts (GM847 and VA13) and two osteosarcoma lines (Saos-2 and U-2 OS), have previously been described (16). Cells were cultured in DMEM supplemented with 10% fetal bovine serum in 10% CO_2. Telomerase-positive cells T24 and MCF7 were cultured similarly. Cell synchronization at late S-G_2 was achieved by a double thymidine block-and-release protocol as described previously (16). For BrdUrd pulse labeling, cells were incubated 30 min with reagents in a cell proliferation kit (Amersham Pharmacia Biotech, Inc., Piscataway, NJ), fixed, and stained as described below.

Immunostaining, Coimmunoprecipitation, and Western Blots. Indirect immunofluorescence staining was performed essentially as described previously (16). Briefly, cells plated on cover slips in 6-cm culture dishes were washed with PBS and fixed for 20 min in 3.7% formaldehyde in PBS with 0.1% Triton X-100. Cells were then permeated with 0.05% Saponin at room temperature for 30 min, followed by washing five times in PBS. After blocking with 10% goat serum in PBS/0.5% NP40 at room temperature for 30 min, cells were incubated with primary antibodies for 2 h at room temperature. FITC or Texas Red-conjugated secondary antibodies (Southern Biotechnology Associates, Inc., Birmingham, AL) were used to detect primary antibodies. Cells were counter stained with 4′, 6′-diamino-2-phenylindole and mounted in Permafluor solution (Shandon Lipshaw, Pittsburgh, PA). Fluorescence microscopy was performed with a Nikon Eclipse TE300, and the captured images were processed with Metamorph software and Adobe Photoshop. Immunoprecipitation was performed in lysis 250 buffer [50 mM Tris-Cl (pH 7.4), 250 mM NaCl, 5 mM EDTA, 50 mM NaF, 0.1% NP40, and 0.5 mM phenylmethylsulfonyl fluoride] at 4°C as described previously (18). Coprecipitates were resolved by 7.5% SDS-PAGE and immunoblotted with Rad50, Mre11, and/or NBS1 antibodies (29).

Antibodies. For TRF1 and hRap1, mouse polyclonal sera were raised against GST-TRF1 and GST-hRap1, respectively, which had been expressed and purified from bacteria. Mouse anti-Mre11(12D7), mouse anti-Rad50 (13B3), and mouse anti-Rad51 (14B4) monoclonal antibodies have been described previously (16, 18). Rabbit anti-Rad51 and mouse anti-BRCA1 monoclonal (Ab-1) antibodies were purchased from Oncogene Research Products (Boston, MA). Rabbit anti-NBS1 antibody was obtained from Novus Biologicals (Littleton, CO). Mouse anti-PML antibody was from Santa Cruz Biotechnology (Santa Cruz, CA). Rabbit anti-Sp100 antibody was purchased from MBL International Corporate (Watertown, MA).

Conditional Expression of NBS1C. To generate cell clones that express a GFP-NBS1C fusion protein, we used a tetracycline-inducible expression system (30). NBS1C (amino acids 543–754 of NBS1) was translationally fused to GFP in the pUHD10 vector. Constructs pUHD10-NBS1C and pCHTV (bearing tet regulator and hygromycin-resistant gene, respectively) were cotransfected (10:1 molar ratio) into human osteosarcoma U-2 OS cells, which were subsequently selected with hygromycin (150 μg/ml) in the presence of tetracycline (1 μg/ml). Hygromycin-resistant colonies were isolated and assayed for conditional expression of GFP-NBS1C. One of the positive clones, named UNBS1C, with tight tet-dependent regulation, was used in this study.

Recombinant Adenoviruses. Constructs directing the expression of NBS1C, GFP, or GFP-TRF1Δmyb were prepared according to a simplified adenovirus amplification system with minor modifications (31). To facilitate virus amplification and evaluation of the titer, TRF1Δmyb and NBS1C were both tagged with GFP. Adenoviruses were produced and amplified in E1-immortalized human embryonic kidney cells 293. ALT cells were infected and harvested at 36 h after infection. To perform double staining (such as Mre11 with PML), cells were treated with 1% H_2O_2 after fixation until the GFP signal was fully quenched and then stained as described above.

RESULTS AND DISCUSSION

Association of BRCA1 with PML Bodies Is Specific to ALT Cell. BRCA1 plays an essential role in the maintenance of genome stability, which is partially attributed to its interaction with the DNA damage response and repair complex NBS1/Rad50/Mre11 (18). In ALT cells, the NBS1/Rad50/Mre11 complex is localized with APBs during late S-G_2 phase, suggesting its involvement in telomere length maintenance (16, 17). We first asked if BRCA1 is involved in the ALT pathway. Indirect immunofluorescence studies showed that BRCA1 colocalized with APB-associated proteins, TRF1, Sp100, and NBS1 in several ALT cells, including GM847 (Fig. 1*A*). Although BRCA1 forms speckles in S-phase cells, they are not APB associated (32). However, when ALT cells are enriched at late S-G_2 phase, after release from a double-thymidine block, BRCA1 associates with APB foci in ~24% of cells, compared with 5–7% in unsynchronized culture (Fig. 1*B*). These data suggest that the association of BRCA1 with APBs is specific for late S-G_2 stage, similar to that of NBS1 and Rad51 (Fig. 1*B* and Ref. 16). In contrast, colocalization was not observed in telomerase-positive cells such as human bladder carcinoma cells, T24, and human breast cancer cells, MCF7 (Fig. 1*C*), suggesting that the association of BRCA1 with APBs is specific to late S-G_2 in ALT cells. These data implicating BRCA1 in the ALT pathway are consistent with its roles in homology-directed DNA repair and microhomology-mediated DNA end-joining (27, 33).

Colocalization of Multiple DSB Repair Factors and hRap1 at APBs. BRCA1 is known to colocalize with NBS1/Mre11/Rad50 complex and Rad51 in response to treatment of cells with DNA damaging agents (18, 20). The NBS1/Mre11/Rad50 complex and Rad51 participate in distinct DNA repair events (34, 35). However, both colocalize with APBs in ALT cells (14–16). To demonstrate these functionally distinct recombination factors and BRCA1 are localized in APBs, we performed pair-wise coimmunostainings in either randomly growing or synchronized ALT cells at late S-G_2 (Fig. 1*D*). We found that Rad51 colocalized with BRCA1 (Fig. 1*D*, *a–d*), NBS1 (*e–h*), and Mre11 (*i–l*) reciprocally, suggesting that these factors may work in concert during a recombination-mediated telomere lengthening that potentially occurs in APBs.

In addition to recombination proteins, it is known that many factors are found at APBs, including telomere repeat binding proteins TRF1 and TRF2 (14, 16). The human homologue of yeast Rap1, hRap1, was recently identified as a telomere-associated protein, which contains a BRCT and is critical for telomere length regulation (36). Using an antibody specific for hRap1, we detected immunoreactivity that colocalized with APBs (Fig. 1*E*). Similar to BRCA1 and the NBS1/Mre11/Rad50 complex, the association of hRap1 with APBs is also most evident when cells are arrested at the late S-G_2 phase (data not shown). Combined, the results of these localization experiments suggest that a wide spectrum of both telomere and DSB repair-associated factors may be operational in human ALT pathway.

Colocalization of Double-Strand Break Repair Factors with IRIF Is Distinct from APB Association. NBS1/Mre11/Rad50 complex and Rad51 are known to play an important role in the repair of ionizing radiation-induced DSBs. Although NBS1/Mre11/Rad50 and Rad51 form nuclear foci upon ionizing radiation, Rad51 cannot be found to be colocalized with NBS1 or Mre11 in a given cell (Ref. 37 and our unpublished observations). This observation is in sharp contrast to what was observed in Fig. 1*D* that both groups of proteins are colocalized at APBs in ALT cells. Therefore, it is likely that recombination-dependent telomere length maintenance is mechanistically related but not identical to DSB repair-associated homologous recombination.

To distinguish the relationship between these two types of nuclear

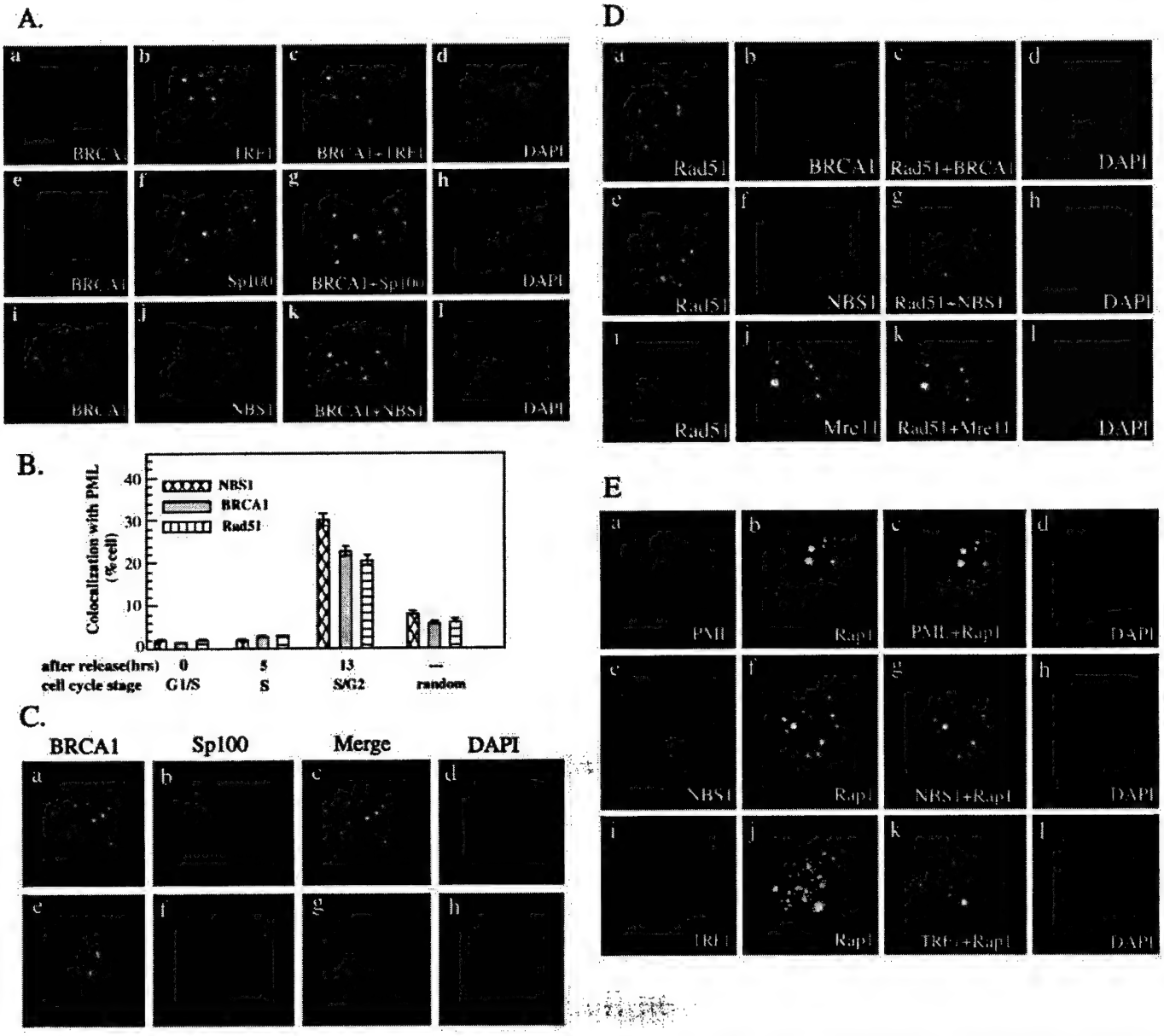

Fig. 1. BRCA1 is a component of the APB in the ALT line GM847. *A*, BRCA1 colocalizes with APB in ALT cells, GM847, as demonstrated by immunofluorescent colocalization with TRF1 (*a–d*), Sp100 (a PML body marker; *e–h*), and NBS1 (*i–l*). Images in *red* represent the detection by a Texas-red-conjugated secondary antibody, whereas *green* represents FITC. Nuclei were visualized by 4′, 6′-diamino-2-phenylindole staining. *B*, association of BRCA1, NBS1, and Rad51, with APBs is most evident in cells enriched at late S-G_2 phase. Cells were either actively growing or synchronized by a double thymidine block and harvested at different time points upon release. For each point, at least 200 cells were counted, and the results were summarized from three independent experiments. *C*, BRCA1 does not associate with PML bodies in telomerase-positive lines such as human bladder carcinoma cells, T24 (*a–d*) and human breast cancer cells, MCF7 (*e–h*). Panels *a* and *e* were immunostained for BRCA1, *b* and *f* for Sp100, whereas *c* and *g* show merged images. *D*, Rad51 colocalizes with BRCA1 (*a–d*), NBS1 (*e–h*), and Mre11 (*i–l*) using antibodies specific for each antigen and procedures described above. *E*, immunostaining with a mouse anti-hRap1 antibody demonstrated its colocalization with APB marker proteins PML (*a–d*), NBS1 (*e–h*), and TRF1 (*i–l*) using antibodies specific for each antigen and procedures described above.

foci, we test whether IRIF and the localization to APBs are dependent on each other. After treatment with γ-irradiation, increased percentage of cells exhibited granular nuclear speckles of BRCA1, Rad51, and NBS1, characteristic of DNA repair foci. These DNA-damaged induced foci did not colocalize with PML or TRF1 in ALT cells such as human osteosarcoma U-2 OS (Fig. 2) and Saos-2 cells (data not shown). However, it was noted that a small fraction of cells demonstrated APB-associated foci positive for the BRCA1, NBS1, and Rad51 antigens in irradiated and mock-irradiated cells. These same patterns of localization were also observed at earlier times (1.5 and 4 h) after exposure to ionizing radiation (data not shown). Combined, these findings suggest that DNA damage-induced foci and APB-associated foci form independently and are morphologically different.

Interrelationships of DSB Repair and Telomere-associated Factors. The association of the above factors with telomeres or APBs in ALT or telomerase-positive cells, their colocalization with BrdUrd under various conditions, and their inclusion in IRIFs are summarized in Table 1. The results were obtained from experiments using either GM847 (ALT line) or T24 (telomerase positive) cells in this study or from other studies using various cell lines (14–16, 19, 37–40). Cumulatively, these data indicate that the distribution of both DSB repair and telomere-associated factors in the nucleus appears to be dynamic and multifaceted. In both telomerase-positive and ALT cells, the NBS1 complex is associated with telomeres and APBs, within which DNA synthesis takes place during late S-G_2 of the cell cycle. The NBS1 complex also associates with replication forks throughout

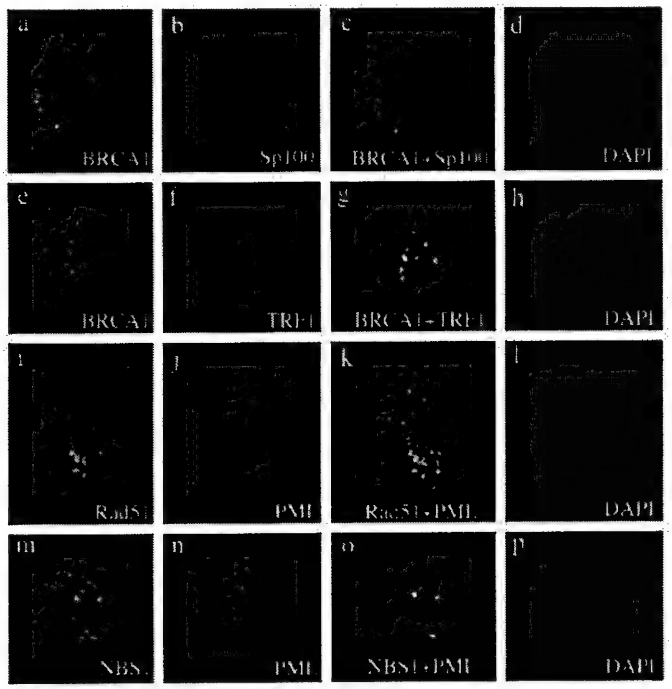

Fig. 2. Association of DSB repair factors with IRIF is distinct from their association with APBs. U-2 OS cells (an ALT line) were harvested and fixed 8 h after radiation (12 gray) and subsequently stained with indicated antibodies. DNA damage-induced foci positive for BRCA1 (usually outnumber PML bodies and are smaller and more homogeneous) do not colocalized with Sp100 (*a–d*) or TRF1 (*e–h*). On the other hand, in a fraction of cells, BRCA1 foci characteristic of APB bodies (larger and brighter but fewer in number) are still present along with newly appearing repair foci that colocalize with TRF1 (*e–h*) after irradiation, suggesting that BRCA1 foci induced by γ-irradiation and colocalization with APBs are independent events. Similar observations were obtained for Rad51 (*i–l*) and NBS1 (*m–p*).

Table 1 *Interrelationships of DSB repair and telomere-associated factors*

	Association w/telomeres or APBs		Colocalize w/BrdUrd			
Factors	ALT cells	TERT(+) cells[a]	S phase	DDI	@APBs	IRIF
Mre11	+	+	+	+	+	+
NBS1	+	+	+	+	+	+
BRCA1	+	−	−	+	+	+
Rad51	+	−	−	+	+	+
Rad52	+	−	?	?	+	+
hRap1	+	+	−	−	+	−

[a] TERT(+), telomerase positive; DDI, DNA damage induced.

S-phase progression and is associated with DNA damage-induced foci when cells are irradiated. On the other hand, BRCA1 and Rad51 are associated with APBs and are also found in replication foci in the presence of DNA damage, regardless of the cell type.

NBS1 Is Essential for the Recruitment and/or Assembly of the NBS1/Mre11/Rad50 Complex into APBs. Elucidating the assembly of functional APBs is central to understanding the ALT pathway. Given the complex spectrum of APB-associated factors, we sought to identify a few key molecules that are critical for their assembly. Because TRF1 is known to interact with both telomeric DNA (41) and NBS1 (16), we hypothesized that both proteins are critical for recruitment and/or assembly of at least BRCA1, Mre11, and/or Rad50 into APBs. To test this model biochemically and cell biologically, we established a subclone of U-2 OS cells, named as UNBS1C, that harbors a stably integrated tet-off system that controls the expression of a GFP-tagged truncated form of NBS1, specifically, a COOH-terminal region encompassed by amino acids 543–754. The rationale for this design is that, although the COOH-terminal region of NBS1 is sufficient for nuclear localization and binding Mre11, the mutated complex does not associate with IRIF (42, 43), an activity that apparently resides within the NH_2-terminal part of the NBS1. If NBS1 is required for APB association, we expected that conditional expression of GFP-NBS1C would result in formation of Rad50/Mre11/NBS1C complexes incapable of APB association. In Fig. 3*A*, immunoblot data demonstrate that removal of tetracycline from the media resulted in a significant induction of GFP-NBS1C expression (compare *Lanes 7* and *8*). Coimmunoprecipitation with α-Mre11 and α-myc and immunoblot detection showed that Rad50 and Mre11 are present in a complex with GFP-NBS1C (Fig. 3*A*, *Lanes 3–6*).

The effects of the truncated NBS1C/Mre11/Rad50 complex on the association of Mre11 and BRCA1 with APBs and DNA synthesis are summarized in Fig. 3*B*. There was a significant reduction in the localization of BRCA1 at APBs upon removal of tetracycline ($P = 0.0153$). The most dramatic effect was on Mre11-associated APBs ($P < 0.0001$), which are normally detected in ~30% of the cells arrested at late S-G_2 stage (16). In contrast, Mre11-associated APBs were completely abolished in late S-G_2 cells upon induction of GFP-NBS1C expression. Consistent with these localization data were the fraction of APBs that displayed BrdUrd incorporation, which was also effectively reduced upon the expression of GFP-NBS1C ($P = 0.0157$). These data suggest that DNA synthesis was reduced in

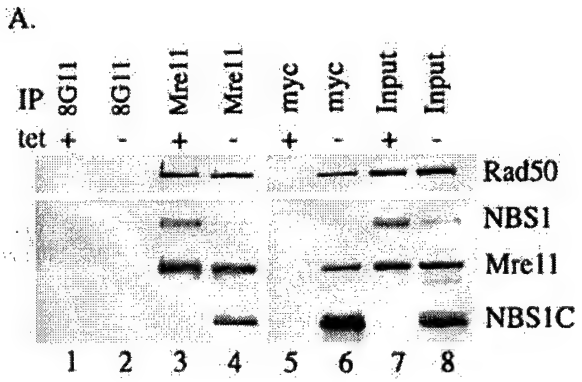

B.

tet	+	-
Mre11	6.4±0.8%	<0.4%
BRCA1	5.3±1.2%	2.1±0.8%
Rad51	5.9±1.4%	4.9±0.9%
TRF1	7.0±1.2%	6.1±1.2%
BrdUrd	3.2±0.6%	1.1±0.6%

Fig. 3. Association of Mre11/Rad50 or BRCA1 with APBs depends on NBS1. *A*, Myc-tagged GFP-NBS1C (amino acid 543–754) competed with the endogenous NBS1 in the formation of NBS1/Mre11/Rad50 complex. Cell lysates prepared from UNBS1C (U-2 OS subclonal line expressing GFP-NBS1C under a tet-off system) were immunoprecipitated with anti-Mre11 antibodies and immunoblotted using antibodies against Rad50, NBS1, and/or Mre11. In the presence of tetracycline, GFP-NBS1C was not expressed and Mre11 coimmunoprecipitated with endogenous NBS1 and Rad50 (*Lane 3*). Upon removal of tetracycline to induce the expression of GFP-NBS1C (induced for 40 h), immunoprecipitation with anti-Mre11 antibodies predominantly brought down GFP-NBS1C instead of the endogenous NBS1 (*Lane 4*). Similarly, Mre11 and Rad50 were specifically immunoprecipitated with GFP-NBS1C by anti-myc antibodies (*Lane 6*) but not control antibodies, mouse anti-GST, 8G11 (*Lanes 1* and *2*). Whole cell lysates from UNBS1C either with (*Lane 7*) or without tetracycline (*Lane 8*) were used to perform straight Western blots probed with each of the specific antibodies as indicated. *B*, effects of the expression of GFP-NBS1C on the colocalization of Mre11, BRCA1, Rad51, TRF1 with APBs. Actively growing UNBS1C cells were plated on the coverslips in the presence or absence of tetracycline in the culture medium. These cells were harvested and immunostained with antibodies against Mre11, BRCA1, Rad51, or TRF1 along with PML (or Sp100). BrdUrd labeling was also performed to evaluate DNA synthesis in APBs (16). Cells that showed positive colocalization of a factor with PML were counted and their percentage relative to the total cell number is presented. A total of at least 140 cells were assessed for each experiment, and the results were summarized from three independent experiments.

A.

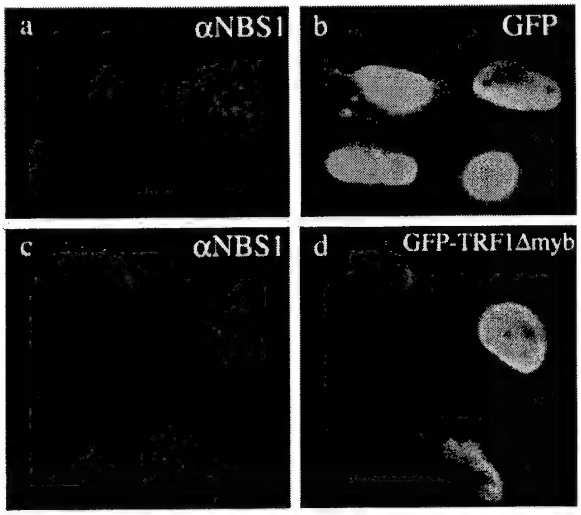

B.

Adenovirus	*(a). GFP*	*(b). GFP-TRF1Δmyb*
NBS1	7.3±1.1%	11.4±1.0%
Mre11	6.2±1.0%	9.1±1.0%

Fig. 4. NBS1 and Mre11 associate with APBs in the presence of overexpressed GFP-TRF1Δmyb. *A*, actively growing GM847 cells were infected with high-titer adenovirus bearing a GFP or GFP-TRF1Δmyb translational fusion, which act as a dominant negative. Cells were harvested at 36 h after infection and stained against NBS1 (*a* and *c*). *b* and *d* show the fluorescent signal of GFP alone (the control) or GFP-TRF1Δmyb in the same field of cells as in *a* and *c*, respectively. Note that some cells overexpressing GFP or GFP-TRF1Δmyb form APB-characteristic NBS1 foci. *B*, fractions of GM847 cells containing APB-characteristic NBS1 or Mre11 foci in cells infected with indicated adenoviruses as described in (*A*). Cells containing more than five APB-characteristic foci for NBS1 or Me11 were counted, and the percentage (*versus* the total population) is presented. For each experiment, at least 220 cells in total were evaluated, and the results are summarized from two independent experiments.

the APBs. Although not investigated here, the data imply an impairment of telomere length maintenance because telomere DNA is the only type known to be present at APBs (14). In contrast to the elimination of Mre11 and reduction of BRCA1 in APBs, the association of TRF1 and Rad51 proteins was only slightly reduced (Fig. 3*B*), although GFP-NBS1C also binds to TRF1 (16). Thus, the mechanism involved in the recruitment of Rad51 to APBs remains unknown.

To eliminate the possibility that the above results were attributable to clonal variations, we designed a system for the expression of GFP-NBS1C using adenovirus, with which highly efficient infection and expression could be achieved. Several ALT lines, including GM847 and VA13, were infected and assessed for the cellular effects of GFP-NBS1C overexpression. Results similar to those with the inducible U-2 OS subline UNBS1C were obtained (data not shown).

These findings suggest that NBS1 is essential for recruitment and/or association of the Mre11/Rad50 complex and BRCA1 with APBs and for APB-specific DNA replication during late S-G_2 phase. It was noted that short-term expression of GFP-NBS1C (within 4 days) did not correlate with significant cell cycle arrest, as quantified by fluorescence-activated cell sorting analysis and immunostaining of the cell cycle marker phosphohistone H3 (data not shown). On the other hand, persistent expression of GFP-NBS1C for >2 weeks led to cell death (data not shown), suggesting that the association of intact NBS1 complex with APBs may be required for growth and proliferation of human ALT cells.

The Association of the NBS1/Mre11/Rad50 Complex with APBs Is Independent of TRF1. We next tested whether TRF1 is required for the association of NBS1, Mre11, and Rad51 with APBs. We used a recombinant adenovirus capable of directing expression of GFP-TRF1Δmyb that forms a nonauthentic TRF1Δmyb/TRF1 dimer, which acts as a dominant negative by depleting endogenous TRF1 from telomere DNA (41, 44). We reasoned that its overexpression would reduce or inhibit the association of NBS1 with telomeres and/or APBs. Unexpectedly however, NBS1 antigen is detected with APBs in a fraction (Fig. 4*B*) of GM847 cells in the presence of overexpressed GFP or GFP-TRF1Δmyb (Fig. 4*A*). Similar results were obtained in two other ALT lines, U-2 OS and VA13 (data not shown). Interestingly, instead of a reduction, a slight increase of the association was observed in cells overexpressing GFP-TRF1Δmyb, compared with the control cells expressing GFP alone (Fig. 4*B*). Taken together, these results suggest that the association of NBS1/Mre11/Rad50 with APBs is independent of TRF1. It is possible that the association could be mediated by another APB component, by other telomeric factors, or by telomere DNA because all of the members of NBS1/Mre11/Rad50 complex have intrinsic DNA binding activity (34, 35).

Structure Requirements for Association of NBS1 with DNA Damage-induced Foci Is Distinct from those Required for APBs. On the basis of the results described above, we concluded that NBS1 plays a central role in the assembly of the functional APBs, which depend on the recruitment of Mre11, Rad50, and BRCA1. Fig. 5 summarizes several sets of experiments designed to elucidate the structural requirement of NBS1 for association with the Mre11/Rad50 complex and localization with APBs. The FHA and BRCT domains are two known conserved modules residing at the NH_2-terminal part of NBS1 (Fig. 5*A* and Ref. 45). In addition, two regions that are also relatively conserved from human to chicken were found and designated as CR1 (amino acids 197–280) and CR2 (amino acids 643–754), respectively (Fig. 5*A*). CR1 is juxtaposed to several SQ-containing phosphorylation motifs that are important for DNA damage response (46–49). CR2 is the interaction domain for several proteins including Mre11 and TRF1 (16, 42, 43).

Using this structural knowledge, we generated a panel of NBS1 mutants and determined their ability to associate with Mre11 complex and APBs by coimmunoprecipitation and/or immunostaining (Fig. 5*B*). Mutation of a conserved residue (His45Ile, Fig. 5*B*) in the FHA domain reduced the association of NBS1 with APBs. Similar reduc-

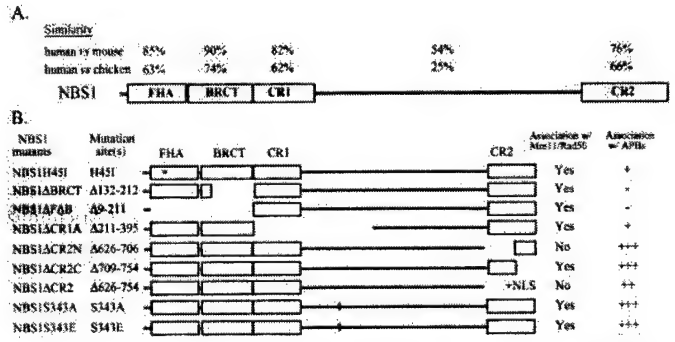

Fig. 5. Structural requirements for the association of NBS1 with Mre11/Rad50 or APBs. *A*, diagram showing the signatory molecular modules in the NBS1 protein. Besides the known NH_2-terminal FHA and BRCT domains, NBS1 contains two relatively CRs (CR1, a.a. 197–280 and CR2, a.a. 643–754). CR1 is juxtaposed to BRCT. CR2 resides at the COOH terminus. The similarities of these signatory domains among human, mouse, and chicken are shown. *B*, a panel of NBS1 deletion mutants COOH-terminally tagged with GFP was constructed and expressed in U-2 OS cells. Colocalization of the expressed NBS1 deletion mutants with Mre11/Rad50 or APBs (represented by TRF1 and PML) were determined by immunostaining as described in "Materials and Methods." Note that NBS1 lacking the BRCT domain no longer associates with APBs.

tions were also observed with several other mutants such as NBS1ΔCR1A (CR1 completely deleted) and NBS1ΔCR2. Strikingly, deletion of the BRCT domain (or both FHA and BRCT domains) completely eliminated the association of NBS1 with APBs. In contrast, deletion of Mre11 interaction domain (NBS1ΔCR2N) did not affect this association, suggesting that the association of NBS1 with APBs is Mre11 independent. Furthermore, expression of NBS1ΔBRCT in U-2 OS cells reduced the colocalization of Mre11/Rad50 and BRCA1, consistent with our observations derived from UNBS1C (data not shown). Serine 343 of NBS1 has been identified as a critical phosphorylation site during DNA damage responses (46–49). However, changing serine 343 to alanine (unphosphorylatable) or glutamate (mimicking phosphorylation) did not affect the association of NBS1 with APBs, suggesting that DNA damage-induced modifications did not play a role in relocalization of NBS1. This result is consistent with our observation that association with DNA damage-induced foci by DSB factors is distinct from their ability to localize with APBs. Taken together, these results strongly suggest that the BRCT domain of NBS1 may mediate an interaction with a PML body component, and this interaction is sufficient to bring in NBS1 and its associated factors critical for telomere elongation to APBs in ALT cells.

In summary, our results implicated the BRCA1 and NBS1 in the human ALT pathway. We established that NBS1 is essential for the assembly of functional APBs, which are probably critical for telomere elongation in human ALT cells. Association of Mre11/Rad50 and BRCA1 with APBs depends on the integrity of NBS1, especially the BRCT module. The recruitment of Rad51 at APBs is NBS1 independent, consistent with the notion that Rad50 complex and Rad51 are required for the generation of different types of ALT cells in yeast (5). Although TRF1 is an integral part of the telomeres, it is dispensable for the recruitment of NBS1 and Rad51 to APBs. Therefore, TRF1 may not be essential for telomere length maintenance in the ALT pathway, but its role at telomeres could be more structurally related. Recombination-associated events responsible for telomere elongation in ALT cells would provide a unique stage for functional cross-talk between BRCA1, Rad51, and the NBS1/Mre11/Rad50 complex, which, in parallel to their roles in DNA recombination and/or DSB repair, contributes to the maintenance of genome stability. Determining whether the BRCA1/NBS1/Mre11/Rad50 complex functions mechanistically in the actual telomere lengthening process or serves as a signal transducer to recruit other recombination and/or DNA synthesis factors awaits additional studies.

ACKNOWLEDGMENTS

We thank Chi-Fen Chen, Yumay Chen, Chang-Ching Liu, Paula Garza, and Diane Jones for their assistance, Qing Zhong for helpful discussion, and Nicolas Ting and Dave Sharp for critically reading the manuscript. We also thank Bert Vogelstein for providing Adeasy system for generating recombinant adenovirus.

REFERENCES

1. de Lange, T. Telomere Dynamics and Genome Instability in Human Cancers, Ed. 1, pp. 265–294. Cold Spring Harbor, NY: Cold Spring Harbor Laboratory Press, 1995.
2. Greider, C. Telomere length regulation. Annu. Rev. Biochem., *65:* 337–365, 1996.
3. Bryan, T. M., Englezou, A., Dalla-Pozza, L., Dunham, M. A., and Reddel, R. R. Evidence for an alternative mechanism for maintaining telomere length in human tumors and tumor-derived cell lines. Nat. Med., *3:* 1271–1274, 1997.
4. Lundblad, V., and Blackburn, E. H. An alternative pathway for yeast telomere maintenance rescues est1-senescence. Cell, *73:* 347–360, 1993.
5. Le, S., Moore, J. K., Haber, J. E., and Greider, C. W. RAD50 and RAD51 define two pathways that collaborate to maintain telomeres in the absence of telomerase. Genetics, *152:* 143–152, 1999.
6. Teng, S. C., and Zakian, V. A. Telomere-telomere recombination is an efficient bypass pathway for telomere maintenance in Saccharomyces cerevisiae. Mol. Cell. Biol., *19:* 8083–8093, 1999.
7. Teng, S., Chang, J., McCowan, B., and Zakian, V. A. Telomerase-independent lengthening of yeast telomeres occurs by an abrupt Rad50p-dependent, Rif-inhibited recombinational process. Mol. Cell, *6:* 947–952, 2000.
8. Chen, Q., Ijpma, A., and Greider, C. W. Two survivor pathways that allow growth in the absence of telomerase are generated by distinct telomere recombination events. Mol. Cell. Biol., *21:* 1819–1827, 2001.
9. Johnson, F. B., Marciniak, R. A., McVey, M., Stewart, S. A., Hahn, W. C., and Guarente, L. The Saccharomyces cerevisiae WRN homolog Sgs1p participates in telomere maintenance in cells lacking telomerase. EMBO J., *20:* 905–913, 2001.
10. Rizki, A., and Lundblad, V. Defects in mismatch repair promote telomerase-independent proliferation. Nature (Lond.), *411:* 713–716, 2001.
11. Cohen, H., and Sinclair, D. A. F. Recombination-mediated lengthening of terminal telomeric repeats requires the Sgs1 DNA helicase. Proc. Natl. Acad. Sci. USA, *98:* 3174–3179, 2001.
12. Reddel, R. R., Bryan, T. M., and Murnane, J. P. Immortalized cells with no detectable telomerase activity. Biochemistry (Mosc.), *62:* 1254–1262, 1997.
13. Dunham, M. A., Neumann, A. A., Fasching, C. L., and Reddel, R. R. Telomere maintenance by recombination in human cells. Nat. Genet., *26:* 447–450, 2000.
14. Yeager, T. R., Neumann, A. A., Englezou, A., Huschtscha, L. I., Noble, J. R., and Reddel, R. R. Telomerase-negative immortalized human cells contain a novel type of promyelocytic leukemia (PML) body. Cancer Res., *59:* 4175–4109, 1999.
15. Lombard, D. B., and Guarente, L. Nijmegen breakage syndrome disease protein and MRE11 at PML nuclear bodies and meiotic telomeres. Cancer Res., *60:* 2331–2334, 2000.
16. Wu, G., Lee, W-H., and Chen, P-L. NBS1 and TRF1 colocalize at promyelocytic leukemia bodies during late S/G_2 phases in immortalized telomerase-negative cells: implication of NBS1 in alternative lengthening of telomeres. J. Biol. Chem., *275:* 30618–30622, 2000.
17. Grobelny, J. V., Godwin, A. K., and Broccoli, D. ALT-associated PML bodies are present in viable cells and are enriched in cells in the G_2/M phase of the cell cycle. J. Cell Sci., *113:* 4577–4585, 2000.
18. Zhong, Q., Chen, C-F., Li, S., Chen, Y., Wang, C. C., Xiao, J., Chen, P-L., Sharp, Z. D., and Lee, W-H. Association of BRCA1 with the hRad50-hMre11–p95 complex and the DNA damage response. Science (Wash. DC), *285:* 747–750, 1999.
19. Scully, R., Chen, J., Ochs, R. L., Keegan, K., Hoekstra, M., Feunteun, J., and Livingston, D. M. Dynamic changes of BRCA1 subnuclear location and phosphorylation state are initiated by DNA damage. Cell, *90:* 425–435, 1997.
20. Scully, R., Chen, J., Plug, A., Xiao, Y., Weaver, D., Feunteun, J., Ashley, T., and Livingston, D. M. Association of BRCA1 with Rad51 in mitotic and meiotic cells. Cell, *88:* 265–275, 1997.
21. Tibbetts, R. S., Cortez, D., Brumbaugh, K. M., Scully, R., Livingston, D., Elledge, S. J., and Abraham, R. T. Functional interactions between BRCA1 and the checkpoint kinase ATR during genotoxic stress. Genes Dev., *14:* 2989–3002, 2000.
22. Zheng, L., Pan, H., Li, S., Flesken-Nikitin, A., Chen, P-L., Boyer, T. G., and Lee, W-H. Sequence-specific transcriptional corepressor function for BRCA1 through a novel zinc finger protein. ZBRK1. Mol. Cell, *6:* 757–768, 2000.
23. Paull, T. T., Cortez, D., Bowers, B., Elledge, S. J., and Gellert, M. Direct DNA binding by Brca1. Proc. Natl. Acad. Sci. USA, *98:* 6086–6091, 2001.
24. Xu, X., Weaver, Z., Linke, S. P., Li, C., Gotay, J., Wang, X. W., Harris, C. C., Ried, T., and Deng, C. X. Centrosome amplification and a defective G_2-M cell cycle checkpoint induce genetic instability in BRCA1 exon 11 isoform-deficient cells. Mol. Cell, *3:* 389–395, 1999.
25. Xu, B., Kim, S., and Kastan, M. B. Involvement of Brca1 in S-phase and G_2-phase checkpoints after ionizing irradiation. Mol. Cell. Biol., *21:* 3445–3450, 2001.
26. Zhong, Q., Boyer, T. G., Chen, P-L., and Lee, W-H. Deficient nonhomologous end-joining activity in cell-free extracts from Brca1-null fibroblasts. Cancer Res., *62:* 3966–3970, 2002.
27. Zhong, Q., Chen, C-F., Chen, P-L., and Lee, W-H. BRCA1 facilitates microhomology-mediated end joining of DNA double strand breaks. J. Biol. Chem., *277:* 28641–28647, 2002.
28. Haber, J. E. The many interfaces of Mre11. Cell, *95:* 583–586, 1998.
29. Dong, Z., Zhong, Q., and Chen, P-L. The Nijmegen breakage syndrome protein is essential for Mre11 phosphorylation upon DNA damage. J. Biol. Chem., *274:* 19513–19516, 1999.
30. Gossen, M., and Bujard, H. Tight control of gene expression in mammalian cells by tetracycline-responsive promoters. Proc. Natl. Acad. Sci. USA, *89:* 5547–5551, 1992.
31. He, T. C., Zhou, S., da Costa, L. T., Yu, J., Kinzler, K. W., and Vogelstein, B. A simplified system for generating recombinant adenoviruses. Proc. Natl. Acad. Sci. USA, *95:* 2509–2514, 1998.
32. Chen, Y., Farmer, A. A., Chen, C-F., Jones, D. C., Chen, P.-L., and Lee, W-H. BRCA1 is a 220-kDa nuclear phosphoprotein that is expressed and phosphorylated in a cell cycle-dependent manner. Cancer Res., *56:* 3168–3172, 1996.
33. Moynahan, M. E., Chiu, J. W., Koller, B. H., and Jasin, M. Brca1 controls homology-directed DNA repair. Mol. Cell, *4:* 511–518, 1999.
34. Paques, F., and Haber, J. E. Multiple pathways of recombination induced by double-strand breaks in Saccharomyces cerevisiae. Microbiol. Mol. Biol. Rev., *63:* 349–404, 1999.
35. Sung, P., Trujillo, K. M., and Van Komen, S. Recombination factors of Saccharomyces cerevisiae. Mutat. Res., *451:* 257–275, 2000.
36. Li, B., Oestreich, S., and de Lange, T. Identification of human Rap1: implications for telomere evolution. Cell, *101:* 471–483, 2000.
37. Maser, R. S., Monsen, K. J., Nelms, B. E., and Petrini, J. H. hMre11 and hRad50 nuclear foci are induced during the normal cellular response to DNA double-strand breaks. Mol. Cell. Biol., *17:* 6087–6096, 1997.

38. Nelms, B. E., Maser, R. S., MacKay, J. F., Lagally, M. G., and Petrini, J. H. *In situ* visualization of DNA double-strand break repair in human fibroblasts. Science (Wash. DC), *280:* 590–592, 1998.
39. Zhu, X. D., Kuster, B., Mann, M., Petrini, J. H., and de Lange, T. Cell-cycle-regulated association of RAD50/MRE11/NBS1 with TRF2 and human telomeres. Nat. Genet., *25:* 347–352, 2000.
40. Mirzoeva, O. K., and Petrini, J. H. DNA damage-dependent nuclear dynamics of the Mre11 complex. Mol. Cell. Biol., *21:* 281–288, 2001.
41. van Steensel, B., and de Lange, T. Control of telomere length by the human telomeric protein TRF1. Nature (Lond.), *385:* 740–743, 1997.
42. Tauchi, H., Kobayashi, J., Morishima, K., Matsuura, S., Nakamura, A., Shiraishi, T., Ito, E., Masnada, D., Delia, D., and Komatsu, K. The Forkhead-associated domain of NBS1 is essential for nuclear foci formation after irradiation but not essential for hRAD50·hMRE11·NBS1 complex DNA repair activity. J. Biol. Chem., *276:* 12–15, 2001.
43. Desai-Mehta, A., Cerosaletti, K. M., and Concannon, P. Distinct functional domains of nibrin mediate Mre11 binding, focus formation, and nuclear localization. Mol. Cell. Biol., *21:* 2184–2191, 2001.
44. Bianchi, A., Smith, S., Chong, L., Elias, P., and de Lange, T. TRF1 is a dimer and bends telomeric DNA. EMBO J., *16:* 1785–1794, 1997.
45. Varon, R., Vissinga, C., Platzer, M., Cerosaletti, K. M., Chrzanowska, K. H., Saar, K., Beckmann, G., Seemanova, E., Cooper, P. R., Nowak, N. J., Stumm, M., Weemaes, C. M., Gatti, R. A., Wilson, R. K., Digweed, M., Rosenthal, A., Sperling, K., Concannon, P., and Reis, A. Nibrin, a novel DNA double-strand break repair protein, is mutated in Nijmegen breakage syndrome. Cell, *93:* 467–476, 1998.
46. Lim, D. S., Kim, S. T., Xu, B., Maser, R. S., Lin, J., Petrini, J. H., and Kastan, M. B. ATM phosphorylates p95/nbs1 in an S-phase checkpoint pathway. Nature (Lond.), *404:* 613–617, 2000.
47. Wu, X., Ranganathan, V., Weisman, D. S., Heine, W. F., Ciccone, D. N., O'Neill, T. B., Crick, K. E., Pierce, K. A., Lane, W. S., Rathbun, G., Livingston, D. M., and Weaver, D. T. ATM phosphorylation of Nijmegen breakage syndrome protein is required in a DNA damage response. Nature (Lond.), *405:* 477–482, 2000.
48. Zhao, S., Weng, Y. C., Yuan, S. S., Lin, Y. T., Hsu, H. C., Lin, S. C., Gerbino, E., Song, M. H., Zdzienicka, M. Z., Gatti, R. A., Shay, J. W., Ziv, Y., Shiloh, Y., and Lee, E. Y. Functional link between ataxia-telangiectasia and Nijmegen breakage syndrome gene products. Nature (Lond.), *405:* 473–477, 2000.
49. Gatei, M., Young, D., Cerosaletti, K. M., Desai-Mehta, A., Spring, K., Kozlov, S., Lavin, M. F., Gatti, R. A., Concannon, P., and Khanna, K. ATM-dependent phosphorylation of nibrin in response to radiation exposure. Nat. Genet., *25:* 115–119, 2000.

Accelerated Publication

THE JOURNAL OF BIOLOGICAL CHEMISTRY
Vol. 278, No. 11, Issue of March 14, pp. 8873–8876, 2003
© 2003 by The American Society for Biochemistry and Molecular Biology, Inc.
Printed in U.S.A.

NFBD1, Like 53BP1, Is an Early and Redundant Transducer Mediating Chk2 Phosphorylation in Response to DNA Damage*

Received for publication, January 2, 2003,
and in revised form, January 21, 2003
Published, JBC Papers in Press, January 24, 2003,
DOI 10.1074/jbc.C300001200

Aimin Peng and Phang-Lang Chen‡

From the Department of Molecular Medicine and Institute of Biotechnology, The University of Texas Health Science Center at San Antonio, San Antonio, Texas 78245

Signaling pathways in response to DNA double strand breaks involve molecular cascades consisting of sensors, transducers, and effector proteins that activate cell cycle checkpoints and recruit repair machinery proteins. NFBD1 (a nuclear factor with BRCT domains protein 1) contains FHA (forkhead-associated), BRCT (breast cancer susceptibility gene 1 carboxyl terminus) domains, and internal repeats and is an early participant in nuclear foci in response to IR. To elucidate its role in the response pathways, small interfering RNA (siRNA) directed against NFDB1 in human cells demonstrated that its absence is associated with increased radio-sensitivity and delayed G_2/M transition, but not G_1 to S. NFBD1 associates with nuclear foci within minutes following IR, a property similar to histone H2AX, 53BP1, and Chk2, which are all early participants in the DNA damage signaling cascade. Temporal studies show that H2AX is required for the foci positive for NFBD1, but NFBD1 is not needed for 53BP1- and H2AX-positive foci. NFBD1, together with 53BP1, plays a partially redundant role in regulating phosphorylation of the downstream effector protein, Chk2, since abrogation of both diminishes phosphorylated Chk2 in IR-induced foci. These results place NFBD1 parallel to 53BP1 in regulating Chk2 and downstream of H2AX in the recruitment of repair and signaling proteins to sites of DNA damage.

Molecules participating in the DNA damage signal pathway can be classified as DNA damage sensors, proximal kinases, transducer kinases, and effectors (1–3). DNA damage sensors, which initiate the DNA damage signal cascade, are minimally characterized. γ-H2AX and the Rad9-Rad1-Hus1 (proliferating cell nuclear antigen-like) clamp complex were considered to be candidates for DNA damage sensors, given their accessibility to damaged DNA (4, 5). Although the phosphorylation and recruitment of these molecules to the DNA damage sites are early actions, the dependence on ATR/ATM[1] for these events challenges their roles as primary sensors (4, 6). Proximal kinases (ATM, possibly ATR and DNA-PK), in cooperation with adaptor proteins, activate a variety of substrates, such as transducer kinases and effectors (1, 3). In yeast, Rad9 is an adaptor protein that plays a central role in transducing and amplifying DNA damage signals by recruiting transducer kinase Rad53 to DNA sites of double strand breaks (7, 8). Based on sequence similarity (9, 10) and early participation in DNA damage responses, three BRCT domain-containing proteins, 53BP1, BRCA1, and NFBD1 (11–14), are possible mammalian orthologs of yeast Rad9. Recent functional studies indicating that 53BP1 only partially regulates the G_2/M checkpoint and Chk2, the human homologue of scRad53, suggests that additional players participate in this crucial cellular response to DNA damage (15–17).

Our initial work on NFBD1 showed that it forms IR-induced foci (IRIF) within 2 min after exposure. Expression of NFBD1-derived BRCT domains compromised association of both Thr^{68}-phosphorylated Chk2 (Chk2T68P) and γ-H2AX within IRIF (13). These data suggest the involvement of NFBD1 in early cellular responses to DNA damage. In the present study, we investigate the precise role of NFBD1 in DNA damage response signaling pathway by using RNAi to suppress NFBD1 protein levels and found that its absence is associated with increased radio-sensitivity and delayed G_2/M transition, but not G_1 to S. NFBD1, together with 53BP1, plays a partially redundant role in regulating phosphorylation of the downstream effector protein, Chk2. These studies place NFBD1 parallel to 53BP1 in regulating Chk2 and downstream of H2AX in the recruitment of repair and signaling proteins to sites of DNA damage.

MATERIALS AND METHODS

Construction of Plasmids—The RNAi vector BS/U6 was kindly provided by Y. Shi (Department of Pathology, Harvard Medical School). Nucleotides sequences from 959 to 981 (GGGCTCAGCCTTTTGGCTTCAT) of NFBD1, sequence from 767 to 789 (GGGCCTTCCGGATGGCCGGCGG) of H2AX, or sequence from 1949 to 1971 (GGGTCTGAGGTGGAAGAAATCC) of 53BP1 were used for construction of the RNAi vectors, BS/U6:NFBD1, BS/U6:H2AX, and BS/U6:53BP1, respectively. The RNAi expression cassette of NFBD1 was also inserted into an pCDNA3 vector that directs expression of GFP and was named pGFP/U6:NFBD1.

Antibodies, Western Blotting, and Immunostaining—Mouse and rabbit anti-NFBD1 were generated as described previously (13). Mouse anti-53BP1 was generated against COOH-terminal 412 amino acids using standard procedures. Rabbit α-γ-H2AX was purchased from Upstate Biotechnology (Lake Placid, NY) and rabbit α-Chk2T68P was from Cell Signaling Technology (Beverly, MA). Rabbit anti-NBS1 and anti-Chk2 antisera were purchased from GeneTex (San Antonio, TX). Immunoprecipitation, Western blotting, and immunostaining were performed as described previously (13, 18). Immunofluorescence images were captured using a Zeiss fluorescence microscope (Zeiss, Axiplan2).

Cell Culture and Treatments with Irradiation—MCF7, a human breast carcinoma cell line, was cultured in Dulbecco's modified Eagle's medium supplemented with 10% fetal bovine serum, 2 mM L-glutamine,

* This work was supported by National Institutes of Health Grant CA 85605 (to P.-L. C.). The costs of publication of this article were defrayed in part by the payment of page charges. This article must therefore be hereby marked "*advertisement*" in accordance with 18 U.S.C. Section 1734 solely to indicate this fact.

‡ To whom correspondence should be addressed: Dept. of Molecular Medicine and Inst. of Biotechnology, The University of Texas Health Science Center at San Antonio, 15355 Lambda Dr., San Antonio, TX 78245. Tel.: 210-567-7353; Fax: 210-567-7377; E-mail: chenp0@uthscsa.edu.

[1] The abbreviations used are: ATR, ataxia telangiectasia and Rad3-related; ATM, ataxia telangiectasia mutated; NFBD1, a nuclear factor with BRCT domains protein 1; BRCT, breast cancer susceptibility gene 1 carboxyl terminus; siRNA, small interfering RNA; 53BP1, tumor suppressor p53 binding protein 1; DSB, double strand break; γ-H2AX, phosphorylated H2AX at serine 139; Chk2T68P, phosphorylated Chk2 at threonine 68; PBS, phosphate-buffered saline; BrdUrd, bromodeoxyuridine; DAPI, 4′,6-diamidino-2-phenylindole; IR, irradiation; IRIF, IR-induced foci; Gy, gray; GFP, green fluorescent protein.

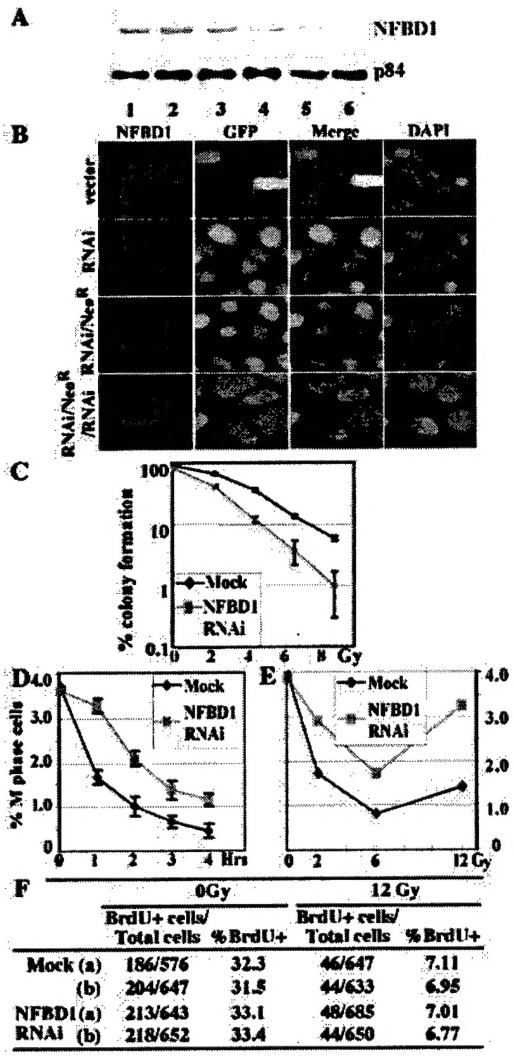

FIG. 1. **Elimination of NFBD1 expression affects IR sensitivity and G_2/M checkpoint.** *A*, Western blot assay of the expression of NFBD1 in MCF7 cells transfected with plasmid (GFP/U6:NFBD1), which directs synthesis NFBD1 siRNA. *Lane 1*, MCF7; *lane 2*, MCF7 transfected with control vector, pCDNA3/GFP. *Lanes 3* and *4*, MCF7 transfected with GFP/U6:NFBD1 for 24 h (*lane 3*) and 48 h (*lane 4*). *Lane 5*, GFP/U6:NFBD1-transfected MCF7 cells were selected with 800 μg/ml G418 for 2 weeks and labeled as RNAi-selected in *B*. *Lane 6*, G418-resistant MCF7 cells were transfected with pBS/U6/NFBD1 and labeled as *RNAi/Neo^R/RNAi* in *B*. Cell extracts were separated by SDS-PAGE and then immunoassayed with antibodies to NFBD1 (*upper panel*) and p84 (*lower panel*). *B*, immunostaining analysis of NFBD1 expression in MCF7 cells transfected with control vector or GFP/U6: NFBD1. Cells were fixed and stained with purified rabbit anti-NFBD1. Panels identified as *NFBD1* represent immunofluorescence staining with anti-NFBD1, and *GFP* represents GFP-expressing cells. *DAPI* indicates cells stained with 4′,6-diamidino-2-phenylindole. *C*, colony formation assay for IR sensitivity. NFBD1 RNAi-transfected or empty vector-transfected cells were irradiated with the indicated doses of IR, and the surviving cells were scored as colonies. *D* and *E*, IR-induced G_2/M checkpoint was examined by counting mitotic phase cells either at the indicated hours after irradiation with 12 Gy (*D*) or at 2 h after the cells were irradiated with indicated dose (*E*). *F*, G_1/S checkpoint control was done by a BrdUrd incorporation assay to monitor S phase entry using NFBD1 RNAi transfected or empty vector controls.

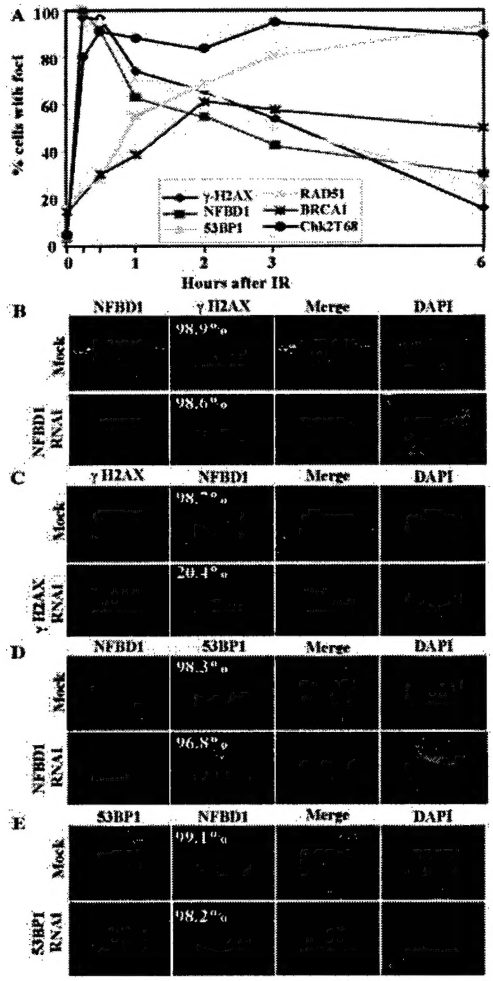

FIG. 2. **Factors recruitment in early DNA damage responses to DSB.** *A*, kinetics of IR-induced foci formation positive for factors involved in DNA damage responses. MCF7 cells were exposed to 1 Gy IR and kept in culture for the indicated times. Treated cells were immunostained with antibodies specific for each the proteins indicated, and the percentage of the cell nuclei containing more than five foci was calculated. *B–E*, *upper panels* are mock-treated cells, and *lower panels* are cells treated with NFBD1 RNAi (*B* and *D*) or H2AX RNAi (*C*) or 53BP1 RNAi (*E*). The percentage of cells either RNAi-transfected or empty vector controls with more than five nuclear foci in each cell was counted and the percentage indicated in the corresponding representative photomicrograph.

50 units of penicillin, and 50 μg/ml streptomycin at 37 °C with 10% CO_2. Cells grown in log-phase were irradiated in a ^{137}Cs radiation source (Mark I, model 68A Irradiator, JL Shepherd & Associates, CA). The medium was replaced immediately after irradiation. All the cells were then cultured at 37 °C and harvested at the indicated time points.

Colony Formation Assay—MCF7 cells transfected and selected with RNAi vectors or empty vector were counted and plated into 10 cm plates. After cell attachment (14 h), the cultures were treated with irradiation at the indicated doses or mock-treated (0 Gy) and then incubated for 14 days. After colony formation, cells were fixed and stained with 2% methyl blue in 50% ethanol. Colony formation was determined by counting a colony with >50 cells. Averages and S.D. values were determined from triplicates. Treated sample percentages were determined by dividing their plating efficiency by the appropriate mock-control.

G_1/S Checkpoint Assay—Cells were plated on cover glasses in 35-mm plates. After 24 h, cultures were either mock-treated or irradiated with 12 Gy of IR and then returned to the incubator. After 24-h incubation, fresh medium containing 10 mM BrdUrd was added and cultured an additional 3 h. Cells were then washed once with PBS and fixed for BrdUrd immunostaining using a cell proliferation kit (Amersham Biosciences). BrdUrd-positive cells were scored by fluorescence microscopy and expressed as a fraction of the total cells.

G_2/M Checkpoint Assay—Cells were plated on cover glasses in 35-mm plates. After 24 h, cultures were either mock-treated or irradiated with 2–12 Gy of γ-radiation and then returned to the incubator. After 1–4 h, cells were gently washed once with PBS, fixed with 4% paraformaldehyde in PBS, and then stained with DAPI. Mitotic cells in prometaphase, metaphase, anaphase, and telophase were identified by fluorescence microscopy, scored, and expressed as a fraction of the total cells.

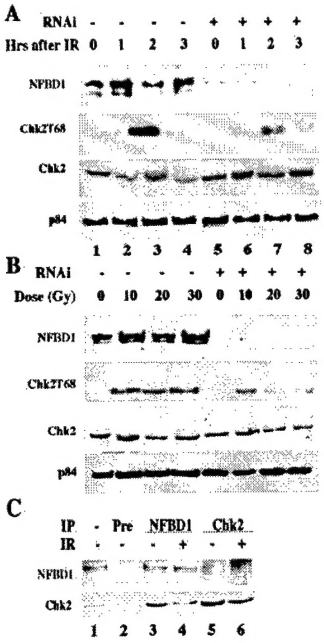

FIG. 3. **Elimination of NFBD1 expression associates with reduced phosphorylation Chk2 at Thr^{68} in response to IR.** *A*, NFBD1 RNAi or empty vector control MCF7 cells were irradiated with 16 Gy. Cell lysates were processed at the indicated times, separated by SDS-PAGE, and then immunoassayed with antibodies to NFBD1 (*top panel*), Chk2T68 (*second panel*), Chk2 (*third panel*), and p84 (*bottom panel*). *B*, Chk2 phosphorylation at Thr^{68} in response to different dose of IR. NFBD1 RNAi-transfected or empty vector control MCF7 cells were irradiated with the indicated doses of IR. Cell lysates were prepared 1 h post-irradiation and processed as described in the legend to A. *C*, Chk2 was reciprocally co-immunoprecipitated with NFBD1. MCF7 were mock-treated (−) or treated with IR (10 Gy) (+) and harvested after 2 h. Cell extracts were immunoprecipitated with preimmune sera (*Pre*, *lane 2*), anti-NFBD1 (*lanes 3* and *4*), or anti-Chk2 (*lanes 5* and *6*) antibodies and analyzed by Western blot probed with anti-NFBD1 (*top panel*) and anti-Chk2 (*second panel*) antibodies. One-tenth of the cell extracts was directly used for Western blot (*lane 1*), serving as references.

RESULTS AND DISCUSSION

Elimination of NFBD1 Expression Affects IR Sensitivity and G_2/M Checkpoint—Our initial work on NFBD1 (nuclear factor that contains BRCT domains 1, KIAA0170) showed that it forms IRIF within 2 min after exposure. Expression of NFBD1-derived BRCT domains compromised association of both Thr^{68}-phosphorylated Chk2 (Chk2T68) and γ-H2AX within IRIF (13). NFBD1 phosphorylation in response to ionizing IR is mediated by ATM (14). Together, these data suggest the involvement of NFBD1 in early cellular responses to DNA damage. To investigate the precise role of NFBD1 in DNA damage response signaling pathway, we generated a vector-based RNAi construct (19) for the *in vivo* expression of a 22-base pair RNA duplex that targets NFBD1. The human breast cancer cell line, MCF7, transfected with the NFBD1 siRNA construct demonstrated significantly reduced expression of NFBD1 protein about 50–60 h after transfection (Fig. 1*B*, compare *lane 1* with *lanes 3* and *4*). In a population of G418-selected cells expressing siRNA, NFBD1 was nearly undetectable (Fig. 1*B*, *lanes 5* and *6*), indicating effective repression by this approach. Using a GFP/NFBD1 siRNA dual expression plasmid, it is apparent that NFBD1 immunofluorescence is inversely correlated with GFP fluorescence, which is not observed using control vectors (Fig. 1*B*, compare rows labeled *RNAi*, *RNAi/Neo^R*, and *RNAi/Neo^R/RNAi* with vector).

Inactivation of genes essential for DNA damage signal transduction, including ATM, H2AX, BRCA1, Chk2 and p53, results in IR sensitivity (see review in Ref. 20). Because NFBD1 is an early participant in this pathway (13), we then examined IR sensitivity in MCF7 cells expressing NFBD1 siRNA. As shown in Fig. 1*C*, NFBD1 RNAi-transfected cells, but not empty vector, formed significantly less colonies upon IR exposure. Similar results were also observed in human HeLa and osteosarcoma U2OS cells (data not shown). To test for the possibility

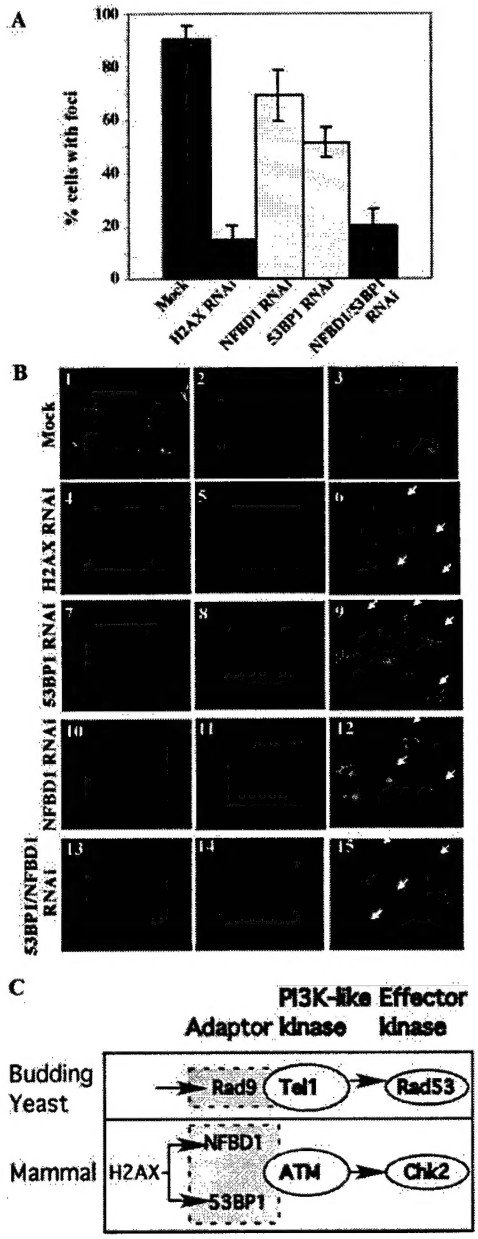

FIG. 4. **NFBD1, like 53BP1, redundantly regulates CHK2.** *A*, empty vector control, H2AX RNAi, NFBD1 RNAi, 53BP1 RNAi, and NFBD1–53BP1 double RNAi-transfected cells were irradiated with 8 Gy. At 2 h post-irradiation, cells were immunostained with anti-Chk2T68p antibody. The percentage of the cells with more than five nuclear foci was calculated. *B*, representative photomicrographs of IR-induced Chk2T68-positive foci are shown. *Panels 1* and *13*, double stained with α-NFBD1 and α-53BP1; *panel 4*, α-H2AX; *panel 7*, α-53BP1; *panel 10*, α-NFBD1; *panels 2*, *5*, *8*, *11*, and *14*, α-CHK2T68p; *panels 3*, *6*, *9*, *12*, and *15*, DAPI. *Panels 1–3* were transfected with empty vector. *Panels 4–6* were transfected for H2AX RNAi. *Panels 7–9* were transfected for 53BP1 RNAi. *Panels 10–12* were transfected for NFBD1 RNAi. *Panels 13–15* were transfected for both 53BP1 and NFBD1 RNAi. *Arrows* indicate RNAi-targeted cells. *C*, a model for the NFBD1 DNA damage checkpoint signaling pathway. In response to DSBs, NFBD1 and 53BP1 both play a central role in transducing DNA damage signals to Chk2.

that IR sensitivity results from defects in checkpoint control, NFBD1 RNAi-transfected MCF7 cells were tested for G_1/S or G_2/M checkpoint control. In both temporal and dose-response protocols (Fig. 1, *D* and *E*, respectively), NFBD1 RNAi-transfected MCF7 cells are partially defective in G_2/M checkpoint, while the G_1/S checkpoint remains intact (Fig. 1*F*).

NFBD1 Association with IR-induced Foci Has Kinetics Similar to γ-H2AX and 53BP1—Previous studies showed that the DNA damage response factors, γ-H2AX, RAD51, 53BP1, and CHK2 form IRIF at sites of DSB (Review in 20). The kinetics of recruitment to DSB sites is useful in exploring their functional relationship. As high dose IR treatment may mask the kinetics of early IRIF formation as reported previously (13), cells were irradiated with 1 Gy, and IR-induced nuclear foci were scored. Similar to γ-H2AX and 53BP1, the percentage of cells with NFBD1-positive IRIF increased immediately after IR treatment and diminished quickly after 60 min (Fig. 2*A*), implying that these proteins have nearly identical kinetics of foci association and participate at the early stages of DSB response. In contrast, CHK2T68-positive IRIF peaked within 30 min after IR, remained at high levels for 6 h, after which they slowly diminished (Fig. 2*A*), suggesting that phosphorylation of Chk2T68 and/or its association with IRIF is a later event compared with that of NFBD1, 53BP1, or γ-H2AX. RAD51- and BRCA1-positive foci were detected at a much later stage under conditions of low dose IR exposure (Fig. 2*A*).

NFBD1 Is Downstream of γ-H2AX and Parallel to 53BP1 in Early Signal Transduction Hierarchy—To determine the relationship of NFBD1, 53BP1, and γ-H2AX in early responses to DSB, cells transfected with plasmids directing expression H2AX, NFBD1, or 53BP1 siRNA were scored for IRIFs positive for each protein. In the H2AX RNAi-transfected cells, NFBD1, similar to 53BP1 (16), was not detected at IRIF (Fig. 2*C*). In the 53BP1 RNAi-transfected cells, the presence of NFBD1 in IRIF was unchanged (Fig. 2*E*). Conversely, in NFBD1 RNAi-treated cells, IRIFs positive for 53BP1 and γ-H2AX was not altered (Fig. 2, *B* and *D*). These results suggest that H2AX is upstream and is required for the recruitment of NFBD1 and 53BP1 into the DSB signal transduction cascade. However, association of NFBD1 and 53BP1 with DSB may represent two independent events downstream of H2AX.

NFBD1 and 53BP1 Regulate Chk2 Redundantly—The function of NFBD1 may serve as an adaptor protein similar to the part played by yeast Rad9 for Rad53, the human homologue of Chk2. To directly test whether NFBD1 has a role in regulating Chk2, phosphorylation of Thr^{68} in cells transfected with NFBD1 RNAi was assayed by Western blotting using phosphorylation state-dependent antibodies. As shown in Fig. 3, *A* and *B*, the immunoreactivity detected with these antibodies was partially reduced relative to total Chk2 protein. These data are comparable with the partial reduction of Chk2T28 phosphorylation observed in 53BP1 RNAi-transfected cells (15–17). Immunoprecipitation of 53BP1 could efficiently bring down Chk2 (15). This observation suggested that 53BP1 might act as an adaptor that facilitates Chk2 phosphorylation. Similarly, Chk2 can be reciprocally co-immunoprecipitated with NFBD1 (Fig. 3*C*). Taken together, these results suggest that NFBD1 binds to Chk2 and mediates its phosphorylation.

To delineate the signaling pathway leading to Chk2 phosphorylation, Chk2T68-positive IRIF in cells transfected with H2AX, 53BP1, and NFBD1 RNAi expression plasmids were scored. A consistent observation is that H2AX is essential for Chk2T68 association IRIF. However, in 53BP1 or NFBD1 RNAi-treated cells, Chk2T68-positive foci were only partially reduced (Fig. 4, *A* and *B*). Interestingly, in 53BP1 and NFBD1 RNAi double transfected cells, CHK2T68-positive IRIF was reduced to a level comparable with H2AX RNAi-transfected cells (Fig. 4, *A* and *B*). These results suggest that NFBD1 and 53BP1 redundantly regulate the participation of the phosphorylated Chk2T28 in IR-induced foci.

In response to DSBs, NFBD1 and 53BP1 both appear to play a central role in transducing DNA damage signals to downstream effectors by serving perhaps as adaptor proteins connecting the upstream signal from γ-H2AX to the downstream effector Chk2 (Fig. 4*C*). This model is consistent with the role of Rad9 function in budding yeast. In yeast, Rad9 is an adaptor protein that plays a central role in transducing and amplifying DNA damage signals by recruiting transducer kinase Rad53 to DNA sites of double strand breaks (7, 8). Chk2 is a major target of ATM, which phosphorylates threonine 68 to activate its kinase activity in response to DNA damage. Activated Chk2, in turn, phosphorylates p53 at Ser^{20}, CDC25A at Ser^{123}, and CDC25C at Ser^{216}, contributing to the G_1/S, S, and G_2/M checkpoint (see review in Ref. 21). The critical question of how adaptor proteins help mediate activation of Chk2 at DSB sites remains to be solved. Our results showing redundancy of NFBD1 and 53BP1 in regulating the recruitment of Chk2T68 to DNA DSB sites probably underscores the importance of this step in mammalian cells. Because of the dissimilarity of their structures (9, 10), it is anticipated that NFBD1 and 53BP1 may also function in different branching pathway.

Acknowledgments—We are grateful to Stanley Fields for providing partial 53BP1 cDNA and Shi Yang for providing pBS/U6 construct. We thank Paula Garza and Diane Jones for antibody preparation and Dave Sharp and Wen-Hwa Lee for critically reading the manuscript.

REFERENCES

1. Zhou, B. B., and Elledge, S. J. (2002) *Nature* **408,** 433–439
2. Khanna, K. K., and Jackson, S. P. (2001) *Nat. Genet.* **27,** 247–254
3. Melo, J., and Toczyski, D. (2002) *Curr. Opin. Cell Biol.* **14,** 237–245
4. Paull, T. T., Rogakou, E. P., Yamazaki, V., Kirchgessner, C. U., Gellert, M., and Bonner, W. M. (2000) *Curr. Biol.* **10,** 886–895
5. Kaur, R., Kostrub, C. F., and Enoch, T. (2001) *Mol. Biol. Cell* **12,** 3744–3758
6. Bao, S., Tibbetts, R. S., Brumbaugh, K. M., Fang, Y., Richardson, D. A., Ali, A., Chen, S. M., Abraham, R. T., and Wang, X. F. (2001) *Nature* **411,** 969–974
7. Sun, Z., Hsiao, J., Fay, D. S., and Stern, D. F. (1998) *Science* **281,** 272–274
8. Gilbert, C. S., Green, C. M., and Lowndes, N. F. (2001) *Mol. Cell* **8,** 129–136
9. Koonin, E. V., Altschul, S. F., and Bork, P. (1996) *Nat. Genet.* **13,** 266–268
10. Callebaut, I., and Mornon, J. P. (1997) *FEBS Lett.* **400,** 25–30
11. Schultz, L. B., Chehab, N. H., Malikzay, A., and Halazonetis, T. D. (2000) *J. Cell Biol.* **151,** 1381–1390
12. Rappold, I., Iwabuchi, K., Date, T., and Chen, J. (2001) *J. Cell Biol.* **153,** 613–620
13. Shang, Y. L., Bodero, A. J., and Chen, P.-L. (2003) *J. Biol. Chem.* **278,** 6323–6329
14. Xu, X., and Stern, D. F. (2003) *J. Biol. Chem.* **278,** 8795–8803
15. Wang, B., Matsuoka, S., Carpenter, P. B., and Elledge, S. J. (2002) *Science* **298,** 1435–1438
16. Fernandez-Capetillo, O., Chen, H. T., Celeste, A., Ward, I., Romanienko, P. J., Morales, J. C., Naka, K., Xia, Z., Camerini-Otero, R. D., Motoyama, N., Carpenter, P. B., Bonner, W. M., Chen, J., and Nussenzweig, A. (2002) *Nat. Cell Biol.* **4,** 993–997
17. DiTullio, R. A., Mochan, T. A., Venere, M., Bartkova, J., Sehested, M., Bartek, J., and Halazonetis, T. D. (2002) *Nat. Cell Biol.* **4,** 998–1002
18. Chen, P. L., Chen, C. F., Chen, Y., Xiao, J., Z. D., S., and Lee, W. H. (1998) *Proc. Natl. Acad. Sci. U. S. A.* **95,** 5287–5292
19. Sui, G., Soohoo, C., Affar el, B., Gay, F., Shi, Y., Forrester, W. C., and Shi, Y. (2002) *Proc. Natl. Acad. Sci. U. S. A.* **99,** 5515–5520
20. Rouse, J., and Jackson, S. P. (2002) *Science* **297,** 537–551
21. Bartek, J., Falck, J., and Lukas, J. (2001) *Nat. Rev. Mol. Cell. Biol.* **2,** 877–886